eman ta zabal zazu

Universidad del País Vasco

Euskal Herriko Unibertsitatea

Role of mitochondria in liver diseases

Tesis doctoral:

Naroa Goikoetxea-Usandizaga

2022

Directores de la tesis:

Dra Malu Martínez-Chantar

Dr Óscar Lorenzo González

Nire familiari.

“Teammates are kind like your family.
You don't get to choose them, you just come in.
And I just got very lucky”

James Clear

Yo también ♥

Naroa

TABLE OF CONTENTS

TABLE OF CONTENTS

RESUMEN

RESUMEN

Las mitocondrias son orgánulos que producen la mayor parte de la energía celular necesaria, y participan también en numerosos procesos metabólicos y de señalización celular. Por lo tanto, las alteraciones mitocondriales no solo afectan al metabolismo, sino que también tienen un impacto en las vías de señalización, la salud y la esperanza de vida (Sorrentino, Menzies, and Auwerx 2018). Debido a la elevada actividad metabólica del hígado, los hepatocitos tienen una gran densidad mitocondrial y son por ello especialmente susceptibles a los trastornos que afectan a la función mitocondrial (Lee and Sokol 2007). De hecho, la disfunción mitocondrial desempeña un papel clave en el inicio y desarrollo de las enfermedades hepáticas crónicas (EHCs). El estrés oxidativo, la desregulación del metabolismo, disminución en la síntesis del ATP y el daño del ADN mitocondrial son prueba de ellos, que en conjunto desencadenan la muerte de los hepatocitos y la liberación de patrones moleculares asociados al daño, potenciando así la patogénesis y progresión de la enfermedad hepática (Xiang, Shao, and Chen 2021).

La morbilidad y la mortalidad de las EHCs son elevadas y su tendencia sigue en alza (Mokdad et al. 2016). Aunque las infecciones virales como la hepatitis B y C están disminuyendo, el abuso de alcohol y la enfermedad del hígado graso no alcohólico (EHGNA) han surgido como importantes factores de riesgo (Cheemerla and Balakrishnan 2021). Sin una terapia adecuada, la progresión de las EHCs puede dar lugar al desarrollo de etapas tardías como la cirrosis o el carcinoma hepatocelular (CHC) (Mishra and Younossi 2012; Riley and Bhatti 2001; Vernon, Baranova, and Younossi 2011), y el trasplante de hígado (TH) puede ser el único tratamiento curativo para estas enfermedades hepáticas en fase terminal. Sin embargo, las tasas actuales cubren menos del 10% de la necesidad mundial de trasplante de órganos (Asrani et al. 2019). Estos datos ponen de manifiesto la ventana de oportunidad para abordar la creciente prevalencia del abuso del alcohol y la EHGNA, y desarrollar nuevas estrategias para mejorar las tasas de trasplante antes de que el manejo de las enfermedades hepáticas crónicas se vuelva insostenible.

Nuestro grupo de investigación, *el Liver Disease Laboratory*, tiene una amplia experiencia en el estudio de las alteraciones metabólicas que subyacen al desarrollo y progresión de las EHCs, con el fin de desarrollar nuevos tratamientos. Entre estas alteraciones, nos hemos centrado en la disfunción mitocondrial como motor principal en

la patofisiología de las EHCs. Teniendo en cuenta las funciones que desempeñan las mitocondrias y su implicación en diversas actividades celulares, la modulación de la disfunción mitocondrial conllevará un gran efecto.

La proteína J controlada por la metilación (MCJ), también conocida como DnaJC15, es un inhibidor endógeno de la actividad mitocondrial que interactúa con el complejo I mitocondrial y lo inhibe (Hatle et al. 2013). Se han observado niveles significativamente elevados de MCJ en pacientes con EHGNA, lesión hepática inducida por APAP y enfermedad hepática colestásica (Barbier-Torres et al. 2017, 2020; Iruzubieta et al. 2021), lo que sugiere una posible relación entre MCJ y la disfunción mitocondrial. Además, hemos podido demostrar previamente que el silenciamiento de *Mcj* específico para el hígado aumenta la actividad mitocondrial y la síntesis de ATP y (1) reduce la formación de ROS y la esteatosis en la esteatohepatitis no alcohólica (EHNA) (Barbier-Torres et al. 2020); (2) previene la disfunción mitocondrial y el daño de los hepatocitos tras la lesión hepática inducida por APAP (Barbier-Torres et al. 2017); y (3) protege contra la lesión hepática inducida por colestasis (Iruzubieta et al. 2021). Por lo tanto, estudiar la relevancia de la disfunción mitocondrial y, específicamente, la contribución de MCJ (1) al desarrollo de la enfermedad hepática alcohólica (EHA) y (2) a las limitaciones actuales que sufre el trasplante hepático (TH) (capacidad regenerativa limitada, daño por isquemia-reperfusión) son uno de los objetivos principales de este trabajo.

El consumo excesivo de alcohol es la principal causa de mortalidad relativa al hígado en los países occidentales y representa la segunda indicación más frecuente de TH en todo el mundo (Louvet and Mathurin 2015). La progresión de la EHA partiendo del hígado graso alcohólico hacia la esteatohepatitis alcohólica, la hepatitis alcohólica, la cirrosis y, finalmente, el CHC está bien caracterizada, pero carece de una terapia que pueda detener e incluso revertir la progresión de la enfermedad (You and Arteel 2019). Actualmente, las únicas opciones para curar el daño hepático relacionado con el alcohol son la abstinencia en etapas tempranas y el TH en las etapas avanzadas (Teschke 2018). Casualmente, el abuso del alcohol deteriora considerablemente la función mitocondrial. De hecho, la disfunción mitocondrial es uno de los primeros indicadores de los daños relacionados con el alcohol (Zhong et al. 2014). El metabolismo de altas concentraciones de alcohol conduce a la formación de acetaldehído tóxico y grandes cantidades de NADH, que, en caso de no ser oxidadas, alteran el poder reductor de la célula, el ratio

NAD^+/NADH, afecta a importantes vías metabólicas, y, sobre todo, causa la acumulación del acetaldehído (Ceni, Mello, and Galli 2014). Por lo tanto, tras el consumo del alcohol, las mitocondrias deben aumentar el consumo de oxígeno, mediante un proceso que se conoce como "*Swift Increase in Alcohol Metabolism*" (SIAM) (Zhong et al. 2014). Si el consumo se cronifica, este fenómeno causa la disfunción mitocondrial, estrés oxidativo y la enfermedad se agudiza. Curiosamente, los pacientes que sufren de alcoholismo en etapas avanzadas muestran una eficiencia metabólica significativamente reducida y un menor contenido de ATP intracelular. En base a lo expuesto anteriormente, nuestro primer objetivo ha sido analizar la implicación de la disfunción mitocondrial, y su regulación mediada por MCJ, en la EHA.

Por otro lado, como hemos mencionado, las tasas de trasplante hepático actuales cubren menos del 10% de la necesidad mundial (Asrani et al. 2019). La lesión por isquemia-reperfusión (IR), la principal causa de disfunción hepática tras el trasplante (Gracia-Sancho, Casillas-Ramírez, and Peralta 2015), y la escasez de órganos de donantes (Campana et al. 2021) son las limitaciones principales del TH. Entre las estrategias para ampliar el grupo de donantes, se ha propuesto el uso de hígados con criterios expandidos, es decir, hígados que provienen de donantes cadavéricos tras un paro cardíaco, donantes añosos (<60 años) o esteatóticos (Ivanics et al. 2021). Desafortunadamente, el uso de estos órganos aumenta la incidencia de disfunción hepática y del síndrome post-reperfusión (Trapero-Marugán, Little, and Berenguer 2018; Younossi et al. 2021), debido a su elevada susceptibilidad a la lesión isquémica y a la alteración de la regeneración hepática. Además, la regeneración del hígado está determinada por el estado energético del hepatocito (Alexandrino et al. 2016) y el daño mitocondrial y la disminución del ATP son característicos de la lesión isquémica (Gracia-Sancho, Casillas-Ramírez, and Peralta 2015). Esto sugiere que la disfunción mitocondrial, puede que a consecuencia de MCJ, esté limitando la capacidad regenerativa y aumentando la susceptibilidad hacia el daño isquémica, especialmente en individuos con un metabolismo comprometido, como pueden ser los donantes añosos y esteatóticos.

El objetivo de esta tesis, en resumen, es caracterizar la contribución de MCJ, un inhibidor endógeno de la respiración mitocondrial, al desarrollo de la EHA y al deterioro de la respuesta regenerativa junto con una mayor susceptibilidad a la lesión isquémica que se observa en los individuos metabólicamente comprometidos, y posibles futuros donantes.

Para el análisis de la EHA, se han examinado muestras de pacientes a distintas etapas de la enfermedad, desde estadios iniciales hasta biopsias de pacientes con hepatitis alcohólica sometidos a trasplante. También se ha empleado el modelo de ratón NIAAA desarrollado por el grupo de investigación de Bin Gao (Bertola et al. 2013) como modelo preclínico de estadios tempranos de EHA. En este modelo los ratones son alimentados con la dieta de Lieber-De Carli suplementada con 5% (vol/vol) de etanol durante 10 días, más un único gavage de etanol 31% (vol/vol) el día 11, y se caracteriza por representar un estadio inicial de la enfermedad, esteatohepatitis alcohólica moderada. Hemos trabajado con ratones que carecen de la proteína MCJ en todo el organismo, conocidos como MCJ-KO, y con ratones control, Wt, a los que se les ha realizado un silenciamiento específico en el hígado inyectando por la vena de la cola un siRNA contra *Mcj* (siMCJ).

En el presente trabajo se ha caracterizado la implicación de MCJ en la fisiopatología de la EHA; el inhibidor está regulado a la baja tanto en pacientes con EHA temprana y en los ratones alimentados con el NIAAA, y sobreexpresado en pacientes con EHA avanzada. Comparado con ratones Wt, los MCJ-KO muestran una mortalidad cuatro veces superior tras la ingesta del alcohol, por lo que la falta de MCJ en todo el cuerpo resulta perjudicial en EHA. Hemos podido observar que esto se debe a los efectos sistémicos del alcohol. Tras el consumo del alcohol, los macrófagos intestinales que carecen de MCJ se sobreactivan y desencadenan una cascada proinflamatoria que causa una disbiosis intestinal, aumenta la permeabilidad intestinal y facilita la traslocación de lipopolisacárido (LPS) o endotoxina bacteriana. El LPS, por un lado, agrava el daño hepático, ya que aumenta la expresión de *Cyp2e1* y la producción consecuente de estrés oxidativo, y por otro, afecta la función pancreática. Los islotes beta pancreáticos de los ratones MCJ-KO pierden la capacidad de sensar la glucosa y liberar insulina, provocando la hiperglucemia, en los casos más graves, la muerte súbita de los ratones MCJ-KO.

Sin embargo, el silenciamiento específico de *Mcj* en el hígado alivia la EHA. En los ratones alimentados con el NIAAA y tratados con el siMCJ se ha observado un aumento en la supervivencia, reducción del daño hepático y ausencia de alteraciones sistémicas, es decir, tanto el intestino como la función pancreática no ha sufrido un daño adicional. Mostramos que el tratamiento con el siMCJ restaura la función mitocondrial y renueva las concentraciones de NAD^+, lo que permite recuperar la actividad de SIRT1 y modificar

el metabolismo lipídico hacia la oxidación de ácidos grasos, inhibiendo la producción *de novo* y acumulación de ácidos grasos, atenuando la esteatosis y previniendo la inflamación y la lesión hepatocelular. Casualmente, los ratones tratados con el siMCJ también muestran una recuperación del daño hepático mediante una mayor regeneración.

En resumen, el presente trabajo demuestra la contribución de MCJ en el desarrollo de la EHA. También subraya la necesidad de generar tratamientos específicos dirigidos al hígado que eviten los efectos secundarios en el resto de los órganos. De hecho, el silenciamiento específico de Mcj en el hígado mediante el uso del siMCJ ha demostrado ser una terapia potencial efectiva, ya que recupera la función mitocondrial y restaura el ratio NAD^+/NADH necesario para un metabolismo catabólico que evite la esteatosis, la inflamación y el daño hepático.

Con relación al trasplante hepático, hemos analizado biopsias de donantes hepáticos tras el daño por isquemia y reperfusión y se han realizado tres aproximaciones quirúrgicas en los modelos preclínicos. La hepatectomía parcial del 70% (Phx) es el modelo por excelencia para el estudio de la capacidad regenerativa (Higgins and Anderson 1931). El modelo de daño por isquemia prolongada (90' IR) permite el estudio del daño isquémico que se da durante el trasplante (Yamauchi and B 1982), y el modelo combinado de Phx junto con IR representa la cirugía de resección hepática que se practica en clínica (Selzner, Camargo, and Clavien 2003). Hemos podido observar la sobreexpresión de MCJ durante la regeneración hepática y la lesión por isquemia. Los ratones MCJ-KO y Wt tratados con el siMCJ muestran una regeneración acelerada, 12 horas respecto a ratones no tratados, una reducción en la lesión isquémica y un aumento en la supervivencia en el modelo combinado de Phx junto con IR, de hecho, la falta de MCJ aumenta de un 50% a un 80% dicha supervivencia. El aumento de la respiración mitocondrial y de la producción de ATP mediante el silenciamiento de *Mcj* permite la adaptación mitocondrial que restablece el suministro bioenergético para mejorar la regeneración y evita la muerte celular tras el daño por IR. En cuanto al mecanismo, el aumento de la secreción de ATP facilita la activación temprana de las células de Kupffer y la producción de TNF, IL-6 y HB-EGF, acelerando el inicio de la regeneración, la entrada en el ciclo celular y la división de los hepatocitos.

En cuanto al posible uso de hígados con criterio extendido, los hígados de ratones añosos y esteatóticos se caracterizan por una disminución en la producción de ATP, lo que reduce la capacidad regenerativa y aumenta la susceptibilidad al daño por isquemia. En este estudio se ha determinado que el tratamiento terapéutico de siMcj en ratones de 15-17 meses y en ratones alimentados con una dieta alta en grasas y fructosa durante 12 semanas, recupera la capacidad mitocondrial, la producción de ATP y por lo tanto alivia la esteatosis, supera las limitaciones regenerativas y reduce la susceptibilidad al daño isquémico. Se abre, por tanto, una nueva perspectiva en el uso de hígados con criterio extendido para trasplante hepático.

En este trabajo hemos podido demostrar la contribución de MCJ en las limitaciones principales del trasplante hepático, que son la regeneración hepática limitada y una susceptibilidad al daño isquémico aumentado, especialmente en hígados metabólicamente comprometidos. Su silenciamiento promueve la regeneración, reduce el daño isquémico y supera las limitaciones regenerativas de los hígados con criterio extendido, permitiendo su uso para el trasplante hepático.

En resumen, nuestros resultados indican que MCJ contribuye a la fisiopatología de la EHA y perjudica la regeneración, además de aumentar la susceptibilidad a la isquemia. Destacamos la necesidad de terapias específicas para las enfermedades hepáticas crónicas, y, por último, proponemos el silenciamiento específico de Mcj como posible solución para aliviar la lista de espera de trasplante, ya que reestablece las capacidades intrínsecas de hígados con criterio extendido, permitiendo, así, su uso clínico.

Conclusiones

En base a los resultados obtenidos e integrados en esta tesis doctoral, hemos concluido:

1) MCJ está regulada a la baja en modelos clínicos y preclínicos de EHA temprana y sobreexpresada en pacientes con EHA avanzada
2) La deficiencia de MCJ en todo el cuerpo exacerba la EHA *in vivo*
    a. La regulación a la baja de la proteína exacerba los efectos sistémicos del alcohol
        i. La sobreactivación de los macrófagos intestinales desencadena una cascada proinflamatoria que altera la microbiota intestinal, aumenta la permeabilidad intestinal y facilita la translocación de LPS
        ii. El LPS circulante agrava la lesión hepática mediante el aumento de la expresión de *Cyp2e1* y el estrés oxidativo
        iii. El LPS circulante deteriora la función pancreática y los ratones MCJ-KO muestran un mal control glucémico
        iv. Los niveles elevados de glucosa en sangre facilitan la entrada de glucosa en el hígado, la lipogénesis *de novo* de los AF y causan esteatosis
    b. Tras el abuso de alcohol, los ratones MCJ-KO mueren debido a la hiperglucemia
3) El silenciamiento hepático de *Mcj* mejora la EHA *in vivo*
    a. La regulación a la baja de la proteína previene la esteatosis
        i. El aumento de la OXPHOS promueve la oxidación de los ácidos grasos y restablece el ratio NAD^+/NADH
        ii. El NAD^+ restaurado aumenta la actividad desacetilasa de SIRT1
        iii. SIRT1 inhibe la activación de mTORC1, la expresión de SREBP1 y la lipogénesis *de novo*
    b. La regulación a la baja de la proteína reduce el estrés oxidativo
    c. Aliviar la esteatosis y reducir el estrés oxidativo previene la inflamación y el daño hepatocelular
4) MCJ se sobreexpresa durante la regeneración hepática y la lesión por isquemia-reperfusión en modelos clínicos y preclínicos

5) El silenciamiento hepático de *Mcj* mejora la regeneración hepática y reduce el daño isquémico *in vivo*
    a. La regulación a la baja de la proteína mejora la respiración mitocondrial y aumenta la producción de ATP
    b. El aumento de la producción de ATP proporciona energía adicional para la regeneración del hígado e inicia la cascada regenerativa
        i. El ATP extracelular activa las células de Kupffer residentes en el hígado y, posteriormente, la producción de citoquinas (TNF, IL-6) y factores de crecimiento (HB-EGF)
        ii. STAT3 y EGFR se activan y facilitan la migración de CyclinD1 al núcleo
        iii. Los hepatocitos comienzan a proliferar rápidamente
    c. El aumento de la producción de ATP evita el vaciado característico de ATP que sucede durante la lesión isquémica
    d. La lesión general del hígado mejora
6) El silenciamiento hepático de *Mcj* supera las limitaciones regenerativas y reduce la susceptibilidad a la lesión isquémica en modelos preclínicos metabólicamente comprometidos
    a. La regulación a la baja de la proteína mejora la bioenergética mitocondrial, aumenta la producción de ATP, atenúa la esteatosis y promueve la regeneración en ratones esteatóticos
    b. La regulación a la baja de la proteína mejora la bioenergética mitocondrial, aumenta la producción de ATP, disminuye el estrés oxidativo, promueve la regeneración y aumenta la supervivencia en ratones envejecidos

Bibliografía

Alexandrino, Henrique et al. 2016. "Mitochondrial Bioenergetics and Posthepatectomy Liver Dysfunction." *European Journal of Clinical Investigation* 46(7): 627–35.

Asrani, Sumeet K, Harshad Devarbhavi, John Eaton, and Patrick S Kamath. 2019. "Burden of Liver Diseases in the World." *Journal of Hepatology* 70(1): P151-171.

Barbier-Torres, Lucía et al. 2017. "The Mitochondrial Negative Regulator MCJ Is a Therapeutic Target for Acetaminophen-Induced Liver Injury." *Nature Communications* 8(1).

———. 2020. "Silencing Hepatic MCJ Attenuates Non-Alcoholic Fatty Liver Disease (NAFLD) by Increasing Mitochondrial Fatty Acid Oxidation." *Nature Communications* 11(1): 1–15. http://dx.doi.org/10.1038/s41467-020-16991-2.

Bertola, Adeline et al. 2013. "Mouse Model of Chronic and Binge Ethanol Feeding (the NIAAA Model)." *Nature Protocols* 8(3): 627–37. http://dx.doi.org/10.1038/nprot.2013.032.

Campana, Lara, Hannah Esser, Meritxell Huch, and Stuart Forbes. 2021. "Liver Regeneration and Inflammation: From Fundamental Science to Clinical Applications." *Nature Reviews Molecular Cell Biology* 22(9): 608–24. http://dx.doi.org/10.1038/s41580-021-00373-7.

Ceni, Elisabetta, Tommaso Mello, and Andrea Galli. 2014. "Pathogenesis of Alcoholic Liver Disease: Role of Oxidative Metabolism." *World Journal of Gastroenterology* 20(47): 17756–72.

Cheemerla, Shantan, and Maya Balakrishnan. 2021. "Global Epidemiology of Chronic Liver Disease." *Clinical Liver Disease* 17(5): 365–70.

Gracia-Sancho, Jordi, Araní Casillas-Ramírez, and Carmen Peralta. 2015. "Molecular Pathways in Protecting the Liver from Ischaemia/Reperfusion Injury: A 2015 Update." *Clinical Science* 129(4): 345–62.

Hatle, Ketki M. et al. 2013. "MCJ/DnaJC15, an Endogenous Mitochondrial Repressor of the Respiratory Chain That Controls Metabolic Alterations." *Molecular and Cellular Biology* 33(11): 2302–14.

Higgins, G M, and R M Anderson. 1931. "Experimental Pathology of the Liver I. Restoration of the Liver of the White Rat Following Partial Surgicla Removal." *Arch Pathol Lab Med* 12: 186–202.

Iruzubieta, Paula et al. 2021. "Boosting Mitochondria Activity by Silencing MCJ Overcomes Cholestasis-Induced Liver Injury." *JHEP Reports* 3(3).

Ivanics, Tommy, Phillipe Abreu, Eleonora De Martin, and Gonzalo Sapisochin. 2021. "Changing Trends in Liver Transplantation: Challenges and Solutions." *Transplantation* 105(4): 743–56.

Lee, Way S, and Ronald J Sokol. 2007. "Liver Disease in Mitochondrial Disorders." *Seminars in Liver Disease* 27(3): 259–73.

Louvet, Alexandre, and Philippe Mathurin. 2015. "Alcoholic Liver Disease: Mechanisms of Injury and Targeted Treatment." *Nature Reviews Gastroenterology and Hepatology* 12(4): 231–42.

Mishra, Alita, and Zobair M. Younossi. 2012. "Epidemiology and Natural History of Non-Alcoholic Fatty Liver Disease." *Journal of Clinical and Experimental Hepatology* 2(2): 135–44.

Mokdad, Ali H. et al. 2016. "Global Burden of Diseases, Injuries, and Risk Factors for Young People's Health during 1990–2013: A Systematic Analysis for the Global Burden of Disease Study 2013." *The Lancet* 387(10036): 2383–2401.

Riley, T. R., and A. M. Bhatti. 2001. "Preventive Strategies in Chronic Liver Disease: Part II. Cirrhosis." *American Family Physician* 64(10): 1735–40.

Selzner, Markus, Carlos A Camargo, and Pierre-Alain Clavien. 2003. "Ischemia Impairs Liver Regeneration after Major Tissue Loss in Rodents: Protective Effects of Interleukin-6." *Hepatology* 30(2): 469–75.

Sorrentino, Vincenzo, Keir J. Menzies, and Johan Auwerx. 2018. "Repairing Mitochondrial Dysfunction in Disease." *Annual Review of Pharmacology and Toxicology* 58: 353–89.

Teschke, Rolf. 2018. "Alcoholic Liver Disease: Alcohol Metabolism, Cascade of Molecular Mechanisms, Cellular Targets, and Clinical Aspects." *Biomedicines* 6(4).

Trapero-Marugán, María, Ester Coelho Little, and Marina Berenguer. 2018. "Stretching the Boundaries for Liver Transplant in the 21st Century." *The Lancet Gastroenterology and Hepatology* 3(11): 803–11. http://dx.doi.org/10.1016/S2468-1253(18)30213-9.

Vernon, G., A. Baranova, and Z. M. Younossi. 2011. "Systematic Review: The Epidemiology and Natural History of Non-Alcoholic Fatty Liver Disease and Non-Alcoholic Steatohepatitis in Adults." *Alimentary Pharmacology and Therapeutics* 34(3): 274–85.

Xiang, Li, Yaru Shao, and Yuping Chen. 2021. "Mitochondrial Dysfunction and Mitochondrion-Targeted Therapeutics in Liver Diseases." *Journal of Drug Targeting* 29(10): 1080–93. https://doi.org/10.1080/1061186X.2021.1909051.

Yamauchi, Hidemi, and B. 1982. "Postischemic Liver Damage in Rats: Effect of Some Therapeutic Interventions on Survival Rate." *Baca, Ibo Mittmann, Ulrich Geisen, Hans Peter Salzer, Manfred* 138(1): 63–70.

You, Min, and Gavin E. Arteel. 2019. "Effect of Ethanol on Lipid Metabolism." *Journal of Hepatology* 70(2): 237–48. https://doi.org/10.1016/j.jhep.2018.10.037.

Younossi, Zobair M. et al. 2021. "Nonalcoholic Steatohepatitis Is the Most Rapidly Increasing Indication for Liver Transplantation in the United States." *Clin Gastroenterol Hepatol* 19(3): 580–89.

Zhong, Zhi et al. 2014. "Acute Ethanol Causes Hepatic Mitochondrial Depolarization in Mice: Role of Ethanol Metabolism." *PLoS ONE* 9(3).

ABBREVIATIONS

ABBREVIATIONS

AA	=	Amino acids
ABC	=	Drug-effluxing ATP-binding cassette transporters
ABI	=	Anoxic brain injury
ABS	=	Absorbance
AC	=	Alcoholic cirrhosis
ACADL	=	Acyl-Coa Dehydrogenase Long Chain
ACC	=	Acetyl-Coa carboxylases 1 and 2
ADH	=	Alcohol dehydrogenase
ADP	=	Adenosine diphosphate
ADW	=	Alcohol in drinking water
AH	=	Alcoholic hepatitis
AKT	=	AKT serine/threonine kinase
AKT	=	Protein kinase B
ALD	=	Alcoholic liver disease
ALDH	=	Aldehyde dehydrogenase
ALF	=	Acute liver failure
ALR	=	Augmenter of liver regeneration
ALT	=	Alanine aminotransferase
AMPK	=	AMP-activated protein kinase
ANG	=	Angiotensin
ANOVA	=	Analysis of variance
ANRP	=	Abdominal normothermic perfusion
AP-1	=	Activator protein 1
APAP	=	Acetaminophen
APOB100	=	Apolipoprotein B100
ARDS	=	Acute respiratory distress syndrome
ARDS	=	Amphiregulin
ASGPR	=	Asialoglycoprotein receptor
ASH	=	Alcoholic steatohepatitis
AST	=	Aspartate aminotransferase
ATP	=	Adenosine triphosphate
ATP2B	=	ATPase Sarcoplasmic/Endoplasmic Reticulum Ca^{2+} Transporting 2
AUD	=	Alcohol use disorder
BAC	=	Blood alcohol concentrations
BAs	=	Bile acids
BAX	=	Bcl2 associated x, apoptosis regulator
BCL-XL	=	B-cell lymphoma-extra large
BCL2	=	Bcl2 apoptosis regulator
BH	=	Brain hemorrhage
BMM	=	Bone marrow derived macrophages
BP	=	Base pairs

BSA	=	3% BSA in TBST-0.1%
BSA	=	Bovine serum albumin
BUBR1	=	Budding uninhibited by benzimidazole-related1
C/EBP	=	Ccaat-enhancer-binding protein
CA2	=	Cyclin A2
CACL2	=	Calcium chloride
CB1	=	Cyclin B1
CCL	=	C-c motif chemokine ligand
CCL4	=	Carbon tetrachloride
CCR	=	C-c motif chemokine receptor
CD1	=	Cyclin D1
CDCD	=	Controlled donation after circulatory death
CE	=	Cholesteryl esters
CE	=	Cyclin E
CHREBP	=	Carbohydrate response element-binding protein
CI	=	Cold ischemia
CLD	=	Chronic liver disease
CNS	=	Central nervous system
COX1	=	Cyclooxigenase-1
CPT1A	=	Carnitine palmitoyltransferase 1a
CXCL1	=	C-X-C motif chemokine ligand 1
CYP2E1	=	Cytochrome p450 family 2 subfamily e member 1
CYPD	=	Cyclophilin D
DAMP	=	Damage-associated molecular patterns
DBD	=	Donations after brain death
DCD	=	Donations after circulatory death
DEN	=	Diethylnitrosamine
DHE	=	Dihydroethidium
DID	=	Drinking in the Dark
DM	=	Diabetes mellitus
DMD	=	Dystrophin
DMEM	=	Dulbecco's modified eagle medium
DNA	=	Deoxyribonucleic acid
DRP	=	Dynamin-related protein
ECAR	=	Extracellular acidification rate
ECM	=	Extracellular matrix
ECMO	=	Extracorporeal membrane oxygenation
EGF	=	Epidermal growth factor
EGFR	=	Epidermal growth factor receptor
EGTA	=	Egtazic acid
ENOS	=	Endothelial nitric oxide synthase
ER	=	Endoplasmic reticulum
ERK1/2	=	Extracellular signal-regulated kinase 1/2

ETC	=	Electron transport chain
ETOH	=	Ethanol
EV	=	Extracellular vesicles
FA	=	Fatty acids
FADH2	=	Flavin adenine dinucleotide
FAO	=	Fatty acid oxidation
FASN	=	FA synthase
FASN	=	Fatty acid synthase
FAT	=	CD36/FA translocase
FATP	=	FA transport protein
FATP2	=	Fatty acid transport protein 2
FBS	=	Fetal bovine serum
FCCP	=	Carbonyl cyanide 4-trifluoromethoxyphenylhydrazone
FDA	=	United States Food and Drug Administration
FGF-21	=	Fibroblast growth factor
FITC	=	Fluorescein isothiocyanate
FMT	=	Faecal microbiota transfer
FWIT	=	Functional warm ischemic time
FXR	=	Farnesoid X receptor
G-CSF	=	Granulocyte colony-stimulating factor
GADD34	=	Growth arrest and DNA damage-inducible protein
GALNAC	=	N-acetylgalactosamine
GAPDH	=	Glyceraldehyde-3-phosphate dehydrogenase
GLUT2	=	Glucose transporter 2
GM-CSF	=	Granulocyte-macrophage colony-stimulating factor
H_2O_2	=	Hydrogen peroxide
HA	=	Hepatic artery
HAMCJ	=	MCJ overexpressing plasmid
HAMP	=	Hepcidin antimicrobial peptide
HB-EGF	=	Heparin binding EGF like growth factor
HBSS	=	Hanks balanced salt solution
HCC	=	Hepatocellular carcinoma
HCV	=	Hepatitis C virus
HE	=	Hematoxylin and Eosin
HFHFD	=	High fat high fructose diet
HGF	=	Hepatocyte growth factor
HGFR	=	Tyrosine-protein kinase Met / hepatocyte growth factor receptor
HH	=	Hedgehog
HMP	=	Hypothermic machine perfusion
HNE	=	4-hydroxynonenal
HNF-1	=	Hepatocyte nuclear factor-1
HO-1	=	Heme oxygenase 1
HOPE	=	Hypothermic oxygenation perfusion

HRP	=	Horseradish-peroxidase
HSC	=	Hepatic stellate cells
IBD	=	Inflammatory bowel disease
ICU	=	Intensive care unit
ICU	=	Intermittent clamping
IGL-1	=	Institute Georges Lopez -1
IL	=	Interleukin
ILK	=	Integrin-linked kinase
IMM	=	Inner mitochondrial membrane
IPA	=	Ingenuity pathway analysis
IPC	=	Ischemic preconditioning
IPGTT	=	Intraperitoneal glucose tolerance test
IPOSTC	=	Ischemic post conditioning
IRI	=	Ischemia/reperfusion injury
ITBL	=	Ischemic-type biliary lesions
KC	=	Kupffer cells
KLF2	=	Kruppel-like factor 2
KO	=	Knockout
KRB	=	Krebs ringer bicarbonate buffer
LD50	=	50% lethal dose
LDC	=	Lieber-DeCarli diet
LPS	=	Lipopolysaccharide
LR	=	Liver regeneration
LSEC	=	Liver sinusoidal endothelial cells
LT	=	Liver transplantation
MAT1A	=	Methionine adenosyltransferase 1A
MCJ	=	Methylation-controlled J protein
MCJ-KO	=	MCJ-Knock out
MEM	=	Minimum essential medium
MEOS	=	Microsomal ethanol oxidation system
MFN	=	Mitofusin
MG2+	=	Magnesium
MILK	=	5% non-fat milk in TBST-0.1%
MP	=	Machine perfusion pump
MPTP	=	Mitochondrial permeability transition pore
MQC	=	Mitochondrial quality control
MSC	=	Mesenchymal stem cells
MTDNA	=	Mitochondria DNA
MTORC1	=	Mammalian Target of Rapamycin Complex 1
MTROS	=	Mitochondrial ROS
NA	=	Noradrenaline
NAC	=	N-acetylcysteine
NADH	=	Nicotinamide adenine dinucleotide

NAFLD	=	Non-alcoholic fatty liver disease
NET	=	Neutrophil extracellular trap
NFkB	=	Nuclear Factor-kappa B
NIAAA	=	National Institute of Alcohol Abuse and Alcoholism
NMN	=	Nicotinamide mononucleotide
NMP	=	Normothermic machine perfusion
NR	=	Nicotinamide riboside
NRF	=	Nuclear respiratory factor
NRF2	=	Nuclear factor erythroid 2-related factor
O_2^-	=	Superoxide anion
OCR	=	Oxygen consumption rate
OCT	=	Optimal cutting temperature
OMM	=	Outer mitochondrial membrane
OMY	=	Oligomycin
OPA1	=	Optic atrophy 1
OXPHOS	=	Oxidative phosphorylation
PAMP	=	Pathogen-associated molecular patterns
PARP	=	Poly (ADP-ribose) polymerase
PBC	=	Primary biliary cholangitis
PBS	=	Phosphate buffered saline
PCNA	=	Proliferating cell nuclear antigen
PCR	=	Real time quantitative polymerase chain reaction
PETCT	=	Positron Emission Tomography and Computed Tomography
PGC1A	=	Peroxisome proliferator-activated receptor gamma coactivator 1-alpha
PHFL	=	Post-hepatectomy liver failure
PHX	=	Partial hepatectomy
Pi	=	Inorganic phosphate
PINK1	=	PTEN-induced kinase 1
PLCTRL	=	Control plasmid
PNF	=	Primary non-function
PPAR	=	Peroxisome proliferator-activated receptor
PSA	=	Penicillin-streptomycin-amphotericin
PSC	=	Primary sclerosing cholangitis
PV	=	Portal vein
RIPC	=	Remote IPC
RNA	=	Ribonucleic acid
ROS	=	Reactive oxygen species
ROT/AA	=	Rotenone/antimycin
RPM	=	Revolutions per minute
SAH	=	S-Adenosyl-L-homocysteine
SAME	=	S-adenosyl-L-methionine
SCD-1	=	Steryl-coa-desaturase-1
SCS	=	Static cold storage

SDH2	=	Succinate dehydrogenase
SDS-PAGE	=	Sodium dodecyl sulphate-polyacrylamide gel electrophoresis
SEM	=	Standard error of the mean
SER	=	Serine
SFS	=	Superfast surgery
SFSS	=	Small-for-size-syndrome
SIAM	=	Swift Increase in Alcohol Metabolism
SIMCJ	=	MCJ-specific small interfering RNA
SIRNA	=	Small interfering RNA
SIRT1	=	Sirtuin
SREPB1	=	Sterol regulatory element-binding protein 1
STAT3	=	Signal transducer and activator of transcription 3
TBST-0.1%	=	Tris buffered saline 0.1% tween-20
TCA	=	Tricarboxylic acid cycle
TFAM	=	Transcription factor a, mitochondrial
TG	=	Triglycerides
TGF	=	Transforming growth factor
THRE	=	Threonine
TIM4	=	T-cell immunoglobulin and mucin domain molecule-4
TLR	=	Toll-like receptors
TM	=	Thrombomodulin
TNF	=	Tumor necrosis factor
TNFR	=	Tumor nuclear factor receptor
TRAIL	=	TNF-related apoptosis-inducing ligand
TYR	=	Tyrosine
UB	=	Ubiquitin
UC	=	Ulcerative colitis
UPA	=	Urokinase
UPR	=	Unfolded protein response
UW	=	University of Wisconsin
VCAM-1	=	Vascular cell adhesion molecule 1
VDAC	=	Voltage-dependent anion channel
VEGF	=	Vascular endothelial growth factor
VLDL	=	Very low-density lipoproteins
VSOP-NO	=	Venous oxygen persufflation with NO gas
WAT	=	White adipose tissue
WD	=	Western diet
WHO	=	World health organization
WLST	=	Withdraw life-sustaining therapy
WNT	=	Wingless-related integration site
WT	=	Wild type
YAP	=	Yes-associated protein

1. SUMMARY

1 SUMMARY

Mitochondrial dysfunction plays a key role in the initiation and development of chronic liver diseases (CLDs). Because of the great metabolic activity of the liver, hepatocytes have a high density of mitochondria and are therefore susceptible to disorders that affect mitochondrial function. Methylation-controlled J protein (MCJ) is an endogenous negative regulator of mitochondrial complex I. Moreover, markedly elevated MCJ levels have been measured in several chronic liver diseases, suggesting a possible link between MCJ and mitochondrial dysfunction.

The main goal of our group, the Liver Disease Laboratory, is to explore the mechanisms underlying CLDs and to develop novel therapeutic approaches. In the present thesis we have studied alcoholic liver disease (ALD) and limitations in liver transplantation (LT), focusing in particular on mitochondrial dysfunction as the driving force of pathology and on MCJ as a potential therapeutic target.

Excessive alcohol consumption is the leading cause of liver-related mortality in Western countries and represents the second most common indication for LT worldwide. The progression of ALD from alcoholic fatty liver to hepatocellular carcinoma (HCC) is well described, but no therapy exists to halt or even reverse it. Interestingly, mitochondrial dysfunction is one of the earliest indicators of alcohol-related liver injury. Metabolism of high alcohol concentrations leads not only to toxic acetaldehyde, but also to decreased NAD^+/NADH ratio and oxidative stress, altering important metabolic pathways such as beta-oxidation. In addition, patients suffering from alcoholism exhibit significantly reduced metabolic efficiency and lower intracellular ATP content. Thus, MCJ-mediated suppression of mitochondrial respiration may contribute to ALD development.

Moreover, ischemia-reperfusion injury (IRI), the major cause of graft dysfunction after transplantation, and the shortage of donor organs significantly affect current transplantation rates, which meet less than 10% of global demand. The use of extended-criteria livers has been proposed as a strategy to improve the donor pool. Unfortunately, these marginal organs increase the incidence of allograft failure because of elevated susceptibility to ischemic injury and impaired liver regeneration. Liver regeneration is determined by the energy status of the hepatocyte and mitochondrial damage and ATP depletion are characteristic of IRI.

The NIAAA mouse model developed by Bin Gao's research group has been used to study the early stages of ALD. Herein, we demonstrate the implication of MCJ in the pathophysiology of ALD, as the inhibitor is downregulated in patients with early ALD and *in vivo* animal models and overexpressed in patients with advanced ALD. Whole body lack of MCJ is detrimental after alcohol abuse because it exacerbates the systemic effects of alcohol. In this work, we have shown that intestinal macrophages lacking MCJ trigger a proinflammatory cascade that facilitates the translocation of LPS, which aggravates hepatic injury and impairs pancreatic function, leading to hyperglycemia and sudden death of ethanol-fed MCJ-KO mice. Meanwhile, liver specific *Mcj* silencing improves ALD, restoring mitochondrial function, attenuating steatosis, and preventing inflammation and hepatocellular injury.

In addition, we have used three preclinical approaches (70% partial hepatectomy (Phx), prolonged IRI, and Phx under IRI) and liver biopsies from donors after IRI to demonstrate overexpression of MCJ during liver regeneration and ischemic injury. Hepatic *Mcj* silencing promotes regeneration, reduces ischemic injury, and increases survival. Regarding the mechanism, enhanced mitochondrial respiration and ATP production by MCJ knockdown enables mitochondrial adaptation that restores bioenergetic supply for enhanced regeneration and prevents cell death after IRI. Mechanistically, increased ATP secretion facilitates early Kupffer cell activation and production of TNF, IL-6, and HB-EGF, accelerating the priming phase and progression through G1/S during liver regeneration. Interestingly, therapeutic silencing of *Mcj* in 15-month-old mice and in mice fed a high-fat-high-fructose diet for 12 weeks improves mitochondrial respiration, reduces steatosis, and overcomes regenerative limitations.

In conclusion, our results indicate that MCJ contributes to the pathophysiology of ALD and impairs regeneration as well as increases susceptibility to ischemia. We also highlight the need for liver-specific targeted therapies. Finally, liver-specific *Mcj* silencing may be the solution to alleviate the transplant waiting list by restoring extended criteria livers.

2. INTRODUCTION

2 INTRODUCTION

2.1 MITOCHONDRIA

What lies behind "the powerhouse of the cell"? The mitochondria. A key organelle involved in energy production, numerous metabolic processes, cell signaling, and so on. There is a growing interest in the role of mitochondrial dysfunction in the pathogenesis of common chronic diseases, as well as in cancer development. This work focuses on understanding the contribution of mitochondrial dysfunction in alcoholic liver disease (ALD) and liver transplantation (LT) and proposes modulation of mitochondrial bioenergetics as a therapeutic approach to treat ALD and improve the outcomes of LT.

2.1.1. Structure and function of mitochondria

Mitochondria originated from a convoluted alpha-proteobacterium 2 billion years ago. Structurally, they have an inner and an outer membrane enclosing an intermembrane space. The outer mitochondrial membrane (OMM) has multiple porins that mediate material transport, whereas the inner mitochondrial membrane (IMM) has multiple invaginations termed cristae that contain proteins involved in mitochondrial dynamics and the five complexes (I-V) of the electron transport chain (ETC) (J. R. Friedman and Nunnari 2014) (**Fig. 2.1**).

- Complex I: NADH-ubiquinone oxidorreductase is the complex that oxidizes NADH to NAD^+ transferring two electrons to the ubiquinone (Q). Four H^+ simultaneously translocate to the mitochondrial intermembrane space to generate a proton gradient.
- Complex II: Succinate dehydrogenase or SDH complex is a complex involved in the ETC and TCA. In ETC, $FADH_2$ is oxidized to FAD, delivering two extra electrons to Q and with no proton pumping to the intermembrane space.
- Complex III: Ubiquinone-cytocrome-c oxidorreductase complex. It is involved in the reduction of cytochrome c oxidizing the ubiquinol to ubiquinone and contributing to H^+ gradient by the release of four more H^+ to the intermembrane space.

- Complex IV: Cytochrome c oxidase complex is linked to complex III and participates in electron transference from C.III to oxygen, producing water and pumping four H^+ to the intermembrane space.
- Complex V/ATPase/ATP synthase: This complex finally couples the ETC to OXPHOS by using the proton gradient created across the ETC for generating ATP. This complex redrives the previously pumped H^+ into the matrix and uses the produced electrochemical energy created by the gradient to phosphorylate

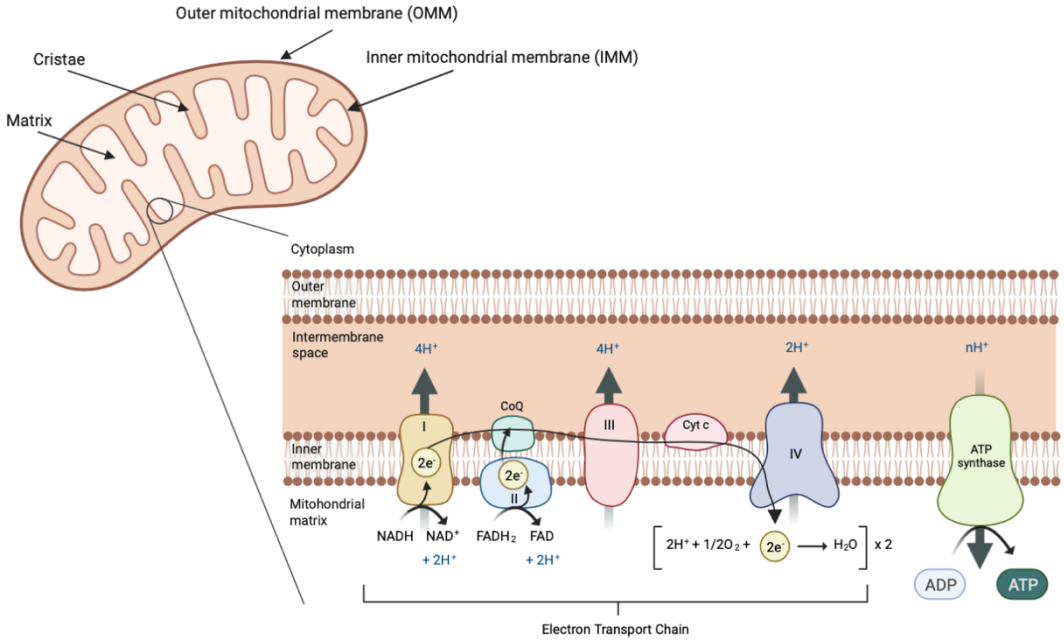

Figure 2.1 Mitochondrial electron transport chain (ETC). The ETC is composed by five complexes that transfer electrons from $FADH_2$ and NADH to the oxygen, which is finally reduced to water. During the process, pumped H^+ from the mitochondrial matrix to the mitochondrial intermembrane space create an electrochemical gradient. Finally, the complex V or adenosine triphosphate (ATP) synthase employs the energy obtained by formed gradient to produce ATP (OMM= Outer mitochondrial membrane; IMM= Inner mitochondrial membrane; NADH= nicotinamide adenine dinucleotide; FADH2= flavin adenine dinucleotide; CoQ= Coenzyme Q; Cyt c= Cytochrome C; ADP= adenosine diphosphate)

These are essential for the main function of mitochondria, which is the production of ATP by oxidative phosphorylation (OXPHOS). In fact, mitochondria provide more than 90% of the ATP for cell growth. Within the IMM is the mitochondrial matrix where vital metabolic processes such as tricarboxylic acid (TCA) occur. Metabolism of energy substrates generates NADH and FADH2, which donate electrons to the ETC. The movement of electrons through the ETC induces the transfer of protons across the inner membrane into the intermembrane space, creating an electrochemical gradient. This proton motivating force is released via ATP synthase (complex V) and drives ATP production. A byproduct of this process is the generation of reactive oxygen species

(ROS), which have cell signaling functions in normal physiology but are harmful in excess (Nunnari and Suomalainen 2012).

Other important mitochondrial functions include maintenance of intracellular Ca2+ homeostasis, redox balance, and control of apoptosis through regulation of mitochondrial membrane permeability (Osellame, Blacker, and Duchen 2012).

2.1.2. Mitochondrial DNA (mtDNA)

Mitochondria retain their own circular genome, which encodes 13 proteins, including subunits of the ETC complexes. Interestingly, mtDNA maintains features of its bacterial heritage and can therefore stimulate immune responses (J. Lee et al. 2020).

2.1.3. Mitochondrial quality control (MQC) mechanisms

Mitochondria own a MQC system to restore normal homeostasis when this organelle results damaged. It includes the regulation of mitochondrial dynamics through fission/fusion, the selective mitophagy-mediated removal of the large irreparable damaged components and the mitochondrial biogenesis for appropriate numbers (Xiang, Shao, and Chen 2021)(**Fig 2.2**).

2.1.3.1. Fission and Fusion

Mitochondria are dynamic organelles that can fuse together and divide to cope with metabolic fluctuations or stress. This allows for coordination of organelle morphology and distribution (Xiang, Shao, and Chen 2021). Mitochondrial fission allows the transport of mitochondria to different cellular locations as well as the isolation of damaged mitochondria to allow mitophagy. This process requires the recruitment of cytoplasmic dynamin-related protein 1 (DRP1) (Liu and Chan 2015). Fusion, on the other hand, enables the transfer of mitochondrial proteins and mitochondrial DNA (mtDNA) and may serve as a repair mechanism. It is mediated by mitofusin 1 and 2 (MFN 1,2), optic atrophy protein 1 (OPA1), and the IMM-specific cardiolipin (Pernas and Scorrano 2016).

2.1.3.2. Mitophagy

Upon irreversible mitochondrial damage, mitophagy enables the removing of local unrepairable mitochondrial units via the phagolysosome. Parkin and PINK1 are the main mediators of this process (Ding and Yin 2012).

2.1.3.3. Mitochondrial biogenesis

Finally, mitochondrial biogenesis involves mitochondrial proliferation and differentiation, which are necessary to maintain the mass and quantity of mitochondria after injury. It is primarily regulated by several transcriptional regulatory factors PGC-1alpha, NRF1/2 and TFAM (Campbell, Kolesar, and Kaufman 2012).

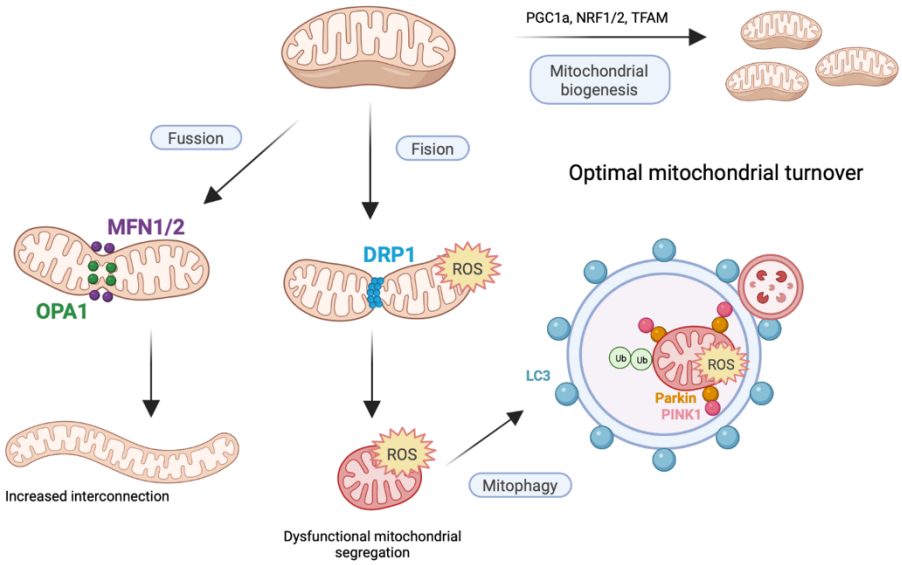

Figure 2.2 Mitochondrial quality control mechanism (MQC). In response to mitochondrial damage, cell commences the MQC mechanism to restore homeostasis. Mitochondrial biogenesis is regulated by several transcription factors, including PGC1a, NRF1/2 and TFAM. Mitochondrial fusion is coordinated by MFN1/2 and OPA1, and DRP1 and its receptors mediate mitochondrial fision. Parkin dependent mitophagy is a common pathway for mitochondial autophagy (PGC1a= peroxisome proliferator-activated receptor gamma coactivator 1-alpha ; NRF1/2= nuclear respiratory factor 1/2 ; TFAM= transcription factor 1, mitochondrial; MFN1/2= mitofusin 1/2 ; OPA1= optic atrophy 1; DRP1= dynamin-related protein 1; PINK1= PTEN-induced kinase 1 ; Ub= ubiquitin; ROS= reactive oxygen species)

2.1.4. Mitochondrial dysfunction and chronic diseases

Changes in mitochondrial function not only affect cellular metabolism, but also have a critical impact on whole-body metabolism, health, and life expectancy. Diseases defined by mitochondrial dysfunction currently include metabolic, cardiovascular,

neurodegenerative, and neuromuscular diseases (Sorrentino, Menzies, and Auwerx 2018). In addition, most liver diseases initially affect hepatic mitochondria, causing oxidative stress (OS), dysregulation of mitochondrial metabolism, ATP synthesis, and mtDNA integrity, Ca^{2+}-compensatory dysfunction and excessive mitochondrial membrane permeability transition pore (mPTP) opening, which together trigger hepatocyte death and release of damage-associated molecular patterns (DAMPs) and exacerbate the pathogenesis and progression of liver disease (Xiang, Shao, and Chen 2021). The underlying mechanisms of mitochondrial dysfunction in ALD and LT will be discussed in more detail in the next chapters, as well as the benefits of a targeted therapeutic approach.

2.2 ALCOHOLIC LIVER DISEASE (ALD)

Chronic liver disease (CLD) encompasses a broad group of liver diseases of various etiologies characterized by slow progression, usually lasting longer than 6 months (up to 20-40 years), and may lead to the development of late stages: Cirrhosis and hepatocellular carcinoma (HCC) (Mishra and Younossi 2012; Riley and Bhatti 2001; Vernon, Baranova, and Younossi 2011). CLDs are a major cause of morbidity and mortality; 29 million people suffer from them in Europe alone, and liver disease is responsible for approximately 2 million deaths per year worldwide (Asrani et al. 2019; Cheemerla and Balakrishnan 2021). Among the various pathologies causing CLDs, viral infections with hepatitis B and C, and alcohol abuse are the most common. Meanwhile, non-alcoholic fatty liver disease (NAFLD), whose prevalence is increasing in many parts of the world, is emerging as a new risk factor (Cheemerla and Balakrishnan 2021). In addition, the global burden of acute and chronic liver disease is expected to increase (Mokdad et al. 2016).

Liver transplantation (LT) is the only curative treatment for acute liver failure and end-stage liver disease. However, current transplantation rates meet less than 10% of global organ transplantation needs (Asrani et al. 2019). These data highlight the window of opportunity to address the increasing prevalence of alcohol abuse and NAFLD and develop new strategies to improve transplantation rates before the global burden of liver disease becomes unsustainable.

Alcohol-related liver disease ALD is one of the most common liver diseases worldwide (Avila et al. 2021a) and a leading cause of morbidity and mortality (Magdaleno, Blajszczak, and Nieto 2017). Globally, alcohol abuse is the most common substance abuse disorder, with approximately 2 million people using alcohol, according to the World Health Organization (WHO) (Asrani et al. 2019) Although usually a preventable cause of death, ALD accounts for up to 60-80% of liver-related mortality in Europe (Benedé-Ubieto et al. 2021) and is the second most common indication for liver transplantation worldwide (LT) (Philippe Mathurin and Lucey 2020). It is a clinical syndrome encompassing a broad spectrum of liver disease, ranging from simple lipid accumulation in hepatocytes (steatosis) to alcoholic steatohepatitis (ASH) characterized by inflammation and fibrosis, with short-term mortality (40-50% at 6 months), to cirrhosis

(Mitra, De, and Chowdhury 2020). Approximately 2% of patients with cirrhosis develop primary HCC (Avila et al. 2021a) (**Fig. 2.3**).

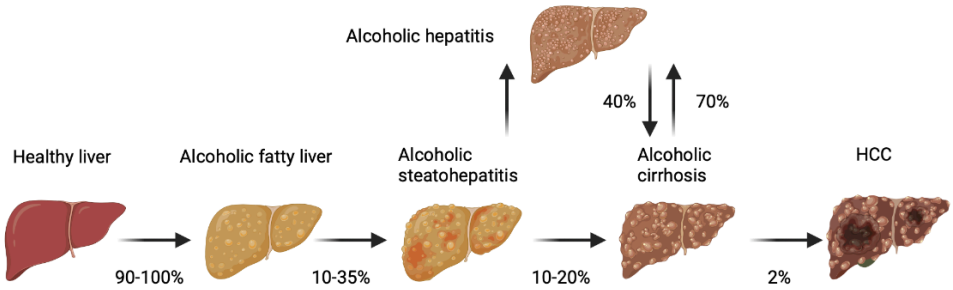

Figure 2.3 Alcoholic liver disease pathogenesis. Most patients develop alcoholic fatty liver disease after chronic alcohol abuse for months or years. Alcoholic steatohepatitis (ASH) develops in up to one third of those who continue to drink heavy alcohol, and alcoholic cirrhosis (AC) develops in up to 20%. Approximately 2% of AC patients progress to primary HCC. Patients with severe ASH, characterized by jaundice and liver failure, may develop alcoholic hepatitis (AH). Those who survive AH, will develop cirrhosis in 70%, and cirrhotic patients may develop acute AH, which has a high mortality rate.

The most common forms of ALD are alcoholic steatosis (ASH), acute and chronic alcoholic hepatitis (AH), and alcoholic cirrhosis (AC), which worsen with chronic alcohol consumption (Magdaleno, Blajszczak, and Nieto 2017). However, it is difficult to determine the true prevalence of ALD due in part to sociocultural factors (Malnick and Maor 2020). Diagnosis relies on individuals' self-report of their alcohol consumption, unlike other liver diseases that can be determined by objective testing. The EASL guideline on NAFLD uses a daily alcohol consumption threshold of 30 g for men and 20 g for women to distinguish ALD from NAFLD (Marchesini et al. 2016). Thus, annual per capita alcohol consumption is used as a marker for disease development (Cheemerla and Balakrishnan 2021). And this marker predicts a bleak future, as alcohol consumption is projected to continue to increase from 5.9 liters in 1990 and 6.5 liters in 2017 to 7.6 liters in 2030. Moreover, in recent years, the interaction with other risk factors that can exacerbate or worsen ALD has been neglected. However, several studies have shown that overweight or obesity in combination with alcohol consumption have an additive effect on the risk of developing ALD and the severity of fibrosis (Avila et al. 2021a). Thus, considering the previous data and adding them to the increasing prevalence of current drinkers and the decline in lifelong abstainers, the burden of ALD will most likely continue to increase and become a global health problem.

Regarding progression of pathology, ALD refers to several symptoms that contribute to liver injury. These include the accumulation of fatty acids (FA), also known as steatosis or alcoholic fatty liver (You and Arteel 2019), the increase in oxidative stress due to the overproduction of reactive oxygen species (ROS) (Ceni, Mello, and Galli 2014), and the activation of immune cells and inflammation, which sequentially or simultaneously lead to significant disease progression toward AH and AC. The pathophysiology of ALD, which is influenced by host and environmental factors, is currently only partially understood (Magdaleno, Blajszczak, and Nieto 2017) and is closely related to the effects of ethanol and its metabolites on the liver and other organs triggered by the effects of alcohol (Teschke 2018a).

Moreover, there is a lack of therapy that could halt and even reverse ALD (You and Arteel 2019). Currently, permanent abstinence in early stages and liver transplantation in more advanced stages are the only options for ALD patients (Teschke 2018a), as there is no evidence to reverse cirrhosis at ALD (Louvet and Mathurin 2015). Unfortunately, access to LT for these patients remains marginal, with fewer than 5-10% of potential ALD candidates estimated to be selected, as they rarely meet the mandatory 6-month abstinence criteria when hospitalized for decompensation and their risk of relapse remains high (Philippe Mathurin and Lucey 2020). Therefore, a better understanding of the mechanisms mediating onset and progression of this disease is critical for the development of targeted therapy for treatment or prevention. These mechanisms are described in the next sections

2.2.1 Alcohol metabolism

As mentioned earlier, the pathogenesis of ALD is still not well understood, but it is closely related to ethanol metabolism. In recent decades, significant progress has been made in understanding the molecular mechanisms by which oxidative ethanol metabolism contributes to the progression of ALD (Ceni, Mello, and Galli 2014). Briefly, the oxidation of ethanol to acetate is a two-step process carried out by the enzymes alcohol dehydrogenase (ADH) and aldehyde dehydrogenase (ALDH) (**Fig. 2.4**)

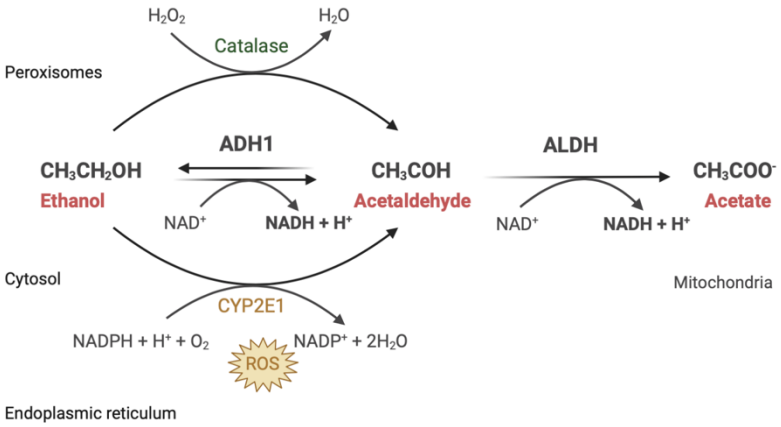

Figure 2.4 Alcohol metabolism. Alcohol dehydrogenase (ADH1) is the main cytosolic enzyme that converts alcohol to acetaldehyde. Toxic acetaldehyde is then further oxidized to acetate by aldehyde dehydrogenase (ALDH) in the mitochondrial matrix. Both enzymes use NAD^+ as a cofactor, leading to increased NADH production. Catalase, in the peroxisome, and the inducible microsomal enzyme (MEOS and CYP2E1), in the endoplasmic reticulum, also oxidize ethanol to acetaldehyde, with increased reactive oxygen species (ROS) due to the latter (MEOS= microsomal ethanol oxidation system; CYP2E1= cytochrome P450 2E1)

ADH catalyzes the first step of ethanol metabolism, it allows the oxidation of ethanol to acetaldehyde using NAD + as a cofactor. ADH is a family of cytosolic enzymes found mainly in the liver but also in the gastrointestinal tract, and of the various isozymes, ADH1 plays the major role in the metabolism of ethanol in the liver (Crabb 1995; Jian et al. 2020). Acetaldehyde is then further oxidized to acetate by ALDH in the mitochondrial matrix, also using NAD + as a cofactor. The rate of this reaction is sufficiently slow to allow accumulation, and an increase in acetaldehyde is usually seen in people who consume alcohol (Ramaiah, Rivera, and Arteel 2004). Indeed, many systemic toxic effects of ethanol abuse are thought to be mediated by the direct or indirect effects of elevated blood acetaldehyde levels (Biewald, Nilius, and Langner 1998; Charles S. Lieber 2004; Tuma 2002).

Metabolism of high alcohol concentrations also leads to accumulation of nicotinamide adenine dinucleotide (NADH) and the consequent decrease in the NAD +/NADH ratio, which significantly affects mitochondrial activity and key biochemical pathways (Ceni, Mello, and Galli 2014; Charles S. Lieber 2004; Ramaiah, Rivera, and Arteel 2004; You and Arteel 2019).

Two other systems can lead to ethanol oxidation: catalase, whose levels in the liver are negligible (Cederbaum 2012), and the microsomal ethanol oxidation system (MEOS), which relies on cytochromes P450 (CYP), particularly ethanol-inducible CYP2E1. Under

physiological conditions, only a small amount of ethanol, about 10%, is oxidized to acetaldehyde by CYP2E1, but chronic alcohol abuse results in induction of the MEOS system and CYP2E1 protein expression (Charles S. Lieber 1997). Unfortunately, the catalytic reaction of CYP2E1 generates a considerable amount of ROS, contributing to the oxidative stress caused by alcohol (Lu and Cederbaum 2008).

Therefore, ethanol oxidative metabolism results in toxic acetaldehyde accumulation, altered redox balance due to decreased NAD^+/NADH ratio and oxidative stress caused by ROS overproduction. All these directly affect the mitochondrial function (Chandramouleeswaran et al. 2020; Charles S. Lieber et al. 2008; Z. Zhong et al. 2014).

2.2.1.1 Swift Increase in Alcohol Metabolism (SIAM)

Following the use of alcohol, hepatic respiration increases, and ethanol oxidation nearly doubles (Lemasters and Holmuhamedov 2006). This phenomenon is named Swift Increase in Alcohol Metabolism (SIAM) (Bradford and Rusyn 2005; Thurman et al. 1982). A single inebriating dose of ethanol is sufficient to stimulate the respiratory burst, which may be an adaptive response to oxidize toxic acetaldehyde more rapidly and to increase oxidation of NADH to NAD^+ supply for ADH-dependent alcohol metabolism (Z. Zhong et al. 2014).

On the one hand, acetaldehyde has an electrophilic nature, what enables its binding and formation of covalent chemical adducts with proteins, lipids and DNA (Freeman et al. 2005; Heymann, Gardner, and Gross 2018). These adducts are broadly pathogenic because they alter cell homeostasis by changing protein structure and promoting DNA damage and mutations (Charles S. Lieber 2004), which contributes to ethanol toxicity in organs. As the major site of acetaldehyde degradation, mitochondria are the first organelle to suffer from its toxic effects (Chandramouleeswaran et al. 2020). Thus, following ethanol consumption, mitochondria undergo SIAM in order to increase its acetaldehyde breakdown capacity. On the other hand, in the process of metabolizing ethanol to acetate through ADH and ALDH, 2 equivalents of reduced NADH are generated per equivalent of ethanol oxidized (You and Arteel 2019). Thus, ethanol oxidation requires cofactor supply in the form of NAD^+, which mitochondria provide through enhanced oxidation of NADH, by undergoing SIAM.

Selective stimulation of mitochondrial metabolism in the liver occurs by mechanisms that are not fully understood (Lemasters and Holmuhamedov 2006). Although increased mitochondrial respiration should theoretically increase adenosine triphosphate (ATP) formation through oxidative phosphorylation, alcohol treatment actually decreases ATP levels in the liver. Indeed, the increased oxygen consumption during SIAM is mediated by reversible uncoupling of hepatocellular mitochondria (Lemasters and Holmuhamedov 2006; Z. Zhong et al. 2014). Moreover, the voltage-dependent anion channel (VDAC) plays a key role in this phenomenon (Lemasters and Holmuhamedov 2006). VDAC is responsible for the permeability of the mitochondrial outer membrane to hydrophilic metabolites such as ATP, ADP, fatty acyl-CoA, and various respiratory substrates. Acetaldehyde, on the other hand, is an uncharged molecule that readily crosses mitochondrial membranes without requiring VDAC. Importantly, increased NADH production during ethanol metabolism inhibits VDAC conductance (Z. Zhong et al. 2014). Therefore, mitochondrial uncoupling combined with VDAC closure promotes faster and more selective oxidation of acetaldehyde by mitochondrial ALDH.

The molecular mechanisms underlying ethanol-induced mitochondrial uncoupling *in vivo* remain to be determined. Ethanol metabolism and altered redox balance are required for mitochondrial depolarization, and ADH plays a greater role than MEOS in causing this phenomenon (Z. Zhong et al. 2014). The finding that 3-methylpyrazole, an ADH inhibitor, strongly blocks the respiratory burst triggered by ethanol supports this idea (Thurman, McKenna, and McCaffrey 1976). In addition, Zhong et al. observed that ALDH activation decreased mitochondrial depolarization, suggesting that acetaldehyde most likely plays an important role in ethanol-induced mitochondrial depolarization. New studies aim to understand the relationship between oxidative stress and mitochondrial depolarization *in vivo*.

2.2.2 Mitochondrial dysfunction

One of the earliest manifestations of hepatocyte injury by alcohol is morphological and functional changes of mitochondria (Ishak, Zimmerman, and Ray 1991; Z. Zhong et al. 2014). Certainly, increased energy expenditure and decreased metabolic efficiency have

long been noted in human drinkers (Levine, Harris, and Morgan 2000; P. M. Suter, Jéquier, and Schutz 1994).

2.2.2.1 Maladaptive SIAM

Chronic ethanol abuse turns SIAM into a maladaptive mechanism consistent with a reduction in overall metabolic efficiency, as reported in ALD patients (Levine, Harris, and Morgan 2000; P. Suter, Jequier, and Schutz 1994), impairing ATP production and increasing liver vulnerability to injury (**Fig. 2.5**).

First, chronic ethanol consumption is found to decrease the expression and activity of mitochondrial complex I, III, IV and ATP synthase (Middleton and Vergis 2021), pushing mitochondrial respiration to its limits as its clearance capacity is overwhelmed. The impaired oxidative capacity of mitochondria interferes with the oxidation of acetaldehyde, initiating a vicious cycle of progressive acetaldehyde accumulation and greater mitochondrial damage (Hasumura, Teschke, and Lieber 1975). Since mitochondria can no longer oxidize acetaldehyde rapidly enough, its accumulation favors the formation of protein adducts in the organelle, with subsequent deleterious effects on mtDNA and the enzymes that catalyze important metabolic pathways (Andringa et al. 2010).

When the oxidative capacity of mitochondria is overwhelmed and impaired due to chronic ethanol abuse, the redox balance is also altered. The overproduction of reducing equivalents from ethanol oxidation and the reduced mitochondrial capacity to regenerate NAD^+ shifts the NAD^+/NADH ratio toward a reduced state. The altered redox balance also has significant effects on metabolism (Ceni, Mello, and Galli 2014). This shift in the pyridine nucleotide redox state has been shown to impair normal carbohydrate and lipid metabolism, which not only reduces ATP supply to cells but also reduces the ability to oxidize fatty acids and leads to rapid accumulation of lipids in hepatocytes (Ramaiah, Rivera, and Arteel 2004). As mentioned earlier, VDAC closure is mediated by increased NADH levels. Indeed, VDAC inhibition alone would suppress mitochondrial uptake of ADP and Pi for ATP synthesis and release, decrease the cytosolic ATP/ADP ratio, and stimulate glycolysis and glycogenolysis. Similarly, VDAC closure, by inhibiting fatty acyl-CoA access to the acylcarnitine shuttle, blocks beta-oxidation and promotes FA

accumulation, which promotes alcoholic fatty liver disease (Lemasters and Holmuhamedov 2006), discussed in detail below.

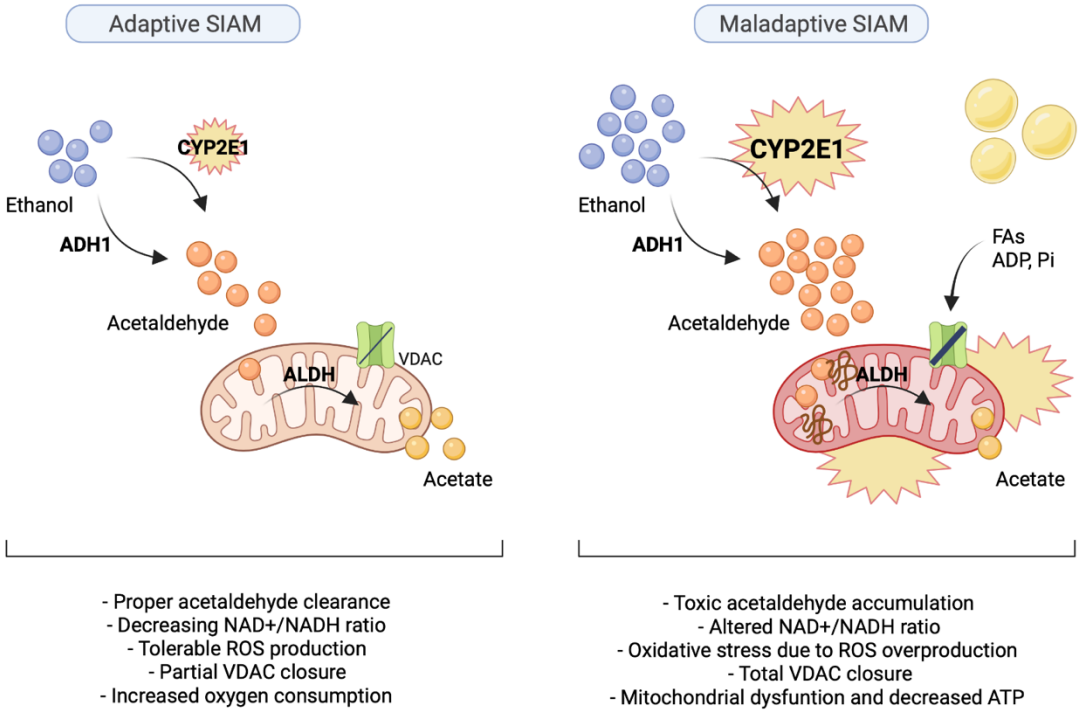

Figure 2.5 Swift Increase in Alcohol Metabolism (SIAM). Following the use of alcohol, mitochondria augment their oxygen consumption, as an adaptive response to oxidize the toxic acetaldehyde faster, and to increase NAD^+ supply both for alcohol metabolism and to restore hepatic metabolism. However, chronic ethanol abuse turns SIAM into a maldaptive mechanism, consistent with a decrease in overall metabolic efficiency as reported in ALD patients, impairing ATP produciton and ehancing hepatic susceptibility to injury (ADH1= alcohol dehydrogenase 1; CYP2E1= cytochrome P450 2E1; ALDH= aldehyde dehydrogenase; VDAC= voltage-dependent anion channel; FAs= fatty acids; ADP= adenosine diphosphate; Pi= inorganic phosphate)

Finally, mitochondrial exhaustion and metabolic alterations are accompanied by ROS overproduction. Besides the oxidative stress generated by ethanol metabolism, mainly hydrogen peroxide (H_2O_2) and superoxide anion (O_2^-) due to the overactivation of the MEOS system and CYP2E1 (Lu and Cederbaum 2008), mitochondria are the other main source for ROS in ALD, through the proton leak in the oversaturated respiratory chain (Louvet and Mathurin 2015). Once generated, these free radicals interact with the polyunsaturated fatty acids found in membranes throughout the cell and its components, generating lipid peroxidation end-products and protein adducts. The cytotoxic effect of oxidative stress leads to cell death and significant liver damage (Luedde, Kaplowitz, and Schwabe 2014).

On top of that, a decrease in the antioxidant defense also characterizes ALD patients (Charles S. Lieber 2001). As alcoholics often replace up to 50% of their total daily calories with ethanol, this leads to nutritional deficiencies, also complicated by malabsorption in the gastrointestinal tract (Ramaiah, Rivera, and Arteel 2004). The combined result is that alcoholics often have lower levels of dietary antioxidant molecules and overall impaired antioxidant system (Charles S. Lieber 2001). In fact, chronic exposure to ethanol induces glutathione depletion, which makes hepatocytes more sensitive to oxidative stress, as reduced glutathione protects cells against ROS (Louvet and Mathurin 2015).

Altogether, SIAM is the way ethanol stimulates a selective mitochondrial oxidation of acetaldehyde but at the same time causes relatively global suppression of other mitochondrial activities, especially fatty acid oxidation, and increases the production of ROS.

2.2.2.2 Altered mitochondrial structure and dynamics

Chronic ethanol exposure is also associated with structural abnormalities of mitochondria leading to changes in mitochondrial dynamics. Acetaldehyde accumulation, protein adducts, and ROS are responsible for mitochondrial swelling and impaired cristae formation in rat and mouse ALD models (Yan et al. 2007). In addition, prolonged alcohol consumption leads to the development of large mitochondria, known as megamitochondria, by downregulating the activation of mitochondrial fission protein Drp1. This has been shown to be a beneficial adaptive response with reduced hepatotoxicity. Megamitochondria detected in human liver biopsies from patients with AH are associated with less severe liver dysfunction and better survival (Chedid et al. 1986).

2.2.2.3 Disrupted calcium homeostasis

The role of mitochondria in calcium homeostasis is also affected by alcohol. Chronic consumption has been found to increase mitochondrial calcium concentrations (Yan et al. 2007). In ALD rat models, increased mitochondrial calcium uniporter (MCU) expression was observed, which was accompanied by increased mitochondrial calcium uptake,

mitochondrial ROS production and decreased NAD^+/NADH ratio, resulting in overall increased mitochondrial ROS (mtROS) and altered metabolic pathways (Middleton and Vergis 2021).

Furthermore, a hallmark of mitochondrial dysfunction is the excessive opening of the mitochondrial permeability transition pore (mPTP); a nonselective voltage-dependent mitochondrial channel is formed by IMM proteins upon failure of MQC mechanisms or Ca^{2+} overload. Opening of the pore allows mitochondrial IMM permeation for molecules including protons, cytochrome C, Ca^{2+} and ROS and leads to proapoptotic events such as loss of the protonmotive force, decreased ATP production, mitochondrial swelling, and rupture of the OMM (Panel, Ghaleh, and Morin 2018). In addition, sustained opening of mPTP mediates mitochondrial calcium release, which enhances ER stress (Y. Zheng et al. 2019).

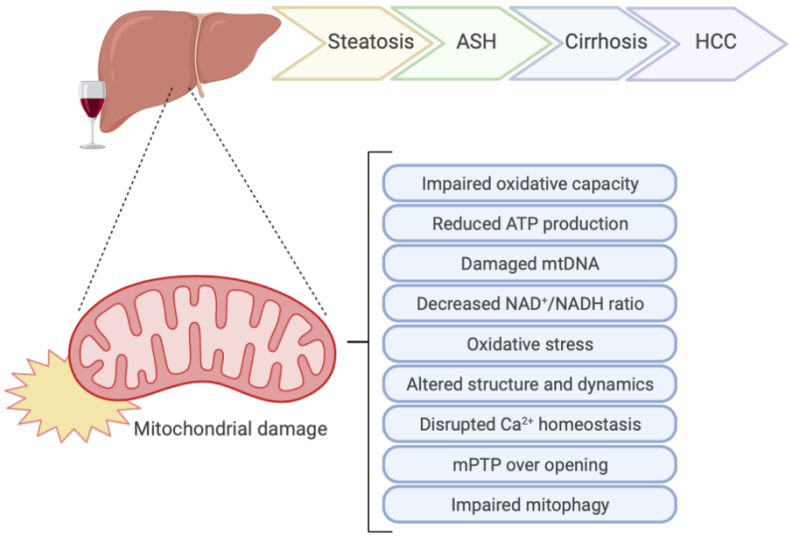

Figure 2.6 Mitochondrial damage in alcoholic liver disease (ALD). Mitochondrial deregulation promotes the pathological development of liver disease (ASH= alcoholic steatohepatitis; HCC= hepatocellular carcinoma; ATP= adenosine triphosphate; mtDNA= mitchondrial DNA; NADH= nicotinamide adenine dinucleotide; mPTP= mitochondrial permeability transition pore)

2.2.2.4 *Impaired mitophagy*

As explained earlier, mitochondrial damage is repaired by mitochondrial fusion or by mitophagy. Alcohol consumption has been shown to inhibit mitophagy in mice, which enhances alcohol-induced steatosis, fibrosis, and mitochondria-associated apoptosis (H. Zhou et al. 2019).

Overall, mitochondrial dysfunction in ALD leads to inhibition of acetaldehyde metabolism and its subsequent deleterious accumulation, increased hepatocyte apoptosis, and liver inflammation. All of these promote the progression of ALD. Therefore, targeting mitochondrial dysfunction, which is an early indicator of alcohol-related liver injury, could halt progression to fibrosis, cirrhosis, and end-stage liver disease.

2.2.3 Pathogenesis of ALD

ALD is the result of a cascade of events that clinically lead first to alcoholic fatty liver and then, usually via alcoholic steatohepatitis, potentially to cirrhosis and HCC (Ramaiah, Rivera, and Arteel 2004; Teschke 2018a). Moreover, patients with underlying cirrhosis and ongoing alcohol abuse are predisposed to developing alcoholic hepatitis (Philippe Mathurin and Bataller 2015). In the next section the most common forms of ALD will be explained, highlighting the biochemical mechanisms that mediate the initiation, perpetuation, and progression of liver injury.

2.2.3.1 Alcoholic Fatty Liver or Alcoholic Steatosis

Steatosis is the abnormal accumulation of FAs in hepatocytes in the form of lipid droplets. In normal lipid metabolism, hepatic free FAs are both synthesized by the liver from glycolytic end products and hepatic catabolism, or actively taken up by the liver from extrahepatic sources. These can be either oxidized for fuel at the mitochondria, used for membrane synthesis or esterified intro triglycerides (TGs). TGs are subsequently packaged as very low-density lipoproteins (VLDLs) that can be secreted into the bloodstream (Bradbury 2006), for use or storage by the peripheral organs. There is an intricate crosstalk between these systems and the dysregulation of the fluxes can cause lipids to accumulate in hepatocyte, leading to steatosis (You and Arteel 2019).

Ethanol alters almost all aspects of hepatic lipid metabolism. Indeed, steatosis is a rapid metabolic response to alcohol abuse, with a prevalence of essentially 100% in those who consume harmful levels of alcohol (Gao and Bataller 2011; Ishak, Zimmerman, and Ray 1991; Magdaleno, Blajszczak, and Nieto 2017; Ramaiah, Rivera, and Arteel 2004). This

is the result of disturbances related to FA uptake, synthesis, oxidation, and export, that disrupt the homeostasis between the processes involved in the increase and decrease of hepatic FA (Charles S. Lieber 1994). Although alcohol induced steatosis is rapidly and readily reversible upon cessation of alcohol consumption, hepatic fat accumulation can invoke metabolic chances that sensitize the liver to further injury (You and Arteel 2019). Thus, understanding the underlying mechanisms of how alcohol induces steatosis could be key in preventing progression to late stages of ALD.

2.2.3.1.1 Effects of ethanol mobilization of fatty acids from adipose tissue

Intrahepatic FA content can increase because of an excess of free FAs supply from the white adipose tissue (WAT), the major source of FAs in the body. Under specific circumstances, TGs contained in the adipose tissue are hydrolyzed releasing free FAs delivered directly to the liver instead of been up taken by other tissues. However, excess FA release from the WAT may cause FA over flux into the liver, leading to development of fatty liver (Wei et al. 2013). Clinical studies have demonstrated that lower fat mass is associated with higher liver fat in alcoholics (W. Zhong et al. 2012). Indeed, alcohol exposure has been found to stimulate adipose lipolysis and FA release from WAT, an event known as reverse triglyceride transport (Wei et al. 2013).

2.2.3.1.2 Effects of ethanol on fatty acid transporters

Circulating FAs are taken up directly by the liver and are the major source for triglyceride synthesis. This process is mediated by FA transporters, CD36/FA translocase (FAT) and FA transport protein (FATP), and FA binding proteins (He et al. 2011). Ethanol exposure increases hepatic uptake of exogenous FAs by upregulating hepatic levels of CD36/FAT, FATP1 and FATP5 (S. L. Zhou et al. 1998). Indeed, suppression of hepatic CD36/FAT expression has been shown to alleviate steatosis and ameliorate experimental alcoholic steatohepatitis, underscoring the involvement of FA transporters in the pathogenesis of ALD (You and Arteel 2019).

2.2.3.1.3 Effects of ethanol on FA and triglyceride synthesis

As previously mentioned, the liver generates FAs from non-lipid precursors via *de novo* lipogenesis, a process regulated mainly by insulin and glucose flux in the liver, which

serves to store a source of energy for periods of fasting. Briefly, pyruvate from glycolysis enters the citric acid cycle (TCA) and is converted to citrate, which is then converted to acetyl- and malonyl-CoA and used to synthesize FAs. Rate limiting enzymes in *de novo* lipogenesis include acetyl-CoA carboxylases 1 and 2 (ACC-1 and -2, which convert acetyl-CoA to malonyl-CoA), FA synthase (FASN, synthesize saturated FAs from malonyl-CoA), and steryl-CoA-desaturase-1 (SCD-1 which converts saturated FAs to monounsaturated FAs) (**Fig. 2.7**).

The net effect of ethanol is to activate *de novo* lipogenesis, while concomitantly inhibiting processes that block this response. And although some of this effect results from the direct action of ethanol or acetaldehyde on the aforementioned lipogenic genes, it is primarily mediated by transcriptional regulation. The most potent inducers of these genes are the transcription factors sterol regulatory element-binding protein 1c (SREPB-1c) (Shimano et al. 1997) and carbohydrate response element-binding protein (ChREBP) (Yamashita et al. 2001). Under normal conditions lipogenesis is induced after the intake of nutrients and downregulated during fasting, as insulin and glucose or citrate are the activators of SREBP-1c and ChREBP, respectively, and glucagon the inhibitor.

Alcohol consumption may activate processes that stimulate the expression of these transcription factors and down-regulate the elements that reduce their expression (Gao and Bataller 2011) .

Activators of *de novo* lipogenesis

a. Endoplasmic reticulum (ER) stress

The endoplasmic reticulum (ER) is involved in the proper folding and assembly of secreted and membrane proteins, and the homeostasis between the protein load and the capacity of ER to process it must be maintained to ensure proper protein folding. When this homeostasis is disrupted, misfolded or unfolded proteins accumulate, leading to ER stress (Xia et al. 2020). In attempts to reestablish homeostasis, the ER activates a signaling network known as the unfolded protein response (UPR), which affects *de novo* lipogenesis, as one downstream effect of UPR activation is the insulin-independent proteolytic activation of SREBP-1c. Several studies have shown that alcohol induces ER stress in the liver (Kaplowitz and Ji 2006).

b. Tumor Necrosis Factor (TNF)

Both basal and lipopolysaccharide (LPS)-stimulated production of TNF are increased in humans consuming alcohol (H. J. Wang, Zakhari, and Jung 2010). Along with the pro-inflammatory role of TNF, this cytokine increases free FAs release from adipocytes, d*e novo* lipogenesis in hepatocytes by transcriptional activation of SREBP-1c and slows fat metabolism by mitochondria, as inhibits b-oxidation (Hardardottir et al. 1992; Lawler et al. 1998; Nachiappan et al. 1994).

Inhibitors of *de novo* lipogenesis

a. AMPK

The AMP-activated protein kinase (AMPK) acts as a "sensor" of cellular energy status and helps to maintain homeostasis. Briefly, the downstream effects of AMPK activation are considered catabolic and favor ATP generation during energy depletion. It also inhibits ATP-consuming processes, such as *de novo* lipogenesis (R. Ren et al. 2020). AMPK is a serine-threonine kinase that can phosphorylate and inactivate ACC, a rate-limiting enzyme for FA synthesis. In addition, AMPK directly phosphorylates and inhibits SREBP-1c activity in hepatocytes, attenuating steatosis (Gao and Bataller 2011). Thus, AMPK inhibits FA synthesis but promotes FA oxidation. However, alcohol consumption inhibits AMPK activity and its downstream effects, thereby disinhibiting *de novo* lipogenesis (You and Arteel 2019).

b. Sirtuin 1

Sirtuin 1 (SIRT1) is an NAD^+ dependent protein deacetylase. Targets of its deacetylase activity include several key players in SREBP-1c and ChREBP-1 signaling. Early studies already reported that ethanol exposure reduces SIRT1 expression levels, and ultimately inhibits SIRT1 deacetylase activity in the liver, due to the altered NAD^+/NADH ratio (R. Ren et al. 2020).

c. Adiponectin

Adiponectin is an adipose-derived hormone that circulates in the plasma and a pivotal player in the regulation of lipid metabolism. Indeed, adiponectin inhibits lipid synthesis and stimulates FA oxidation in part by activating SIRT1, AMPK1, PGC1-alpha and PPARalpha, and suppressing SREBP-1 (You and Rogers 2009). Ethanol abuse has been

seen to hamper the production of adipokines by the adipose tissue and downregulate hepatic adiponectin receptors (W. Zhong et al. 2012).

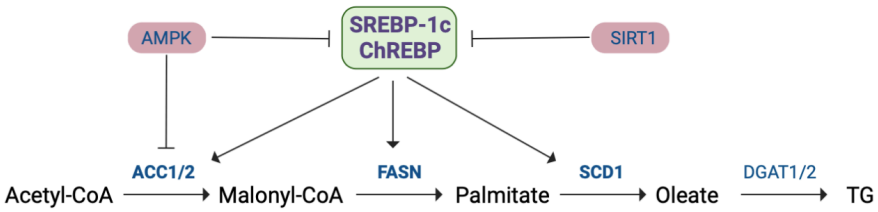

Figure 2.7 Effect of alcohol on *de novo* lipogenesis. The principal steps implicated in triglyceride (TG) synthesis from acetyl-CoA. SREBP-1c and ChREBP, transcription factors (TFs) that regulate the expression of different enzymes implicated in determined steps of lipogenesis. This process is enhanced in ALD, as alcohol upregulates the levels of TFs (in green) and downregulates the main inhibitors of *de novo* lipogenesis: AMPK and SIRT1 (in red) (ALD= alcoholic liver disease; AMPK= AMP-activated protein kinase; SREPB-1c= sterol regulatory element-binding protein 1c; ChREBP= carbohydrate response element-binding protein; SIRT1= sirtuin1; ACC1/2= acetyl-CoA carboxylase 1/2 ; FASN= fatty acid synthase; SCD1= steryl-CoA-desaturase-1; DGAT1/2= diglyceride acyltransferase)

2.2.3.1.4 Effects of ethanol on mitochondrial b-oxidation

Free FAs are catabolized through mitochondrial b-oxidation or fatty acid oxidation (FAO) in a series of steps that produce energy in form of ATP and ketone bodies. FAs need to be activated into acyl-CoA and translocated by carnitine palmitoyl transferase (CPT) into mitochondria, where they undergo cycles of four sequential reactions until they are converted into acetyl-CoA. At this point, acetyl-CoA can either enter the TCA cycle for ATP production or be used as ketogenic substrate in extrahepatic tissues.

Despite the net increase in the supply of FAs for b-oxidation, there is no apparent induction of b-oxidation genes during alcohol exposure. The major mechanism of action underlying this effect is hypothesizes to be the inactivation of peroxisome proliferator-activated receptor (PPAR)-alpha, a nuclear hormone receptor that controls transcription of a range of genes involved in free FA transport and oxidation. The toxic metabolite acetaldehyde, but not ethanol itself, directly inhibits the transcriptional activity and DNA-binding ability of PPAR-alpha in hepatocytes (Gao and Bataller 2011).

Moreover, ethanol also inhibits b-oxidation activity. Firstly, the decreased NAD^+/NADH ratio caused by alcohol metabolism directly inhibits mitochondrial b-oxidation, mainly mediated by the NAD^+ reducing enzyme, 3-hydroxy-CoA dehydrogenase, the final step

in generating acetyl-CoA during b-oxidation. Furthermore, increased ACC activity, due to impaired AMPK activity, inhibits CPT1 activity through augmented malonyl-CoA (You and Arteel 2019). As previously mentioned, VDAC closure impairs the entrance of FAs to mitochondria for b-oxidation (Lemasters and Holmuhamedov 2006). Finally, ethanol exposure, its toxic metabolite and oxidative stress hamper mitochondrial respiration, what directly impacts the ability of the organelle to oxidize free FAs. The fact that long-term alcohol consumption inhibits autophagy likely exacerbates the latter (Gao and Bataller 2011).

2.2.3.1.5 Effects of ethanol on VLDL export

Excess FAs are conjugated in the liver to TGs, which can be stored in the hepatocyte or released into the bloodstream in the form of VLDLs for delivery to peripheral tissues. VLDLs are macromolecular complexes composed mainly of TGs and cholesterol esters (CE) surrounded by phospholipids and unesterified cholesterol and stabilized by a molecule of apolipoprotein B100 (ApoB100) (Venkatesan, Ward, and Peters 1988). Studies have observed that hepatic secretion of VLDLs is significantly impaired after alcohol abuse (Kharbanda et al. 2009; Venkatesan, Ward, and Peters 1988; Wei et al. 2013).

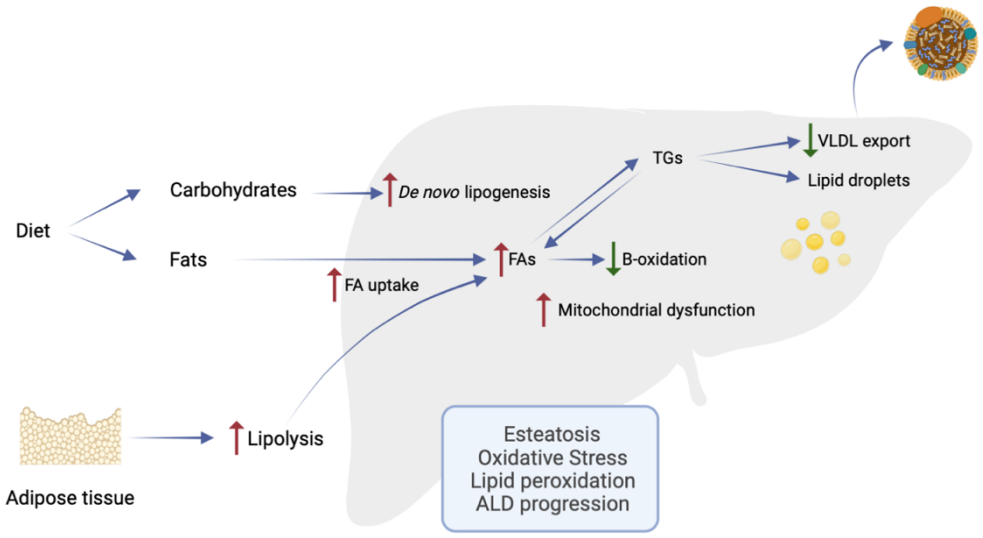

Figure 2.8 Altered pathways in alcoholic steatosis. Steatosis is a rapid metabolic response to alcohol abuse, as ethanol alters almost all aspects of hepatic lipid metabolism. Alcohol augments lipolysis in the adipose tissue, increasing the circulating fat content. Besides, also increases fatty acid (FA) uptake, enhances *de novo* lipogenesis, decreases mitochondrial beta oxidation, and impairs the VLDL secretion. Mitochondrial dysfunction leads to oxidative stress, that together with FA accumulation, cause lipid peroxidation, what promotes hepatocellular injury and the progression of the disease towards ASH and AH (TGs= triglycerides; VLDL= very low-density lipoproteins; ALD= alcoholic liver disease; ASH= alcoholic steatohepatitis; AH= alcoholic hepatitis)

Overall, ethanol affects almost all aspects of hepatic lipid homeostasis (**Fig. 2.8**), as mentioned previously. Although alcohol induces hepatic influx and de novo synthesis of FAs, fatty liver should not develop if the liver can efficiently metabolize and/or excrete TGs into the blood. Therefore, impaired mitochondrial function and VLDL secretion should coexist with hepatic fatty acid influx and fatty acid synthesis in the development of alcoholic steatosis. Because alcoholic steatosis is rapidly reversible, it provides an opportunity for therapeutic intervention to prevent progression of ALD because the degree of steatosis is an early predictor of overall disease severity (Day and James 1998).

2.2.3.2 Alcoholic Fibrosis (AF) and Alcoholic Cirrhosis (AC)

Up to one-third of individuals who continue heavy alcohol use develop ASH (Avila et al. 2021a). ASH and AH are not easily distinguished; however, a clear distinction is necessary because the two have different natural clinical courses and treatment options (Teschke 2018b). ASH A mild stage of ALD, characterized by steatosis and hepatitis, has a good clinical course. AH In contrast, ALD, a severe stage, has marked hepatocellular necrosis, apoptosis, and inflammation and is considered a life-threatening disease. With a mortality rate of 30-50% after 3 months (Philippe Mathurin and Bataller 2015) due to jaundice, hepatic failure, and hepatic encephalopathy, AH represents one of the most lethal diseases in clinical hepatology (Teschke 2018a).

Determining physiopathological details and specific molecular mechanisms driving ASH and AH is complicated because ALD is usually diagnosed at late stages, making adequate characterization of pathogenesis difficult, and because animal models representing human ASH and AH are lacking (Teschke 2018b).

Priming and sensitization are key concepts in alcohol-induced liver injury. Ethanol metabolism and acetaldehyde toxicity generate ROS, causing lipid peroxidation, mitochondrial dysfunction, and glutathione depletion, which subsequently activate and sensitize hepatocytes to further injury (Gao and Bataller 2011). ALD is characterized by chronic inflammation; indeed, continued heavy alcohol consumption leads to infiltration of polymorphonuclear cells and hepatocellular damage (Farooq and Bataller 2016). The presence of fat accumulation in the liver seems to be a prerequisite for the development

of the disease, possibly because a steatotic liver is more susceptible to various factors that trigger inflammation (Ramaiah, Rivera, and Arteel 2004).

After alcohol abuse, bacterial overgrowth of the gut, changes in the composition of the microbiota, and increased gut permeability cause pathogen-associated molecular patterns (PAMPs) such as LPS and bacterial DNA to migrate from the gut to the liver. This ultimately leads to the elevated LPS levels observed in patients with ALD (Fairfield and Schnabl 2021). PAMPs are then sensed by various receptors and activate pro-inflammatory innate immune activation pathways, contributing to hepatocyte damage and the release of damage-associated molecular patterns (DAMPs). Several Toll-like receptors (TLRs) are involved in the recognition of PAMPs and DAMPs, which form an amplification loop to increase pro-inflammatory cytokine production and enhance liver injury and disease severity. These signaling pathways are mainly activated in recruited macrophages and activated Kupffer cells in the liver (Avila et al. 2021a).

In addition, AH recruits many neutrophils to the liver, which are attracted in part by Kupffer cell activation and pro-inflammatory cytokines. Based on animal models, neutrophils exhibit an activated phenotype after chronic alcohol exposure, and once they migrate into the liver parenchyma, they kill sensitized hepatocytes by releasing ROS and proteases, likely contributing to alcohol-induced liver injury (Gao and Bataller 2011).

Finally, activation of adaptive immunity is also involved in the pathogenesis of alcohol. Indeed, patients with AH have elevated levels of circulating antibodies to lipid peroxidation adducts, as protein adducts may serve as antigens to activate the adaptive immune response (Arsene, Farooq, and Bataller 2016).

Overall, progression from ASH to AH appears to define a point of no return, as this stage appears to be a rate-limiting step for progression to cirrhosis and HCC in patients with ALD (Ramaiah, Rivera, and Arteel 2004).

2.2.3.3 Alcoholic Fibrosis (AF) and Alcoholic Cirrhosis (AC)

Persistent alcohol abuse leads to progressive liver fibrosis and cirrhosis, which carries a high risk of complications. It is estimated that approximately 20% of ASH patients

develop fibrosis/cirrhosis (Avila et al. 2021a). Excessive alcohol consumption is the most common cause of cirrhosis in Europe and has become an important public health problem and a significant cause of morbidity and mortality worldwide (Magdaleno, Blajszczak, and Nieto 2017). In fact, fibrosis is considered the first irreversible step in ALD (Ramaiah, Rivera, and Arteel 2004).

Liver fibrosis is a wound healing response to almost all forms of chronic liver injury. It is characterized by excessive accumulation of collagen and other extracellular matrix (ECM) proteins. The accumulation of ECM proteins alters normal liver architecture, converting the parenchyma into fibrotic scar tissue and producing hepatocyte regenerative nodules that eventually lead to cirrhosis (S. L. Friedman 2008b). AC Is considered end-stage liver disease characterized by changes in liver parenchyma, nodule formation, and hepatic dysfunction.

Activated hepatic stellate cells (HSCs) are the main source of increased ECM protein production. Following liver injury, HSCs become activated and differentiate into myofibroblast-like cells that migrate through the liver, accumulate at damaged sites, and replace injured or dead hepatocytes while secreting ECM (Celli and Zhang 2014).

As mentioned earlier, fibrosis can be chronic and in many cases progress to cirrhosis without symptoms. Compensated cirrhosis, referred to when the liver has normal or unimpaired liver function, often leads to progression to decompensated cirrhosis. Decompensated cirrhosis is characterized by the rapid development of various complications related to hypertension and hepatic dysfunction, which may progress even more rapidly to HCC and are associated with poorer survival rates (S. L. Friedman 2008b).

Acetaldehyde plays an important role in the initiation and maintenance of fibrosis. It acts on HSCs in a paracrine manner by increasing the expression of collagen I, and it also reacts rapidly with cellular components to generate adducts that help maintain HSC activation. Similarly, ROS also simulates fibrosis, both by activating pro-fibrogenic signaling pathways in HSCs and by directly inhibiting metalloproteinases that degrade collagen. Finally, LPS is considered an extrinsic inducer of liver fibrosis. It not only

stimulates Kupffer cells to produce ROS and cytokines that subsequently promote HSC activation, but also activates HSCs directly via TLR4 (Purohit and Brenner 2006).

2.2.3.4 Hepatocellular Carcinoma

Liver cancer is the fifth most common cancer type in the world and the second cause of cancer-related death. HCC is the most frequent presentation of liver cancer (70-85%) over other types (cholangiocarcinoma, hemangiosarcoma and hepatoblastoma) (Suriawinata and Thung 2002). Chronic alcohol abuse is considered a major risk for its development.

Like cirrhosis of any other etiology, AC promotes progression to HCC; around 2% of cirrhotic patients develop HCC (Avila et al. 2021a). The mechanisms that contribute to development of HCC in AC patients are complex and include telomere shortening, alterations in tumor microenvironment, hepatocyte proliferation, loss of cell cycle checkpoints and activation of oncogenic pathways. There are some unique mechanisms that contribute to the development of HCC specifically in patients with ALD. These include acetaldehyde, a carcinogen with mutagenic properties, induction of CYP2E1, which metabolized many of the procarcinogenic compounds in alcoholic drinks, and the immunosuppressive effect of alcohol (Morgan, Mandayam, and Jamal 2004).

2.2.4 Animal models of ALD

Animal models are essential to understand the pathophysiology of progression of ALD and to define effective treatments, but their use in ALD is limited. To date, none of the current animal models can reproduce all major features of human ALD. Indeed, rodent models are characterized by relatively mild liver damage and an impaired ability to achieve and maintain high blood alcohol concentrations (BAC) (Arsene, Farooq, and Bataller 2016; Nevzorova et al. 2020). This could be explained by certain physiological characteristics: (1) high basal metabolic rate, (2) natural aversion to alcohol, (3) fast catabolism of alcohol, (4) spontaneous reduction of alcohol intake when blood acetaldehyde levels increase, (5) different progression times between humans and rodents, (6) absence of addictive behaviors and (7) differences in the innate immune system (Delire, Stärkel, and Leclercq 2015). Nevertheless, current animal models remain

a very useful tool for studying ALD. **Table 2.1**, adapted from Nevzorova *et al*. (Nevzorova et al. 2020), provide a brief description of each diet and its modifications.

Alcohol in drinking water (ADW) is the simplest model of experimental alcohol administration, originally developed in the late 1970s. Briefly, increasing amounts of ethanol are gradually added to the available drinking water (usually starting at 5% (v/v)), and the highest ethanol concentration is used throughout the study.

There are several variations: Mice might have free access to a single drinking bottle containing alcohol in water and standard chow diet (ADW Single Bottle) (Lamas-Paz et al. 2018); a second bottle might be incorporated that offers choice between water and alcohol at different concentrations, which is more suitable for animals that prefer no or little alcohol (ADW Multiple Bottles) (D'Souza El-Guindy et al. 2010); the "Drinking in the Dark" modification (DID) is based on replacing the water bottle with a bottle containing 20% ethanol for 2 to 4 hours, starting 3 hours after the onset of the dark cycle (Thiele and Navarro 2014). ADW for 8-10 weeks is sufficient to induce steatosis, and long-term (months) alcohol feeding has been reported to induce oxidative stress, steatosis, very mild fibrosis, inflammatory cell infiltrates, increased liver injury, and depletion of cellular antioxidant defenses in mice (Brandon-Warner et al. 2012). The available variations of this model make it one of the most suitable models of chronic alcohol abuse for a variety range of studies, and alternatively, flavors might be added to make the alcohol more tasteful.

Western lifestyles often include an overlap of alcohol consumption and high fat consumption. Some animal models have already been proposed to investigate the influence of dietary factors on chronic alcohol-induced liver injury: Combining ADW (5%) with high-fat diet (HFD) for 6 weeks leads to inflammation, activation of HSCs, and initial fibrosis development (Gäbele et al. 2011); a complementary model that combines HFD feeding followed by single-dose ethanol administration leads to inflammation and liver injury and could be used to study the effects of the interactions between obesity and binge drinking on liver injury (Chang et al. 2015); and finally, the DUAL model, developed by Benedé-Ubieto *et al*. (Benedé-Ubieto et al. 2021), is based on 10%vol/vol alcohol in sweetened drinking water in combination with a Western diet (WD) for 10, 23, and 52 weeks. Mice fed the DUAL diet exhibit increased body max index, altered glucose and lipid metabolism, significant liver damage, lobular

inflammation, and advanced hepatic fibrosis that progresses to cirrhotic changes after 12 months. It mirrors advanced steatohepatitis in humans (Benedé-Ubieto et al. 2021).

Although the ADW model was widely used for mild ALD, the need for a method to achieve significant BAC and allowed control over nutrition led to the development of a unique liquid diet procedure by Charles Lieber and Leonore M. DeCarli (LdC diet) over 25 years ago (Lamas-Paz et al. 2018) that incorporates ethanol into a liquid diet. Since rodents have nothing to eat or drink except the ethanol-containing liquid diet, the ingestion ensures high ethanol consumption. The amount of ethanol in the diet should be gradually increased, up to the final concentration of 6.4% v/v to allow the animal to adjustt. Four weeks of LdC is a suitable model to study the initial phase of ALD (Nevzorova et al. 2016). Modifications have been developed for the advanced form of ALD.

First, the NIAAA model developed by Bin Gao's group (Bertola et al. 2013). Mice receive LdC (5%) for 10 days and a single oral gavage of ethanol on day 9. It can be extended to longer periods of chronic feeding and combined with multiple binges. It represents early ASH, and chronicity could cause more severe steatohepatitis, although body weight loss and high mortality are challenging. On the other hand, in addition to binge drinking, other hepatotoxins such as diethylnitrosamine (DEN), carbon tetrachloride (CCl_4), lipopolysaccharide (LPS), or acetaminophen (APAP) can be added during chronic LdC to provide a "second hit", exacerbating liver injury and providing useful insights into the effects of ethanol on the progression of severe liver injury such as cirrhosis or HCC (Delire, Stärkel, and Leclercq 2015; Nevzorova et al. 2020; Hidekazu Tsukamoto et al. 2009)

To overcome the limitations of LdC and reach the advanced stages of ALD, Tsukamoto developed a new feeding model of direct ethanol infusion through a surgically implanted gastric cannula (Tsukamoto-French model) in 1984. Briefly, a catheter is implanted in the stomach under aseptic conditions, and alcohol is added to the LdC diet and infused directly into the stomach (H. Tsukamoto et al. 1984). Ethanol intake, administration rate, and route of administration are fully controllable and allow for manipulation of dietary factors and addition of secondary hits (Lazaro et al. 2015). Animals can be maintained on this diet for several months, and the pathological changes obtained are similar to those in

Table 2.1 Most extended models for the study of alcoholic liver disease (ALD) Adapted from *Nevzorova et al. 2020* (HCC=hepatocellular carcinoma; DEN=dietylnitrosamine; NIAAA=national institute of alcohol abuse and alcoholism; ASH=alcoholic steatohepatitis; LPS=lipopolysaccharide; CCl4=carbon tetrachloride; LdC=Lieber-DeCarli; HFD= high fat diet; WD= western diet)

Model	Administration	Time	Steatosis	Inflammation	Fibrosis	HCC	Mortality rate	Weakness
Ad libitum alcohol-drinking water	Oral alcohol consumption by drinking water	8-70 weeks	+	-	-	With DEN	+ ++ (Long-Term)	General: it induces moderate steatosis and comparatively low elevation of serum aminotransferases, but no signs of fibrosis or inflammation DID variation: Nutritional effects associated with ethanol consumption difficult to assess and control, difficult to sustain considerable BAC long term, possible dehydration
Ad libitum liquid diet (Lieber-DeCarli diet)	Oral alcohol consumption with alcohol-containing liquid diet formula but with no other food or drink	3-12 weeks	++	+/-	-	-	+	It is not completely physiological since forces ethanol consumption when animals are hungry or thirsty, requires daily change of the liquid diet during the experimental period and it does not induce liver inflammation or hepatic fibrosis even after prolonged administration.
Chronic and binge alcohol feeding (The NIAAA or Gao-binge model)	A single or repeated intragastric gavage of alcohol following chronic feeding with the Lieber-DeCarli liquid diet	10 days-8 weeks	++	+	+	-	++	The model still represents only moderate ASH. The combination of long-term chronic feeding and multiple binges of ethanol feeding is rather challenging, because of body weight loss and high mortality. In addition, an improper technique during the oral gavage is other leading cause of mortality
Lieber-DeCarli diet + other hepatotoxins (Second-hit model)	Addition of hepatotoxins such as DEN, LPS or CCl4 during the chronic feeding phase of the Lieber-DeCarli liquid diet	4-10 weeks	++	++	++	With DEN	++	LdC variations may promote advanced liver disease but are usually accompanied by lower reproducibility and higher mortality.
Intragastric infusion (Tsukamoto-French model)	Direct enteral feeding through a surgically implanted intragastric cannula	4 weeks-4 months	++	++	++	-	+++	Not a physiological model, requiring skilled surgical implantation in combination with expensive equipment. It needs extensive animal monitoring.
Ad libitum alcohol-drinking water + HFD	Oral alcohol consumption by drinking water (5%) combined with a high fat diet	6 weeks	++	+	+	-	+	The model still represents only moderate ASH.
Ad libitum alcohol-drinking water + WD	Oral alcohol consumption by drinking water (10%) combined with a western diet	10-52 weeks	++	++	++	-	++	The perfectly mirrors advanced ASH, but lacks complications of advanced ALD injury, such as HCC.

human ALD, including steatosis, inflammation, and fibrosis, but not cirrhosis or other irreversible changes.

Although the chronic-plus-binge ethanol feeding model and the hybrid feeding model are useful for studying ASH, there are no models yet that show all characteristics and complications observed in AH, such as cirrhosis, jaundice, renal failure, and bacterial infections, do not yet exist (Arsene, Farooq, and Bataller 2016). Related to the experimental models using secondary hepatic stressors, although hepatotoxins can be included in the rodent models previously described to study more advanced ALD stages, these are more likely to represent the effects of the toxin more than ALD. Therefore, more physiological models that mimic human ALD progression are needed (Avila et al. 2021a).

2.2.5 Treatment for ALD

Currently, there is no United States Food and Drug Administration (FDA)-approved therapy for ALD and prolonged abstinence is the standard of care. Despite some important advances in understanding the underlying pathogenesis and clinical features of ALD, there have been no significant advances in therapy over the past 40 years (Farooq and Bataller 2016).

The first and most important step in the treatment of ALD is to achieve complete and sustained abstinence, regardless the stage of the disease. In fact, abstinence is associated with better clinical outcomes across the spectrum of ALD, from early asymptomatic to complicated severe cases (Argemi et al. 2021). In addition, given the high prevalence of malnutrition and vitamin deficiencies, ensuring a proper nutrition is recommended in patients with ALD (Shah et al. 2019). In fact, heavy drinkers consume almost half of the total calories in the form of alcohol, which significantly decreases the intake of proteins and fats as well as vitamins and minerals (C. S. Lieber 1988). Increased catabolism, decreased food intake, pancreatic insufficiency, or the presence of encephalopathy may contribute to malnutrition in ALD, favoring complications of portal hypertension and bacterial infections (Argemi et al. 2021). Therefore, it is recommended to support nutrition by providing high-protein, low-fat diet, and to balance the levels of vitamins B, C, K, and folic acid (Suk, Kim, and Baik 2014).

Primary and secondary prophylaxis of complications are other important goals in patients with advanced ALD. Alcohol-related damage to extrahepatic organs is described in more detail in **Chapter 2.2.6**. It should be noted, however, that such changes affecting, for example, the nervous system, pancreatic function, intestinal integrity, or cancer development should be prevented, screened, and treated when present.

Treatment of the underlying alcohol use disorder (AUD) is critical at early stages. In addition to an addiction specialist and psychosocial support, specific alcohol withdrawal medications are used as adjuvant treatment (Kong et al. 2019). Disulfiram is an irreversible alcohol dehydrogenase inhibitor commonly used to treat alcoholism. However, because of its potentially severe hepatotoxicity, it is not recommended for advanced-stage ALD patients (Stickel et al. 2017). Drugs that are not metabolized by the liver are more suitable for ALD patients, even in advanced stages. Among them, Baclofen, a gamma-aminobutyric acid B receptor agonist, has been shown to be effective in maintaining a withdrawal, even in patients with cirrhosis (Argemi et al. 2021; Gitto et al. 2016).

Nevertheless, treatments for alcohol addicts depend on the degree of alcohol consumption. Early diagnosis is critical to ensure appropriate treatment. ALD is a particularly silent disease that is not recognized until the physical consequences of irreversible AH or AC occur (Shah et al. 2019). Therefore, early detection programs are urgently needed.

As mentioned earlier, AH in its more severe form has a 30-day mortality rate of 40% of patients (P Mathurin et al. 2011). Initially, patients with AH need to be hospitalized for treatment because bacterial infections are common in these patients and lead to multiorgan failure and death. Since the first placebo-controlled trials in the 1970s, specific treatment of AH has invariably consisted of administration of oral prednisolone for 28 days (Argemi et al. 2021). Because ALD is associated with increased levels of oxidative stress, antioxidants such as vitamin E, N-acetylcysteine (NAC), S-adenosylmethionine (SAMe), and silymarin have been studied and evaluated for the treatment of AH patients (Gao and Bataller 2011). Emerging therapies for the treatment of AH, including those that target the systemic effects of ALD, are discussed in Section 2.2.7.

Once alcoholic fibrosis/cirrhosis is diagnosed in ALD patients, alcohol withdrawal can only slow the onset of the disease. There are no FDA-approved antifibrotic agents to reduce the progression of fibrosis in ALD patients, leaving alcohol abstinence and liver transplantation as the only effective therapeutic approaches. Some agents such as angiotensin blockers, losartan, can reduce the progression of fibrosis and the development of stem cell therapy research has discovered the potential of mesenchymal stem cells (MSCs) in regenerative liver medicine (Kong et al. 2019). These cells have the inherent ability to migrate to sites of inflammation following tissue injury, where they can differentiate into hepatocyte-like cells and secrete a wide range of cytokines. These secretions inhibit the proliferation of HSCs, reduce inflammation and fibrosis, and ameliorate damaged tissues by providing them with nutrients and stimulating angiogenesis and tissue regeneration (R. Ji et al. 2012).

For patients with decompensated ALD cirrhosis and/or developing HCC, LT is the only therapeutic option. ALD represents the second most common indication for LT worldwide, accounting for about 30% of all primary transplants in Europe and approximately 25% in the U.S. (Avila et al. 2021a). LT is the most effective therapeutic option for patients with end-stage liver disease, and both graft and patient survival rates for AUD are comparable to those after transplantation for other etiologies (Argemi et al. 2021). Nevertheless, ALD is still considered a controversial indication for LT, mainly because it is considered a self-inflicted disease with negative consequences for society, and because of the potential risk of alcohol relapse after LT. This explains the existence of the six-month abstinence rule as a prerequisite for LT in many centers, although its relevance has never been demonstrated and the ideal duration of abstinence before LT is still controversial (Gitto et al. 2016). Regarding early LT for AH who do not respond to drug therapy, there is growing evidence that rigorous patient selection is key to positive outcomes (P Mathurin et al. 2011). The presence of close supportive family members, absence of coexisting disorders, and agreement to lifelong complete alcohol abstinence were some of the stringent selection criteria that challenge the requirement for long-term abstinence prior to LT and underscore the need for psychosocial assessment for long-term survival after LT at AH.

2.2.6 Systemic effects of alcohol abuse

The enzymes that metabolize alcohol (i.e., ADH1, CYP2E1, and ALDH) are mainly expressed in hepatocytes, so most of the direct cellular toxicity of ethanol affects these cells (Louvet and Mathurin 2015). However, the toxic effects of acetaldehyde and ROS extend far beyond liver damage; alcoholism is, in fact, a multisystemic disease (González-Reimers et al. 2014) (**Fig. 2.9**).

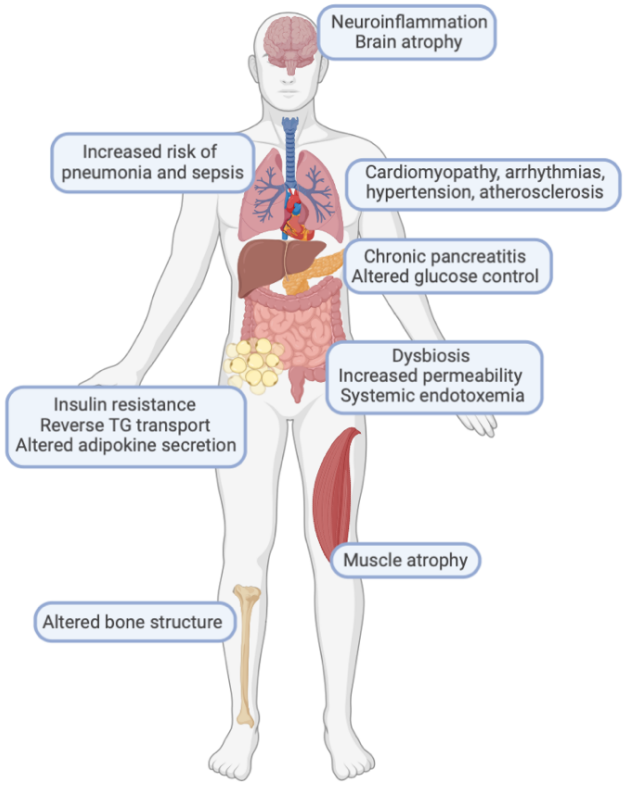

Figure 2.9 Systemic effects of alcohol abuse. Although alcohol is mainly metabolized in the liver, the toxic acetaldehyde and ROS affect the whole organism, such as brain, lungs, circulatory system, pancreas, gut, adipose tissue, muscle, and bone (ROS= reactive oxygen species; TG= triglycerides)

2.2.6.1 Gut-liver axis in ALD

Alcohol consumption affects the gut on several levels. More than 100 trillion microbes live in the human digestive system, collectively known as the *gut microbiome.* The physiological link between the microbiome and the human host is extensive and includes important roles in digestion, metabolism, and immunity. The balance between commensal and pathological bacteria is important for homeostasis in the gut, as well as for protection

against various systemic disease states (Cani 2018). ALD is associated with changes in the gut microbiota, and although these depend on the stage of the disease (Avila et al. 2021b), overall bacterial diversity is reduced in the microbiome of patients with all forms of alcohol-related liver disease. Regarding specific bacterial taxa, there are some common microbial associations in patients with ALD. Alcohol consumption alone, without the presence of significant liver disease, is associated with a reduction in *Bacteroidaceae* and an increase in Gram-negative *Proteobacteria* in general (Fairfield and Schnabl 2021), which are associated with higher concentrations of endotoxins (Ceni, Mello, and Galli 2014; Louvet and Mathurin 2015). Patients with alcohol-related cirrhosis and AH have an enrichment of more commonly pathogenic taxa, such as *Enterobacteriaceae, Streptococcaceae,* and *Enterococcus*.

Until recently, the study of microbial changes and associations with ALD was limited to the bacterial domain. Fungi are commensals in the human digestive tract and fungal dysbiosis is similarly associated with progression of ALD. Mycobiome dysbiosis in patients with alcohol-related liver disease is characterized by increased abundance of *Candida* and decreased fungal diversity (Yang et al. 2017). In addition, the human digestive tract is also colonized by numerous commensal viruses that together form the enteric virome. Indeed, patients with ALD exhibit an increase of eukaryotic viruses known to cause disease in humans, as well as increased viral diversity in the enteric environment (Shkoporov et al. 2019).

The importance of intestinal dysbiosis in the development of ALD was shown by faecal microbiota transfer (FMT). Mice transplanted with faeces from patients with AH develop more severe liver disease compared with mice transplanted with faeces from patients with less severe disease after receiving of an oral LdC diet for 28 days (Llopis et al. 2016). Interestingly, the development of intestinal dysbiosis does not occur in all patients with AUD. However, those who develop this condition have a higher degree of intestinal permeability than those who do not (Poole, Dolin, and Arteel 2017).

Heavy alcohol consumption is associated with an increase in gut permeability and leakage of endotoxins, with or without liver disease. And abstinence for 2 weeks or longer is necessary for increased gut permeability to return to baseline levels (Qin et al. 2007). Alcohol can increase the leakage of endotoxins from the gut through a variety of

mechanisms. Alcohol and/or acetaldehyde can directly alter gut permeability and leakiness by causing structural defects in the barrier. Acetaldehyde contributes to altering intestinal barrier function and to promoting translocation by disrupting tight and adherens junctions in the colon mucosa (Ceni, Mello, and Galli 2014). And indirectly, by enhancing the deficiency of Zn^{2+}, which is necessary for maintaining the integrity of intestinal epithelium, and increasing circulating inflammatory cytokines (H. J. Wang, Zakhari, and Jung 2010).

Microbial products, including bacterial endotoxins (such as lipopolysaccharide [LPS] secreted by gram-negative bacteria), bacterial exotoxins (such as cytolysin secreted by *Enterococcus*), fungal exotoxins (such as candidalysin), and microbial pathogen-associated molecular patterns (PAMPs) from all types of microbiota can promote hepatocellular injury (Fairfield and Schnabl 2021). Indeed, LPS in the interstitial fluid can enter the systemic circulation after passing through the intestinal epithelium via two pathways: the portal vein and the GI tract lymphatic vessels. The liver plays a critical role in the degradation and inactivation of LPS. Most LPS is detoxified by both Kupffer cells and hepatocytes, and only that which escapes this process can enter the bloodstream. However, by the lymphatic route, where there is no major detoxification organ, most of the bioactive LPS is released into the bloodstream, making it available to different organs (H. J. Wang, Zakhari, and Jung 2010). Endotoxins bind hepatic Toll-like receptors (TLRs) and PAMPs bind directly to pattern-recognition receptors on Kupffer and hepatic stellate cells. All of the above microbial products can lead to an inflammatory cascade of cytokine activation, oxidative stress, and fibrotic changes (Tripathi et al. 2018).

Importantly, alcohol abuse impairs the liver's ability to detoxify LPS. Consequently, more LPS escapes from the liver and remains in the bloodstream, which in turn increases systemic inflammatory conditions and damage to various organs. The effect of ROS and pro-inflammatory cytokines in distant organs such as the brain, adipose tissue, and heart will be discussed in more detail in the next section.

2.2.6.2 Central nervous system (CNS)

Brain atrophy is the most common CNS complication of heavy alcohol consumption and can lead to dementia even in young drinkers (González-Reimers et al. 2014). Alcohol abuse can lead to regional structural brain damage and cognitive dysfunction, neuronal

death, and inhibition of neurogenesis, resulting in a reduction in brain volume (H. J. Wang, Zakhari, and Jung 2010). Indeed, peripheral endotoxemia leads to inflammation of the brain. Although LPS does not cross the blood-brain barrier, systemic endotoxemia leads to an increase in the pro-inflammatory cytokine TNF in the serum and CNS (Qin et al. 2007). Alcohol-related brain atrophy recovers slowly after months of abstinence (Demirakca et al. 2011).

2.2.6.3 Adipose-liver organ crosstalk

The normal function of adipose tissue is profoundly affected by excessive alcohol consumption, causing changes similar to those seen in obese patients (H. Wang et al. 2021). Alcohol directly provokes the death of adipocytes and inflammation of adipose tissue. As explained earlier, these processes cause adipose tissue resistance to insulin, increase lipolysis, and lead to lipid accumulation in the liver through reverse triglyceride transport. Alcohol consumption also alters adipokine secretion of leptin, visfatin, resistin, and adiponectin and activates both KCs and HSCs, leading to accelerated liver inflammation and fibrosis. Regarding inflammation, alcohol promotes the production of TNF, CCL2, and IL-6 in adipose tissue, and the levels of these molecules correlate with the severity of ASH in patients (H. Wang et al. 2021).

2.2.6.4 Chronic pancreatitis

Chronic pancreatitis is common in alcoholics, is partly responsible for the nutritional problems of these patients and is a risk for the development of pancreatic cancer (Clemens and Mahan 2010; Rasineni et al. 2020). Ethanol causes progressive inflammation and fibrosis in the pancreas. Indeed, LPS can directly stimulate pancreatic stellate cells, and in early stages of the necrotic-fibrotic process, macrophages invading the pancreas produce proinflammatory cytokines that exacerbate pancreatic damage (Detlefsen et al. 2006). In addition, altered glucose and insulin levels were found in a model with chronic ethanol consumption (Z. Ren et al. 2016).

2.2.6.5 Lung

Ethanol consumption has been associated with an increased incidence of acute respiratory distress syndrome (ARDS). Besides, because alcohol alters the normal barrier function of the alveoli and induces oxidative stress, there is a higher incidence of pneumonia, the main cause of sepsis in advanced stage ALD patients (Mehta and Guidot 2012).

2.2.6.6 Other systemic effects

Chronic ethanol abuse may also contribute to muscle atrophy (in 40-60% of alcoholics), cardiovascular disease (cardiomyopathy, arrhythmias, hypertension, and atherosclerosis), and bone alterations, by directly inhibiting osteoblast function and increasing bone resorption, both mediated by the overproduction of ROS (González-Reimers et al. 2014).

Overall, chronic alcohol consumption impairs not only gut and liver functions, but also multi-organ interactions, leading to persistent systemic inflammation and ultimately, organ damage; what calls for a multidisciplinary and social approach to treating these conditions (Mitra, De, and Chowdhury 2020).

2.2.7 Novel therapeutic targets for ALD

Although alcohol withdrawal is the standard therapy for patients with all stages of ALD, the need for a specific FDA-approved therapy has led to the search for new therapeutic approaches that target specific pathway (**Fig. 2.10**). In patients with early stages of ALD, molecules that limit oxidative stress and alleviate steatosis and/or reduce fibrosis progression should be developed in close association with alcohol dependence management.

However, early diagnosis and therapy of silent ASH in patients with AUD is uncommon. As mentioned earlier, ALD progresses silently until complications arise, and patients are usually not discovered until late stages. Therapeutic options for acute, severe forms of ALD, such as AH, have remained unchanged since the 1970s and are based on treatment with corticosteroids (Argemi et al. 2021). However, the efficacy of prednisolone is limited and applies to only a minority of patients (H. Wang et al. 2021). Therefore, the

development of effective therapeutics for AH is an important unmet clinical need. Despite this need, there have been relatively few clinical trials addressing AH; clinicaltrials.gov (April 2022) lists 99 registered clinical trials. 42 of these have been completed, and only 8 trials have published their results.

Advances in understanding the molecular mechanisms of ALD have led to the identification of new therapeutic targets, resulting in more pathophysiologically oriented approaches. The focus of new therapeutics in preclinical testing is on normalizing gut dysbiosis and permeability, alleviating the inflammatory response, and finding hepatoprotective agents.

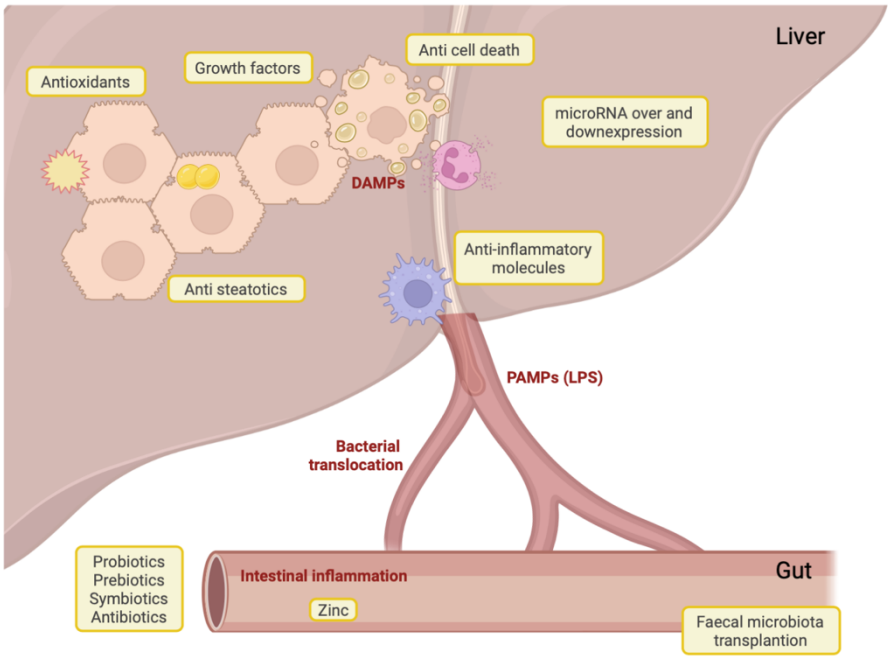

Figure 2.10 Novel therapeutic targets for alcoholic liver disease (ALD). There are many potential targets to treat ALD including gut dysbiosis, increased permeability, inflammation, cell death, regeneration, and oxidative stress (PAMPs= pathogen-associated molecular patterns; LPS= lipopolysaccharide; DAMPs= damage-associated molecular patterns)

2.2.7.1 Targeting gut dysbiosis and intestinal barrier function

Intestinal dysbiosis associated with ALD is well described (see **Chapter 2.2.6**) and has recently been targeted for therapy. Interestingly, transfer of human microbiota from patients with ALD or healthy controls affects the susceptibility of mouse models to AH.

Small clinical studies using transfer of faecal microbiota have shown a positive effect on mortality in patients with AH who are ineligible for steroid treatment and improvement of hepatic encephalopathy in patients with decompensated AC (Bajaj et al. 2017; Philips et al. 2017; Wrzosek et al. 2021).

Other more targeted approaches might include restoring intestinal eubiosis using prebiotics, probiotics, or symbiotics because they reduce the production of proinflammatory bacterial products, enhance anti-inflammation, and improve barrier integrity, resulting in reduced endotoxin release (Y. Wang et al. 2013). Probiotics such as *Lactobacillus rhamnosus* GG, *Akkermansia muciniphila,* or *Lactobacillus fermentum* show encouraging results (Kong et al. 2019). In addition, modulating the intestinal microbiota with bacteriophages could be a promising therapeutic approach. This was recently demonstrated using bacteriophages specifically targeting *Enterococcus faecalis*, a bacterium that accumulates in the gut of patients with AH and releases a hepatotoxic exotoxin (Duan et al. 2020).

The results of a placebo-controlled study showed that the nonabsorbable antibiotic rifaximin alters the gut microbiota and protects alcoholic patients from hepatic encephalopathy (Bass et al. 2010). Similar results were observed with TLR4 antagonists (Mencin, Kluwe, and Schwabe 2009).

A number of dietary supplements have also been tested in mouse models for their ability to improve intestinal integrity and limit the transfer of PAMPs to the portal circulation and liver. To date, only zinc supplementation has been tested in patients with AH.

Finally, the farnesoid X receptor (FXR)-bile acid axis/FXR agonists may also be a promising therapeutic target for ALD. In mouse models of liver disease, FXR agonists have been shown to improve intestinal mucosal integrity, leading to reduced microbial translocation and HSC activation (Carr and Reid 2015).

2.2.7.2 Alleviating inflammation

The use of anti-inflammatory agents is by far the best studied therapeutic route for AH. Prednisolone does indeed dramatically reduce inflammation but, as noted above, is not

effective in most patients and increases the risk for secondary infections (Singal et al. 2018). Preclinical studies suggest that strategies that interrupt activation of the inflammatory cascade may be beneficial in ALD and AH. For example, inhibition of the interleukin-1 (IL-1) pathway by administration of the IL-1 receptor antagonist anakinra attenuated alcohol-induced steatosis, liver injury, inflammation, and early fibrosis in mice (Petrasek et al. 2012). Anakinra and the IL-1b specific monoclonal antibody canakinumab are currently being evaluated in clinical trials. Chemokines are also important therapeutic targets for interrupting inflammation in AH patients. Preclinical studies with a dual inhibitor of chemokine receptor, CVC, have shown promising results (Ambade et al. 2019).

Alternatives to strategies that directly interrupt the cycle of proinflammatory cytokine and chemokine signaling are also of interest. IL-22 is a member of the IL-10 cytokine family and plays an important role in regulating bacterial infection, tissue repair, and homeostasis. In rodent models of ALD IL-22 protects against liver injury, reduces steatosis and fibrosis, and promotes liver regeneration (Ceni, Mello, and Galli 2014). In addition, IL-22 may be a good therapeutic target that overcomes the promotion of corticosteroid-mediated infections (Kong et al. 2019).

2.2.7.3 Reducing hepatocyte injury and promoting liver regeneration

Hepatocytes suffer a variety of insults during ALD. Deregulation of PPAR transcriptional activity during steatosis and ASH suggests a possible role of PPAR agonists in ALD treatment. Indeed, in alcohol-treated mice, the PPARgamma agonists rosiglitazone and pioglitazone increase circulating adiponectin levels and activate the SIRT1-AMPK signaling cascade, which correlates with enhanced expression of FAO enzymes and a reduction in hepatic steatosis (Ceni, Mello, and Galli 2014).

While PAMPs that enter the portal circulation from the gut are a source of inflammatory signals that contribute to ALD, DAMPs that originate from injured or dead cells are other potential targets. Two approaches have been proposed: agents that reduce oxidative stress and treatments that decrease hepatocyte death. Current studies are testing whether antioxidants that target mitochondria might be more therapeutically useful than general antioxidant (Singal and Shah 2019; P. Zhang et al. 2015). Regarding hepatocyte death,

hepatocytes can undergo cell death via multiple pathways including apoptosis, necroptosis, pyroptosis, and ferroptosis. Strategies targeting multiple forms of cell death are underdevelopment, as preliminary results using only apoptosis inhibitors failed to prevent either inflammation or cell injury (Roychowdhury et al. 2012). Complementary strategies to promote hepatocyte regeneration are also being explored, as patients with AH, who do not respond to drug therapy, have a marked deficiency in hepatocyte proliferation markers. Granulocyte colony-stimulating factor (G-CSF) can promote liver regeneration and has recently been shown to increase survival in ALD (Argemi et al. 2021).

2.2.7.4 microRNA based therapies

Increasing evidence suggests that miRNAs and extracellular vesicles (EVs) play a role in the pathomechanisms of ALD. These microRNAs are involved in oxidative stress, inflammatory responses, lipid metabolism, and activation of HSCs by regulating transcription of target proteins (Kong et al. 2019). Chronic alcohol abuse has been shown to reduce liver and hepatocyte expression of miRNA-122, the most abundant microRNA essential for hepatocyte functions. And its replacement in vivo alleviated liver injury, steatosis, and fibrosis in ALD mouse models (Satishchandran et al. 2018). Moreover, inflammation-related miRNA-155 is increased by alcohol in immune cells, and miRNA-155-deficient mice were protected from ALD (Bala et al. 2016). Therefore, downregulation or overexpression of certain microRNAs can be used as a therapeutic target for ALD.

2.2.7.5 Combination therapies

Finally, many of the ongoing or registered clinical trials on AH involve the use of combination therapies. Indeed, given the many tissues affected by chronic alcohol abuse, combined therapeutic approaches targeting multiple pathways may be the best strategies for future interventions. For example, a combination of zinc to improve gut health and anakinra to inhibit inflammation, as well as the influence of G-CSF with NAC or prednisolone, are being investigated (H. Wang et al. 2021).

Overall, specific pathways involved in alcohol-induced liver injury are helping to decipher new therapeutic targets, highlighting the need to establish new mouse models that mimic human ALD more precisely. Future efforts should be directed toward developing early detection programs and testing the new therapeutic approaches in controlled clinical trials in early to advanced ALD patients.

2.3 LIVER TRANSPLANTATION

The remarkable regenerative capacity of the liver allows the implementation of several therapeutic strategies. The regenerative response can be used in the context of hepatobiliary surgery, as it allows resections such as for malignancies and liver transplantation (LT).

In this sense, LT is the only curative treatment for acute liver failure and end-stage liver disease. Hepatocellular carcinoma and hepatitis C virus cirrhosis have been the most common diseases leading to liver transplantation, although increasing numbers of patients with alcoholic cirrhosis and nonalcoholic steatohepatitis are receiving transplants (Younossi et al. 2021).

However, this life-saving technique is also associated with complications. Ischemia-reperfusion injury (IRI) is an important cause of liver damage in surgical procedures such as hepatic resection and liver transplantation and the main cause of graft dysfunction post-transplantation (Gracia-Sancho, Casillas-Ramírez, and Peralta 2015). Moreover, the success of this procedure depends on the quality of the graft. If its regenerative capacity is compromised in any way, this may lead to poor or delayed graft function, occasionally the need for re-transplantation, or ultimately the death of the recipient (Forbes and Newsome 2016). Additionally, the gap between supply and demand for liver grafts is expanding, so that not all patients on liver transplant waiting lists are guaranteed a liver graft (Campana et al. 2021).

In the next section, we analyze the regenerative capacity of the liver, the mechanisms underlying IRI, factors that may affect liver regeneration and exacerbate IRI, the implication of mitochondrial dysfunction, and therapeutic strategies to improve the current organ donor pool.

2.3.1 Liver regeneration

In the absence of injury, the liver epithelium is maintained by the slow turnover of hepatocytes and/or ductal cells within their own compartment. Experiments in rats have shown that between 0.2% and 0.5% of liver cells divide at any given time (MacDonald

1961). This mitotic quiescence is misleading, however, because when liver tissue is attacked, it shows remarkable regenerative capacity and restores homeostasis within a few days. The best studied form of liver regeneration is that which occurs after the loss of hepatocytes from a single acute injury, such as partial two-thirds hepatectomy (Phx) or administration of noxious chemicals (CCl4, acetaminophen...).

Up to 70% of the liver can be surgically removed and the organ grows back to its original size by compensatory hyperplasia. In contrast to true anatomical regeneration, the remaining liver tissue expands to meet the metabolic needs of the organism, but it does not regain its original anatomical structure, and the liver mass is replaced without activation of progenitor cells (S. A. Mao, Glorioso, and Nyberg 2014). Liver regeneration after acute injury requires a coordinated process in which cytokines, growth factors, and metabolic changes drive the regeneration of both epithelial cells (hepatocytes and bile duct cells) and stromal cells (Kupffer cells, HSCs, and hepatic sinusoidal endothelial cells -LSECs). The interaction of these cell populations is essential for the restoration of homeostasis (Nelson Fausto, Campbell, and Riehle 2006). This phenomenon was recorded and mythologized in ancient times, as in the myth of Prometheus (**Fig. 2.11**).

Figure 2.11 Prometheus (1762) by Nicolás Sébastien Adam. Louvre Museum.

As discussed earlier, the hepatectomy-induced healing response has clinical relevance to resections and transplants, but it is distinct from that seen in chronic liver diseases such as NAFLD or cirrhosis, which are more common in the clinical setting and are responsible for high morbidity rates worldwide (Pimpin et al. 2018). Hepatocytes are particularly vulnerable to such pathologies because they are exposed to exogenous and endogenous

toxins (such as alcohol, viruses, and FAs) on a daily basis as part of their metabolic, digestive, and detoxification activities. Considering how much the rest of the organism depends on liver function, the liver is under unique evolutionary pressure to develop robust, but not infallible, regenerative mechanisms against toxic damage (Campana et al. 2021; Verma et al. 2021).

Indeed, the liver is the only solid organ that, through regenerative mechanisms, ensures that the ratio of liver to body weight is always 100% of what is required for body homeostasis (Michalopoulos and Bhushan 2021). This is an energy-consuming process that is influenced by the energy status of the main parenchymal cell, the hepatocyte (Alexandrino et al. 2018). However, several factors can affect regenerative capacity. Metabolically damaged livers (aged, steatotic) show reduced or delayed regeneration compared to controls (Ivanics et al. 2021). On the other hand, inflammation, viruses, or toxins can alter tight regulation of liver regeneration and lead to continuous proliferation of hepatocytes, fibrosis, cirrhosis, and liver cancer (Michalopoulos and Bhushan 2021). With the increasing prevalence of chronic liver disease and rising indications for LT, new strategies are needed to improve liver surgery outcomes.

2.3.1.1 Regeneration following Partial Hepatectomy

Two-thirds partial hepatectomy (Phx) was first described by Higgins and Anderson in 1931 (Higgins and Anderson 1931). It takes advantage of the multilobular structure of the rodent liver to efficiently remove 2/3 of the liver mass with a simple surgical procedure (**Fig. 2.12**). The advantage of this approach is that removal of the lobes is not accompanied by destruction of the remaining liver tissue and the subsequent inflammatory response that typically occurs in hepatotoxic models, in which necrosis plays a key role. Besides, hepatectomy allows accurate timing of the event and a clean chronology of the observed changes (Michalopoulos 2013). In rodents, most of the liver mass is restored within 7-8 days, with full recovery achieved within 3 weeks.

In all species, liver regeneration is significantly affected when more than two-thirds of hepatic mass is removed. This clinical syndrome is termed “Small-for-size-syndrome” (SFSS) and is probably due to the fact that the amount of liver remaining is insufficient to maintain body functions (Demetriou et al. 1988). Besides, because all portal vein flow

passes through the remnant liver, if this is very small, the pressure in the portal vein may exceed the pressure in the hepatic artery, resulting in its obstruction (Demetris et al. 2006). Conversely, after removal of less than one-third of the liver tissue in rodents, there is not only proliferation of hepatocytes, but also hypertrophy.

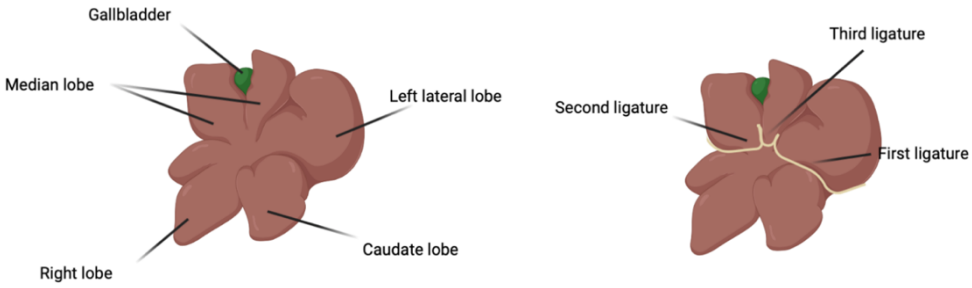

Figure 2.12 Two-thirds partial hepatectomy (Phx). The image on the left shows a schematic representation of murine liver anatomy. For the 70% Phx the left lateral lobe and the left and right parts of the median lobe are resected. The image on the right depicts the optimal ligature of the liver lobes. Adapted from *Nevzorova YA*, et al. 2015

During liver regeneration after partial hepatectomy, normally quiescent hepatocytes undergo a rapid series of coordinated changes to enter the cell cycle and restore structural and functional hepatic loss through a process of compensatory hyperplasia (Verma et al. 2021). The study of the mechanisms underlying liver regeneration has evolved considerably. Initially, it was believed that a single humoral agent could act as a key that could triggers all the events required for liver regeneration. Then it was suggested that activation of a pathway involving multiple components might be responsible for regeneration. And more recently, we are working with the idea that the activity of multiple signaling pathways is required for liver regeneration (Taub 2004). Although liver regeneration requires the activation of multiple signaling pathways, they do not act independently. These pathways may occur simultaneously and/or sequentially, in different liver cell types and at specific stages of liver regeneration. Redundancy is indeed a characteristic feature of these networks, such that loss of a single gene rarely results in complete inhibition of liver regeneration (Nelson Fausto, Campbell, and Riehle 2006).

The entire regeneration process occurs in three phases: Priming (activation of transcription factors to promote hepatocyte division), Progression (attainment of required functional cell mass through DNA replication and hepatic division), and Termination

(balance of cell division and apoptosis to control organ size). Each phase is executed by a well-coordinated parenchymal and non-parenchymal cell and signaling networks, primarily: cytokines, growth factors and metabolic (Nelson Fausto, Campbell, and Riehle 2006; Verma et al. 2021). Briefly, the innate immune system, especially the liver resident Kupffer cells and secreted cytokines such as TNF and IL-6, play an important role in initiating liver regeneration after Phx. Hepatocytes primed by these agents readily respond to growth factors and enter the cell cycle in the progression phase. Indeed, it is the activation and migration of cyclin D1 into the nucleus that commits hepatocytes to DNA synthesis. The peak of hepatocyte proliferation varies from species to species. In the rat, this peak is reached after at 24 hours, whereas in mice it occurs between 36 and 48 hours (N Fausto 2000). Finally, once the hepatostat is reached, stop signals are responsible for the decline in DNA synthesis, involving transforming growth factor-beta (TGFb) and feedback inhibition from the cytokine and growth factor pathways (S. A. Mao, Glorioso, and Nyberg 2014; Tarlá et al. 2006) (**Fig. 2.13**).

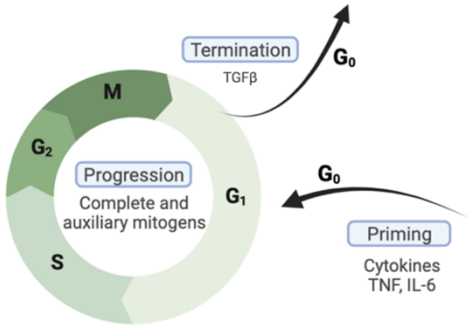

Figure 2.13 The outline of liver regeneration process (TNF=Tumor necrosis factor; IL-6=Interleukin-6; TGFb=Transforming growth factor beta)

It should be noted that the expression of many genes related to hepatocyte differentiation decreases in proliferating hepatocytes. This means that only a portion of hepatocytes undergo partial dedifferentiation at any given time, allowing those that do not actively proliferate to maintain liver functions. If proliferation were to occur in all hepatocytes simultaneously, liver, and systemic failure would be inevitable (Michalopoulos and Bhushan 2021).

As discussed earlier, liver regeneration after Phx requires a coordinated process of epithelial and stromal interactions that reinforce each other until homeostasis is restored (**Fig. 2.14**). Interestingly, proliferating hepatocytes produce many growth factors that are

mitogenic for other liver cells. In fact, hepatocytes are at the center of coordinated histogenesis through which liver regeneration not only restores the required amount of hepatocytes, but also the formation of histologically complete liver tissue. Hepatocytes and cholangiocytes are the first hepatic cell types to enter the cell cycle and proceed to mitosis. HSCs replicate 1-2 days later than hepatocytes. Liver sinusoidal endothelial cells (LSECs) have a very complex and prolonged response as they are replaced by bone marrow endothelial progenitor cells after 3-6 days. And Kupffer cells can proliferate locally, but migration of monocytes from the blood and bone marrow also contributes to their regeneration (Michalopoulos 2017).

Overall, given the complexity of the liver as an organ and the speed at which regeneration occurs, the process must be orderly. The next section will describe the major stages of liver regeneration and the signals that regulate each step.

2.3.1.1.1 Immediate events after Phx

An immediate consequence of Phx is the channeling of all portal vein flow through a narrowed path. The narrowing increases portal pressure and produces shear stress on LSECs. Previous studies have shown that diverting part of the portal vein flow delays and decreases liver regeneration (Marubashi et al. 2004). Thus, the increased flow of portal venous blood per unit of liver, as well as the resulting increased availability of all contents normally present in the portal circulation, plays an important role in initiating the regeneration process, although it has not yet been well defined. Indeed, portal venous blood contains many signaling molecules, including epidermal growth factor (EGF), bile acids, and insulin. These signaling mechanisms have been analyzed independently, but none of them alone can trigger the spectrum of changes observed immediately after Phx (Michalopoulos and Bhushan 2021).

In addition, several signaling pathways are initiated shortly after Phx. At the onset of liver regeneration, ECM remodeling and degradation is required. It is initiated by the increased activity of urokinase (uPA) and a proteolysis cascade by which urokinase activates metalloproteinases, leading to the degradation of ECM proteins, the release and activation of matrix-bound growth factors (such as hepatocyte growth factor, HGF), and the initiation of the regenerative signaling cascades. Notably, the increase in urokinase

activity is the earliest documented biochemical change in the regenerating liver, but there is no clear signaling link between increased portal flow and urokinase activation (Michalopoulos 2013).

It is very likely that many of the very early events associated with liver regeneration have not yet been described because they are a variety of rapid, coordinated, and sometimes redundant changes. The combination of the above events results in rapid and profound changes in gene expression patterns in hepatocytes. Hundreds of new genes that are not normally expressed in quiescent hepatocytes are rapidly activated, and this altered gene expression with episodic increases and decreases persists for more than 14 days (Taub 1996).

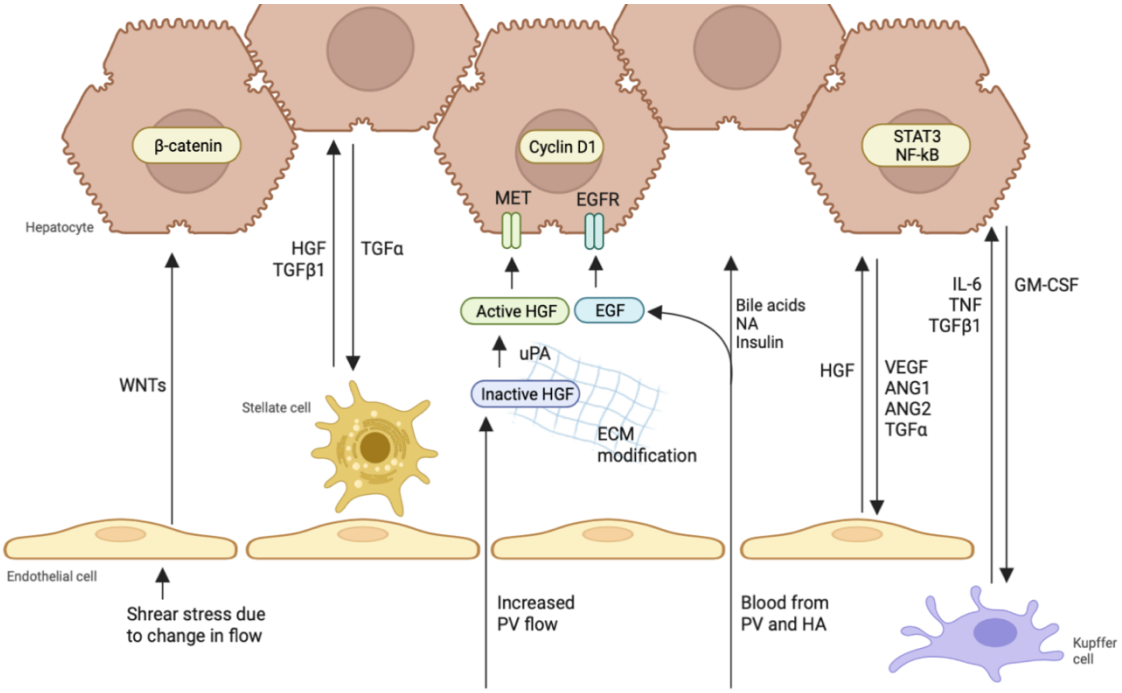

Figure 2.14 Multiple signaling molecules regulate cell proliferation during liver regeneration. As urokinase-type plasminogen activator (uPA) and metalloproteinases remodel the hepatic extracellular matrix (ECM) during liver regeneration, hepatocyte growth factor (HGF) is locally activated and also released into the peripheral blood. Epidermal growth factor (EGF) is constantly available from portal venous (PV) blood. There are local, mutually paracrine signals and between hepatocytes and other hepatic cell types. Hepatic stellate cells (HSCs) also generate paracrine signals and make specialized contacts with both liver sinusoidal endothelial cells (LSECs) and hepatocytes. In that capacity, they might be the origin of non-humoral stimuli mediated by direct contact between hepatocytes and HSCs driving b-catenin into hepatocyte nuclei within a few minutes after partial hepatectomy (Phx). (ANG= angiopoietin; GM-CSF=granulocyte-macrophage colony-stimulating factor; HA=hepatic artery; NA=noradrenaline; NF-kB=nuclear factor-kB; STAT3=signal transducer and transcription activator 3; TGF=transforming growth factor; TNF=tumor necrosis factor; VEGF=vascular endothelial growth factor) Adapted from *Michalopoulos et al., 2021*

2.3.1.1.2 Priming phase: initiation of liver regeneration and the cytokine network

The initiation of liver regeneration is driven by the innate immune system and the releasee of cytokines. After Phx, increases in liver mRNA and serum levels of TNF and IL-6 are observed, as well as activation of the transcription factors Nuclear Factor-kappa B (NF-kB) and Signal Transducer and Activator of Transcription 3 (STAT3). The cytokine network is initiated by the binding of TNF to its receptor TNFR1 and subsequent activation of NF-kB and production of IL-6 in Kupffer cells, which promotes STAT3 activation in hepatocytes (Nelson Fausto, Campbell, and Riehle 2006). These events prime hepatocytes for the transition from quiescence to cell cycle entry (G_0 to G_1). It is important to understand the mechanisms that trigger activation of this network. It has been suggested that after Phx, increased LPS concentrations in the portal vein per liver unit may be responsible for Kupffer cell activation and TNF production (Cornell 1985), although further experiments are needed.

2.3.1.1.3 Progression phase: cell division and complete and auxiliary mitogens

Once hepatocytes enter the cell cycle, progression is driven by growth factors that abolish a restriction point in late G_1. Hepatocyte progression from G_1 to S phase is associated with an activation cascade of cyclins and cyclin-dependent kinases (Mullany et al. 2008). Activation of cyclin D1 and migration into the nucleus commits hepatocytes to DNA synthesis. This activation is driven by the previously activated transcription factors NFkB, STAT3, and C/EBP (Michalopoulos 2017).

As discussed earlier, several extracellular signals affect hepatocytes very early after Phx. They all contribute in meaningful way to selected aspects of the regeneration process, and there is no single signaling pathway to date whose complete elimination is associated with a prolonged and complete failure of the regeneration response. However, based on their mode of action, extracellular signals can be divided into two main categories (**Fig. 2.15**).

HGF and ligands of EGFR can induce proliferation of hepatocytes when injected into nonoperated rodents, and they can also induce complete replication of hepatocytes in culture with serum-free, chemically defined media. In this sense, they are considered "complete mitogens" (Tao et al. 2017). On the other hand, many other signals (described below) have been discovered based on the observation that liver regeneration is delayed, although still completed several days later, in the absence of a particular signal. These

signals do not induce hepatocyte proliferation in animals *in vivo* or in hepatocytes in serum-free, chemically defined media. In this sense, they are considered "auxiliary mitogens". However, this term in no way diminishes their importance, as they control the precise timing of essential transcription factors associated with the initiation of hepatocyte proliferation (Michalopoulos 2013).

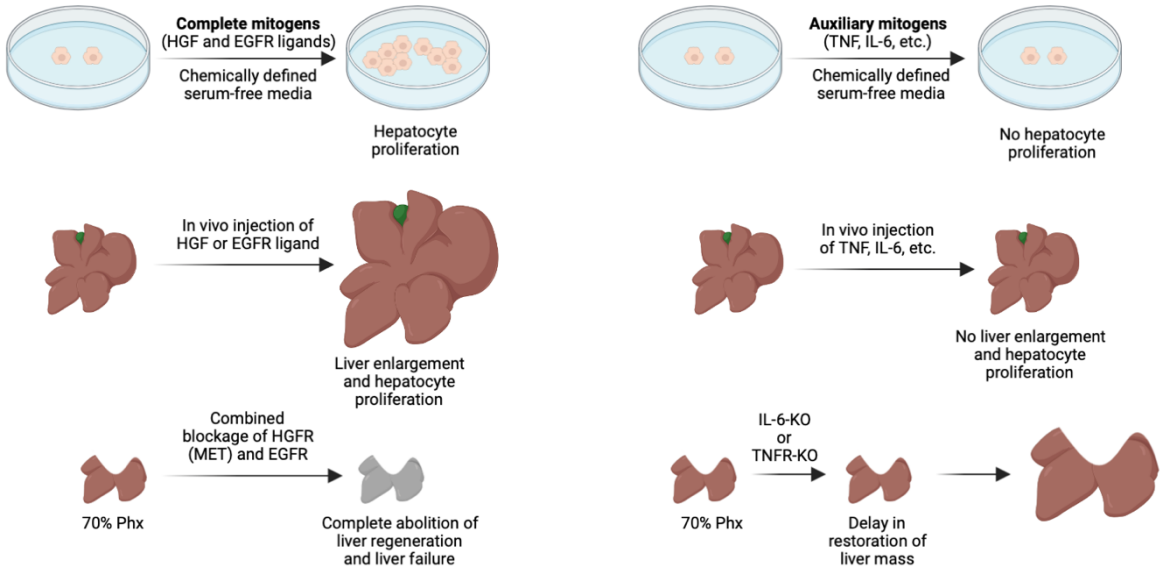

Figure 2.15 Extracellular signals involved in liver regeneration are classified according to their actions on hepatocytes and their overall effect on liver regeneration. Complete mitogens (hepatocyte growth factor (HGF) and epidermal growth factor receptor (EGFR) and its ligands stimulate proliferation. When both signalings are eliminated, liver regeneration is abolished. Auxiliary mitogens do not induce proliferation, but liver regeneration is delayed when their signals are inhibited (HGFR=HGF receptor; KO=Knockout; Phx=Partial hepatectomy; TNF=tumor necrosis factor; TNFR=TNF receptor) Adapted from *Michalopoulos et al., 2021*

Complete mitogens: receptor tyrosine kinases and their ligands

HGF and the EGFR ligand family are important growth factors that control cell cycle progression during liver regeneration. HGF is strongly embedded in the ECM of the liver; after Phx and ECM remodeling, HGF is activated by urokinase and released into the peripheral blood. Activation of its receptor MET and complete formation of the MET signalosome are detected within 30 minutes after Phx. A second wave of HGF synthesis begins in the liver 3 hours after Phx peaking at 24h, and it its synthesized by both HSCs and LSECs. EGFR is expressed in all hepatic cell types and its ligands relevant to liver regeneration are EGF, TGFalpha, heparin-binding EGF-like growth factor (HB-EGF) and amphiregulin (AR) (Nelson Fausto, Campbell, and Riehle 2006). Both MET and EGFR

are receptor tyrosine kinases. Their activation therefore leads to the activation of numerous intracellular signaling pathways that regulate a variety of transcription factors, initiate translation, and regulate metabolic pathways. For example, they are responsible for the activation of extracellular signal-regulated kinase 1/2 (ERK1/2), which correlates with DNA replication in hepatocytes and proliferation. In mice, knockdown of both signaling pathways completely disrupts liver regeneration (Paranjpe et al. 2016). There is no other extracellular signaling interruption that completely inhibits liver regeneration.

Auxiliary mitogens

As mentioned earlier, auxiliary mitogens orchestrate and optimize the timing and intensity of intracellular signals important for the control of hepatocyte proliferation and paracrine cell interactions. When their signaling is turned off, regeneration is delayed but not abrogated because alternative compensatory signaling pathways are activated.

a. TNF: produced by hepatic and spleen macrophages, increased rapidly after Phx. While it activates cell death pathways in many circumstances, it is also associated with enhancement of cell proliferation signals when its receptor interacts with cells that have already been stimulated to proliferate (Michalopoulos 2017). Mice lacking TNFR1 or 2 have delayed regeneration and decreased NF-kB activation (Yamada et al. 1998). Infusion of TNF does not induce cell proliferation, but as explained earlier, it "primes" hepatocytes to respond better to the mitogenic effects of HGF and EGF.
b. IL-6: produced by both hepatic macrophages and hepatocytes, also increases rapidly in the blood after Phx. In mice deficient in TNFR, the increase in IL-6 is lower (N Fausto 2000). In addition, mice lacking IL-6 have delayed liver regeneration due to insufficient activation of STAT3. However, regeneration is eventually completed, likely due to delayed activation of STAT3 by other ligands such as HGF and EGF (Runge et al. 1999).
c. Noradrenaline: produced by the terminal synapses of sympathetic neurons, adrenal medulla, and HSCs, increases to the same extent as HGF after Phx (Cruise et al. 1987). It has been shown to enhance the production of EGF and HGF, the mitogenic effects of EGFR and MET, transactivates STAT3, and suppresses hepatocyte mitoinhibition by Tgfb.
d. Bile acids: increase on day 2 after Phx and their depletion leads to decreased regeneration (W. Huang et al. 2006). The action of bile acids is mediated by the

transcription factor farnesoid X receptor (FXR). Indeed, FXR-deficient mice have increased mortality after Phx and delayed liver regeneration.

e. Insulin: although not a complete mitogen for hepatocytes, it is required for EGF and HGF action in hepatocyte cultures (Michalopoulos and Bhushan 2021). It is constantly supplied to the liver by the pancreatic islet b-cells via the portal circulation.

Complex mitogenic pathways

There are also more complex extracellular signals that control intracellular pathways that, when disrupted, delay but do not abolish regeneration. It has not been fully explored whether they can trigger liver regeneration in intact rodents.

a. Wnt/b-catenin: The Wnt/b-catenin signaling system plays an important in liver biology. Much of the involvement of Wnt family members in liver regeneration has been derived from the actions of beta-catenin, the major signaling molecule for Wnt actions. Migration of beta-catenin to the nuclei of hepatocytes is one of the first signals observed in liver regeneration. However, it should be noted that beta-catenin activation and migration are also in part mediated by MET and EGFR (Michalopoulos 2013).
b. Hedgehog: Members of the HH family appear to play important roles in hepatic metabolism, response to chronic injury, fatty liver, and HSC activation. Recently, inhibition of the HH pathway was shown to delay liver regeneration in the first 48 hours, with most mice dying within 72 hours.
c. TGF beta: The role of TGF beta in liver regeneration is intriguing. It is produced by HSCs and inhibits proliferation of hepatocytes in cell culture, but also increases their motility. Administration of TGF beta shortly after Phx delays liver regeneration (Russel et al. 1988). Remodeling of the ECM allows TGF beta to be released into the blood, removing it from the immediate periphery of hepatocytes before proliferation. However, Tgfbeta mRNA levels increase within 2-3 hours after Phx, and several studies suggest that MET and EGFR signaling trigger its induction. Interestingly, regenerating hepatocytes become resistant to the mitoinhibitory effects of TGF beta by downregulating its receptors and due to increased levels of norepinephrine. It should be noted that TGF beta stimulates the production of connective tissue proteins in fibroblasts and promotes the formation of capillaries by endothelial cells (Michalopoulos 2013). Because these functions are essential for the formation of

complete liver tissue, the presence of TGF beta at an early stage, when its receptor is still downregulated in hepatocytes, allows hepatocytes to continue proliferation while it is available to regulate other necessary functions for the formation of liver tissue.

2.3.1.1.4 Termination phase: hepatostat is achieved

The time of onset of liver regeneration is determined by the time Phx is performed. However, the timing of cessation of liver regeneration is difficult to determine. Hepatectomy studies suggest the existence of a homeostatic "hepatostat" system that controls tissue size for optimal performance (Michalopoulos 2017). Indeed, the liver can increase in size when the physiological needs of the body require it (e.g., pregnancy, childhood). Conversely, the liver decreases in size in situations where the body's metabolism changes or during disease (e.g., cachexia, chemotherapy, and chronic inflammation (Michalopoulos 2013). Therefore, in order to achieve hepatostat, it is important that liver regeneration is properly initiated after acute tissue loss and terminated at the correct liver size.

Wound healing is characterized by transient remodeling, de novo synthesis, and deposition of ECM, which, as explained earlier, releases latent cytokines (pro-HGF) and ensures repositioning of epithelial cells within the 3D histoarchitecture (Friedl and Gilmour 2009). Thus, as hepatocytes gradually adopt a quiescent phenotype, the ECM is restored. An important regulator of ECM restoration is the communication between hepatocytes and HSCs. This communication is regulated in part by integrin-linked kinase (ILK), a hepatocyte growth suppressor and regulator of hepatocyte differentiation (Gkretsi et al. 2008). In normal mouse liver regeneration, expression of ILK is increased when hepatocyte proliferation ends (5-7 days), and ILK-knockout mice have enlarged livers and excessive ECM. In addition, TGF beta inhibits hepatocyte proliferation in culture, but there is no clear relationship between TGF beta and the end of regeneration. Although it is expelled from the liver at the beginning of liver regeneration, it is resynthesized and restored at the end of regeneration by binding to decorin in the immediate vicinity of hepatocytes. Decorin itself has an inhibitory effect on both MET and EGFR, which may also play a role in termination of regeneration (Bagy, Iozzo, and Kovalszky 2012; Buraschi et al. 2010).

There is evidence that the number of hepatocytes produced at the end of regeneration exceeds that of the original liver and that a small wave of apoptosis occurs at the end of regeneration that corrects the final number, supporting hepatostat function.

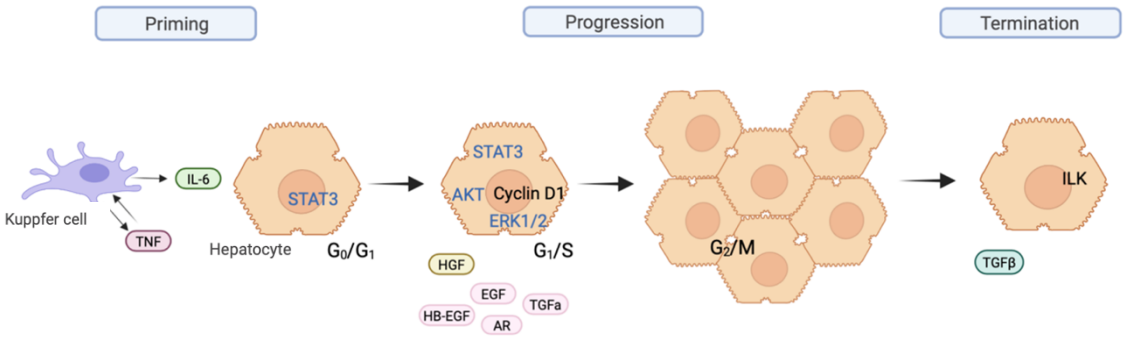

Figure 2.16 The three phases of liver regeneration. The innate immune system, especially the liver resident Kupffer cells and secreted cytokines such as tumor necrosis factor (TNF) and interleukin-6 (IL-6), play an important role in **initiating** liver regeneration after 70% partial hepatectomy (Phx). Hepatocytes primed by these agents readily respond to growth factors and enter the cell cycle in the **progression phase**. Finally, once the hepatostat is reached, **stop** signals such as transforming growth factor-beta (TGFb), are responsible for the decline in DNA synthesis (AKT=Protein kinase B; AR=amphiregulin; EGF=epidermal growth factor; ERK1/2=extracellular signal-regulated kinase 1/2; HB-EGF=heparin-binding EGF-like growth factor; HGF=hepatocyte growth factor; ILK=integrin-linked kinase; STAT3=signal transducer and transcription activator 3)

2.3.1.1.5 Alternative regenerative pathways

Regenerative activities in liver regeneration are characterized by phenotypic fidelity: Hepatic epithelial cells (hepatocytes and cholangiocytes) proliferate to form more of them. However, there are situations in which one of the two epithelial compartments cannot to regenerate. In such situations, alternative regenerative schemes are activated in which hepatocytes and cholangiocytes act as “facultative stem cells” for each other.

Hepatocytes and cholangiocytes are derived from embryonic hepatoblasts. In situations of liver regeneration in which hepatocyte proliferation is suppressed, cholangiocytes give rise to progenitor cells with hepatobiliary properties that gradually transform into hepatocytes. When cholangiocyte proliferation is suppressed, periportal hepatocytes transform into cholangiocytes in situ mimicking a similar transformation that occurs during embryonic development (Michalopoulos and Bhushan 2021).

Despite numerous studies searching for “stem cells” in the liver comparable to those observed in other organs, such cells have not been convincingly identified in the liver. Given the critical dependence of the entire body on liver function, liver regeneration appears to be a much faster and more efficient strategy than reliance on “stem cells”, which is a slower process.

2.3.1.1.6 Metabolic remodeling during liver regeneration

After Phx, the liver faces increased metabolic demands. It must continue to support the organism during the regenerative process while attempting to meet the energy demands for DNA replication and cell division (S. A. Mao, Glorioso, and Nyberg 2014). Therefore, coordinated regulation of metabolism and cell division during regeneration is a prerequisite for tissue recovery after injury (Locasale and Cantley 2011).

Several studies have suggested that metabolic changes after Phx may also be physiological determinants of liver regeneration (S. A. Mao, Glorioso, and Nyberg 2014; Verma et al. 2021). In short, changes in intermediate metabolism in response to hepatic insufficiency could provide essential signals for initiation of liver regeneration, and conversely restoration of metabolic homeostasis after hepatostatic recovery could also provide signals for termination (Rudnick and Davidson 2012).

Within hours of surgery, mice subjected to Phx develop significant hypoglycemia (J. Huang and Rudnick 2014; Weymann et al. 2009). This is probably due to the acute removal of two-thirds of the glycogen content and gluconeogenic capacity. The liver then induces the hepatic gluconeogenic machinery and suppresses its glycolytic activity to limit the decline in blood glucose levels after hepatectomy (Brinkmann et al. 1978). However, the physiological importance of hypoglycemia is underscored by the fact that dextrose supplementation suppresses both Phx and toxin induced hepatocellular proliferation. Similarly, caloric restriction accelerates the onset of hepatocellular proliferation. Thus, the hypoglycemic response to hepatic insufficiency could trigger the signals that promote liver regeneration (Rudnick and Davidson 2012).

By 12 hours after surgery, hypoglycemia accelerates a systemic catabolic response characterized by a decrease in lean mass and adipose tissue and the subsequent increase in circulating and hepatic free FAs (Gazit et al. 2010). It has long been known that the early regenerating liver transiently develops steatosis after Phx, and several studies have

pointed to systemic catabolism as the primary source (Klingensmith and Mehendale 1982). Upregulation of genes involved in *de novo* lipogenesis, such as perilipin (Plin2), provokes lipid droplet formation, an energy source for replicating hepatocytes. Interestingly, liver regeneration is inhibited when hepatic lipid accumulation is pharmacologically or genetically suppressed (Verma et al. 2021). The stimulatory effects of lipids on liver regeneration can be partially explained by their enhanced hepatic utilization for the synthesis of phospholipids and cholesterol, and provision of energy during reparative processes, since b-oxidation of FAs serves as the major source of new ATP production in the regenerating liver (Rudnick and Davidson 2012; Solhi et al. 2021).

As regeneration progresses, these perturbations of hepatic and systemic metabolism resolve. For example, liver enzymes TG decline, and blood glucose levels and body mass normalize as hepatostat is completed (J. Huang et al. 2016).

Overall, the metabolic changes that occur in response to liver failure provide energy and macromolecular precursors necessary for regeneration and generate specific molecular signals that initiate regenerative hepatocellular proliferation.

Mitochondrial bioenergetics during liver regeneration

As explained earlier, liver regeneration is a highly energy-dependent process. After Phx, hepatocytes undergo the cell cycle, DNA replication, and protein synthesis, processes that require a large amount of energy (Alexandrino et al. 2018). Thus, liver regeneration is affected by the energy status of hepatocytes.

The required amount of energy is provided by oxidative phosphorylation of FAs in mitochondria. Caldez et al. observed that the transition from a quiescent state to a proliferative state is accompanied by an increase in the oxygen consumption rate (OCR). And that mitochondrial dysfunction not only reduces ATP production and increases oxidative stress, but also alters metabolism, reduces cell division, and increases liver injury after Phx (Caldez et al. 2018). The clinical aspects of how impaired mitochondrial bioenergetics affects liver regeneration and thus surgical outcomes of liver resection and transplantation are further discussed.

2.3.1.2 Regeneration after toxic injury

The toxin-based, pharmacologic, or hepatotoxic models are relatively easy to perform and have greater clinical relevance. However, these models also have several drawbacks such as lack of reproducibility, different regeneration responses depending on the dose and route of administration, animal species, age, and nutritional status (Verma et al. 2021). **Table 2.2** shows the commonly used drugs for liver injury and subsequent regeneration.

Table 2.2 Commonly used drugs for hepatotoxic/pharmacologic liver regeneration models. Adapted from *Verma et al. 2021* (CCl4=Carbon tetrachloride)

Drug/Hepatotoxin	Principal Cell Affected	Effect
Carbon tetrachloride	Hepatocytes	Cell membrane damage, dependent on lipid peroxidation by radicals produced due to metabolism of CCl4; acute liver injury that manifests itself in the form of centrilobular necrosis, followed by hepatocyte regeneration.
Thioacetamide	Hepatocytes	Acute liver damage by biotransformation into thioacetamide sulfoxide and sulfone causing centrilobular necrosis, followed by hepatocyte regeneration. Continued exposition induces hepatic cirrhosis.
Acetaminophen	Hepatocytes/Oval cells	Acute liver failure, due to formation of N-acetyl-benzoquinoneimine, resulting in centrilobular apoptosis and necrosis, activation of Kupffer cells, followed by hepatocyte regeneration. Exerts its effect only when present in excess and normal detoxifying pathways are saturated. Higher dose leads to oval cell activation.
D-Galactosamine	Hepatocytes/Oval cells	Acute liver injury by causing intracellular depletion of uridine nucleotides and consequent pan-lobular necrosis, followed by hepatocyte regeneration. Increased/repeated dose leads to activation of progenitor oval cells.
Ethanol	Hepatocytes/Oval cells	Damage due to hepatocyte steatosis and necrosis, but large variations seen among different studies due to mode and duration of administration. Causes weakened and delayed liver regeneration after Phx.

In clinical practice, liver regeneration after drug-induced liver injury is critical for recovery. Acetaminophen overdose is a major cause of acute liver failure in the Western world and therefore a particularly important DILI mouse model (Bhushan and Apte 2019). Hepatotoxics cause centrilobular liver necrosis and sterile inflammation when administered acutely. The extent of damage depends on the dose of the chemical. Shortly after hepatocyte necrosis, infiltration of the affected areas by polymorphonuclear leukocytes and macrophages occurs, resulting in elimination of the dead cells. Regeneration occurs by the hepatocytes of the unaffected areas of the lobule, restoring

the structural integrity of the lobule and repairing the injury (Michalopoulos and Bhushan 2021).

Most evidence suggests that the signaling pathways that act after Phx are also involved in this process. Similar to the Phx model, early dose-dependent activation of EGFR and MET, as well as expression of TNF/IL-6 and their downstream signaling via NF-kB and STAT3, occur after acetaminophen overdose in mice (Bhushan et al. 2014).

In contrast to the Phx model, where EGFR inhibition alone has little effect, EGFR inhibition following acetaminophen overdose nearly abrogates compensatory liver regeneration and increases mortality (Bhushan et al. 2017). The source of these signals could be the same as after Phx, but it is very likely that infiltrating macrophages also play a very important role.

Chronic administration of these chemicals results in prolonged and unrecovered hepatocyte death and subsequent activation of HSCs with deposition of an altered ECM, leading to fibrosis, extensive scarring, and eventually liver cirrhosis (S. L. Friedman 2008a).

2.3.2 Ischemia/Reperfusion Injury (IRI)

Ischemia/reperfusion injury (IRI) is an important cause of liver damage during surgical procedures such as hepatic resection and liver transplantation and is the major cause of graft dysfunction post- transplantation (Gracia-Sancho, Casillas-Ramírez, and Peralta 2015). During LT donor livers are exposed to two types of ischemia-mediated damage. After retrieval, donor livers are cold stored for transport and until the recipient's native livers are retrieved (cold ischemia). Such ex vivo preserved livers are then implanted (onset of warm ischemia) and the vasculature is reconstructed to initiate blood flow (cessation of warm ischemia) (Hirao, Nakamura, and Kupiec-Weglinski 2022).

Despite the clinical importance of IRI, the underlying mechanisms are only partially understood. In the initial phase of IRI, the ischemic insult exposes liver cells to oxygen deprivation, pH changes, and ATP depletion, which increases their dependence on

glycogen for energy. These events trigger production of ROS, increase intracellular calcium concentration, and promote organelle damage, leading to hepatic injury. Subsequent reperfusion is even more damaging, as it disturbs liver metabolism and elicits inflammatory cascades that exacerbate hepatocellular damage.

2.3.2.1 Cold vs Warm injury

Damage to the liver endothelium during cold preservation is the first factor leading to hepatic IRI. Indeed, LSECs have been recognized as early targets in liver transplantation after cold preservation (Peralta, Jiménez, and Gracia-Sancho 2013). Their phenotype is rapidly deregulated and activated after 6 hours of cold storage and is strongly apoptotic and proinflammatory. Cold stress downregulates Kruppel-like factor 2 (KLF2) in LSECs, leading to impairment of endothelial nitric oxide synthase (eNOS), thrombomodulin (TM), and nuclear factor erythroid 2-related factor (NRF2), resulting in poor graft microcirculation, platelet activation, vasoconstriction, oxidative stress, and activation of the innate immune system (Gracia-Sancho, Casillas-Ramírez, and Peralta 2015). In addition, rapid repopulation of LSEC is observed after transplantation, which is associated with upregulation of several pro-angiogenic and endothelial survival mechanisms.

The injury process that begins during hypothermia is subsequently favored by the rewarming process during graft implantation.

While LSECs are more sensitive to cold IRI, hepatocytes are particularly sensitive to warm hypoxia. A central mechanism underlying parenchymal injury is mitochondrial damage. Briefly, warm ischemia causes intracellular metabolic disturbances such as ATP depletion and increased anaerobic glycolysis, which elevates lactate production and alters pH homeostasis (Peralta, Jiménez, and Gracia-Sancho 2013). In addition, similar to cold IRI, Kupffer cells play a key role in warm IRI. They are a source of many pro-inflammatory mediators that promote neutrophil activation and recruitment (Jaeschke 1998).

2.3.2.2 Key mediators of the ischemic injury

Overall, microcirculatory failure, the inflammatory cascade, and mitochondrial dysfunction appear to be the three major mechanisms mediating the ischemic liver injury.

2.3.2.2.1 Microcirculatory failure

As explained earlier, LSEC damage after IRI is the first event in the development of graft failure. LSEC damage involves cell activation, apoptosis, and detachment, resulting in disruption of hepatic microcirculation.

KLF2 is a transcription factor predominantly expressed by the endothelial cell that induces the expression of vasodilator, antithrombotic, and anti-inflammatory genes (eg, eNOS and TM) and inhibits the expression of adhesion molecules (vascular cell adhesion molecule 1 (VCAM-1) and E-selectin), thereby maintaining a vasoprotective endothelial phenotype.

After IRI, oxygen deprivation in hepatocytes leads to ionic changes that impair cell volume regulation and result in LSEC swelling. This fact, together with the imbalance between the decreased bioavailability of NO and the increased levels of endothelin and thromboxane A2, contributes to the constriction of the sinusoidal lumen and, consequently, to microcirculatory dysfunction. Hide et al have shown that a brief period of warm ischemia is sufficient to increase intrahepatic vascular resistance and portal pressure and markedly decrease liver perfusion (Hide et al. 2016). The study conducted by Russo et al showed that the lack of hemodynamic stimulation during storage conditions is the most important detrimental factor for the above processes (Russo et al. 2012). Indeed, blood flow-induced shear stress maintains a vasoprotective endothelial phenotype due to the activation of KLF2, which mediates the transcription of several protective genes. Thus, blockade of blood inflow during the ischemic period decreases KLF2 expression and leads to loss of hepatic vasoprotection during reperfusion.

Different mechanisms for endothelial injury during cold (Russo et al. 2012) or warm (Hide et al. 2016) IRI have been described. However, the consequences are similar: downregulation of the KLF2 vasoprotective pathway, impaired vasodilatory capacity, and

endothelial activation, leading overall to increased hepatic vascular resistance and liver inflammation with significant leukocyte infiltration, oxidative stress, and cell death

2.3.2.2.2 Inflammation

IRI is also a local sterile inflammatory response driven by innate immunity. DAMPs released from injured liver cells initiate and maintain the noninfectious sterile inflammatory response. Subsequent reperfusion facilitates the leakage of DAMPs into the circulation, leading to activation of the innate immune system and robust hepatocellular injury. The immunological cascade includes activation of liver resident Kupffer cells and infiltration of circulating lymphocytes, neutrophils and monocytes. All in all, the liver, an immunologically quiescent milieu, becomes an inflamed organ during IRI.

Macrophages play a central role in the mechanism of IRI. They not only perceive the initial DAMPs to trigger inflammation and recruit host immune cells, but also contribute to the termination of the inflammatory response and homeostatic tissue repair. Neutrophil granulocytes are not only activated and infiltrate the liver, where they trigger local inflammation, but they also migrate into the bloodstream and, in cooperation with platelets, promote distal organ injury through neutrophil extracellular traps (NET) and associated thrombosis (Hirao, Nakamura, and Kupiec-Weglinski 2022).

Thus, the failure of the microcirculation is also closely related to the activation of the innate immune system. During infection, the ability of NETosis to block blood flow to or from damaged tissues could prevent the spread of DAMPs and pathogens to distant organs, thereby preventing distal injury. However, IRI-induced thrombosis by activated platelets and NET has the potential to cause disruption of sinusoidal microcirculation, leading to necrotic inflammation and further accelerating IRI (McDonald et al. 2017).

2.3.2.2.3 Mitochondrial dysfunction

Mitochondrial function is severely impaired by IRI. During the ischemic period, there is a shift from aerobic respiration to anaerobic glycolysis. However, the prolonged hypoxia leads to a shutdown of redox processes, a reduced capacity for ATP generation, and a parallel acidification of the cellular milieu as lactic acid and ketone bodies accumulate.

These processes lead to metabolic acidosis and alter pH homeostasis, further exacerbating enzymatic, organelle, and even cellular damage (Teodoro et al. 2022).

Together with the depletion of intracellular energy, hypoxic conditions favour the formation of ROS. Many studies have confirmed that microvascular and parenchymal damage are mainly caused by oxidative stress (S. Zhang et al. 2022). ROS alter mitochondrial dynamics (biogenesis, fission, fusion, and mitophagy), induce the formation of mPTP, and increase cytosolic Ca^{+2} levels, leading to overall mitochondrial reduction, increased oxidative stress and cell death, increasing morbidity and mortality.

2.3.2.3 Animal models

Numerous experimental animal models have been used in the field of warm (and cold) IRI injury. Clinical application of strategies developed on laboratory benches depends on the use of preclinical models that resemble as closely as possible the clinical condition in which the strategy is to be applied. As explained earlier, pathophysiological mechanisms differ according to the type of ischemia. Indeed, it should be taken into account that the extent and duration of ischemia, the type of liver undergoing IRI, and the presence of liver regeneration lead to differences in the mechanisms of hepatic IRI and, therefore, preclinical approaches must be carefully planned according to clinical application.

2.3.2.3.1 Preclinical normothermic ischemia

Normothermic ischemia may be complete or partial (70%). It is known that the extent of liver injury as well as hepatic IRI mechanisms, including restoration of blood flow and energy charge during reperfusion, depend on the extent of ischemia. The model of global liver ischemia with portal decompression ideally simulates the clinical situation of warm ischemia after the Pringle maneuver for liver resection and LT (Mendes-Braz et al. 2012). Partial hepatic ischemia was described by Yamauchi et al in 1982 and is induced by clamping the portal triad (hepatic artery, portal vein, and bile duct) that irrigates the medial and left lateral lobes with an atraumatic clamp (Yamauchi and B 1982). This model of 70% partial ischemia has been widely used in experimental studies of hepatic I/R (**Fig. 2.17**).

In addition to the extent, the duration of ischemia is also an important factor. Indeed, the severity of hepatocellular injury depends on the duration of ischemia. The objective of the study determines the appropriate duration. Short periods (up to 60 minutes) of warm ischemia result in reversible cell injury, with liver oxygen consumption returning to control levels when oxygen is reperfused after ischemia. Conversely, reperfusion after prolonged warm ischemia (more than 90 minutes) leads to irreversible cell damage. Sham or control mice must be included in these studies. The abdomen is opened during the ischemia period without manipulating the liver.

Importantly, reperfusion follows the initial ischemia phase. During reperfusion, two phases can be distinguished: an early phase (within 2-4 hours after reperfusion) characterized by the release of ROS and the production of inflammatory mediators, and a late phase (6-48 hours after reperfusion) in which inflammatory responses exacerbate liver injury through the infiltration of neutrophils and macrophages (Hide et al. 2016). Therefore, reperfusion time varies depending on the study of short- or long-term damage. Other factors such as age and degree of steatosis may also affect the outcome. Indeed, they exacerbate ischemic injury and will be described in more detail in the next section.

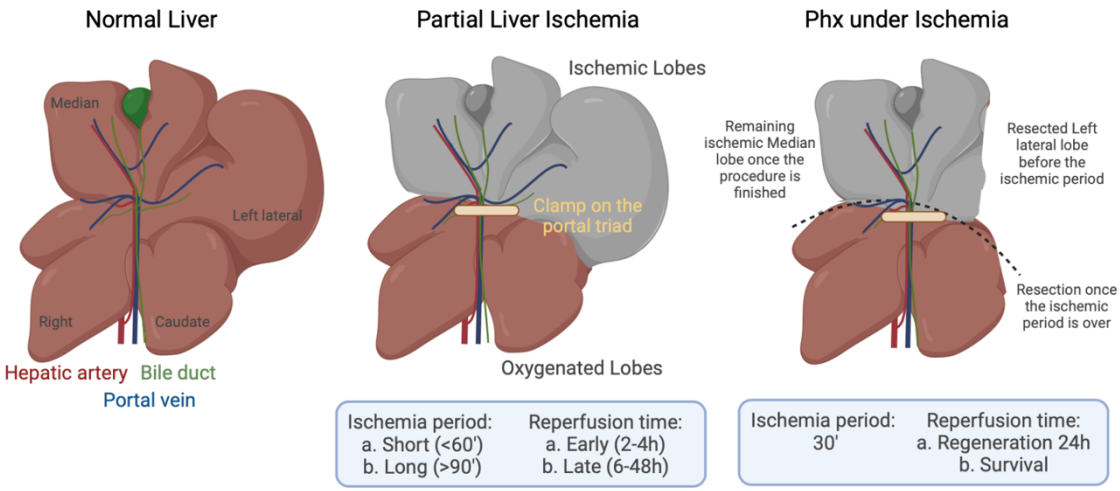

Figure 2.17 Partial liver ischemia and Partial hepatectomy under ischemia. The image on the left shows an schematic representation of murine liver anatomy. For partial liver ischemia (image on the center), the portal triad is clamped for a hort or long ischemic period, and then reperfused, obtaining ischemic and oxygenated lobes. For partial hepatectomy under ischemia (image on the right), the left lateral lobe is firsly resected previous the ischemic period. Then the portal trial is clamped for 30 minutes, and once the ischemic period is over, the right and caudate lobes will be resected. At the end just the ischemic median lobe will be obtained (Phx=partial hepatectomy)

In clinical situations, Phx under IRI is usually performed to control bleeding during parenchymal dissection. In the experimental model, after resection of the left lateral lobe, a microvascular clamp is placed over the portal triad supplying the median lobe (30% partial ischemic model). At the end of the ischemia time, the right lobe and the caudate lobe are resected, and reperfusion of the median lobe is achieved by releasing the clamp (**Fig. 2.17**). The ischemia time is usually 30 minutes because of the aggressiveness of this model. Indeed, the survival rate in 3-month-old c57/BL6 Wt mice is approximately 50%. The remnant is an ischemic lobe that must overcome the ischemic injury and limited regenerative capacity to reach the hepatostat. However, the ease of performance and good reproducibility make Phx under IRI a suitable preclinical model (M. Selzner, Camargo, and Clavien 2003).

2.3.2.3.2 Preclinical hypothermic ischemia

Preclinical hypothermic ischemia models are usually ex situ. Biberthaler et al developed an in situ model in which the temperature of the ischemic organ was adjusted to 4ºC or 37ºC by superfusion with 0.9% NaCl (Biberthaler et al. 2001). However, this model might suffer from some standardization problems and might not have good reproducibility.

In contrast, in the hypothermic ex situ ischemia model, livers are exsanguinated, flushed with cold preservation solution via the portal vein, and cold stored (4ºC) in the preservation solution for 1 to 24 hours, depending on the study (von Heesen et al. 2015; Russo et al. 2012). After cold storage, livers are exposed to room temperature for a short time to mimic the warm ischemia period and reperfused ex vivo via the portal vein with Krebs buffer (37ºC) (Russo et al. 2012). Sham or control livers (without cold storage) are perfused, rinsed with cold preservation solution, and immediately reperfused ex vivo.

2.3.3 Organ Shortage

The indications for liver transplantation have changed and expanded. Fewer patients are undergoing LT for hepatitis C virus (HCV)-related cirrhosis, and in the United States, Europe, and the United Kingdom, the need for LT is increasing primarily because of the rising incidence of NASH -related cirrhosis and cancer indications (Ivanics et al. 2021). These changing indications have the potential to exacerbate the existing imbalance between organ supply and demand.

Organ donors have also changed. In fact, eligibility is declining. First, life expectancy and obesity have increased in the general population, so older and steatotic liver donations are associated with comorbidities and graft failure. In addition, the ratio of donations after circulatory death (DCD) to donations after brain death (DBD) has increased, reducing the utilization of available organs due to the increased susceptibility of DCD to ischemic damage (Ivanics et al. 2021).

Despite the mismatch between organ need and availability, 8.4% of livers are discarded annually in the United States, and globally, the rate ranges from 3.4% in Argentina to 44.9% in Brazil (Kwong et al. 2021).

All of this leads to the high mortality on the LT waiting list, which averages 25% in most centers (Northup et al. 2015). Unfortunately, if the indications for LT continue to increase without a concomitant increase in the number of available organs, the mortality on the waiting list will continue to rise. Therefore, there is a clear need for strategies to increase the number of livers available for transplantation.

2.3.3.1 Strategies to increase the donor pool

Some strategies aimed at closing the gap between the number of patients who need a LT and the number who receive a transplant include policy changes. While they are outside our scope, examples such as the possibility of increasing donation by optimizing donor authorization or rethinking European policy to consider soft opt-out consent for organ donation are showing some improvements (Trapero-Marugán, Little, and Berenguer 2018).

Others depend more directly on a better understanding of the options available to increase the donor pool (**Table 2.3**). As noted earlier, the number of organs discarded because they are considered to be of suboptimal quality remains high. The most common reasons for discarding an available organ are advanced donor age, graft steatosis, and DCD because these organs are more susceptible to IRI. However, the use of organs from historically marginal donors has increased. The term "marginal organ" with negative labeling has

been replaced by the more appealing term "expanded criteria donor," and several strategies have been developed to address the shortage of much-needed organs.

Table 2.3 Challenges and solutions for suboptimal quality and size liver grafts Adapted from *Ivanics et al. 2020* (ATP= adenosine triphosphate; DBD=donation after brain death; DCD=donation after circulatory death; HCV=Hepatitis C virus; RNA= ribonucleic acid; SFSS= small for size syndrome)

Topic	Challenges	Solutions and future prospects
Older donors	Use of liver allografts from older donors is increasing High susceptibility to ischemic injury Associated with increased organ failure and biliary complications Acceleration of fibrosis in HCV-patients Mitochondrial dysfunction, reduced intracellular ATP and necrotic injury Impaired regenerative capacity	Careful patient selection Appropriate donor-recipient matching Prevent ischemic injury Alleviate mitochondrial dysfunction Enhance endogenous regenerative capacity
Steatotic grafts	Increasing number of steatotic grafts High susceptibility to cold preservation and ischemic injury Mitochondrial dysfunction Increased oxidative stress and inflammation Microcirculatory failure No reliable and consistent means to measure steatosis	Avoid high-risk clinical situations (prolonged cold ischemia, older donors) Appropriate donor-recipient matching New steatosis measuring tools Organ reconditioning Prevent ischemic injury Alleviate mitochondrial dysfunction Enhance endogenous regenerative capacity
Donation after cardiac death	Increasing proportion of DCD Compared to DBD, implies a period of warm IRI Substantial ATP depletion High susceptibility to ischemic injury Associated with graft dysfunction and biliary complications	Careful donor selection, avoiding further comorbidities Reduce prolonged cold ischemic preservation Prevent ischemic injury Alleviate mitochondrial dysfunction Enhance endogenous regenerative capacity
HCV-positive grafts	Increasing number of HCV positive livers Not much information	Careful donor selection (positive for HCV antibodies but not HCV RNA) Appropriate matching Use of antiviral eradication Organ reconditioning
Living donation and split liver transplantation	Alternative to increase the organ pool Suboptimal size Challenged regenerative capacity Small for size syndrome (SFSS)	Discriminatory donor and receptor selection Reduce prolonged cold ischemic preservation Appropriate donor-recipient matching Alleviate mitochondrial dysfunction Enhance endogenous regenerative capacity

2.3.3.1.1 Organs with suboptimal quality

Older donors

The use of liver grafts from older donors has increased in recent years due to increased life expectancy (Dicker et al. 2018) and the prevailing organ shortage. Donor age is not limited, but early reports of older donors (> 65) showed a higher risk of early mortality and graft nonfunction compared with young donors (Detre et al. 1995), so age has been included in most liver transplant risk indices. However, the impact of donor age on LT outcome is complex because of associated comorbidities.

Morphologic changes in the ageing liver have been described, particularly after the age of 50 years, including a progressive decline in cell number due to a decreased regenerative capacity, and microcirculatory changes (Fiel et al. 2011). In addition, ageing is associated

with a number of decreased mitochondrial functions. Compared with young donors, impaired energy metabolism leads to decreased ATP production and increased formation of ROS, which exacerbates the inflammatory response. All of this aggravates ischemic injury (Seizner et al. 2007).

However, because liver cells are in a compensatory state of hyperfunction, relatively well-preserved functions have been described in livers from older donors (Furrer et al. 2011). Furthermore, recent evidence suggests that the new environment in which the liver graft is placed may be of greater importance than the age of the graft cells themselves. This suggests that careful matching between donor and recipient, along with proper donor selection that excludes those with additional risk factors for poor graft outcome, could lead to better outcomes.

All in all, transplants from older donors are a safe option for expanding donor selection when considered in the context of other donor and recipient variables. Strategies aimed at reducing ischemic injury, alleviating mitochondrial dysfunction, and improving regenerative capacity may be of further help.

Steatotic grafts

The obesity epidemic is expected to further increase the proportion of steatotic grafts. As with aged livers, steatotic livers are particularly susceptible to IRI, oxidative stress, and biliary complications, which increases the risk of graft dysfunction. The increased susceptibility is related to mitochondrial dysfunction and reduced microcirculation due to sinusoidal vasoconstriction. After cold ischemia, steatotic livers are ATP-depleted due to OXPHOS impairment, which induces irreversible hepatocellular necrosis (Tashiro et al. 2014). In addition, hepatic steatosis reduces regenerative capacity (Truant et al. 2013; Veteläinen, van Vliet, and van Gulik 2007).

Hepatic steatosis is the accumulation of lipid droplets in hepatocytes. In most cases, both macrosteatosis and microsteatosis are present in varying degrees in steatotic livers. Depending on the percentage of fat content, steatosis is classified as mild (< 30%), moderate (30-60%), or severe (> 60%). Macrosteatosis was originally recognized as a risk factor for primary graft dysfunction, with more severe steatosis being associated with

worse outcomes (Chu et al. 2015). Therefore, the consensus is that severely steatotic grafts should be avoided, grafts with mild steatosis should be accepted, and grafts with moderate steatosis should be evaluated in conjunction with other risk factors. However, a combination of risk factors rather than a single factor appears to influence the outcome of LT with a steatotic graft. Indeed, Zheng et al reported good survival rates with the use of highly steatotic grafts despite initial complications (D. Zheng et al. 2017).

Again, the use of steatotic livers depends on the context. Avoiding high-risk clinical situations, such as a long cold ischemia period and older donors, could ensure positive outcomes. To improve donor-recipient matching, the degree of steatosis must be adequately assessed. Currently, there are no reliable and consistent means to measure steatosis because biopsy is not standardized and depends on the retrieving surgeon. In addition, organ reconditioning, which would allow less ischemic injury and improved liver regeneration, may be a promising approach to increase the use of steatotic grafts for LT.

Donation after circulatory death

Most deceased donor organs come from patients declared dead by neurological criteria, which is knows as donation after brain death (DBD). However, the shortage of organs for transplantation and technical developments leading to better outcomes after transplantation have led to a renewed interest in donation after circulatory death (DCD) (Miñambres et al. 2018).

Compared to DBD, DCD necessarily implies a period of warm IRI that lies between circulatory arrest and cold flush and results in substantial ATP depletion prior to cooling. Altered intracellular bioenergetics increase susceptibility to ischemia and reduce regenerative capacity. Therefore, DCD donors are considered to have extended criteria for LT, as the risk of IRI leading to graft dysfunction and biliary complications is higher than DBD donors (Foley et al. 2011).

Machine perfusion during organ preservation, discussed in detail in the next section, allows reconditioning of DCD organs. Interestingly, the use of DCD organs continues to

increase and is recognized as a potential source of transplantable organs that has not yet been fully exploited.

Grafts from donors with active hepatitis C virus infection

Another strategy to reduce the gap between the number of donors and recipients is to use grafts from donors positive for HCV. This strategy is similar to strategies used in the past with grafts from donors positive for cytomegalovirus and Epstein-Barr virus (Ramanan and Razonable 2013) and more recently with grafts from patients positive for hepatitis B virus core antibodies (Huprikar et al. 2015).

Eradication of HCV is now feasible with new oral antivirals. In this sense, the use of organs from donors positive for HCV antibodies provides a unique opportunity to expand the donor pool. Of note, the number of donations from deceased LT donors, particularly deceased HCV-seropositive and intravenous drug users, has increased by 20% in the past 5 years. In fact, the opioid crisis in the United States has led to a substantial increase in the retrieval of organs from HCV-positive donors. These organs come from young people who are otherwise healthy and normally considered ideal donors. With the development of highly effective antiviral agents, the use of these grafts is expected to increase (Trapero-Marugán, Little, and Berenguer 2018).

2.3.3.1.2 Organs with suboptimal size

Living donor liver transplantation and split liver transplantation are considered donations with grafts of suboptimal size.

Living donation has successfully increased the overall number of liver transplants in Asian countries where cultural factors significantly limit DCDs (Trapero-Marugán, Little, and Berenguer 2018). Split liver transplantation was developed in the 1980s as a potential solution to the severe shortage of size-matched pediatric whole organs. In practice, a liver from a single deceased donor is split between two recipients. Usually, a smaller left side segment is used for children and a larger right trisegment for adults. Although split liver transplantation has been shown to be a safe alternative in young children, several authors have estimated the adjusted risk of graft failure in adult recipients to be 1.5-2-5-fold that in whole liver recipients (Cauley, Vakili, and Fullington 2016).

Discriminate donor and recipient selection and specific surgical skills appear to be the most important success factors. Donor age should be limited, as should additional comorbidities such as macrosteatosis, inflammation, and fibrosis. Minimizing cold ischemia times also ensures good graft quality. Selection and matching of suitable recipients, especially adults, is the next important step. Adults of short stature, small stature, and with minimal portal hypertension are considered ideal candidates (Trapero-Marugán, Little, and Berenguer 2018).

Both procedures rely on regeneration of the donor graft to achieve the correct liver mass. When regeneration fails in these cases, small-for-size syndrome (SFSS) can occur, resulting in poor or delayed graft function, prolonged stays in the intensive care unit, occasionally the need for repeat transplantation, or eventually even death of the recipient (Forbes and Newsome 2016). However, this serious condition occurs very rarely.

Despite significant improvements, there is still a large discrepancy between the potential and actual number of grafts of suboptimal size. Although the outcomes of living donation are equivalent to those of DCD, the total number of liver transplants in the United States or Europe performed with organs from living donors remains relatively small (about 5% of all transplants) (Goldberg et al. 2014). It is likely that split liver transplants account for between 1% and about 10% of all liver transplants, with similar graft survival rates compared with whole liver transplantation (Wan et al. 2015).

The solution may be to improve donor selection and donor-recipient match, increase regenerative capacity, and reduce ischemic damage.

2.3.3.2 Strategies to improve the quality of extended criteria donation

As observed, preventing or alleviating ischemic injury and improving endogenous liver regeneration are the key measures to recondition and enhance the use of extended criteria organs in order to strengthen the current donor pool.

2.3.3.2.1 Strategies to alleviate IRI

IRI refers to a cascade of cellular damage resulting from the combination of anaerobic metabolism (ATP-depletion, ROS overproduction) and reperfusion (metabolic dysfunction, activation of proinflammatory signaling pathways) and, as discussed earlier, is closely related to an increased incidence of delayed graft function and primary graft nonfunction. Attenuation of IRI is critical for LT and surgery, especially for grafts with extended criteria, such as old, steatotic, or DCD organs, because they are more susceptible to ischemic damage (de Rougemont, Lehmann, and Clavien 2009).

In the next section, protective surgical and pharmacological strategies are described (**Table 2.4**).

Table 2.4 Surgical and pharmacological strategies to alleviate ischemia reperfusion injury (IRI)

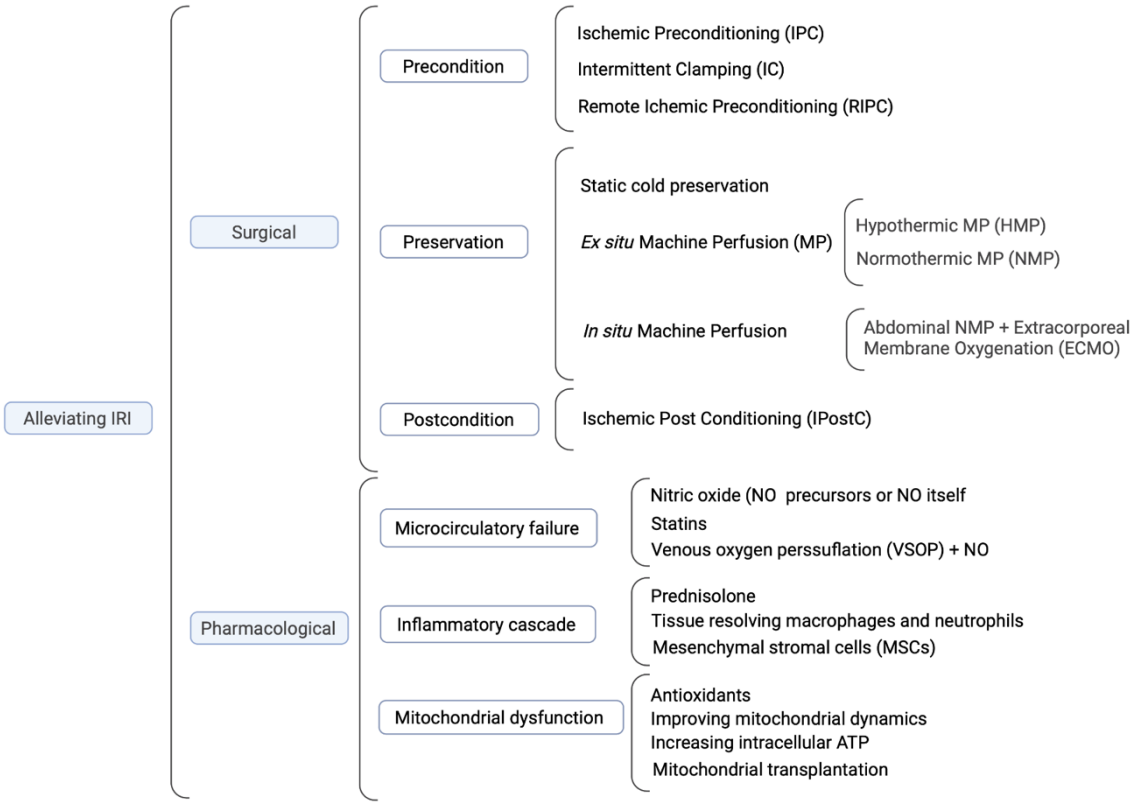

Surgical and machine perfusion-based strategies

There are three phases at which the surgeon can intervene. First, the donor or patient can be preconditioned before surgery. Second, a harvested organ can be stored under

optimized conditions. Finally, reperfusion injury in the recipient or patient can be attenuated after surgery (de Rougemont, Lehmann, and Clavien 2009).

Preconditioning

Strategies in the preconditioning phase are mostly based on so-called "damage priming," i.e., inducing minor damage through mild, brief, controlled events in which blood flow is removed and restored.

a. Ischemic Preconditioning

Ischemic preconditioning (IPC) is a short-term ischemia usually triggered by clamping of the portal triad, followed by a brief reperfusion before an expected prolonged ischemic phase (X. L. Mao et al. 2022). Numerous experimental studies in animals have provided compelling preclinical evidence that IPC can significantly improve hepatocyte survival and reduce the severity of hepatic IRI.

In general, IPC improves liver IRI and restores ATP levels and mitochondrial function. On the one hand, mitochondria damaged during IPC could be identified and removed by mitodynamic processes and replaced by newer and more competent mitochondria, contributing to cell resistance. This is referred to as mitohormesis (Teodoro et al. 2022). On the other hand, a slight increase in oxidative stress during IPC may trigger cellular adaptation by decreasing ATP synthase activity, thereby increasing tolerance to mPTP and maintaining ATP levels during IRI. In addition, the increased expression of heme oxygenase-1 (HO -1) after IPC may indicate that enhanced autophagy also maintains mitochondrial function (X. L. Mao et al. 2022).

Inflammation is another important process during ischemic injury. The protective effect of IPC may also be related to its anti-inflammatory effect. T-cell immunoglobulin and mucin domain molecule-4 (TIM4) is mainly expressed in mature dendritic cells and macrophages and is necessary for macrophage migration, phagocytosis, and activation of pathological processes during IRI (H. Ji et al. 2014). Zhang et al. found that IRI significantly increased the expression of TIM4, whereas IPC decreased it, suggesting that inhibition of TIM4 may be another potential therapeutic strategy for IPC to minimize IRI (Y. Zhang et al. 2018).

As for extended criteria organs, IPC protects steatotic livers by maintaining energy homeostasis. Selzner et al showed that IPC protects steatotic livers from IRI-induced necrosis by preserving and restoring tissue ATP content (N. Selzner et al. 2003). Conversely, although IPC is highly protective against reperfusion injury in young mice, it is an ineffective strategy in old mice. Selzner et al. even observed increased necrotic injury after preconditioning. Older livers have dramatically decreased ATP levels, and the additional ischemia time during preconditioning could cause a further decrease, leading to the increased necrosis. Interestingly, Selzner et al have shown that restoration of intrahepatic ATP levels by administration of glucose before surgery improved reperfusion injury and restored the protective effect of IPC (Seizner et al. 2007).

Nevertheless, there are criticisms of the efficacy of this approach, as some meta-analyzes have concluded that IPC does not always guarantee alleviation of ischemic injury because of the heterogeneity of the patients studied. In addition, the optimal protocol, particularly with respect to ischemic intervals, remains poorly understood. Current methods for performing IPC mainly include 5 minutes of ischemia/10 minutes of reperfusion and 10/10; however, Lin et al. recently compared several pretreatment protocols in a rat IRI model to determine the optimal IPC protocol and found that 5/5, repeated three times, provided the best protection against IRI (J. Lin et al. 2020).

Given the above results, the use of IPC in actual patients appears premature.

b. Intermittent Clamping

A similar surgical procedure to IPC is intermittent clamping (IC). The main difference is the number of cycles of occlusion and flow restoration and the timing of performance. Whereas IPC involves only one cycle before IRI by default, IC consists of multiple cycles of flow occlusion and restoration, and these are not limited to the period before IRI. Several studies have concluded that IPC is superior for shorter procedures because it improves transaminase levels and surgical complications, but for longer periods they are virtually the same procedure (Teodoro et al. 2022).

c. Remote Ischemic Preconditioning

Remote IPC (RIPC) is a rather peculiar phenomenon in which IRI events localized in distant organs lead to enhanced liver resistance to ischemic injury. While the release of protective elements is likely involved and may flow into the circulation, the protection of distant tissues, particularly mitochondrial function, is apparently necessary for the action of RIPC in the liver (E. K. Choi et al. 2020). Koh et al. showed that serum transaminases, hepatic expression of inflammatory cytokines, and apoptosis-associated genes were lower in IR mice treated with RIPC than in untreated mice (Koh et al. 2019).

However, conflicting results have been obtained in ongoing clinical trials. Qi et al. observed no improvements in transaminase levels or early allograft dysfunction in patients treated with RIPC (Qi et al. 2021), and a recent randomized clinical trial published in Ann Surg reported that RIPC was not associated with clinical improvements (Jung et al. 2020).

Preservation

From donor liver procurement to transplantation, liver grafts are in the phase of preservation and repair. Currently, there are two main strategies for organ preservation, namely static and dynamic.

a. Static Cold preservation

Static cold storage (SCS) consists in preserving organs at low temperatures (0-4ºC) to reduce metabolic activity and consequently cellular damage. Cold storage aims to delay the depletion of ATP levels and slow down the damaging processes associated with ischemia. Cold storage involves perfusing the organ with a cold solution and then storing it statically in a container filled with the cold solution until it is transplanted.

The composition of the preservation solution determines the quality and duration of graft preservation by preventing energy loss, acidosis, edema and oxidation, among other things. The University of Wisconsin (UW) solution, developed in the 1980s, is considered the gold standard for liver graft preservation solution. However, its high potassium concentration leads to cellular depolarization and vasoconstriction. In an attempt to

improve the preservation solution, the effect of different oncotic agents was investigated. The Institute Georges Lopez (IGL)-1 solution, characterized by high sodium and low potassium concentrations and the presence of polyethylene glycol 35 (PEG35) as an oncotic agent has shown beneficial effects compared to UW (Czigany et al. 2022). Liver grafts preserved in IGL-1 have been associated with better mitochondrial protection, reduced oxidative stress, and less inflammatory response, suggesting that PEG35 may be a critical agent for mitochondrial preservation (Bardallo et al. 2021). Indeed, addition of glutathione to PEG35 containing IGL solution (IGL-2) enhanced mitochondrial function and reduced ROS production in cold stored steatotic grafts (Bardallo et al. 2022).

To date, SCS is still the most commonly used method for liver preservation because it is simple and inexpensive. However, the low temperature and hypoxia of SCS have been reported to damage LSECs, resulting in delayed recovery or even loss of graft function.

b. Dynamic Organ Preservation or Machine Perfusion

In dynamic perfusion, the graft is continuously perfused with a preservative solution using a machine perfusion pump (MP). Continuous perfusion allows for better distribution of the preservative solution throughout the graft as well as washout of blood, continuous delivery of nutrients, and elimination of toxic metabolites, resulting in a better outcome (Czigany et al. 2020). In addition, this technique allows real-time monitoring of the functional and biochemical performance of the graft and, interestingly, the possibility of applying a pharmacological agent.

Mechanical perfusion devices are not a new technology but have rarely been used for organ preservation, mainly for logistical reasons. Nowadays, they are more portable and efficient and therefore represent a promising therapeutic strategy for graft preservation (Teodoro et al. 2022). Initial reports on MP have confirmed the safety and feasibility of the system in standardized criterion livers. However, evidence suggests that MP is most beneficial when applied to extended criteria livers.

There are several factors that can be modified during the process of MP, such as perfusion time, timing (continuous, preischemic, or endischemic), temperature (hypothermic, midthermic, subnormothermic, and normothermic), and oxygenation. In addition, the MP

strategies can be performed ex situ or in situ. The optimal conditions remain to be fully explored.

Ex situ MP strategies

The strategies described here are considered ex situ because the organ is harvested and placed in a chamber where it is continuously perfused (**Fig. 2.18**). To minimize ischemic insult, it is important to initiate organ protection quickly. Superfast surgery (SFS) has been the method of choice for many years and is the standard in most countries (Rubio Muñoz et al. 2022).

Hypothermic Machine Perfusion (HMP)

HMP (0-12ºC) combines hypothermia, which slows cellular metabolism and prevents ATP depletion, with a perfusate containing various metabolic substrates and other protective mediators that circulate through the donor organ and flush cytokines and toxins from the organ. It also allows monitoring by determining pump parameters and enzymes in the preservation solution (de Meijer, Fujiyoshi, and Porte 2019).

Hypothermic oxygenation perfusion (HOPE) seems to be the key to prevent IRI. The mechanism is to maintain mitochondrial integrity and function and reduce ROS HOPE formation. This combines the benefits of cold preservation conditions with active oxygenation of the perfusate so that the mitochondria of the graft are able to produce and restore ATP in similar amounts as before reperfusion (Schlegel et al. 2020). The cold preservation solution has typically been UW, although recent results support switching to IGL-1 or IGL-2 preservation solutions (Rosello et al. 2020).

Interestingly, drugs can also be added to the HOPE perfusate. Lin et al added a defatting cocktail to HOPE perfusate in a rat liver transplantation model, which was shown to improve steatotic liver graft and postoperative survival compared with HOPE alone (F. Lin et al. 2021).

However, there are two parameters for HOPE that have not yet been elucidated: the optimal perfusion pathway and the optimal level of oxygen delivery. Dutkowski et al have shown that HOPE treatment of DCD livers significantly reduced graft damage compared with matched cold-stored DCD livers. In addition, HOPE -perfused DCD livers achieved

similar outcomes to the group that received a DBD liver graft (Dutkowski et al. 2015), suggesting that a simple endischemic perfusion approach may help to expand the field for the safe use of DCD liver grafts.

Normothermic Machine Perfusion (NMP)

NMP (35-38ºC) uses a blood-based perfusate to preserve the liver under near-physiological conditions. Usually, normal function of the donor organ can be maintained for 3-19 hours. Numerous experimental studies have reported that NMP reduces the severity of hepatic IRI, possibly by maintaining physiological liver temperature and blood flow rate, regulating endothelial function, and replenishing ATP stores (Boteon et al. 2017). In addition, one clinical study showed that NMP successfully inhibited the proinflammatory response and promoted graft regeneration (Jassem et al. 2019), and others showed that NMP reduced both graft injury and organ shedding rate by 50% compared with SCS (Nasralla et al. 2018).

In addition, compared with HMP, NMP allows the generation of data to evaluate liver viability. Indeed, lactate, glucose, pH, and transaminases can be measured in the perfusate and glucose, bicarbonate, pH, and bilirubin in the bile (de Meijer, Fujiyoshi, and Porte 2019). Another unique property of NMP compared with HMP is that it allows ex vivo reconditioning during liver preservation. Reconditioning or improvement of liver graft quality before transplantation is based on the addition of defatting cocktails, anti-inflammatory drugs, mesenchymal stem cells (MSCs), or genetic therapies (C. Hu, Wu, and Li 2020; X. L. Mao et al. 2022; Thijssen et al. 2019).

Although NMP has the greatest potential to minimize the deleterious effects of cold ischemia, it is also more costly and logistically challenging than HMP and SCS. Namely, the technique requires a blood-based perfusate that may not always be available, and if the normothermic temperature changes, the quality of the liver is compromised and may not be suitable for subsequent transplantation (Trapero-Marugán, Little, and Berenguer 2018).

NMP is expected to expand the donor pool and improve the efficiency of expanded criteria organs by allowing reprocessing and modification of these grafts. Therefore, future studies should focus on donors with expanded criteria.

Prospects

Different approaches can also be combined. For example, a recently proposed solution to the logistical challenges is a so-called back-to-base approach, in which a liver is placed on NMP after a SCS phase required for transport to the recipient center. The combination of HOPE and NMP could also help mitigate oxidative stress and tissue inflammation and improve metabolic recovery (Ivanics et al. 2021).

In situ MP strategies

In contrast to superfast surgery, abdominal normothermic perfusion (ANRP) with extracorporeal membrane oxygenation (ECMO) has become an established alternative in Spain and is being used with increasing frequency (Rubio Muñoz et al. 2022).

Briefly, after cannulation of the donor femoral artery and vein, an aortic occlusion balloon is filled to prevent ascending flow and reperfusion of the heart and brain, and ECMO is initiated. Frequent analytical checks can be performed by measuring arterial gases, lactate, hematocrit and haemoglobin, ionogram, and liver and kidney profiles. Prior to abdominal organ retrieval, ECMO is interrupted, the arterial cannula is used for cold preservation fluid perfusion, and the venous cannula is used for exsanguination. The maximum duration of ANRP-ECMO is not yet established, but it is usually 1.5-2 hours.

Figure 2.1 Ex situ machine perfusion. The figure compares the protective mechanism of both hypothermic and normothermic machipe perfusion, together with temperature variations and potential viability tests of normothermic machine perfusion (NMP). Adapted from *de Mejier et al. 2019* (ATP=adenosine triphosphate; HMP=hypothermic machine perfusion; ROS=reactive oxygen species; O_2=oxygen)

ANRP-ECMO is considered the best strategy to shorten the duration of warm ischemia and alleviate the injury because it reverses metabolic changes, restores cellular physiology after energy deprivation, and eliminates metabolites produced by ischemic injury. In this way, preconditioning is used first as a backup for static cold preservation and then for warm ischemia of the recipient, thereby attenuating IRI (Rubio Muñoz et al. 2022).

Although this system is not yet available in many hospitals, the establishment of mobile ECMO teams has encouraged its use. Indeed, it is used in more than 50% of donors. Interestingly, Hessheimer et al. have recently shown that ANRP-ECMO allows the use

of older donors compared with SFS (Hessheimer et al. 2022). It has also shown positive results in moderately steatotic grafts, although it has not yet been used in severe grafts.

Postconditioning

Ischemic Post Conditioning (IPostC) is a novel approach to minimize IRI during liver surgery. In contrast to IPC, IPostC is defined as multiple short cycles of reperfusion and ischemia after prolonged ischemia, with controlled reperfusion preceding continuous reperfusion. This method produces virtually the same results as IPC without the time-consuming sequence of restriction/reperfusion events before surgery, which may be more practical because the onset of ischemia cannot always be predicted, and one may be in a hurry to start LT.

Pharmacological strategies

Since the pathophysiology of hepatic IRI involves multiple targets and mechanisms, several pharmacological interventions are currently being tested. As discussed earlier, there are three main mechanisms underlining ischemic injury (failure of microcirculation, inflammation, and mitochondrial dysfunction) that can be targeted. It should be noted that clinical trials with some of the next approaches are still pending, and most of them have not been used to treat grafts with extended criteria.

Attenuation of microcirculatory failure

Sinusoidal lumen narrowing, increased vascular resistance, and microcirculatory dysfunction occur at early stages of ischemic injury and are exacerbated in organs with extended criteria, such as steatotic grafts. Reduced bioavailability of NO plays a key role in the loss of vasoprotection during reperfusion.

The reduction in bioavailability of NO is explained by a combination of two factors: decreased synthesis due to reduced KLF2 expression and consequent eNOS activity and increased NO scavenging due to the large amount of oxidative radicals generated during reperfusion (Hide et al. 2016). Interestingly, de Rougemont et al. demonstrated the beneficial effects of inhalation of NO after LT, as it accelerated the recovery of liver functions (de Rougemont, Lehmann, and Clavien 2009). However, Kageyama et al. noted

that in vivo administration of NO after LT can cause vascular hyporeactivity and decompensation and suggested that NO should be restricted to liver grafts during storage (Kageyama et al. 2014).

Along these lines, Peralta et al. found that the addition of a NO donor to hepatic IRI attenuated both TNF and transaminase increases and that inhibition of NO synthesis during IPC resulted in an increased inflammatory response, underscoring the protective role of NO during preconditioning (Peralta et al. 1999). In addition, the addition of simvastatin to cold UW preservation solution (Russo et al. 2012) or administration in vivo 30 minutes before warm ischemia injury (Hide et al. 2016) has been shown to increase the production and bioavailability of NO in a KLF-2 manner, thereby attenuating microcirculatory failure. And the use of venous oxygen persufflation with NO gas (VSOP-NO) during dynamic hypothermic storage of DCD grafts has been shown to decrease portal vein pressure (Kageyama et al. 2014; Nebrig, Neuhaus, and Pascher 2014).

Inhibition of the inflammatory cascade

Prednisolone is a glucocorticoid steroid that has anti-inflammatory effects in liver resection and transplantation. A meta-analysis by Hai et al showed that perioperative administration of steroids in clinical liver resection can reduce overall complications, postoperative bilirubin levels, and inflammation (Hai et al. 2021). Kotsch et al. found in a prospective randomized clinical trial that treatment of the donor with intravenous prednisolone significantly decreased proinflammatory cytokines and adhesion molecules, alleviated IRI, and reduced acute rejection (Kotsch et al. 2008).

Macrophage activation and neutrophil infiltration are key events during the inflammatory response. However, global depletion of macrophages or neutrophils is not necessarily beneficial, as they play an important role in resolving inflammation and protecting immunocompromised transplant recipients. Indeed, global deletion of liver resident Kupffer cells exacerbated acute IRI in mice and delayed regeneration after Phx. As LT recipients are immunosuppressed, neutrophils represent the main weapon of host defense against pathogens, and therapies that limit their effector functions could increase the risk of life-threatening infections. Therefore, differentiating both cell populations into a

tissue-resolving phenotype may be a better strategy (Hirao, Nakamura, and Kupiec-Weglinski 2022).

Interestingly, mesenchymal stromal cell (MSC) therapy has gradually become a hot topic for promoting liver regeneration and repairing liver injury in various liver diseases, as MSCs have been reported to migrate into injured tissues, undergo hepatogenic differentiation, inhibit the release of inflammatory factors, and promote the proliferation of liver cells in vivo. Acute rejection after LT is usually treated with high doses of immunosuppressants, which have severe toxicity and side effects. In this regard, immunomodulatory cell therapy with MSCs may be a suitable approach to complement standard pharmacotherapy in LT recipients (Shi et al. 2017). Indeed, MSCs exert immunoregulatory effects via cell-cell contacts and secretion of anti-inflammatory factors that inhibit liver inflammation, prolong allograft survival, and reduce the side effects of LT (C. Hu, Wu, and Li 2020).

Prevention of mitochondrial dysfunction and oxidative stress

Mitochondrial dysfunction is the cause of ischemic injury, and preservation or restoration of mitochondrial function is a key indicator of successful organ recovery (Teodoro et al. 2022). Increased susceptibility of grafts with extended criteria for ischemic injury is related to the reduced ability of the liver to generate ATP and subsequent necrotic cell death.

Melatonin and N-acetylcysteine (NAC) protect the liver from ischemic injury through their antioxidant effects. Melatonin may act directly as a free radical scavenger or indirectly by upregulating the expression of various antioxidant enzymes. Importantly, melatonin attenuates liver IRI by maintaining mitochondrial membrane stability, promoting ATP synthesis in the liver, and improving liver function in preclinical models of cold storage (C. Hu et al. 2021; Ma et al. 2017). NAC, on the other hand, a glutathione precursor, reduces apoptosis, attenuates ROS induced ER stress, and inhibits activation of the inflammatory response via TLRs signaling, thereby reducing the incidence of graft dysfunction and improving liver function in clinical studies (Ntamo et al. 2022).

Targeting mitochondrial dynamics by improving biogenesis and mitophagy or increasing

cellular NAD^+ pools by using NAD^+ precursors such as nicotinamide riboside (NR) and nicotinamide mononucleotide (NMN) are other plausible strategies to improve mitochondrial quality and increase respiration along with ATP production (Teodoro). Indeed, Selzner et al improved intrahepatic ATP content in aged mice by preoperative injection of glucose, which protected against reperfusion injury and restored the protective effect of IPC, resulting in additive protection when both strategies were combined (Seizner et al. 2007).

Finally, mitochondrial transplantation is a novel technique to improve mitochondrial function. In a recently published study, Rousselle et al. intravenously administered mitochondria isolated from healthy mouse livers to living mice 1 day before LT. Hepatocellular mitochondrial uptake was demonstrated and was associated with higher ATP levels, oxygen consumption, improved histology, and higher levels of energy metabolism-enhancing genes. Interestingly, diet induced obese mice were also subjected to mitochondrial transplantation previous to LT and showed reduced steatosis when compared to vehicle treated (Rousselle et al. 2020).

2.3.3.2.2 Strategies to enhance the regenerative capacity

Liver regeneration is a robust, well-orchestrated, but not infallible process. Regenerative capacity may be impaired in certain contexts, such as extended criteria organs or after ischemic injury (M. Selzner, Camargo, and Clavien 1999), and it may require additional support in living donor and split liver transplantation when graft size is suboptimal.

Strategies to enhance liver regeneration include removal of deleterious agents (such as HCV, alcohol, inadequate nutrition), reconditioning of damaged tissue (e.g., defatting agents, reduction or resolution of fibrosis, alleviation of ischemic injury), and direct stimulation of hepatocyte proliferation (Forbes and Newsome 2016).

The next section focuses on reconditioning and direct stimulation of endogenous regenerative capacity, primarily through the targeted use of mitochondria.

Regenerative capacity is a highly energy-consuming chain of events and depends on the energy status of hepatocytes. Thus, reversing mitochondrial dysfunction in organs with

expanded criteria would not only ameliorate ischemic damage but also overcome regenerative limitations and allow for improved graft function (Alexandrino et al. 2018).

Indeed, Alexandrino et al. found "a direct relationship between mitochondrial bioenergetics and postoperative outcome after liver surgery." Their study showed that decreased oxidative phosphorylation correlated with poorer postoperative synthetic and excretory function of the liver, and that mitochondrial dysfunction was associated with an increased risk of post-hepatectomy liver failure (PHFL), which is an independent risk factor for liver-specific morbidity (Alexandrino et al 2016).

S-adenosyl-L-methionine (SAMe) is a methyl donor and a precursor of glutathione that can enhance mitochondrial respiration and OXPHOS while reducing mitochondrial ROS. Its protective effects have been described in chronic ethanol exposure, DILI, and IRI in preclinical models (Bailey et al. 2006; Brown et al. 2014; Jeun and Lee 2001). Two randomized trials have shown that liver injury in patients undergoing resection of cirrhotic HCC decreased slightly after the use of SAMe as pharmacological conditioning, although no mechanistic study linked the effect to improvement in mitochondrial respiration and OXPHOS (Liu et al. 2014; Su et al. 2013). Augmenter of liver regeneration (ALR) is another candidate due to its potent mitogenic effect, which seems to depend on its effect on mitochondrial biogenesis (Han et al. 2015). Indeed, transfection of ALR in rodent models of IRI and DILI showed improvement in OXPHOS, ATP production, and overall survival (Weng et al. 2017). In addition, selective removal of damaged mitochondria by promoting mitophagy also improves energetic efficiency and reduces oxidative stress, which improves regeneration and survival in a rodent model of 90% Phx (Lin et al. 2015).

There are other several strategies aimed at enhancing the endogenous hepatic regenerative capacity. These include growth factors (J. S. Choi et al. 2019; Forbes and Newsome 2016), metabolism (Fan et al. 2022; Solhi et al. 2021), inflammation (C. Hu, Wu, and Li 2020; S. M. Lee et al. 2021) or even tissue engineering (H. Hu et al. 2018; Messina et al. 2020; Nadi et al. 2020; J. Wang et al. 2022) that have been extensively reviewed.

2.4 METHYLATION CONTROLLED-J PROTEIN (MCJ)

We have already explained that mitochondria are essential organelles for eukaryotic cells because of their role in controlling cellular metabolism and that they generate ATP through OXPHOS within the respiratory chain. In this sense, tissues with high metabolism, such as heart, liver, skeletal muscle or kidney, have a greater content of mitochondria. We have also described the mitochondrial quality control mechanisms that maintain mitochondrial function under physiological conditions, such as the balance between biogenesis and autophagy that mediates periodic (approximately 17 days) turnover of the organelle (Gottlieb and Gustafsson 2011).

However, there are other mechanisms that contribute to the regulation of ETC according to metabolic needs or in response to acute or chronic metabolic changes. Fasting, caloric restriction, obesity, hyperglycemia, hypercholesterolemia, and hypoxia are some of the metabolic changes that may affect mitochondrial function (Hatle et al. 2013).

Since high turnover of mitochondria can affect cell longevity, the presence of alternative mechanisms that can rapidly regulate mitochondrial respiration would be beneficial to cells (Hatle). Several molecules that are not intrinsic components of the respiratory chain have been found to contribute positively to the activity of ETC complexes (e.g., STAT3, Rcf1, and GRIM -19) (Tammineni et al. 2013). Less is known about the presence of inhibitory mechanisms for the regulation of ETC.

Methylation-controlled J protein (MCJ) or DnaJC15, a member of the DnaJC family of chaperones, is an endogenous negative regulator of the mitochondrial respiratory chain (Hatle et al. 2013). MCJ is a small protein of 147 amino acids (aa) with features that distinguish it from other members of the DnaJC family. While most are soluble proteins, MCJ contains a transmembrane domain and has a unique N-terminal domain that does not share significant sequence similarity with other known proteins (Champagne et al. 2016). It was first discovered in human ovarian cancer cell lines, where MCJ gene expression was found to be negatively regulated by CpG island methylation (Shridhar et al. 2001; G Strathdee et al. 2004).

MCJ localizes to the inner mitochondrial membrane, where it interacts and negatively regulates complex I activity, leading to disruption of the respirasomes and reduction in ATP synthesis (Hatle et al. 2013; Schusdziarra et al. 2013). Although dispensable under normal physiological conditions, its absence leads to increased complex I activity and ATP synthesis and stimulates the formation of respiratory supercomplexes, limiting the production of ROS, as they facilitate the efficient transfer of electrons and minimize the risk of "electron leak" that leads to oxidative stress (Acín-Pérez et al. 2008) (**Fig. 2.18**).

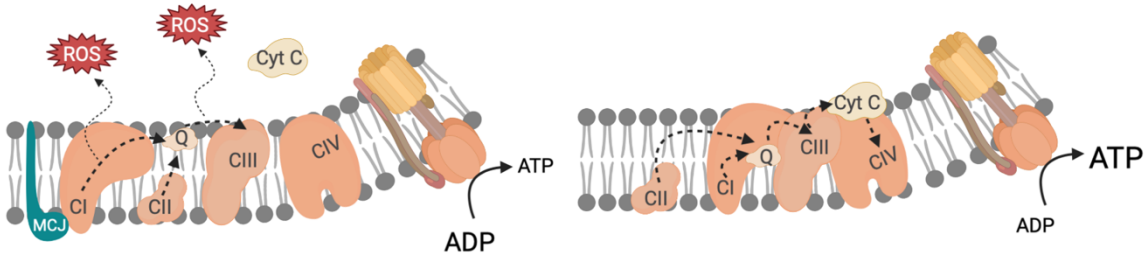

Figure 2.18 Methylation-controlled J protein (MCJ). The image on the left shows an schematic representation of the electron transport chain where MCJ interacts and inhibits the complex I activity. Reactive oxygen species (ROS) are produced consequently. The image on the right shows MCJ lacking ETC, formation of supercomplexes, absence of ROS and augmented adenosine triphosphate (ATP) production. Adapted from *Iruzubieta et al. 2021* (C=Complex; Cyt C=Cytocrhome C; Q=Coenzyme Q)

Regarding the expression of MCJ, it is expressed not only in human ovarian cancer cells but also in breast and uterine cancer cells, where it correlates with response to chemotherapy (Giddings et al. 2021). Within the immune system, MCJ is highly expressed in CD8 cells but not in CD4 and B cells (Hatle et al. 2013), and it is also expressed in macrophages, although to a lesser extent (Navasa et al. 2015). Interestingly, MCJ is found primarily in tissues with very active mitochondrial metabolism, including heart and liver (Barbier-Torres et al. 2017; Hatle et al. 2013).

Overall, MCJ, one of the first described endogenous negative regulators of complex I, is a potent inhibitor of mitochondrial metabolism. The next section describes its role in various cells and tissues and the therapeutic potential of regulating mitochondrial respiration by targeting MCJ.

2.4.1 MCJ associated chemoresistance

Several studies have shown that loss of MCJ expression in tumors correlates with chemotherapy resistance and poor prognosis in breast and ovarian cancer patients (Fernández-Cabezudo et al. 2016; Gordon Strathdee et al. 2005). Indeed, inhibition of MCJ expression in drug-sensitive breast cancer cell lines results in an increased 50% lethal dose (LD50) for certain chemotherapeutic agents (e.g., doxorubicin and paclitaxel) (Hatle et al. 2007).

The study by Giddings et al. uncovered the underlying mechanism between loss of MCJ and development of chemoresistance, focusing on drug-releasing ATP-binding cassette transporters (ABC). ABC Transporters use mitochondria-derived ATP as an energy source to deliver drugs out of cancer cells (Locher 2016). Giddings et al. examined the energy requirements of ABC transporters in the context of metabolic adaptations of chemoresistant cancer cells and found that loss of MCJ increases their ability to produce ATP and supply ABC transporters, which promotes drug efflux (Giddings et al. 2021)..

Interestingly, Giddings et al. have also developed MCJ mimetics that can attenuate mitochondrial respiration and safely overcome chemoresistance, both in vitro and in vivo. As mentioned earlier, the N-terminal region (35 aa) of MCJ does not show significant homology to other eukaryotic proteins. Therefore, they developed peptide mimetics of MCJ containing the first 20 aa of the N-terminus (N-MCJ). Unlike standard inhibitors of complex I (rotenone) or complex V (oligomycin), which completely block their activity, MCJ is an endogenous modulator that negatively regulates complex I activity. Like MCJ, N-MCJ mimetics do not completely block or reduce mitochondrial respiration in cells expressing endogenous MCJ, confirming the lack of toxicity of N-MCJ mimetics in these tissues or cells expressing MCJ (Giddings et al. 2021).

Overall, their results suggest that attenuating mitochondrial respiration by restoring MCJ in combination with standard chemotherapy may be an alternative therapeutic approach to increase sensitivity to chemotherapy in cancer cells that have lost MCJ.

In addition, Sinha et al. also investigated the role of MCJ in modulating cellular sensitivity to chemotherapeutic agents. Mitochondria play a central role in the intrinsic pathway of

apoptosis and involve the activation of multiple transmembrane channels that lead to the release of death factors (Gulbins, Dreschers, and Bock 2003). One of the major transporters activated during apoptotic stimuli is the mitochondrial mPTP. Sinha et al. found that MCJ modulates the activity of mPTP by recruiting cyclophilin D (CypD), an essential component of mPTP, and induces apoptosis by opening the channel. Thus, in the absence of MCJ, cancer cells show increased resistance to cell death and activation of the mPTP (Sinha and D'Silva 2014).

2.4.2 Expression of MCJ within the immune system

Metabolism is emerging as an important factor regulating immune cell function and differentiation and influencing the course of an immune response (Saravia et al. 2020). Indeed, naive, effector, and memory T cells have different metabolic profiles to provide the required energy and bioenergetic precursors. Switching metabolism from OXPHOS in naive and memory T cells to glycolysis in effector T cells is critical for their rapid proliferation and synthetic capacity (Secinaro et al. 2019). In this context, Champagne et al. found that MCJ tightly regulates mitochondrial respiration in CD8 T cells. Increased OXPHOS and ATP production caused by loss of MCJ increases cytokine secretion in CD8 effector cells. MCJ also serves to adjust effector CD8 T cell metabolism during the contraction phase, and consequently, memory CD8 cells lacking MCJ show enhanced protection against influenza virus infection (Champagne et al. 2016).

In attempting to understand the evolutionary reasons for MCJ expression in CD8 T cells, Champagne et al. suggest that although CD8 cells are key to protection, an exaggerated cytotoxic response could cause nonspecific tissue damage. Indeed, an effective adaptive immune response requires rapid proliferation of responding T cells followed by equally rapid cell death. Secinaro et al. observed that MCJ expression in CD8 T cells is closely associated with glycolysis and activation of caspase-3, which serves to prevent accumulation and promote timely death of highly proliferative CD8 T cells (Secinaro et al. 2019).

As for macrophages, mitochondria contribute to macrophage immune function through the generation of ROS, a mitochondrial byproduct (West et al. 2011). Navasa et al. found that MCJ is essential for the production of TNF by macrophages in response to a variety

of TLR ligands and bacteria. Interestingly, MCJ-deficient mice are resistant to the development of fulminant liver injury after administration of LPS because the absence of MCJ results in inhibition of TNF release from the plasma membrane (Navasa et al. 2015).

Therefore, MCJ provides a novel mechanism for fine-tuning mitochondrial metabolism in immune cells and thus regulating their activity.

2.4.3 MCJ and microbiota

The gut microbiota plays a key role in the physiological homeostasis of the intestine and in the pathophysiology of diseases such as inflammatory bowel disease (IBD) and ulcerative colitis (UC). Recent studies suggest an interplay between the gut microbiota and mitochondria of mucosal cells, including epithelial and immune cells. Altered mitochondrial metabolism and overproduction of ROS may affect gut composition, activate immune cells, and alter epithelial barrier function (Jackson and Theiss 2020).

Pascual-Itoiz et al. showed that MCJ deficiency disrupts the regulatory relationship between host mitochondria and the gut microbiota during UC and influences disease severity. They observed that induction of experimental colitis in MCJ-deficient mice leads to activation of the innate immune system, increased levels of proinflammatory cytokines, intestinal permeability, and dysbiosis characterized by proliferation of *Ruminococcus gnavus* (Pascual-Itoiz et al. 2020).

2.4.4 MCJ, liver metabolism and chronic liver diseases

Mitochondrial dysfunction plays a key role in the development of metabolic disorders (Bhatti, Bhatti, and Reddy 2017). Initial studies by Hatle et al. previously found that enhanced mitochondrial respiration in the absence of MCJ prevented pathological accumulation of lipids in the liver in response to both fasting and a high-cholesterol diet, and hypothesized that loss of MCJ expression might lead to a "fast" metabolism that mitigates the consequences of metabolic disorders. Furthermore, they proposed that the acquisition of MCJ in vertebrates may have been an evolutionary adaptive phenomenon to slow mitochondrial respiration in response to inadequate food intake and to prolong lipid reserve (Hatle et al. 2013).

Mitochondrial dysfunction is also associated with the pathogenesis of many acute and chronic liver diseases (Mansouri, Gattolliat, and Asselah 2018). However, alleviating mitochondrial dysfunction by improving respiration has not been widely considered due to the potential ROS overproduction.

NAFLD, considered the next major health epidemic with an estimated worldwide prevalence of 25%, is triggered by excessive accumulation of lipids in the liver due to an increased supply of FAs from adipose tissue, accompanied by an imbalance between lipid catabolism and de novo lipid synthesis (S. L. Friedman et al. 2018). Hepatic lipid catabolism is highly dependent on mitochondrial metabolism because FAs are degraded in the liver by b-oxidation in mitochondria. Barbier-Torres et al hypothesized that an increase in mitochondrial respiration in the liver might improve the degradation of FAs, thereby preventing their accumulation and disease progression. Indeed, liver-specific therapeutic targeting of MCJ improves the ability of hepatocytes to mediate b-oxidation of FAs and minimizes lipid accumulation without collateral oxidative stress, resulting in less hepatocyte damage and fibrosis (Barbier-Torres et al. 2020). Importantly, Barbier-Torres et al. used FDA-approved small-interfering RNA (siRNA) in the form of nanoparticles and N-Acetylgalactosamine (GalNAc) to efficiently target hepatic MCJ, laying the foundation for a direct, rapid, and already accessible therapeutic approach.

Mitochondrial dysfunction also contributes to APAP-induced liver injury (Ramachandran and Jaeschke 2019). It is estimated that more than 60 million people in the United States consume APAP weekly, and it is the leading cause of acute liver failure (ALF) in both the United States and Europe (Bernal and Wendon 2013). It is noteworthy that the timing of APAP intake is critical to treatment. Currently, treatment with the antioxidant NAC is the standard therapy, which has a 66% chance of saving the liver if administered within 8 hours of intoxication. In general, current therapeutic approaches provide very small time windows and low probabilities of saving the liver after acute failure. Therefore, approaches are needed to improve the prognosis of these patients (Smilkstein et al. 1988). Although the mechanisms underlying APAP-induced liver injury are not fully understood, mitochondrial dysfunction plays a key role. Barbier-Torres et al found that APAP impairs the formation of mitochondrial respiratory supercomplexes via MCJ, leading to decreased production of ATP and increased formation of ROS. Interestingly,

in vivo treatment with an inhibitor of MCJ expression protects the liver from APAP-induced liver injury at a time when NAC has no effect, because suppression of MCJ expression prevents APAP-mediated inhibition of complex I activity and ATP production and oxidative stress by maintaining supercomplex formation (Barbier-Torres et al. 2017).

Finally, during experimental cholestasis, a reduction in overall mitochondrial function was observed, associated with a decrease in oxidative metabolism and ATP synthesis and an overproduction of ROS (Arduini et al. 2012). Cholestasis, defined as any condition leading to hepatic retention and accumulation of potentially toxic bile acids (BAs), can eventually lead to cirrhosis, liver failure, and death (European Association for the Study of the Liver 2017). Primary biliary cholangitis (PBC) and primary sclerosing cholangitis (PSC) are the most common cholestatic CLDs, and there are few available therapies. Iruzubieta et al showed that the absence of MCJ in a mouse BDL model reduced neutrophil activation and prevented mitochondrial dysfunction, thereby attenuating cholestatic liver injury. In addition, loss of MCJ protected hepatocytes from ROS overproduction and ATP deprivation, resulting in reduced BA-induced hepatocyte death (Iruzubieta et al. 2021).

Up-regulated hepatic MCJ levels in patients suffering from NAFLD, NASH, ALF and cholestasis (Barbier-Torres et al. 2017, 2020; Iruzubieta et al. 2021) highlight the therapeutic applicability of MCJ silencing in the treatment of chronic liver disease.

3. HYPOTHESIS AND OBJECTIVES

3 HYPOTHESIS AND OBJECTIVES

The morbidity and mortality of chronic liver diseases (CLDs), and thus the global burden, are high and expected to continue to increase (Mokdad et al. 2016). Although viral infections such as hepatitis B and C are declining, alcohol abuse and NAFLD have emerged as important risk factors (Cheemerla and Balakrishnan 2021).Without appropriate therapy, CLDs can progress to cirrhosis and hepatocellular carcinoma (HCC) (Mishra and Younossi 2012; Riley and Bhatti 2001; Vernon, Baranova, and Younossi 2011), and liver transplantation (LT) may be the only curative treatment for these end-stage liver diseases. However, current rates cover less than 10% of the global need for organ transplantation (Asrani et al. 2019). These data highlight the window of opportunity to address the increasing prevalence of alcohol abuse and NAFLD and develop new strategies to improve transplantation rates before the global burden of liver disease becomes unsustainable.

Our group, the Liver Disease Laboratory, has broad expertise studying the mechanisms underlying the development and progression of CLDs in order to develop new therapeutic strategies. The search for treatments with a broad spectrum of activity has become our priority. As presented in this work, research is focused on mitochondrial dysfunction that leads to the development and progression of the disease. Considering that mitochondria perform many functions and are involved in a variety of activities, modulating mitochondrial dysfunction will have many implications.

In this context, methylation-controlled J protein (MCJ), also known as DnaJC15, is an endogenous negative regulator of mitochondrial activity that interacts with and inhibits the mitochondrial complex I (Hatle et al. 2013). Significantly elevated MCJ levels have been observed in patients with NAFLD, APAP-induced liver injury, and cholestatic liver disease (Barbier-Torres et al. 2017, 2020; Iruzubieta et al. 2021), and mitochondrial dysfunction is considered a key player in the development of these diseases. Moreover, we have previously shown that hepatic *Mcj* silencing improves mitochondrial activity, ATP production and reduces oxidative stress, thereby alleviating steatosis in NASH

(Barbier-Torres et al. 2020) and liver injury after both APAP-induced liver injury (Barbier-Torres et al. 2017) and cholestatic liver injury (Iruzubieta et al. 2021).

Excessive alcohol consumption is the leading cause of liver-related mortality in Western countries and represents the second most common indication for LT worldwide (Louvet and Mathurin 2015). The progression of ALD from alcoholic fatty liver to alcoholic steatohepatitis, alcoholic hepatitis, cirrhosis, and finally to HCC is well described, but there is no therapy that could halt or even reverse ALD progression (You and Arteel 2019). Alcohol metabolism is known to impair mitochondrial function. In fact, mitochondrial dysfunction is one of the earliest indicators of alcohol-related damage (Zhong et al. 2014).

Therefore, we hypothesized that MCJ might trigger the development and progression of ALD.

Moreover, we have focused on liver transplantation and the major complications it currently faces. Ischemia-reperfusion injury (IRI), the main cause of graft dysfunction after transplantation (Gracia-Sancho, Casillas-Ramírez, and Peralta 2015), and a shortage of donor organs due to the widening gap between supply and demand (Campana et al. 2021) are significantly affecting current transplantation rates. The use of extended-criteria livers has been proposed as one of the strategies to improve the donor pool. Unfortunately, the use of these marginal organs increases the incidence of allograft dysfunction and post-reperfusion syndrome (Trapero-Marugán, Little, and Berenguer 2018; Younossi et al. 2021), due to their elevated susceptibility to ischemic injury and impaired liver regeneration. Notably, liver regeneration is determined by the energy status of the hepatocyte (Alexandrino et al. 2016) and mitochondrial damage and ATP depletion re characteristic of IRI (Gracia-Sancho, Casillas-Ramírez, and Peralta 2015).

Therefore, we hypothesized that mitochondrial dysfunction due to elevated MCJ levels might impair the regenerative response and increase susceptibility to ischemic injury, particularly in individuals with compromised metabolism.

Overall, the main objective of this work is to characterize the contribution of MCJ, an endogenous negative regulator of mitochondrial respiration, to the development of ALD

and to the impaired regenerative response and increased susceptibility to ischemic injury observed in individuals with compromised metabolism.

Hence, the aims of this work are:

1. Characterize the contribution of MCJ to the pathogenesis of ALD by examining its expression at different stages of the disease and its impact on key ALD features, e.g., lipid metabolism, inflammation, and oxidative stress

2. Analyze the possibility of targeting mitochondrial dysfunction by silencing *Mcj* as an alternative therapeutic approach to treat ALD

3. Identify the role of MCJ in the regenerative response after partial hepatectomy and ischemia-reperfusion injury, characterizing the expression of the protein and its effects on liver damage, metabolism, and survival

4. Determine the implication of mitochondrial dysfunction and, in particular, the role of MCJ in the impaired regenerative response and increased ischemic injury observed in metabolically compromised individuals, such as DCD, steatotic, and elderly donors

5. Analyze of the possibility to target mitochondrial dysfunction in metabolically compromised individuals by silencing *Mcj* as a strategy to increase the organ donor pool

4. EXPERIMENTAL PROCEDURES

4 EXPERIMENTAL PROCEDURES

4.1 HUMAN SAMPLES

All studies were performed in accordance with the Declaration of Helsinki and local/national laws. The Human Ethics Committee of each hospital approved the study procedures, and written informed consent was obtained from the legal representatives of the potential donors.

4.1.1 Alcoholic liver disease

A public data repository was used to analyze expression of *MCJ* in ALD patients. Patient data was included in the study by Argemi et al., (Argemi et al. 2019). Patients (n=61) were divided into different clinically relevant stage groups: (1) patients with early alcoholic steatohepatitis (ASH), who were non-obese with high alcohol intake, and presented mild elevation of transaminases and histologic criteria of steatohepatitis (Early ASH, N = 11); (2) patients with histologically confirmed non-severe alcoholic hepatitis (AH) who were biopsied before any treatment (Non-Severe AH, N=11); (3) patients with histologically confirmed AH who were biopsied before any treatment (Severe AH, N = 18) and (4) explants from patients with AH who underwent early transplantation (Explant AH, N = 11). Samples from these groups were compared with fragments of non-diseased human livers (Control N = 10). Patients with malignancies were excluded from the study. Clinical characteristics of this cohort are described in the study by Argemi et al. (Argemi et al. 2019) (Related to Figure 5.1).

4.1.2 Transplantation

Controlled donation after circulatory death (cDCD) was considered for patients in whom the treating team had made the decision to withdraw life-sustaining therapy (WLST). No upper age limit was set. Only donors whose livers were ultimately transplanted were included in analyses. Functional warm ischemic time (FWIT) for abdominal grafts was defined as the time from systolic blood pressure <60 mmHg to the onset of normothermic regional perfusion (NRP) (including a 5-minute no-touch period). For FWIT, an upper time limit of 30 minutes for livers was applied. The extracorporeal membranous

oxygenation (ECMO) device used was a Maquet Rotaflow (Maquet, Rastatt, Germany). Patient data are shown in **Table 4.1**.

Table 4.1 Characterization of the cohort of controlled donation after circulatory death (cDCD) donor patients used for the immunohistochemical characterization of Methylation-controlled J (MCJ) protein levels. (ABI=Anoxic brain injury; BH=Brain hemorrhage; CI=Cold ischemia; FWIT=Functional warm ischemia time; ICU=Intensive care unit; ITBL=Ischemic-type biliary lesions; PNF=Primary nonfunction; VHC=Hepatitis C related liver cirrhosis) (Related to Figure 5.10)

Donor gender, age	Cause of death	ICU stay (days)	FWIT (min)	Recipient gender, age	MELD	Cause of transplant	CI (min)	ITBL	PNF
Female, 65	BH	6	34	Male, 68	13	Hepatocarcinoma	225	No	No
Male, 18	Meningitis	19	6	Male, 50	12	Alcoholic cirrhosis and VHC	420	No	No
Female, 51	ABI	8	17	Male, 63	16	Alcoholic cirrhosis	147	No	No
Male, 55	ABI	7	14	Male, 55	21	Hepatorenal syndrome	300	No	No
Female, 14	BH	19	11	Male, 47	15	Alcoholic cirrhosis	390	No	No
Female, 56	ABI	6	14	Female, 70	14	Hepatocarcinoma + VHC	370	No	No
Male, 26	ABI	4	7	Male, 66	15	Alcoholic cirrhosis and Hepatocarcinoma	350	No	No
Male, 72	BH	3	9	Male, 60	9	VHC cirrhosis	309	No	No
Male, 73	BH	6	9	Female, 62	27	Autoimmune liver disease	310	No	No
Female, 72	ABI	2	23	Female, 56	16	Poliquistosis hepatorenal	275	No	No
Male, 35	ABI	18	8	Male, 39	22	Alcoholic cirrhosis + VHC	301	No	No
Male, 35	ABI	6	12	Male, 56	14	Alcoholic cirrhosis and hepatocarcinoma	180	No	No
Female, 58	BH	10	7	Male, 68	6	Alcoholic cirrhosis	270	No	No
Female, 69	ABI	10	6	Male, 47	19	Alcoholic cirrhosis + VHC	353	No	No
Female, 69	BH	5	6	Female, 65	10	Alcoholic cirrhosis	290	No	No

4.2 ANIMAL EXPERIMENTS

The animal procedures were performed in accordance with the European Research Council for animal care and use and the National Institute of Health guide for care and use of laboratory animals. The maximum authority of the Country Council of Bizkaia and the Institutional Animal Care and Use Committee of CIC bioGUNE approved the animal procedures (REGA 48/901/000/6106) (P-CBG-CBBA-218). MCJ-KO and Wt mice were bred at the CIC bioGUNE AAALAC-accredited animal facility. Adult (three-month-old) male C57BL/6J mice were acquired from Charles River Laboratories and accommodated into the AALAC-accredited CIC bioGUNE animal facilities. All mice were maintained at 21ºC, 45 humidity, and a 12/12 h light/dark cycle. Animal maintenance was based on ad libitum access to water and the respective diet.

4.2.1 Mouse model of chronic and binge ethanol feeding (The NIAAA model)

The National Institute on Alcohol abuse and Alcoholism (NIAAA) experimental model of ALD synergistically induces liver injury, inflammation, and fatty liver, which mimics acute-on-chronic alcoholic liver injury in patients (Bertola et al. 2013). Mice were initially fed the control Lieber-DeCarli diet (F1259, BIO-SERV) *ad libitum* for 5 days to acclimatize them to liquid diet and tube feeding. Afterwards, ethanol-ed groups were allowed free access to the ethanol Lieber-DeCarli diet (F1258, BIO-SERV) containing 5% (vol/vol) ethanol for 10 days, and control groups were pair-fed with the isocaloric control diet. At day 11, ethanol-fed and pair-fed mice were gavaged in the early morning with a single dose of ethanol (5g/kg body weight) or isocaloric maltose dextrin, respectively, and euthanized 9 h later (**Fig. 4.1**).

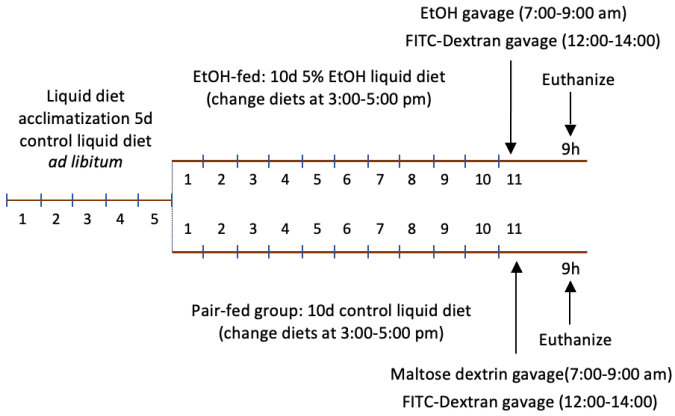

Figure 4.1 Schematic overview of the NIAAA model in Wt and MCJ-KO mice. (EtOH=Ethanol; FITC=Fluorescein isothiocyanate)

We set four different experimental groups:

Group 1: 3-month-old male Wt and MCJ-KO mice were fed with the NIAAA model. At day 11, 5 h after the gavage, mice were orally administered with 100ul 0.6mg/gr body weight of FITC-Dextran and sacrificed 4 h after. Serum samples were directly assayed for the FITC-dextran measurement to study intestinal permeability (**Fig. 4.1**).

Group 2: 3-month-old male Wt and MCJ-KO mice were fed with the NIAAA model. At day 11, after an overnight fasting period and following the gavage, mice were subjected

to an intraperitoneal glucose tolerance test (IPGTT). 2 h after, once the glucose tolerance test was finished, mice were sacrificed.

Group 3: 3-month-old male Wt and MCJ-KO mice were fed with the NIAAA model. At day 6 of the ethanol-diet, after an overnight fasting period, mice were subjected to an IPGTT. At day 11, 9 h after the oral gavage, mice were sacrificed.

Group 4: 3-month-old male c57BL/6J wild-type mice followed the NIAAA model. After the initial acclimatization period, at day 5 of the ethanol Lieber-DeCarli diet, animals were subjected to an *in vivo* silencing RNA targeting *Mcj* (position 294-312) or an unrelated siRNA control, receiving either 1.7 mg/Kg of specific *in vivo* siRNA (Custom Ambion, USA) or control siRNA (Sigma-Aldrich, USA) complexed with Invivofectamine ® 3.0 Reagent (Invitrogen, USA) following the manufacturer's instructions. At day 11, after an overnight fasting period and following the gavage, mice were subjected to an IPGTT. 2 h after, once the glucose tolerance test was finished, mice were sacrificed (**Fig. 4.2**).

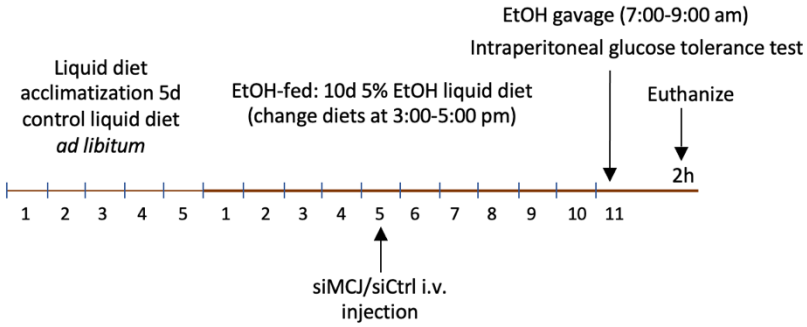

Figure 4.2 Schematic overview of the NIAAA model in siCtrl and LSS-MCJ mice (EtOH=Ethanol; i.v.=intravenous)

4.2.2 70% Partial Hepatectomy

Two-thirds partial hepatectomy (Phx) was first described by Higgins and Anderson in 1931 (Higgins and Anderson 1931). For the 70% Phx the left lateral lobe and the left and right parts of the median lobe are resected.

Before surgery, mice are weighed and carprofen is administered subcutaneously. After 15 minutes, the mice are anesthetized with 4% isoflurane, the abdomen is shaved, and the

isoflurane is lowered to 2% while the surgery is performed. During surgery, a small incision (1-2 cm) is made from the sternum after sterilizing the abdomen with Betadine (Mylan, USA). After both skin layers are opened, the median and left lateral lobes of the liver are carefully extracted. Each lobe (left lateral lobe, left and right part of the median lobe) is ligated and resected separately. The inner skin layer is sutured and the outer one is stapled. After completion of surgery, the mice are placed in a new cage with food on the bedding and ad libitum access to water and a hot plate under half of the cage for the first hour. Weight and suture are checked daily, and subcutaneous buprenorphine is administered every 24 hours for the first 72 hours.

We set four experimental groups:

Group 1: Phx was performed in 3-month-old Wt and MCJ-KO mice. Animals were sacrificed at 3, 6, 12, 24, 33 and 48 hours and 5 days after surgery.

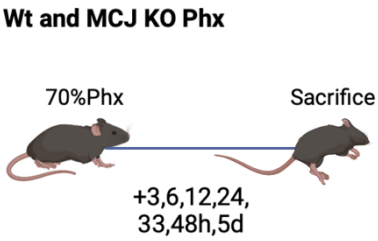

Figure 4.3 Group 1: Partial Hepatectomy in 3-month-old Wt and MCJ-KO mice

Group 2: Phx was performed in 3-month-old c57BL/6J Wt mice. Animals were subjected to an *in vivo* silencing RNA targetting *Mcj* (position 294-312) or an unrelated siRNA control, receiving either 1.7 mg/Kg of specific *in vivo* siRNA (Custom Ambion, USA) or control siRNA (Sigma-Aldrich, USA) complexed with Invivofectamine ® 3.0 Reagent (Invitrogen, USA) following the manufacturer's instructions. Tail vein injection was performed 24h before the Phx and mice were sacrificed at 33 hours after surgery.

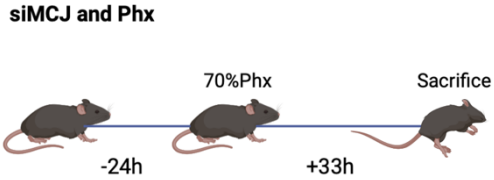

Figure 4.4 Group 2: Partial Hepatectomy in 3-month-old siCtrl and siMCJ mice

Group 3: Phx was performed in 15/17-month-old c57BL/6J Wt mice. Animals were subjected to *in vivo* silencing of *Mcj* or were treated with an unrelated siRNA control, receiving either 1.7 mg/Kg of specific *in vivo* siRNA (Custom Ambion, USA) or control siRNA (Sigma-Aldrich, USA) complexed with Invivofectamine ® 3.0 Reagent (Invitrogen, USA) following the manufacturer's instructions. Tail vein injection was performed 24h before the Phx and mice were sacrificed at 72 hours after surgery.

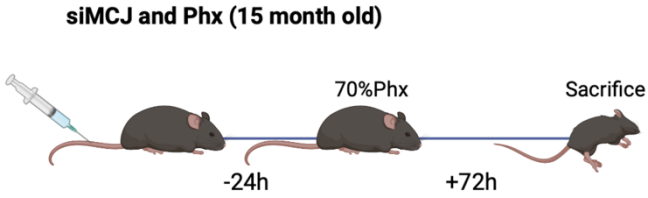

Figure 4.5 Group 3: Partial Hepatectomy in 15-month-old siCtrl and siMCJ mice

Group 4: Phx was performed in 5-month-old c57BL/6J Wt mice. Animals were fed with a high-fat high-fructose (15%) diet (Research Diets, D124511 Rodent Diet with 45% Kcal% Fat) for 12 weeks and they were subjected to *in vivo* silencing of *Mcj* or were treated with an unrelated siRNA control, receiving either 1.7 mg/Kg of specific *in vivo* siRNA (Custom Ambion, USA) or control siRNA (Sigma-Aldrich, USA) complexed with Invivofectamine ® 3.0 Reagent (Invitrogen, USA) following the manufacturer's instructions. Tail vein injection was performed 72h before the Phx and mice were sacrificed at 33 hours after surgery.

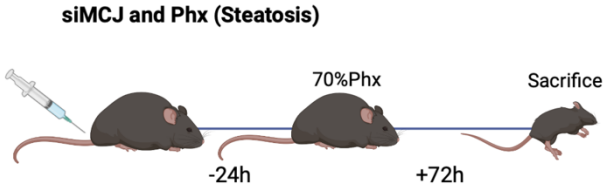

Figure 4.6 Group 4: Partial Hepatectomy in high-fat-high-fructose diet fed 5-month-old siCtrl and siMCJ mice

4.2.3 Partial Hepatectomy under Ischemia-Reperfusion Injury

In clinical situations, Phx under IRI is usually performed to control bleeding during parenchymal dissection. In the experimental model (M. Selzner, Camargo, and Clavien 2003), mice are weighed before surgery and carprofen is administered subcutaneously. After 15 min, the mice are anesthetized with 4% isoflurane, the abdomen is shaved, and the isoflurane is decreased to 2% while surgery is performed. During surgery, a larger incision (5 cm) is made from the sternum after sterilizing the abdomen with Betadine (Mylan, USA). After both skin layers are opened, a retractor is placed near the sternum to open the field of view and working area. Then, a microvascular clamp is placed on the portal triad supplying the median lobe, for 30 minutes. At the end of the ischemia period, the microvascular clamp is released, and both the right and caudate lobes are resected. Thus, the ischemic median lobe remains. The inner layer is sutured and the outer one is stapled. After completion of surgery, the mice are placed in a new cage with food on the bedding and ad libitum access to water and a hot plate under half of the cage for the first hour. Weight and suture are checked daily, and subcutaneous buprenorphine is administered every 24 hours for the first 72 hours.

Three experimental groups were set:

Group 1: Phx under IRI was performed in 3-month-old Wt and MCJ-KO mice. Animals were sacrificed at 24 hours and 7 days after the procedure.

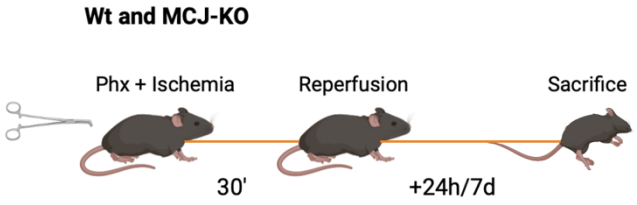

Figure 4.7 Group 1: Partial Hepatectomy under ischemia in 3-month-old Wt and MCJ-KO mice

Group 2: Phx under IRI was performed in 15/17-month-old Wt and MCJ-KO mice. Animals were sacrificed 7 days after the procedure.

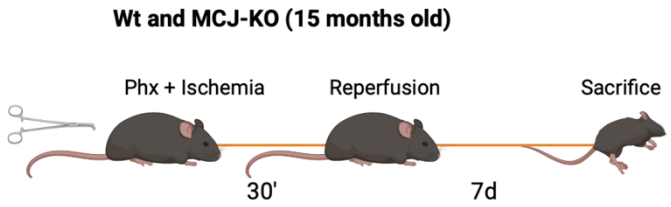

Figure 4.8 Group 2: Partial Hepatectomy under ischemia in 15-month-old Wt and MCJ-KO mice

Group 3: Phx under IRI was performed in15/17-month-old c57BL/6J Wt mice. Animals were subjected to *in vivo* silencing of *Mcj* or were treated with an unrelated siRNA control, receiving either 1.7 mg/Kg of specific *in vivo* siRNA (Custom Ambion, USA) or control siRNA (Sigma-Aldrich, USA) complexed with Invivofectamine ® 3.0 Reagent (Invitrogen, USA) following the manufacturer's instructions. Tail vein injection was performed 24h before the Phx under IRI and mice were sacrificed 7 days after surgery.

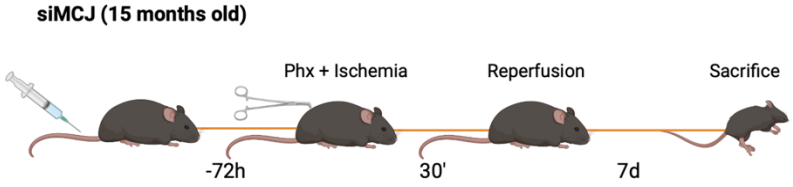

Figure 4.9 Group 3: Partial Hepatectomy under ischemia in 15-month-old siCtrl and siMCJ mice

4.2.4 Ischemia-Reperfusion Injury

Partial hepatic ischemia was described by Yamauchi et al in 1982 and is induced by clamping the portal triad that irrigates the median and left lateral lobes with an atraumatic microvascular clamp (Yamauchi and B 1982). Before surgery, mice are weighed and carprofen is administered subcutaneously. After 15 minutes, the mice are anesthetized with 4% isoflurane, the abdomen is shaved, and the isoflurane is decreased to 2% while surgery is performed. During surgery, a small incision (1-2 cm) is made from the sternum after sterilizing the abdomen with Betadine (Mylan, USA). Using 0.9%NaCl-moistened swabs, the liver lobes are carefully displaced to reach the portal triad, and a microvascular clamp is applied for 90 minutes (prolonged warm ischemia). Reperfusion is initiated by removing the clamp at 4 hours (early phase) and 24 hours (late phase). Ischemic (median and left lateral) and oxygenated (right and caudate) lobes are obtained. In sham-operated

mice (control mice), the liver lobes are gently displaced, and the cavity remains open during the "ischemic" 90 minutes. The inner skin layer is sutured, and the outer is stapled. Upon completion of surgery, the mice are placed in a new cage with food on the bedding and ad libitum access to water and a hot plate under half of the cage for the first hour. Weight and suture are checked daily, and subcutaneous buprenorphine is administered every 24 hours for the first 72 hours.

Two experimental groups were set:

Group 1: 3-month-old Wt and MCJ-KO mice were sham operated.

Group 2: Partial IRI was performed in 3-month-old Wt and MCJ-KO mice. Reperfusion was initiated by removal of the clamp for 4 and 24 hours and animals were then sacrificed.

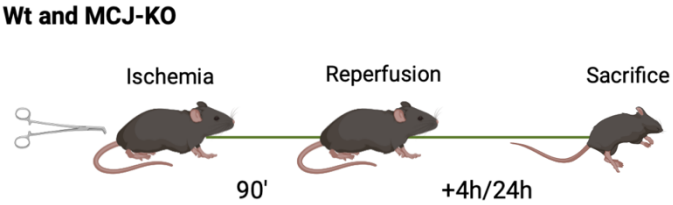

Figure 4.10 Ischemia Reperfusion Injury in 3-month-old Wt and MCJ-KO mice

After the sacrifice, in all experimental groups tissue samples were immediately frozen in liquid nitrogen for RNA and protein extraction, cryopreserved in optimal cutting temperature compound for staining, or fixed in 4% paraformaldehyde for immunohistochemical analysis. Gut samples were protected from RNAses using RNAlater (Thermo Fisher, USA). Blood samples were centrifuged 5 minutes 6000rpm to get the serum, which was kept at -80ºC.

4.3 CELL ISOLATION, CULTURE AND TREATMENTS

4.3.1 Primary cells

In this work primary cell cultures (hepatocytes, Kupffer cells, bone marrow derived macrophages and pancreatic islets) have been used.

4.3.1.1 Primary hepatocytes isolation

Primary hepatocytes were obtained by *in situ* perfusion of the liver with collagenase Type I (Worthington, USA). Briefly, animals were anesthetized with isoflurane (1.5% isoflurane in O_2). Then, the abdomen was opened, and a catheter was inserted into the inferior vena cava. Liver was perfused with buffer A (1x phosphate buffered saline (PBS), 5mM egtazic acid (EGTA), 37ºC and oxygenated) and the portal vein was cut. Next, liver was perfused with buffer B (1xPBS, 1mM calcium chloride ($CaCl_2$) 37ºC and oxygenated) to remove EGTA, and finally perfused with buffer C (1xPBS, 2mM $CaCl_2$, 0.65 bovine serum albumin (BSA), collagenase type I, 37ºC and oxygenated). After buffer C perfusion, liver was separated from the resto of the body and placed into a petri dish with MEM (Gibco, USA). Gall bladder was carefully removed and then, the liver was mechanically disaggregated with forceps. The digested liver diluted in Minimum Essential Medium (MEM) was filtered through a sterile gauze and filtered liver cells were collected and washed three times (1x4' at 400 revolutions per minute (rpm) and 2x5' at 500rpm) in 10% fetal bovine serum (FBS) (Gibco)/1% Penicillin-Streptomycin-Amphotericin (PSA)/1%Glutamine (Gibco) supplemented MEM, conserving all supernatant Kupffer and Hepatic Stellate cells isolation. After the final wash, hepatocytes contained in the pellet were resuspended in 10% FBS 1% PSA/1%Glutamine MEM for subsequent culturing.

Primary hepatocytes were seeded over previously collagen-coated culture dishes at a density of 7600 cells/mm^2 in 10% FBS/1% PSA supplemented MEM and placed in an incubator at 37ºC, 5% CO_2-95% air. After 6 hours of attachment, culture medium and unattached hepatocytes were removed with fresh 0% FBS/1% PSA/1%Glutamine MEM for the aimed treatment.

4.3.1.2 Kupffer cells isolation

Following isolation of mouse hepatocytes by perfusion with Collagenase Type I, supernatants from the hepatocyte wash were joined together and centrifuged (1350g, 10', 4°C). The pellet was resuspended in 10mL preservation buffer and then loaded onto a 25/50% Percoll PLUS (GE Healthcare, UK) gradient and again centrifuged (1350g, 30', 4°C) with minimum acceleration/deceleration. The non-parenchymal cells were collected with a pipette from the interface between the two density cushions of 25% and 50%. Collected cells were centrifuged again (1350g, 10', 4°C) and the resulting pellet was resuspended in DMEM (Gibco). Kupffer cells were removed from the media by selective adherence, by incubating the resuspended cells on uncoated plastic culture plates for 8 min at 37°C. Primary Kupffer cells were incubated in 10% DMEM medium supplemented with 1% PSA and 1% Glutamine at 37°C in a humidified atmosphere of 5% CO2-95% air.

4.3.1.3 Bone marrow derived macrophages (BMMs)

Bone marrow cells were obtained from the femoral and tibial shafts and subjected to erythrocyte lysis with ACK buffer (NH_3Cl 150 mM; $KHCO_3$ 10 mM; Na_2EDTA 0.1 mM). The cells were incubated in non-treated 100 mm x 15 mm plates (Thermo Fisher Scientific) for 6 days at 37ºC in DMEM (Gibco) supplemented with 10 % FBS and 1% penicillin/streptomycin plus 30 ng/ml of M-CSF (Miltentyi Biotech). The medium was changed every 3 days. Non-adherent cells were discarded, and the differentiated macrophages were scraped in PBS (Thermo Fisher Scientific) + 1%FBS, counted and seeded at the appropriate concentrations for the following experiments.

4.3.1.4 Primary human pancreatic islets obtention

Human islets were either obtained from The Cell Isolation and Transplantation Center (Department of Surgery, Geneva; Switzerland) or purchased from Tebu-Bio (Barcelona, Spain) from deceased individuals with informed consents obtained from their families. The donors did not have a previous history of glucose intolerance. The use of human islets was performed in compliance with the Declaration of Helsinki, ICH/Good Clinical Practice. To recover after arrival, human islet preparations were washed, handpicked, and subsequently cultured for 2 days in CMRL-1066 (ThermoFisher

Scientific) containing 5.6 mM glucose, and supplemented with 10%FCS, 100 U/ml penicillin, 100 µg/ml streptomycin, and 100 µg/ml gentamycin (Sigma-Aldrich, Madrid).

4.3.1.5 Primary mouse pancreatic islets isolation

The mice were sacrificed by cervical dislocation. The abdomen was opened, and micro forceps were placed below the ampulla of Vater to better visualize the bile duct (Fig. X). The entire procedure was performed with a magnifying glass. Using ultrafine forceps, two knots were tied: one between the bile duct and the ampulla of Vater to prevent the collagen solution from drifting toward the duodenum, and the other at the proximal end of the bile duct to prevent it from ascending to the liver. A syringe containing 9mL Krebs Ringer buffer with collagenase type V (C9263, Sigma) was prepared for each mouse. A small incision was made with microscissors near the proximal end of the bile duct, just above the knot. The syringe, whose needle (BC Microlance 3 30G ½ 0.3x12) was bent 90º, was then inserted into the bile duct and the isolation solution was injected. Once the pancreas was swollen, it was removed and placed in a 15-mL tube containing 2 mL of ice-cold Krebs-Ringer buffer with collagenase type V. The tube was then placed in a water bath at 37 ºC for 10 minutes, shaking vigorously in the middle and at the end of the incubation to facilitate islet disruption. To stop collagenase digestion, ice-cold Krebs Ringer was used and the 15-ml tube was placed on ice for 10 minutes to allow the islets to settle. The supernatant was discarded, the islets were resuspended in new ice-cold Krebs Ringer solution, and the volume was transferred to a black-bottomed Petri dish to facilitate hand-picking isolating and counting of the islets.

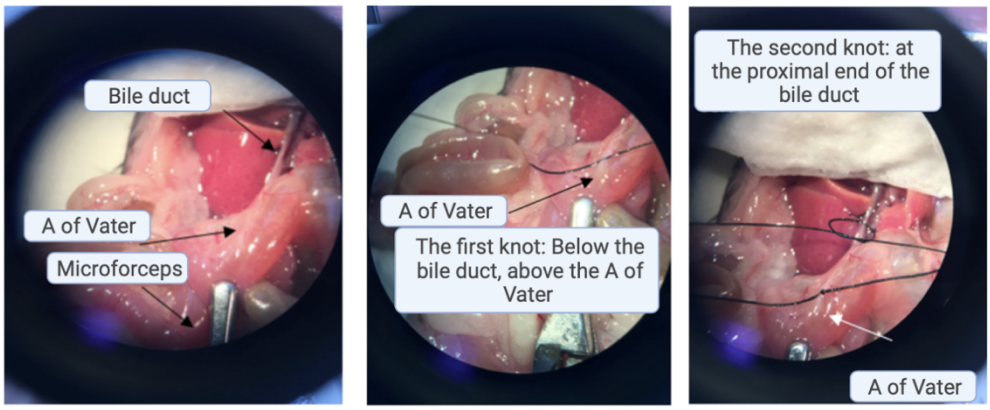

Figure 4.11Primary mouse pancreatic islets isolation. The image on the left shows the liver, bile duct, the ampulla of Vater and the microforceps. The images on the center and on the right show where to tie the knots.

Once isolated, islets were cultured in RPMI-1640 supplemented with 10% FBS, 2 mM L-glutamine, 3 mM glucose, 1% sodium pyruvate, 1% HEPES 1M and 1% penicillin/streptomycin (Invitrogen-Thermo Fisher Scientific, Spain), allowing them to recover.

4.3.2 Cell treatments

4.3.2.1 BMMs and Kupffer cells

BMM and KCs were incubated with ATP (Sigma Aldrich) at a concentration of 3mM for 4 hours, in 0% Dulbecco's Modified Eagle Medium (DMEM) medium supplemented with 1%PSA and 1% Glutamine, to study the activation of the inflammatory response. Supernatants were collected to measure TNF and IL-6 by ELISA and to treat primary hepatocytes.

4.3.2.2 Primary hepatocytes

Primary Wt hepatocytes were incubated with EGF (Sigma-Aldrich) at a concentration of 20ng/mL for 24 hours in 0% MEM medium supplemented with 1%PSA and 1% Glutamine to analyze the proliferative response.

Primary Wt and MCJ KO hepatocytes were also treated with conditioned media from control or ATP treated Kupffer cells for 4 and 24 hours, to study the implication of the inflammatory response in the initiation of hepatocyte proliferation.

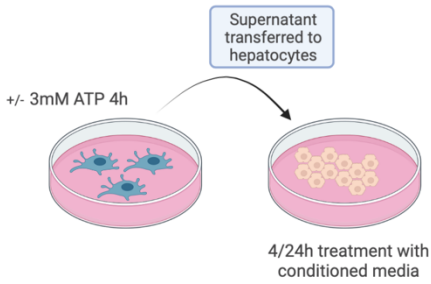

Figure 4.12 Schematic representation of the hepatocyte experiment with Kupffer cell-derived conditioned media (ATP=adenosine triphosphate)

4.3.3 Cell transfection

4.3.3.1 Gene silencing by siRNA transfection

Wt primary hepatocytes were transfected with specific siRNAs at a final concentration of 100nM using DharmaFECT 1 reagent (Dharmacon) following manufacturer's protocol. DharmaFECT 1 and siRNA were diluted separately in 0% FBS/1% PSA MEM for 5' at room temperature (RT). Dilutions were then mixed and incubated 20' at RT. siRNA transfection mixes were then added to the cell suspension medium and replaced for fresh medium after 6h. Controls were transfected with an unrelated siRNA (Qiagen). Protein knockdown was confirmed by western blotting. siRNA transfection volumes, indicated for 6-well plates) and sequences are summarized in **Table 2.2**.

Table 4.2 siRNAs transfected with DharmaFECT 1 indicated for 6-well seeded cells. (mm= murine mouse; F= forward/sense sequence; R= reverse/antisense sequence)

siRNA	DharmaFECT 1 volume	siRNA (100uM) volume	Sequence	Medium volume
mmMCJ	8ul in 0.2mL	1ul in 0.2mL	F 5'-AAGCGAGAGGCUAGUCUUATT-3' R 5'-UAAGACUAGCCUCUCGCUUAC-3'	2 ml

4.3.3.2 Gene overexpression by plasmid transfection

pCMV6-MCJ plasmid was transfected into primary mouse hepatocytes using jetPRIME® (Polyplus, USA). Transfection protocol was realized following manufacturer's instructions. Briefly, 3µg pCMV6-MCJ plasmid were mixed with 200µl jetPRIME® buffer and resuspended during 10s. Then, 6 µl jetPRIME® transfection reagent was added and resuspended again. After a 20-minute incubation, transfection mixture was added to $0.5*10^6$ cells in a 6-well plate. Transfections were performed in cell suspension medium and transfection mix was replaced for fresh medium 6h after transfection unless indicated. pcDNA3-LacZ (Invitrogen) was used as a negative control. The transfection efficiency was confirmed by western blotting. pCMV6-MCJ plasmid was kindly provided by Dr. Juan Anguita.

4.4 RNA ISOLATION AND CDNA EXPRESSION DETERMINATION

4.4.1 RNA isolation

Total RNA from tissue or cultured cells was isolated using TRIzol reagent (Invitrogen) according to manufacturer's instruction. In case of cell mRNA extraction, 5 µg of Glycogen (Ambion, USA) were used in the RNA precipitation step to facilitate the visibility of the RNA pellet. RNA concentration was determined spectrophometrically using the Nanodrop ND-100 spectrophotometer (ThermoFisher Scientific, USA)

4.4.2 Retrotranscription

1-2 µg of isolated RNA were treated with DNAse I (Invitrogren) and used to synthesize cDNA by M-MLV reverse transcriptase in the presence of random primers, ribonucleotides and RNAseOUT (all from Invitrogen). Resulting cDNA was diluted 1/10 (1/20 if 2 µg were used) in RNAse free water (Sigma-Aldrich).

4.4.3 Real time quantitative polymerase chain reaction (qPCR)

qPCRs were performed using either the ViiA 7 or the QS6 Real time PCR System with SYBR Select Master Mix (Applied Biosystems, USA). 1.5 µl of cDNA were used and including the specific primers for a total reaction volume of 6.5 µl in a 384-well plate (Applied Biosystems). All reactions were performed in triplicate. PCR conditions for the primers were optimized and 40 cycles with a melting temperature of 60ºC and 30s per step were used. *Mus musculus* primers were designed using the Primer 3 software via the NCBI-Nucleotide webpage (http://www.ncbi.nlm.nih.gov/nucleotide/) and synthesized by Sigma Aldrich. Primer sequences are detailed in **Table 4.3**. After checking the specificity of the PCR products with the melting curve, data were normalized to the expression of a housekeeping gene (9S, ARP).

Table 4.3 List of primers used to determine mRNA expression of *Mus musculus* genes.

Gene symbol	Forward sequence	Reverse sequence
9S	GACTCCGGAACAAACGTGAG	CTTCATCTTGCCCTCGTCCA
Acadl	GTCCGATTGCCAGCTAATGC	CACAGGCAGAAATCGCCAAC
Acc	GCCTCAGGAGGATTTGCTGT	AGGATCTACCCAGGCCCACAT
Adh1	GTGGCCAAAATCGATGGAGC	GCAGAGCCATAGCCAGTTGA
Aldh2	GCTGGGCTGACAAGTACCAT	CAGGCTCATGGCGGGTATAG
Ap-1	GCACATCACCACTACACCGA	GGGAAGCGTGTTCTGGCTAT
Arp	CGACCTGGAAGTCCAACTAC	ATCTGCTGCATCTGCTTG
Bax	GATCAGCTCGGGCACTTTAG	TGCAGAGGATGATTGCTGAC
Bcl-xL	GGCCTTTTTCTCCTTTGGCG	GATCCACAAAAGTGTCCCAGC
Bcl2	GACCACAGGTGGCACAGGGC	ATGCTGGAGATGCGGACGCG
Ca2	CGTGGATGAGTTTGTCTACATCA	AACAGCCTGCCTTCACCATT
Cb1	TCTTCACAACGGTGAATGGAC	ATGCAGCACCTGGCTAAGAAT
Ccl2	GACCCCAAGAAGGAATGGGT	ACCTTAGGGCAGATGCAGTT
Ccl5	TCGAGTGACAAACACGACTGC	GCTGCTTTGCCTACCTCTCC
Ccr2	ATCCACGGCATACTATCAACAT	CAAGGCTCACCATCATCGTAG
Ccr5	GTGTGGAAAATGAGGACTGCAT	GTCAGAACGGTCAACTTTGGG
Cd1	TCAGTGTGACCCGGACTG	CCTTGGGGTCGACGTTCTG
Ce	GAAATTGCCAAGATTGACAAGAC	TGTTTAACATGATCCTCCAAACC
Chrebp	GCAAAAACTGTCTGCAAGGGT	GGCAGCTCTGAGTCCCATAC
Cpt1a	GACTCCGCTCGCTCATTCC	GAGATCGATGCCATCAGGGG
Cxcl1	GGTGTCCCCAAGTAACGGAG	TTGTCAGAAGCCAGCGTTCA
Cyp2e1	TCACTGGACATCAACTGCCC	ACATGGGTTCTTGGCTGTGT
FasN	GGCCCCTCTGTTAATTGGCT	GGATCTCAGGGTTGGGGTTG
Fatp2	CCGCAGAAACCAAATGACCG	TGCCTTCAGTGGATGCGTAG
Fgf-21	CTGCTGGGGGTCTACCAAG	CTGCGCCTACCACTGTTCC
Hamp	AGGGCAGACATTGCGATACC	GCAACAGATACCACACTGGGA
Hb-egf	GTTGGTGACCGGTGAGAGTC	TGGTTTGTGGATCCAGTGGG
Ho-1	AAGCTTTTGGGGTCCCTAGC	ACAGCTGCTTTTACAGGCCA
Il-10	GCACCCACTTCCCAGTCGGC	GCCATGCTTCTCTGCCTGGGG

Il-1b	ACACTCCTTAGTCCTCGGCCA	CCATCAGAGGCAAGGAGGAA
Il-6	ACCACGGCCTTCCCTACTTCAC	TTCTCATTTCCACGATTTCCCAG
Mcj	ACGCCGACATCGACCACACAG	AATCTTCCTTGCTGTTGCVGTG
p21	ACCATGGTCGGAACTCCATA	CATCTCAAGACAGCGGTTCA
Pcna	TACAGCTTACTCTGCGCTCC	TTGGACATGCTGGTGAGGTT
Ppara	GAGGGTTGAGCTCAGTCAGG	GGTCACCTACGAGTGGCATT
Pparg	GAATGCGAGTGGTCTTCCAT	TGCACTGCCTATGAGCACTT
Sirt1	GATTGGCACCGATCCTCGAA	ACAATCTGCCACAGCGTCAT
Srebp1	GAGGCCAAGCTTTGGACCTGG	CCTGCCTTCAGGCTTCTCAGG
Tgfb	ACTGGAGTTGTACGGCAGTG	GGGGCTGATCCCGTTGATTT
Tlr2	GCATCCGAATTGCATCACCG	GAGCCAAAGAGCTCGTAGCA
Tlr4	CCCACTGCTTCAGGCTACAA	GACCCTGACTGGCACTAACC
Tlr5	AATCCCGCTTGGGAGAACAA	CAGGGGAACCAGGTATGCAG
Tnf	AGCCCACGTCGTAGCAAACCAC	ATCGGCTGGCACCACTAGTTGGT
Trail	CCAACGAGATGAAGCAGC	CCATCAGTGGAGTCCCAG

4.5 GUT METAGENOMIC

4.5.1 Fecal DNA extraction

Genomic DNA was extracted from 180 mg approximately of faecal samples using the Qiagen Fast DNA Stool Mini Kit (Qiagen, Germany) following the manufacturer instructions. Briefly, an initial step of bead beating was included to enhance homogenization, and the lysis temperature was increased up to 95 ºC to recover DNA from bacteria that are difficult to lyse. DNA concentration was measured with a NanoDrop-1000 spectrophotometer (NanoDrop Technologies, USA) and DNA samples were stored at -20 ºC until further analysis.

4.5.2 16S Data analysis methods

The amplicon sequencing protocol targets a fusion fragment containing the V3 and V4 regions (about 459 base pairs (bp)) of the 16S genes with the primers designed

surrounding conserved regions. The full-length primer sequences, using standard IUPAC nucleotide nomenclature, to follow the protocol targeting this fusion region are:

16S Amplicon PCR Forward Primer

5'TCGTCGGCAGCGTCAGATGTGTATAAGAGACAGCCTACGGGNGGCWGCAG

16S Amplicon PCR Reverse Primer

5'GTCTCGTGGGCTCGGAGATGTGTATAAGAGACAGGACTACHVGGGTATCTAATCC

DNA amplicon libraries were generated following Illumina Inc.'s recommendations. The amplification reactions consisted of:

Table 4.4 Constituents of the amplification reaction

	Volume (ul)
Microbial DNA (5 ng/µl)	2.5
Amplicon PCR Forward Primer 1 µM	5
Amplicon PCR Reverse Primer 1 µM	5
2x KAPA HiFi HotStart ReadyMix (KK2602)	12.5
Total	25

PCR cycling was programed with an initial denaturation at 95ºC for 3 min, followed by 25 cycles of annealing (95ºC - 30 seconds, 55ºC - 30 seconds, 72ºC - 30 seconds) and an extension at 72ºC for 5 min.

Then, lllumina Inc.'s sequencing adaptors and dual-index barcodes (Nextera XT index kit v2, FC-131-2001) were added to each amplicon (see Illumina Inc.'s Protocol for details) and, after PCR purification, libraries were normalized and pooled prior to sequencing. The pool containing indexed amplicons was loaded onto the MiSeq reagent cartridge v3 (MS-102-3003), spiked with 25% PhiX control to improve base calling during sequencing, as recommended by Illumina for amplicon sequencing. Sequencing was conducted using a paired end, 2x300pb cycle run on an Illumina MiSeq sequencing system.

Sequencing was done by FISABIO Sequencing Core Facility, who also performed the quality assessment, using *prinseq-lite* (Schmieder and Edwards 2011) with the following parameters (min_length: 50, trim_qual_right: 30, trim_qual_type: mean, trim_qual_window: 20), and the sequence joining, with *FLASH* software (Magoč and Salzberg 2011) using default parameters.

4.5.3 Microbiome sequences bioinformatics analysis

Joined reads were uploaded to QIIME2 software (v2019.7) (Caporaso et al. 2011), specifying the type parameter (SampleData[SequencesWithQuality]) and QIIME2 format option for FASTQ data input (SingleEndFastqManifestPhred33). Samples were then clustered *de novo* into Operational Taxonomic Units (OTUs), using the 97% similarity threshold using dada2 plugin (Callahan et al. 2016). The resulting OTU table was then rarefied to 45,000 reads per sample, when no increase in diversity was obtained from including more reads. Rarefied table was aligned with mafft plugin (Katoh and Standley 2013) and the OTUs phylogenetic tree was then obtained using fasttree plugin (Price, Dehal, and Arkin 2010). Several alpha and beta diversity indexes were computed with diversity plugin and exported for posterior analysis. Finally, OTUs were annotated with GreenGenes 13_8 database and the resulting table was exported for posterior analysis.

4.5.4 Data analysis

OTU table was then clustered into both phylum and genus levels, using the R package *phyloseq*. Genus-clustered dataset was then transformed using the center log-ratio approach, in order to assess for the compositional nature of microbiome data (Gloor et al. 2017) using *ALDEx2* R package (Fernandes et al. 2014). Differential abundance significance between EtOH mice groups was assessed following the ALDEx2 pipeline, with default parameters, using Student's t-test approach. Significance results were then corrected for multiple testing using Benjamini-Hochberg approach (False Discovery Rate). Significance was established at 10% FDR threshold. Both statistical analyses and data visualization was done in R v3.6 (R Development Core Team; http://cran.r-project.org).

4.6 PROTEIN

4.6.1 Protein extraction and analysis

Extraction of total protein was performed as indicated. 50 mg of liver tissue were homogenized using a Precellys-24 apparatus (Bertin Technologies) in 1mL of RIPA lysis buffer (NaH_2PO_4 1.6 mM, Na_2HPO_4 8.4 mM, 0.1% Triton X-100, NaCl 0.1 M, 0.1% SDS, 0.5% sodium azide, 5mg sodium deoxycholate) supplemented with a protease and phosphatase inhibitor cocktail (Roche, Switzerland). In the case of cells, these were washed with cold PBS and resuspended in 200ul of supplemented RIPA lysis buffer.

In all cases, the lysates were centrifuged (13000 RPM, 20 min, 4 °C) and the supernatant (protein extract) was quantified for total protein content by the Bradford protein assay or by BCA protein assay (Pierce, USA) depending on the type of lysis buffer used and determined using a Spectramax M3 spectrophotometer.

4.6.2 Western Blotting

Protein extracts were boiled at 95ºC for 10 min in SDS-PAGE sample buffer (250 mM Tris-HCl pH 6.8, 500 mM β-mercaptoethanol, 50% glycerol, 10% SDS, bromophenol blue). An appropriate amount of protein (5-50ug), depending on protein abundance and antibody sensitivity, were separated by sodium dodecyl sulphate-polyacrylamide gel electrophoresis (SDS-PAGE) in 7% to 15% acrylamide gels, using a Mini-PROTEAN Electrophoresis System (Bio Rad). Gels were transferred onto nitrocellulose or PVDF blotting membranes (GE Healthcare Life Science). Membranes were blocked with 5% non-fat milk in TBS pH 8 containing 0.1% Tween-20 (Sigma Aldrich) (TBST-0.1%) for 60 min at RT, washed three times for 10’ with TBST-0.1% and incubated overnight at 4ºC with commercial primary antibody (1:1000). Primary antibodies and their optimal incubation conditions are detailed in **Table 2.5**. Membranes were then washed three times for 10’ with TBST-0.1% and incubated for 1 hour at RT in blocking solution containing secondary antibody conjugated with horseradish-peroxidase (HRP). Immunoreactive proteins were detected by using Western Lightning Enhanced Chemiluminescence reagent (ECL, PerkinElmer, USA) and exposed to Super RX-N X-ray films (Fuji, Japan) in a Curix 60 Developer (AGFA, Belgium).

Table 4.5 List of antibodies used for Western Blot. (BSA=3% BSA in TBS-Tween 0.1%; Milk=5% non-fat milk in TBS-Tween 0.1%).

Antibody	ID	Supplier	Dilution	Incubation solution
b-ACTIN	a5441	Sigma	1/1000	Milk
BAX	2772S	Cell Signaling	1/1000	Milk
BCL2	Ab7973-1	Abcam	1/1000	Milk
BCL-XL	Sc-7195	Santa Cruz Biotechnology	1/1000	Milk
CYCLIN D1	92G2	Cell Signaling	1/1000	Milk
GAPDH	Ab8245	Abcam	1/1000	Milk
HRP-conjugated secondary antibody to mouse	7074	Cell Signaling	1/1000	Milk
HRP-conjugated secondary antibody to rabbit	7076	Cell Signaling	1/1000	Milk
MCJ	B0027R	BioMosaics	1/1000	Milk
mTORC1	2972	Cell Signaling	1/1000	Milk
PARP	9542	Cell Signaling	1/1000	Milk
PCNA	Sc-25280	Santa Cruz Biotechnology	1/1000	Milk
Phospho-AKT (Ser476)	9271S	Cell Signaling	1/1000	BSA
Phospho-AMPK (Thr172)	2531	Cell Signaling	1/1000	BSA
Phospho-EGFR (Tyr1068)	#3777	Cell Signaling	1/1000	BSA
Phospho-ERK1/2 (Thr202/204)	9101	Cell Signaling	1/1000	BSA
Phospho-mTORC1 (Ser2481)	2974	Cell Signaling	1/1000	BSA
Phospho-S6 (Ser235/236)	4857	Cell Signaling	1/1000	BSA
Phospho-STAT3 (Tyr705)	9131S	Cell Signaling	1/1000	BSA

4.7 PROTEOMIC ANALYSIS

4.7.1 In solution digestion

Protein was extracted in a sample containing 7M urea, 2M Thiourea, 4% CHAPS and 5mM DTT. Samples were incubated for 30 at RT and then digested following the filter-aided FASP protocol described by Wisnieski et al (Wisnieski et al. 2009) with minor modifications. Trypsin was added to a trypsin:protein ratio of 1:20, and the mixture was incubated overnight at 37ºC, dried out in a RVC2 25 speedvac concentrator (Christ, Germany), and resuspended in 0.1% FA. Peptides were desalted and resuspended in 0.1% FA using C18 stage tips (Millipore,USA).

4.7.2 Mass spectrometry analysis

Samples were analyzed in a timsTOF Pro with PASEF (Bruker Daltonics, USA) coupled online to a Evosep ONE liquid chromatograph (Evosep Biosystems, Denmark). 200ng were directly loaded onto the Evosep ONE and resolved using the 30 samples-per-day method.

Protein identification and quantification was carried out using PEAKS X software (Bioinformatics Solutions Inc., Canada). Searches were carried out against a database consisting of *Mus musculus* entries (Uniprot/Swissprot), with precursor and fragment tolerances of 20 ppm and 0.05 Da respectively. Only proteins identified with at least two peptides at FDR<1% were considered for further analysis. Protein abundances inferred from PEAKS were loaded onto Perseus platform (Tyanova et al. 2016), log2 transformed and imputated. A t-test was used to address significant differences in protein abundances within each sample group under analysis.

4.7.3 Functional enrichment proteomic analysis

To elucidate the possible molecular mechanisms, we required the use of bioinformatics tools that helped us to understand the whole protein interactions, pathways, and upstream regulators, with Ingenuity Pathway Analysis (IPA, QIAGEN, USA). The program assesses the protein network using t-test and ratios between groups. IPA studies the protein enrichment using Fisher´s exact *p* value that measures overlap of observed and

predicted regulated gene sets. Using *Z* score, IPA is able to predict the upstream regulators and its expectable functions.

4.8 TISSUE STAINING ASSAYS

Paraffin-embedded sections (5 µm thick) of formalin-fixed samples were initially deparaffinized in xylene or xylene-substitute (Histoclear I solution-Electron Microscopy Sciences) and rehydrated through graded alcohol solutions. Once hydrated, sections were subjected to the following stainings:

4.8.1 Haematoxylin and eosin

After the deparaffinization and rehydration process, sections were subjected to conventional hematoxylin and eosin staining. Images were taken with an upright light microscope (Zeiss, Germany).

4.8.2 Sirius Red

Rehydrated sections were then stained with Sirius red solution 1 (0.01% Fast Green FCF in picric acid, Sigma Aldrich) for 15 min and then with Sirius red solution 2 (0.04% Fast Green FCF/0.1% Sirius Red in picric acid, Sigma Aldrich) for another 15 min. The sections were then dehydrated directly in 100% alcohol and mounted in DPX mounting medium (Sigma Aldrich). Images were taken with an upright light microscope (Zeiss).

4.8.3 Lipid determination by Sudan Red and Oil Red O

Optimal cutting temperature (O.C.T)-included frozen liver samples were cut into 8-10 µm sections. Sections were washed in 60% isopropanol and then stained with fresh Sudan III (0.5% in isopropanol; Sigma Aldrich) solution for 30 min. Samples were then washed again in 60% isopropanol and then counterstained with eosin. The sections were then washed with distilled water and mounted in DPX mounting medium. Images were taken with an upright light microscope (Zeiss).

For the Oil red O staining, frozen O.C.T-embebed 8 µm samples were fixed in 10% Formalin solution, neutral buffer (Sigma-Aldrich) (2´, RT) and washed with running tap water. The samples were stained with Oil red O (Sigma-Aldrich) (15´, RT) and washed

with 60% isopropanol (2´, RT). The sections were counterstained with Mayer´s Hematoxylin and mounted with aqueous mounting medium. Images were taken with an upright light microscope (Zeiss).

4.8.4 ROS determination by DHE

O.C.T-embebed 8 µm sections were incubated with MnTBAP 150 µM 1h at RT. The samples were then incubated with dihydroethidium (DHE) 5 µM for 30 min at 37 ºC and sections were mounted with Fluoromount-G (Southern Biotech, USA) containing 0.7 mg/l of DAPI to counterstain nuclei. Images were taken using an Axioimager D1 fluorescence microscope (Zeiss).

4.8.5 Immunohistochemistry

Paraffin-embebed sections (5µm thick) were unmasked according to the primary antibody to be used and subjected to peroxide blocking (3% H_2O_2 in PBS, 10', RT). For staining with mouse-hosted antibodies in mouse tissues, samples were blocked with goat anti-mouse Fab fragment (Jackson Immunoresearch, USA) (1:10, 1h, RT) and then blocked with 2,5% normal goat serum (Vector, USA) (30', RT). Sections were then incubated in a humid chamber with the primary antibody in antibody diluent with 0,02g/ml BSA followed by Envision anti rabbit or anti-mouse (DAKO) or ImmPRESS anti-rat (Vector, USA) HRP-conjugated secondary antibody incubation (30', RT). Unmasking and incubation conditions for each antibody are indicated in **Table 4.6.** Colorimetric detection was confirmed with Vector VIP chromogen (Vector, USA) and sections were counterstained with Mayer's hematoxylin. Samples were dehydrated in increasing concentrations of ethanol solutions until 100%, cleared in Histoclear I solution and mounted using DPX mounting medium. Images were taken with an upright microscope (Zeiss).

Table 4.6 List of antibodies used for immunohistochemistry or immunofluorescence.

Antibodies	Dilution	Incubation solution	Unmasking	Source	Identifier
4Hydroxynonenal antibody (4-HNE)	1:100	PBS-azide (0.01%)-BSA (2%)	none	Abcam	ab46545
Cleaved Caspase-3 (Liver)	1:50	PBS-azide (0.01%)-BSA (2%)	EDTA 5M, pH 8, 97ºC	Cell Signaling	9661
Cleaved Caspase-3 (Pancreas)	1:400	PBS-Tween (0.2%)- BSA (2%)	Heat-induced antigen retrieval in citrate buffer (pH=6)	Cell Signaling	9661
Cyclin D1	1:100	PBS-azide (0.01%)-BSA (2%)	citrates	Santa Cruz	Sc-450
F4/80	1:50	PBS-azide (0.01%)-BSA (2%)	Proteinase K, 15' at RT	Serotec	MCA497-BB
iNOS (Pancreas)	1:100	PBS-Tween (0.2%)- BSA (2%)	Heat-induced antigen retrieval in citrate buffer (pH=6)	Thermo	PA1-036
Insulin (Pancreas)	1:400	PBS-Tween (0.2%)- BSA (2%)	Heat-induced antigen retrieval in citrate buffer (pH=6)	Cell Signaling	C27C9
Insulin (Pancreas)	1:500	PBS-Tween (0.2%)- BSA (2%)	Heat-induced antigen retrieval in citrate buffer (pH=6)	Sigma	I2018
Ki67	1:2000	PBS-azide (0.01%)-BSA (2%)	citrates	Abcam	Ab66155
MCJ	1:50	PBS-azide (0.01%)-BSA (2%)	citrates	Bio Mosaics	B0027R
PCNA	1:400	PBS-azide (0.01%)-BSA (2%)	citrates	Santa Cruz	sc-25280
PhosphoEGFR (Tyr1068)	1:1000	PBS-azide (0.01%)-BSA (2%)	none	Cell Signaling	#3777
ZO-1	1:500	PBS-azide (0.01%)-BSA (2%)	Proteinase K, Tris-EDTA, pH 8, 30'	Thermo	40-2300
Anti-Mouse, Alexa Fluor 488	1:300	PBS-Tween (0.2%)- BSA (2%)	-	Invitrogen	A11001
Anti-Rabbit-biotinylated, HRP-linked antibody	1:300	PBS-Tween (0.2%)- BSA (2%)	-	Jackson	111-035-003
Anti-Rabbit, Alexa Fluor 568	1:300	PBS-Tween (0.2%)- BSA (2%)	-	Thermo	A11011
Anti-Rabbit, Cy3	1:200	PBS-Tween (0.2%)- BSA (2%)	-	Jackson	711-165-152

4.8.5 Immunofluorescence

Immunofluorescence stainings were carried out in pancreatic islets. Purified islets were washed twice with KRB 5.6 mmol/L glucose and 3% BSA, fixed with 4% paraformaldehyde for 4 min in 0.1 mol/L PBS, washed with PBS and permeabilized with 0.02% Triton X-100 overnight. The primary antibodies were anti-insulin mouse monoclonal antibody (1:500 dilution; Sigma-Aldrich, St. Louis, MO, USA), anti-cleaved caspase-3 rabbit polyclonal antibody (1:400 dilution; Abcam, Cambridge, UK) and anti-iNOS rabbit polyclonal antibody (1:100 dilution; Thermo Fisher Scientific, Waltham, MA, USA). The primary antibody localization was detected using anti-mouse Alexa Fluor 488 for insulin (1:300 dilution; Invitrogen, Waltham, MA, USA) and anti-rabbit Alexa Fluor 568 for caspase 3- and iNOS (1:300; Thermo Fisher Scientific, Waltham, MA, USA). Nuclei were counterstained with 300 nM DAPI (Sigma Aldrich, Madrid, Spain). Confocal fluorescence images were captured with a Leica TCS SP5 confocal microscope (Leica, Wetzlar, Germany) at 2-µm intervals in the z-dimension. Images were analyzed using the open-source image processing package FIJI.

4.8.6 Data analysis

The average sum of intensities or stained area percentage of each sample were calculated using the open-source image processing package ImageJ/FIJI.

(https://imagej.nih.gov/ij/download.html)

4.9 HISTOPATHOLOGICAL STUDY

Samples of livers and colon were sectioned 4µm thick and stained with hematoxylin-eosin. Histopathological lesions were classified according to current histological scores (Isayama et al. 2006; Nishida et al. 2013). All slides were analyzed by a pathologist in a blind manner regarding the genotype of the mice.

4.10 ELECTRON MICROSCOPY

Cells were fixed with 2% glutaraldehyde in PBS (pH 7.4) and sent for conventional Epon resin embedding at the Microscopy Service at the Centre for Molecular Biology “Severo

Ochoa" (CBMSO). Thin sections (~150 nm) were obtained using an ultramicrotome (Leica Microsystems, Germany) and a diamond knife (Diatome, Switzerland), placed on 100 mesh hexagonal, Cu/Pd EM grids, and counterstained with uranyl acetate and lead citrate. Cell sections were visualized using our in-house JEOL JEM-1230 transmission electron microscope operating at 100 kV and equipped with an Orius SC1000 (4008×2672 pixels) cooled slow-scan CCD camera (GATAN, UK). Although several 2D images were collected at different magnifications (from 1000 to 20000X), only those at 2500X magnification showing a balance among the cellular elements contained were used for mitochondria inspection and counting. We selected: 33 sections of MCJ KO basal cells; 30 sections of MCJ KO regenerated cells; 32 sections of wt MCJ cells; and 30 sections of wt MAT A1 cells. The inspected images were Gaussian filtered (with a σ = 2.0) and the mitochondria manually annotated in 2D for visualization using the SuRVoS software. Subsequently, the areas corresponding to the cytosol (excluding nucleus and lipid droplets) were estimated using the ImageJ software and the number of mitochondria per unit area calculated across the distinct cell-types. The median and standard deviation were calculated in GraphPad Prism 8 software.

4.11 METABOLISM ANALYSIS

4.11.1 Liver lipid metabolism

4.11.1.1 Liver Triglycerides (TGs) quantification

30 mg of liver tissue were homogenized with 10 volumes of ice-cold PBS, and mixed gently with chloroform-methanol (2:1, V:V). Samples were then centrifuged at 4200*g* at 4ºC for 10 min. The organic phase was evaporated. The pellet was then re-suspended with 1% Triton X-100 in ethanol and re-evaporated. Finally, the samples were re-suspended in 500 µl of PBS and aliquoted to analyze TGs using an automatized Selectra Junior Spinlab 100 analyzer (Vital Scientific, The Netherlands).

4.11.1.2 Liver Fatty Acid Oxidation Assay

Fatty Acid Oxidation (FAO) was measured by using a commercial Kit (Biomedical Research, USA). Briefly, 20 mg of liver tissue were homogenized in 750 µl of cell lysis

solution and centrifuged at 10000 rpm for 5 min. Protein determination was determined in supernatant fractions using a Bradford Assay. Protein samples were normalized and 15ug were loaded per well with the respective loading control and samples. Samples were incubated for 2 h at 37 ºC with 50 µl FAO assay solution. Reaction was stopped by adding 50ul of 3% Acetic Acid and colorimetric determination was finally determined at 492nm using a spectrophotometer.

4.11.1.3 Serum Mouse Fibroblast Growth Factor (FGF-21) determination

Mouse serum FGF-21 concentration was determined by ELISA using the Mouse/Rat FGF-21 Quantikine ELISA Kit (R&D Systems) according to the manufacturer´s instruction.

4.11.2 Glycaemic control and pancreatic function

4.11.2.1 Glucose quantification in mouse serum

The tip of the tail vein was nicked using a pair of sterile scissors and a blood drop was obtained by gently massaging the tail. Blood glucose was measured by following the instructions of the automatic glucometer (Accu-Chek Aviva, Roche, USA).

4.11.2.2 Insulin quantification in mouse serum

Blood insulin levels were determined by ELISA using Mouse Insulin ELISA (Mercodia AB, Sweden, Ref.10-1247-01) according to the manufacturer´s recommendations.

4.11.2.3 Insulin Tolerance Test (ITT)

Animals followed a 6h fasting period before starting the ITT. Insulin and glucose solutions were freshly prepared: Actrapid (Novo Nordisk) 100U/mL was diluted 1:1000 in sterile PBS in order to obtain 0.1 U/mL and 1gr of glucose (Sigma) was resuspended in 5mL of sterile PBS. Mice were then weighed, and the tip of the tail vein was nicked using a pair of sterile scissors. After a baseline glucose measure, insulin was injected into the intraperitoneal cavity using an insulin syringe (BD-MicroFine^{TM}, USA), 7.5ul per gr. At 15, 30, 60 and 90 minutes blood glucose was measured by gently massaging a small drop of blood onto the glucometer strip (Accu-Chek Aviva, Roche, USA). Glucose

solution was prepared in case glycaemia resulted lower than 40mg/dL; in that case 150ul were injected into the intraperitoneal cavity.

4.11.2.4 Intraperitoneal Glucose Tolerance Test (IPGTT)

Animal followed an overnight fasting period before starting the IPGTT. The glucose solution was freshly prepared: 1 g of glucose (Sigma, USA) was resuspended in 5mL of sterile PBS and filtered through 0.22um Millipore filter. Mice were then weighed, and the tip of the tail vein was nicked using a pair of sterile scissors. After a baseline glucose measurement, glucose was injected into the intraperitoneal cavity using an insulin syringe (BD-MicroFine™, USA), 2g/kg body weight. At 15, 30, 60 and 120 min blood glucose was measured by gently massaging a small drop of blood onto the glucometer strip. Blood glucose was measured using an automatic glucometer (Accu-Chek Aviva, Roche, USA).

4.11.2.5 Static insulin secretion

Following the protocol described in Martín et al., the fresh collagenase-isolated islets were incubated for 1 h at 37 °C in fresh Krebs Ringer Bicarbonate Buffer (KRB) supplemented with 5.6 mmol/L glucose and 3% BSA (Sigma-Aldrich, USA). The medium was continuously bubbled with a mixture of 95% O_2:5% CO_2 to obtain a final pH of 7.4. The medium was then replaced, and the islets were incubated in groups of 5 in 1 mL of KRB supplemented with 1% BSA and glucose at various concentrations (2.75, 5.5, 11.1, 16.7 and 22.2 mmol/L) for an additional 60 min at 37 ºC. Then, the supernatant was collected and stored at −80 °C for the subsequent insulin measurements (Martín et al. 1999). Insulin was assayed by ELISA using the kit from Mercodia per the manufacturer's instructions and Quant-iT PicoGreen dsDNA Assay kit (Invitrogen, USA) was used to measure islet DNA. Insulin values were normalized to DNA content from each batch. Standard curves and experimental points were performed in triplicate.

4.11.2.6 Pancreatic islets ATP determination

Total ATP content was determined as previously described (Qi et al. 2017). Briefly, pancreatic islets total ATP was first extracted. Islets were washed twice in cold KRB supplemented with 5.6 mmol/L glucose and 3% BSA (Sigma-Aldrich, USA) and centrifuged for 1 min at 100x *g*. Then, supernatant was removed, 600 µL of somatic cell ATP releasing reagent (Merck Life Science, Spain) was added to the islet pellets and

samples were sonicated on ice for 1 min (Branson 450 Digital Sonifier, Marshall Scientific, USA). Afterwards, 400 µL of the ATP releasing reagent was added to the samples and they were centrifuged for 15 min at 1400x *g* (4ºC). Finally, 800 µL of supernatant was collected and stored at -80ºC for further measurement of total ATP. Finally, the total ATP content was quantified using the ATP Assay kit (Abcam, UK) following manufacturer´s instructions. Fluorescence (Ex/Em= 535/587/nm) was read using a Varioskan Flash microplate reader (Thermo Scientific, Finland). ATP values were normalized to DNA content from each batch.

4.11.2.7 PET-CET analysis in mouse liver

PET-CT was performed in anesthetized mice using isoflurane. Ophthalmic gel was placed in the eyes to prevent drying. PET-CT studies were performed with a small-animal PET/CT scanner (nanoScan, Mediso, Hungary). Images were acquired 60 minutes after intraperitoneal administration of 8-10 MBq of 18F-FDG using an X-ray beam current of 178 µA and a tube voltage of 45 kVp. After the CT scan, PET data were collected for 30 minutes and reconstructed using the Teratomo 3D algorithm, in a 105 x 105 x 235 matrix (voxel dimensions of 0,4 mm). The region of interest (ROI) was delimited to the liver to obtain the liver uptake (KBq/cc). Biomedical imaging was conducted at the Advanced Imaging Unit of the CNIC (Centro Nacional de Investigaciones Cardiovasculares Carlos III), Madrid, Spain.

4.11.3 Respiration studies in hepatocytes (Seahorse Analysis)

Cellular metabolic profile was determined using high resolution respirometry, the Seahorse Bioscience XF24 Extracellular Flux Analyzer (Seahorse Biosciences, USA), providing real-time measurements of oxygen consumption rate (OCR) and extracellular acidification rate (ECAR). Primary Wt, MCJ-KO and silenced mouse hepatocytes were plated in a collagen type I coated XF24 cell culture microplate (Seahorse Bioscience) at 2.0-3.0 x10^4cells per well, with 500 µl of assay medium prewarmed to 37°C, composed of MEM without bicarbonate, containing 10 mM sodium pyruvate, 10 mM l-glutamine and 1X non-essential amino acids. Cells were then placed on a CO_2 free incubator, at 37ªC, for at least one hour. Meanwhile, the XF assay cartridge (Seahorse Bioscience) was prepared. The following pharmacologic inhibitors were used with the following final concentration: oligomycin (1 µM), an inhibitor of ATP synthase, which allows the

measurement of ATP-coupled oxygen consumption through OXPHOS; carbonyl cyanide 4-trifluoromethoxyphenylhydrazone (FCCP) (0.3 µM), an uncoupling agent that allows maximum electron transport, and therefore a measurement of the maximal OXPHOS respiration capacity; and Rotenone (0,5µM)/Antimycin (0,5µM) mix, mitochondrial Complex I and III inhibitors, respectively. Once the cartridge was ready, after an equilibration step, cells were placed within the Seahorse Bioscience XF24 and upon the sequential delivery of the inhibitors, changes in the OCR were recorded. The normalized data were expressed as pmol of O_2 per minute, per amount of protein quantified by crystal violet staining.

4.11.4 Determination of hepatic Krebs Cycle Intermediate Levels

Liver samples were homogenized in 500 µl of ice-cold extraction liquid with a tissue homogenizer (FastPrep) in one 40 seconds cycle at 6000 rpm. The extraction liquid consisted of a mixture of ice-cold methanol/water (50/50 %v/v). Subsequently 400 µl of the homogenate plus 400 ul of chloroform was transferred to a new aliquot and shaken at 1,400 rpm for 60 minutes at 4 °C. The aliquots were then centrifuged for 30' at 14,000 rpm at 4 °C. 100 µl of the aqueous phase was transferred to a fresh tube. The chilled supernatants were evaporated in a speedvac for approximately 1h. The resulting pellets were resuspended in 250 µl water/acetonitrile (MeCN)/ (40/60/ v/v/).

Samples were measured with a UPLC system (Acquity, Waters Inc., Manchester, UK) coupled to a Time-of-Flight mass spectrometer (ToF MS, SYNAPT G2, Waters Inc.). A 2.1 x 100 mm, 1.7 µm BEH amide column (Waters Inc.), thermostated at 40 °C, was used to separate the analytes before entering the MS. Mobile phase solvent A (aqueous phase) consisted of 99.5% water and 0.5% FA while solvent B (organic phase) consisted of 4.5% water, 95% MeCN and 0.5% FA. Extracted ion traces are obtained for malic acid (m/z = 133.0137), succinic acid (m/z = 117.0188) and fumaric acid (m/z = 115.0031) in a 20 mDa window for the most abundant isotopes and subsequently smoothed and integrated with QuanLynx software (Waters, Manchester, UK). Measured concentrations were converted into amount of analyte per mg liver tissue, taking in account analyte loss due to sample work up.

4.11.5 ATP detection assay

Hepatocytes and cell culture media were used to quantify ATP production and secretion. Quantification of intracellular and extracellular ATP levels was performed in OptiPlate-96 white opaque 96-well microplates (PerkinElmer) using the ATPlite™ luminiscence ATP detection kit (PerkinElmer) and following the manufacturer´s instruction. In brief, 50 µl of the mammalian cell lysis solution were added to 100 µl of the cell suspension or cell media and incubated on an orbital shaker (700 rpm, 5', RT). 50 µl of the substrate solution were added and incubated (700 rpm, 5', RT). Plate was adapted to the dark for 10' and the luminescence was measured in a luminometer. ATP concentration was calculated by extrapolation to an ATP standard curve and subsequent normalization with the total protein content of each sample determined by the Bradford assay (Bio-Rad).

4.11.6 Liver Succinate Dehydrogenase (SDH_2) activity assay

Mitochondrial succinate dehydrogenase (SDH_2) activity was measured in frozen liver tissue with Succinate Dehydrogenase Activity Colorimetric Assay Kit (MAK197, Sigma Aldrich) following the manufacturer's procedure. 5mg of frozen liver were homogenized in 100 µl of the SDH_2 Assay Buffer and kept on ice for 10 minutes. Then, samples were centrifuged (10000g, 5'). A reaction mix of 50 µl was prepared containing (46 µl of SDH assay buffer; 2 µl of SDH_2 substrate mix and 2 µl of SDH_2probe) and added to the supernatant. Absorbance was measured at 600 nm ($A_{initial}$) at initial time ($T_{initial}$). The plate was incubated at 25ºC, and absorbance was measured every 5 minutes during 40 minutes (after this time values were not within the standard curve linearity). SDH_2 activity was calculated and represented as nmol of succinate converted to fumarate per volume and per minute as indicated by manufacturer's recommendations.

4.11.7 Quantification of hepatic reduced to oxidized glutathione (GSH/GSSG)

Liver extracts were analyzed with a UPLC system (Acquity) coupled to a Time-of-Flight mass spectrometer (ToF MS, SYNAPT G2, Waters). A 2.1 x 100 mm, 1.7 mm BEH amide column (Waters), stabilized at 40ºc, was used to separate the analytes before entering the MS. Solvent A (aqueous phase) consisted of 99.5% water, 0.5% formic acid, and 20mM ammonium formate, while solvent B (organic phase) consisted of 29.5% water, 70% MeCN, 0.5% formic acid and 1mM ammonium formate. The extracted ion trace was obtained for GSH (m/Z= 308.0916) and GSSG (m/z= 613.1598) and

subsequently smoothed (2 points, 2 iterations) and integrated with QuanLynx software (Waters).

4.11.8 NAD^+/NADH determination in liver and gut tissue

Hepatic NAD^+/NADH levels were measured using a commercial Kit (ab65348, Abcam, UK). 10mg of frozen tissue were homogenized in 300ul of Extraction buffer and briefly sonicated. Samples were then centrifuged at top speed for 10 min at 4ºC and the supernatant was assayed. Protein concentration was determined in supernatant fractions using a Bradford Assay. Protein samples were normalized to 100ug in 100ul; 50ul were kept on ice while 50ul were warmed for 30 min to degrade NAD^+. Samples were incubated for 5 min with the Reaction Mix and after adding the NADH Developer, the colorimetric determination was finally done at 450nm using the SpectraMax M2 microplate reader**.**

4.11.9 Hepatic Sirtuin (SIRT1) activity assay

Hepatic SIRT1 activity was measured using a commercial Kit (ab156065, Abcam, UK). Briefly, 20mg of liver tissue were used to extract the nuclei as shown in Papageorgiou et al. (Papageorgiou, Demmers, and Strouboulis 2013). Protein concentration was determined using a Bradford Assay and the purity of the fractions was confirmed by western blot. Nuclei were normalized to 60ug in 60ul, and samples were assayed in duplicates, 25ul per well, enzyme sample and the background control. The fluorometric determination was done using the SpectraMax M2 microplate reader, with excitation at 340-360nm and emission at 440-460nm.

4.11.10 Measurement of Hepatic Ethanol and Acetaldehyde content

250mg of liver tissue was used to measure either the hepatic Ethanol or Acetaldehyde content. Homogenized biological tissue was mixed with 500 µL of 1 M perchloric acid and mixed for 2 min and adjusted the pH to 7.0 - 8.0 using approximately 500 µL of 1 M KOH. Samples were stored on ice for 20 min to precipitate potassium perchlorate and allow separation of the fat (if present). Volumes of the samples were centrifuged at 13000*g*, 4ºC for 10 min and the clarified supernatant recovered for use in the assay.10 µL of standards, blanks, and samples were mixed with 200 µl of distilled water, 20 µl of

buffer and 20 µl of NAD+, the absorbances of the initial solutions were read after a 2 min reaction. After that, an aliquot of 2 µl of either alcohol dehydrogenase (ADH) or aldehyde dehydrogenase (ALDH2) (for hepatic ethanol and acetaldehyde, respectively) was added; the absorbance was registered after approx. 5 min. All measurements were analyzed on a costar 96-well clear flat-bottomed plate (Corning, USA) in a Citation 3 (BioTek Instruments Inc., USA) with UV-Vis absorbance monochromators at 340 nm. The amount of NADH formed in this reaction is stoichiometric with twice the amount of ethanol, and stoichiometric with the amount of acetaldehyde.

4.12 IMMUNE SYSTEM ANALYSIS

4.12.1 Isolation of liver infiltrating immune cells for flow cytometry

80mg of fresh liver tissue were digested with Type I collagenase (LS004196, Worthington Biochemical Corp., USA) (2mg/ml in HBSS), at 37ºC, 200rpm for 40 min. Samples were filtered through a 70uM strainer (22363548, Fisher Scientific, Spain) and washed with PBS-2%FBS at 500*g* for 5 min. Then, a 33,75% Percoll™ PLUS (17-5445-01, GE Healthcare, USA) gradient at 693*g*, for 12 min 20ºC was used to separate the hepatocytes and stellate cells from the immune cells, that led in the bottom. The pellet was resuspended in 1mL red blood cell lysis solution (A10492-01, Gibco, USA) and incubated for 4 min RT to eliminate erythrocytes. The reaction was stopped using PBS (14190-094, Gibco, USA). Another washing step was performed, and cells were resuspended in 200ul PBS, ready for staining.

4.12.2 Isolation of pancreas infiltrating immune cells for flow cytometry

The procedure described by Villarreal et al. was followed for the isolation of pancreas infiltrating immune cells (Villarreal et al. 2019). Briefly, pancreas was digested with Type V collagenase (17104-019, Gibco, USA) by cannulating the common bile duct near the Ampulla of Vater with the syringe containing Type V collagenase 1mg/ml in HBSS, once having placed the clamp at the near end of the liver, closing the Bile duct and the Hepatic artery. Pancreas was extracted, mechanically chopped, and digested 10 minutes on a shaking water bath at 37ºC, followed by 30s of mixing by hand. Samples were then filtered through a 70uM strainer (22363548, Fisher Scientific, Spain) and washed twice

with ice cold HBSS at 300xG for 3 min. Cells were resuspended in 200ul PBS, ready for staining.

4.12.3 Flow cytometry and Fluorescent Activated Cell Sorter (FACS)

After isolation, cells were stained with live/dead fixable green (1:1000 in PBS, Invitrogen, USA, L23101) at 4ºC for 30 min. A wash step was performed at 600*g* 5 min before adding 1:200 of Fc Blocker (Biolegend, USA, 101319) for 5 min. Then, 1:200 of primary antibodies was added in staining buffer (00-4222-26, Thermofisher, USA) and incubated for 30 min at 4ºC. Another washing step was performed, and cells were resuspended in 200 µL of staining buffer for acquisition in FACSymphony (BD, USA) and results were analyzed by flowjo (BD, USA). Antibodies used for staining are indicated at **Table 4.7**.

Table 4.7 List of antibodies used for flow cytometry

Antibodies	Fluorochrome	Source	Identifier
CD11b	BUV805	BD	741934
CD11c	PE	Biolegend	117307
CD19	APC	Biolegend	115512
CD3	BUV737	BD	612803
CD4	BUV395	BD	563790
CD45	BV480	BD	566073
CD8	BUV563	BD	748535
F4/80	APC-fire750	Biolegend	117307
GR1	BV711	Biolegend	108443
NK1.1	BV605	Biolegend	108753

4.12.4 Mouse Tumor Necrosis Factor (TNF) quantification in serum

Serum TNF levels were determined by ELISA using the DuoSet II kit (R&D Systems) according to the manufacturer´s recommendations.

4.12.5 Mouse Interleukin-6 (IL-6) quantification in serum

Serum IL-6 levels were determined by using IL-6 Mouse ELISA kit (Invitrogen) according to the manufacturer´s recommendations.

4.13 LIVER INJURY ANALYSIS

4.13.1 Liver transaminase activity determination in mouse serum

Aspartate aminotransferase (AST) and alanine aminotransferase (ALT) serum activity was determined by using the Selectra Junior Spinlab 100 automated analyzer (Vital Scientific) according to the manufacturer's instructions. Standard controls were run before each determination.

4.13.2 Hepatic Calpain activity assay

Calpain Activity Assay Kit (ab65508, Abcam) was used to measure hepatic calpain activity in 10mg of frozen livers manually homogenized in 100ul of Extraction Buffer (Abcam) and centrifuged at 14,000 rpm for 10 minutes at 4ºC. Samples, positive and negative controls were incubated with 10ul of Reaction Buffer (Abcam) and 5ul of Calpain Substrate (Abcam), for an hour, at 37ºC, and fluorescence was measured using a SpectraMax M2 microplate reader (excitation wavelength 400, emission wavelength 505).

4.14 MITOCHONDRIAL ROS ANALYSIS

Mitochondrial Reactive Oxygen Species (ROS) production in primary hepatocytes was assessed using MitoSOX$_{TM}$ Red mitochondrial superoxide indicator (Life Technologies), following manufacturer´s instructions.

4.15 INTESTINAL PERMEABILITY ANALYSIS

4.15.1 Analysis of intestinal permeability using FITC-Dextran

Mice where administered 100ul of FITC-dextran 0.6mg/g of animal by oral gavage and after 4h mice were sacrificed. Serum samples were diluted 1:1 in dPBS and added into a

96-well microplate, where the FITC concentration was determined using a SpectraMax M2 microplate (excitation of 485nm and emission wavelength of 528nm). Serum from mice not administered with FITC-dextran was used to determine the background.

4.15.2 Lipopolysaccharides (LPS) quantification as a marker of increased permeability

4.15.2.1 Quantification in serum

Serum LPS levels were determined by ELISA using the Mouse Lipopolysaccharides (LPS) ELISA Kit (CSB-E13066m, Cusabio, USA) according to the manufacturer´s recommendations.

4.15.2.2 Quantification in liver tissue

Mouse Lipopolysaccharides (LPS) ELISA Kit (CSB-E13066m, Cusabio, USA) was used to measure hepatic LPS content in 5mg of frozen livers manually homogenized in 200ul PBS 1x with protease inhibitors, stored overnight at -20ºC and centrifuged at 5,000*g* for 10 min at 4ºC. Supernatants were diluted 1:500 and 50ul were assayed. Optical density was determined using a SpectraMax M2 microplate reader (Molecular Devices, USA) set to 450nm (correction was set to 540nm and the reading was subtracted).

4.16 STATISTICAL ANALYSIS

All the experiments were performed at least in triplicate. Data is expressed as mean ± SEM and represented as fold change vs. control mean value when indicated. Prism 9 (GraphPad Software, version 9.2.0, USA) was used to perform statistical analyses. A one-way analysis of variance (ANOVA) followed by Tukey (comparing all pairs of columns) was used for three or more groups, while Student's t-test was used for 2 groups. For human samples the Mann-Whitney U test was used for 2 groups. Grubbs' test was performed to determine the significant outliers. A $p < 0.05$ was considered statistically significant. Statistical parameters are reported in the figure legends.

5. RESULTS

5 RESULTS

5.1 THE OUTCOME OF BOOSTING MITOCHONDRIAL ACTIVITY IN ALCOHOLIC LIVER DISEASE (ALD) IS ORGAN-DEPENDENT

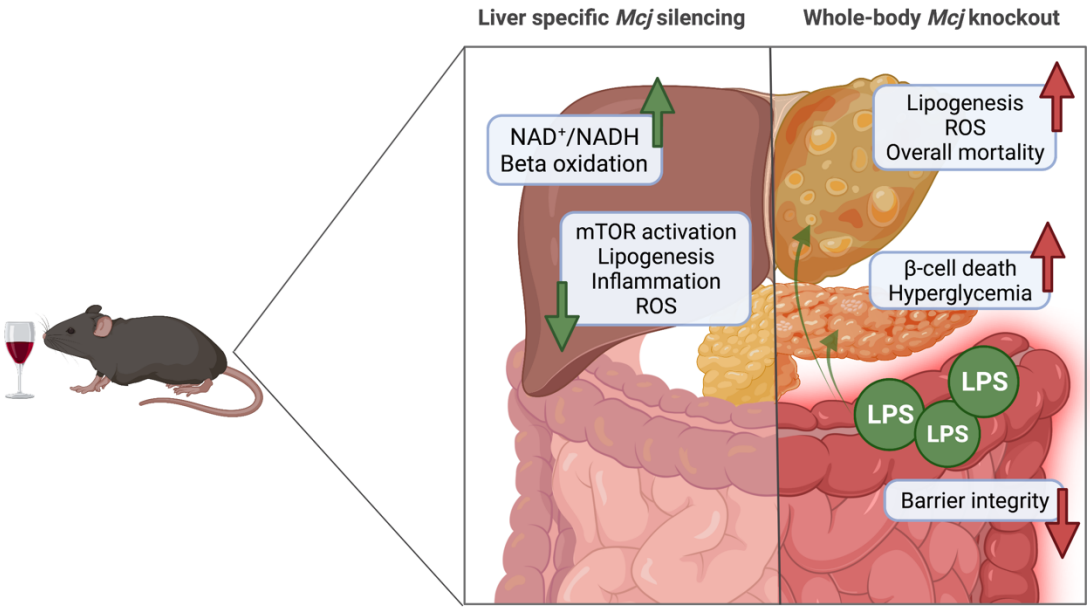

Fig. Opposite results are obtained when silencing *Mcj* specifically in the liver vs in the whole-body during ALD, what highlights the need of an organ or even cell specific therapy to treat liver diseases

5.1.1 MCJ expression in human liver with severe alcoholic hepatitis (AH)

Although mitochondrial dysfunction is known to play a key role in the pathogenesis of alcoholic liver disease (ALD), up to date, no studies have investigated *MCJ/DNAJC15* in ALD patients. To this end, first we compared *MCJ* expression in liver biopsies from patients with early ASH, non-severe and severe AH, and explants of undergoing liver transplantation. Our results showed that, compared to healthy individuals, expression of *MCJ* was downregulated in early stages, and significantly increased in the explants of AH patients undergoing liver transplantation (Fig. 5.1 A). Likewise, *MCJ* showed a tendency to increase in patients suffering from severe AH, compared to non-severe disease (Fig. 5.1 A).

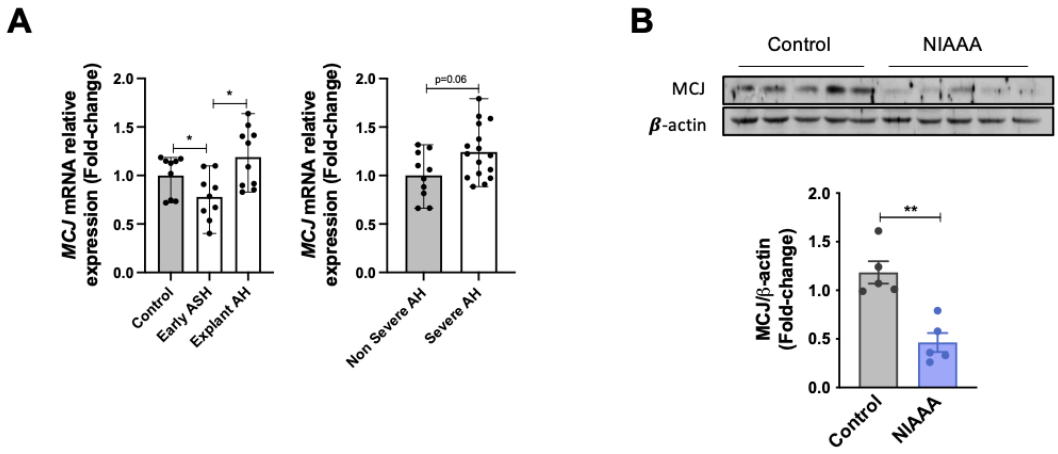

Fig. 5.1 MCJ expression is regulated in alcoholic liver injury. (A) Liver biopsies from patients with Early ASH (n=11), Non-Severe AH (n=11), Severe AH (n=18) and Explanted AH (n=11), together with healthy control individuals (n=10) were used to determine *Mcj* expression by qPCR. Values are represented as Median ± Range. U-test was used to compare two groups. (ASH=alcoholic steatohepatitis, AH= alcoholic hepatitis). **(B)** MCJ levels by western blotting (upper panel) and densitometric quantification (bottom panel) in WT liver extracts with control (n=5) and NIAAA diet (n=5). ß-actin was used as a loading control. Values are represented as mean ± SEM. Student's t-test was used to compare two groups. *p<0.05 and **p<0.01 versus control.

On the other hand, while none of the current animal models can reproduce all major features of human ALD, they remain a very useful tool to study this disease (Nevzorova et al. 2020). In this sense, we determine MCJ protein levels in livers from mice fed the NIAAA model (Bertola et al. 2013), used to study early stages of alcohol steatohepatitis (ASH). Following 10 days of ad libitum oral feeding with the Lieber-DeCarli ethanol liquid diet (5% vol/vol), plus a single binge ethanol feeding at day 11 (31,5% vol/vol) (NIAAA model), MCJ was downregulated compared to control liquid diet (Fig. 5.1 B).

These results confirmed that at early stages of ALD mitochondrial activity was already altered, as MCJ expression was significantly downregulated.

5.1.2 Whole body knockout of MCJ increased ethanol consumption-induced liver injury

Based on previous studies that proved hepatoprotection in MCJ-KO mice (Barbier-Torres et al. 2017, 2020; Goikoetxea-Usandizaga et al. 2022; Iruzubieta et al. 2021), it was surprising to find increased mortality in MCJ-KO mice (55%) compared to Wt mice (15%) that were subjected to the NIAAA protocol (Fig. 5.2A). Ethanol-fed MCJ-KO mice showed increased liver injury; samples were analyzed by histopathology, and it was concluded that ethanol-fed MCJ-KO mice showed more severe steatosis and inflammation, with a final injury score of 3,7 vs 2,3 obtained by ethanol-fed Wt mice (Fig. 5.2B). Besides, we also observed significantly increased necrotic areas and cleaved caspase-3 staining levels (Fig. 5.2B). In mRNA levels of pro-apoptotic genes *Trail, Bax, Bcl2* and *BclxL* no significant changes were found (Fig. 5.2C). A trend to increased serum ALT levels was also seen in MCJ-KO mice (Fig. 5.2D), whereas AST levels remained unchanged (data not shown). In sum, ethanol-fed MCJ-KO mice exhibit milder increased hepatocellular injury compared with ethanol-fed Wt mice.

Since alcohol can interfere with lipid metabolism and induce fat deposition, the effect of MCJ expression manipulation was investigated. The lack of MCJ significantly increased liver steatosis, measured as Sudan Red staining and triglyceride accumulation (Fig. 5.2 E,F). Interestingly, both hepatic fatty acid oxidation and *de novo* lipogenesis/accumulation were augmented; in line with previous results (Barbier-Torres et al. 2020), hepatic beta-oxidation was significantly enhanced in MCJ-KO mice (Fig. 5.2G) and significantly increased mRNA levels of *Fatp2, Ppara, Acc1* and *Chrebp* were found compared to Wt mice (Fig. 5.2H). Moreover, significantly increased *Glut2* expression levels were found in MCJ-KO mice (Fig. 5.2H).

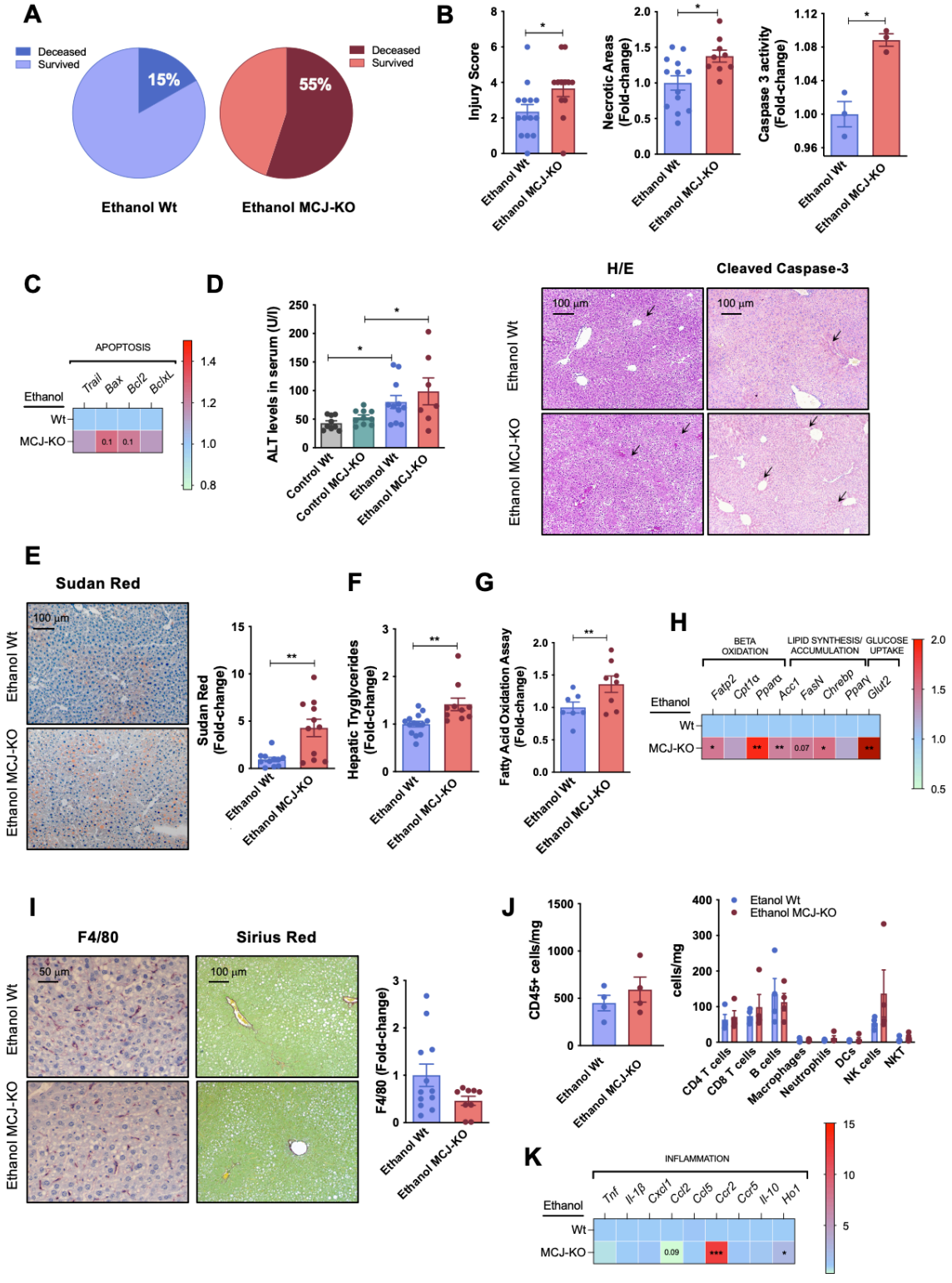

Fig. 5.2 Whole body MCJ-KO show increased liver injury, steatosis and inflammation after ethanol consumption. (A) Pie charts represent the percentage of Survived and Deceased Wt (Left panel) and MCJ-KO (Right panel) mice following the NIAAA model. **(B)** Hepatic injury score obtained after the histopathological evaluation and immunohistochemical staining and quantification of both Necrotic Areas, based on H&E staining, and Cleaved Caspase-3 in Wt versus MCJ-KO mice following the NIAAA model. **(C)** Heatmap representing the differential hepatic expression of mRNA levels from genes involved in Apoptosis in Wt and MCJ-KO mice after NIAAA model (*Trail*= TNF-related apoptosis-inducing ligand; *Bax*= Bcl-2-associated X protein). **(D)** Serum alanine aminotransferase (ALT)

levels in Control and NIAAA fed Wt and MCJ-KO mice. **(E)** Liver immunohistochemical staining and quantification for Sudan Red, a maker for hepatic steatosis, in Wt versus MCJ-KO mice following the NIAAA model. **(F)** Hepatic triglyceride content in Wt versus MCJ-KO mice after the NIAAA model. **(G)** Fatty Acid Oxidation rate was assayed in liver tissue in ethanol-fed Wt and MCJ-KO mice. **(H)** Heatmap showing the differential hepatic expression of mRNA levels from genes involved in Lipid Metabolism in Wt and MCJ-KO mice after NIAAA model (*Fatp2*= Fatty acid transport protein 2; *Cpt1a*= Carnitine Palmitoyltransferase 1A; *Ppara*= Peroxisome proliferator-activated receptor alpha; *Acc*= Acetyl-CoA carboxylase; *FasN*= Fatty acid synthase; *Chrebp*= Carbohydrate-responsive element-binding protein; *Pparg*= Peroxisome proliferator-activated receptor gamma; *Glut2*= Glucose transporter 2). **(I)** Liver immunohistochemical staining and quantification for F4/80, macrophage infiltration, and Sirius Red, fibrosis in ethanol fed Wt and MCJ-KO mice. **(J)** Quantification of hepatic total CD45+ cells and a further characterization of different CD45+ populations using FACS in ethanol fed Wt and MCJ-KO mice. **(K)** Heatmap showing the differential hepatic expression of mRNA levels from genes involved in inflammation in Wt and MCJ-KO mice after NIAAA model (*Tnf*= Tumor necrosis factor; *Il-1b*= Interleukin 1 beta; *Cxcl1*= C-X-C Motif Chemokine Ligand 1; *Ccl2*= C-C Motif Chemokine Ligand 2; *Ccl5*= C-C Motif Chemokine Ligand 5; *Ccr2*= C-C Motif Chemokine Receptor 2; *Ccr5*= C-C Motif Chemokine Receptor 5; *Il-10*= Interleukin-10; *Ho-1*= Heme oxygenase-1). Values are represented as mean ± SEM. Student's t-test was used to compare two groups and one-way ANOVA followed by Tukey post-test was used to compare between multiple groups. *p<0.05, **p<0.01 and ***p<0.001 versus Wt.

Inflammation is another hallmark of ethanol induced liver injury (Avila et al. 2021a). Although ethanol consumption increased hepatic inflammation compared to control mice, we did not observe any differences between ethanol-fed Wt and MCJ-KO mice. F4/80 staining depicted hepatic macrophage infiltration in liver parenchyma (Fig. 5.2I), and flow cytometry was used to interrogate the composition of liver infiltrating immune cells (Fig. 5.2J). NK cells, B cells, $CD8^+$ T and $CD4^+$T cells were the most represented populations, with no evident changes between Wt and MCJ KO mice. Analysis of the expression of inflammatory cytokines revealed significantly increased *Ccr2* levels in ethanol-fed MCJ-KO mice, although the rest of pro-inflammatory cytokines remained unaltered (Fig. 5.2K). Finally, we found no signs of liver fibrosis in MCJ-KO mice (Fig. 5.2I).

The metabolism of high concentrations of alcohol results not only in acetaldehyde, but also in the production of ROS that alter mitochondrial activity and other signaling pathways (Ceni, Mello, and Galli 2014). Analysis of the main enzymes related to alcohol metabolism revealed significantly increased *Adh1* and *Cyp2e1* mRNA levels in MCJ-KO mice (Fig. 5.3A), hinting an accelerated metabolism. Ethanol-fed MCJ-KO mice had a slight tendency towards a reduced hepatic accumulation of both ethanol and acetaldehyde, in line with previous results (Fig. 5.3B). In accordance, MCJ-KO showed increased ROS production, proved by higher levels of DHE staining, along with augmented levels of 4HNE staining, a marker for lipid peroxidation, consequence of increased hepatic steatosis and ROS production (Fig. 5.3C). Finally, we observed no differences in the reduced (GSH)/oxidized (GSSG) glutathione ratio, a potent antioxidant (Fig. 5.3D).

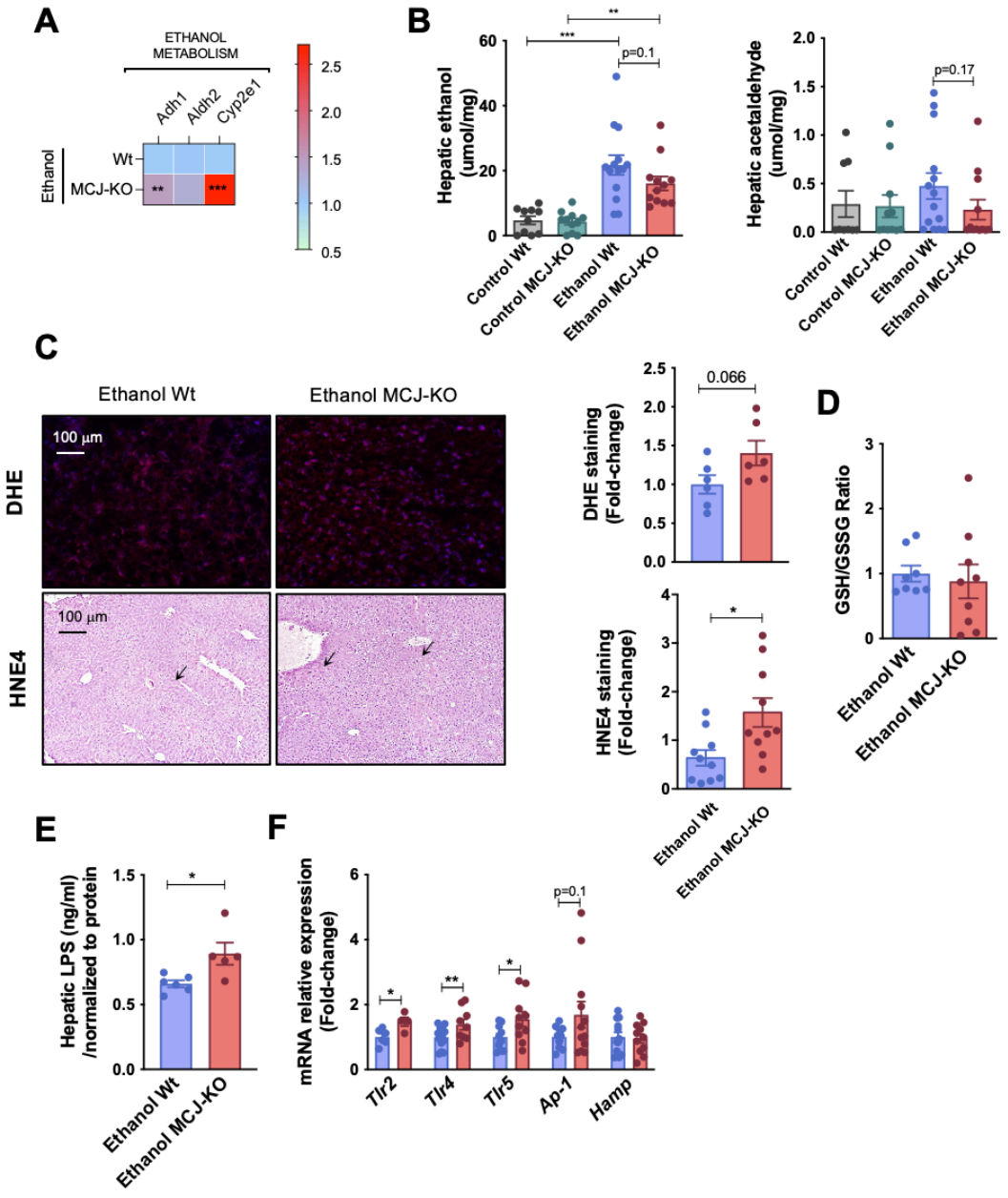

Fig. 5.3 Accelerated ethanol metabolism, increased oxidative stress and altered gut-liver axis in whole body MCJ-KO. (A) Heatmap showing the differential hepatic expression of mRNA levels from genes involved in Ethanol metabolism in Wt and MCJ KO mice after NIAAA model (*Adh1*= Alcohol dehydrogenase 1; *Aldh2*= Aldehyde dehydrogenase 2; *Cyp2e1*= Cytochrome P450 Family 2 Subfamily E Member 1). **(B)** Hepatic ethanol (left panel) and acetaldehyde (right panel) quantification in Control and NIAAA fed Wt and MCJ-KO mice. **(C)** Liver immunohistochemical staining (left panel) and respective quantification (right panel) for DHE and 4-HNE in ethanol-fed Wt versus MCJ-KO mice. **(D)** Hepatic reduced to oxidized glutathione ratio in ethanol fed Wt versus MCJ-KO mice. **(E)** Hepatic amount of LPS in Wt versus MCJ-KO mice following NIAAA model. **(F)** Differential hepatic expression of mRNA levels from genes involved in LPS recognition in Wt and MCJ-KO mice after NIAAA model (*Tlr*= Toll Like receptor; *Ap-1*= Activator protein-1; *Hamp*= Hepcidin antimicrobial peptide). Values are represented as mean ± SEM. Student's t-test was used to compare two groups and one-way ANOVA followed by Tukey post-test was used to compare between multiple groups. *p<0.05, **p<0.01 and ***p<0.001 versus Wt.

The pathophysiology of ALD is closely related to the effect of ethanol and its metabolites not only on the liver, but also on other organs. Alcohol consumption affects the gut at multiple levels, and through its relation to the liver via the portal vein, these effects become visible at the hepatic level, as the gut-liver axis results altered (Avila et al. 2021a). We found significantly increased hepatic lipopolysaccharide (LPS) concentrations, a Gram-negative bacteria derived harmful product (Fig. 5.3E); and significantly elevated expression of Toll-like receptors (TLRs) (Fig. 5.3F) involved in the recognition of LPS, in ethanol-fed MCJ-KO mice, suggesting an increased gut injury and presumably endotoxemia.

Altogether, the NIAAA murine model represents an early alcoholic liver injury, with mild hepatocellular damage, altered lipid metabolism and inflammation, lacking any signs of fibrosis. Importantly, MCJ-KO mice showed increased mortality, liver injury and an apparent gut injury following ethanol consumption.

5.1.3 Augmented intestinal permeability and translocation of bacterial products in ethanol-fed MCJ-KO mice

Alcohol leads to changes in the composition of the gut microbiome, the disruption of the gut barrier and increased intestinal permeability, facilitating the translocation of microbial products (Bishehrashi et al. 2017).

The histopathological evaluation of the colon showed neither injury nor differences between control-fed Wt and MCJ-KO mice, as Pacual-Itoiz et al. (Pascual-Itoiz et al. 2020) had already seen (Fig. 5.4A). On the other hand, compared to control diet, ethanol-treated mice presented lesions in the mucosa and submucosa. Focal ulceration, mononuclear cell infiltration and edema were observed in the mucosa, while the submucosa exhibited mononuclear infiltration and edema. MCJ-KO mice displayed a mean injury score value of 3.42 and Wt mice 1.63, indicating that ethanol-fed MCJ-KO mice had more severe lesions at the colon level (Fig. 5.4A). Elevated expression of *Tnf* and *Il-1ß* were detected by qPCR (Fig. 5.4B), and IHC revealed higher levels of F4/80 staining in the gut of ethanol-fed MCJ-KO mice (Fig. 5.4C); confirming that whole-body MCJ silencing causes an elevated infiltration of macrophages in the intestine, increasing the proinflammatory response.

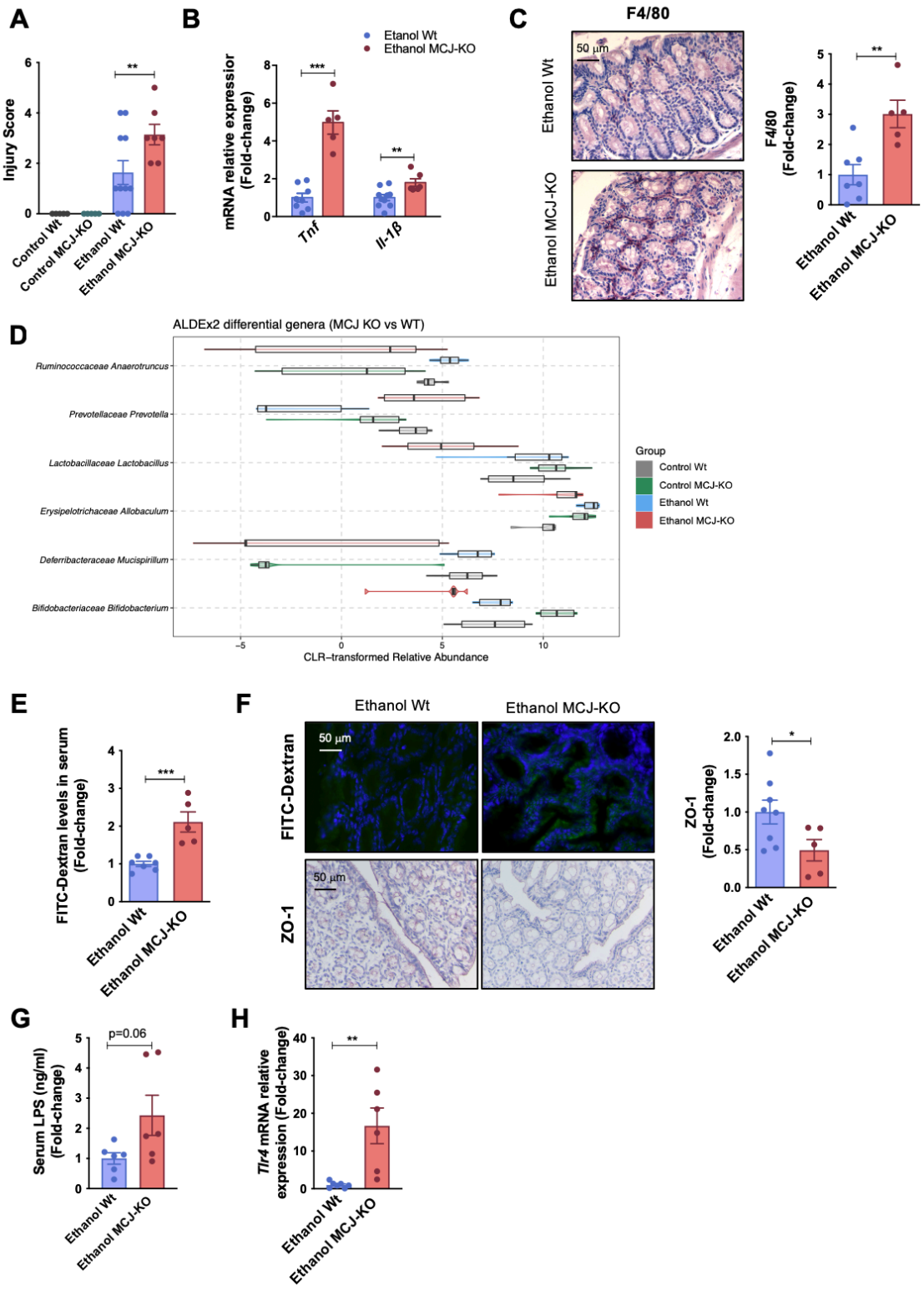

Fig. 5.4 Increased intestinal permeability and translocation in ethanol-fed MCJ-KO mice. (A) Gut injury score obtained after the histopathological evaluation in control and ethanol-fed Wt and MCJ-KO mice. **(B)** Differential gut expression of mRNA levels from *Tnf* and *Il-1b* in Wt and MCJ-KO mice after NIAAA model (*Tnf*= Tumor necrosis factor; *Il-1b*= Interleukin 1 beta). **(C)** Immunohistochemical staining (left panel) and respective quantification (right panel) for F4/80, a marker for macrophage infiltration, in ethanol-fed Wt versus MCJ-KO mice. **(D)** Central Log-Ratio (CLR) transformed abundance for the significant genera (FDR < 10%) found for the comparison between the gut microbiome of MCJ-KO mice versus Wt mice. For each genera, distribution of the CLR-transformed is represented for

each of the 4 study groups using a combination of violin plot for the general distribution and a boxplot for the summary distribution, colored accordingly. **(E)** Serum FITC-Dextran levels, as a marker for intestinal permeability, in ethanol-fed Wt versus MCJ-KO mice (FITC= fluorescein isothiocyanate). **(F)** Immunohistochemical representation of intestinal FITC-Dextran levels, and immunohistochemical staining (left panel) and respective quantification (right panel) for ZO-1, tight junction, in ethanol-fed Wt and MCJ-KO mice (ZO-1= Zonula occludens). **(G)** Serum LPS concentrations in ethanol-fed Wt and MCJ-KO mice. **(H)** Differential gut expression of mRNA levels from *Tlr4* in Wt and MCJ-KO mice following NIAAA model (*Tlr4*= Toll Like receptor 4). Values are represented as mean ± SEM. Student's t-test was used to compare two groups and one-way ANOVA followed by Tukey post-test was used to compare between multiple groups. *p<0.05, **p<0.01 and ***p<0.001 versus Wt.

The V3-V4 regions of 16S rRNA amplicon sequencing identified alterations of the gut microbiota composition in ethanol-fed MCJ-KO mice, suggestive of a dysbiosis event following ethanol consumption (Fig. 5.4D). Compared to Wt mice, higher levels of *Prevotella*, a bacterium known to degrade mucin leading to the gut barrier integrity disruption; and lower abundance of Bifidobacteriaceae, Lactobacillaceae and Ruminococcaceae, which maintain mucosal barrier integrity, were identified in ethanol-fed MCJ-KO mice. The hypothesis of a dysbiotic event following ethanol consumption is further supported by the reduction of Ruminococcaceae and the increase of Bifidobacteriaceae found in the gut microbiome of control MCJ-KO mice's gut microbiome compared to control Wt. Indeed, evaluation of intestinal permeability with FITC-labelled dextran showed higher levels in serum from ethanol-fed MCJ-KO mice (Fig. 5.4E). Besides, reduced levels of tight junction proteins (ZO-1) detected by IHC (Fig. 5.4F) confirms augmented intestinal permeability and decreased junctional integrity in ethanol-fed MCJ-KO mice, facilitating bacterial and microbial products translocation. In fact, higher serum levels of LPS were measured in ethanol-fed MCJ-KO mice (Fig. 5.4G), along with an increased intestinal expression of *Tlr4* (Fig. 5.4H).

Altogether, ethanol consumption caused a significant dysbiosis event in ethanol-fed MCJ-KO mice, inducing intestinal immune dysregulations, increasing intestinal permeability and facilitating the translocation of bacterial endotoxins. This "leaky" gut might be aggravating the hepatic injury and affecting other organs.

5.1.4 Dysregulation of pancreatic beta-cells and hyperglycemia in ethanol-fed MCJ-KO mice

The effects of ethanol metabolism and increased translocation of bacterial endotoxins are by no means restricted to the liver. Increased hepatic *Glut2* expression levels (Fig. 5.2H) together with altered glucose levels in ethanol-fed MCJ-KO mice suggested possible

pancreatic damage (Fig. 5.5A). Indeed, chronic pancreatitis and endocrine dysfunctions are common in alcoholic individuals (Rasineni et al. 2020; Z. Ren et al. 2016).

Expression of *Mcj* was confirmed in both human and mouse pancreatic islets (Fig. 5.5B). After an ethanol bolus on day 11, we performed an intraperitoneal glucose tolerance test (IPGTT), which showed no difference between Wt control mice and MCJ-KO mice. Ethanol consumption significantly worsened the glycemic control and increased blood glucose concentrations. Moreover, ethanol-fed MCJ-KO mice were unable to control their blood glucose levels and reached concentrations of ≥600mg/dL (Fig. 5.5C), which was associated with the death of these animals. To clarify whether the pancreas was already damaged due to chronic ethanol intake prior to ethanol bolus administration, an IPGTT was performed on day 6. Ethanol-fed MCJ-KO mice had significantly higher glucose levels and they already showed poorer glycemic control (Fig. 5.5D).

Blood samples were collected during GTT to analyze insulin levels in response to glucose stimuli. We observed impaired insulin secretion in ethanol-fed MCJ-KO mice compared with Wt mice, as insulin levels dropped significantly 90 minutes after GTT, consistent with the onset of the hyperglycemic event (Fig. 5.5E).

Consistent with the decreased insulin levels, ethanol consumption also significantly decreased the number of pancreatic islets, although we did not observe any differences between ethanol-fed groups (Fig. 5.5F). At the end of the model, pancreatic islets were isolated so that the functionality of pancreatic islets could be tested in vitro. Since insulin secretion depends on ATP production and Ca^{+2} signaling (Klec et al. 2019) intracellular ATP concentrations were measured, and we observed that MCJ-KO islets produced significantly higher ATP concentrations in response to glucose both in the basal state and after ethanol consumption, although these were lower after ethanol consumption in both groups (Fig. 5.5G). However, the static insulin release assay highlighted the lower ability of MCJ-KO islets to detect glucose, as higher glucose levels were required to release the same amounts of insulin (Fig. 5.5H)

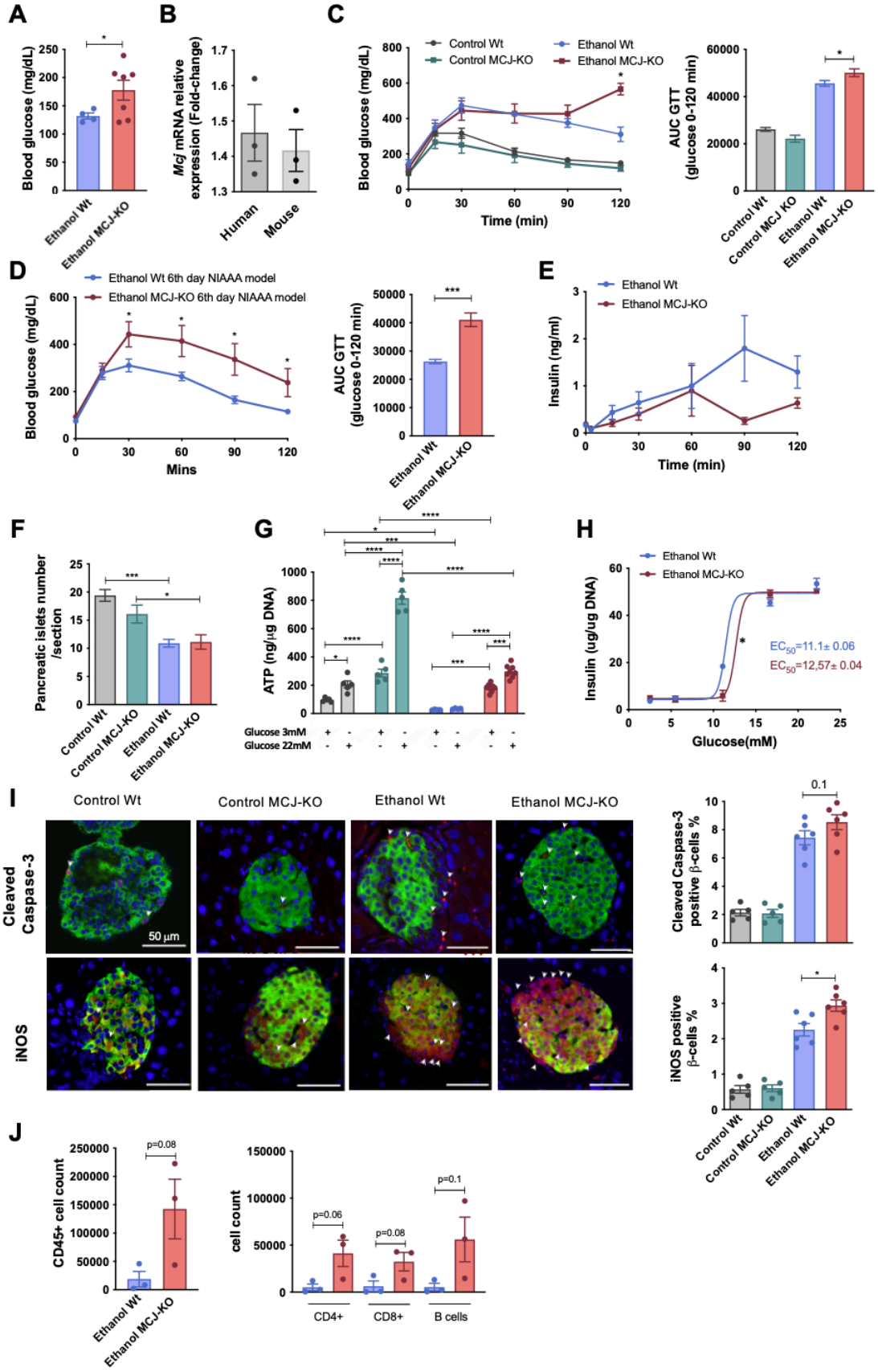

Fig. 5.5 Augmented pancreatic injury and hyperglycaemia in ethanol-fed MCJ-KO mice. (A) Blood glucose levels following the acute ethanol administration**. (B)** Relative *Mcj* mRNA expression in human and mice pancreatic islets. **(C)** Curves showing the blood glucose levels (left panel) and the resulting area under curve (right panel) during the

IPGTT in Control and NIAAA fed Wt and MCJ-KO mice at the end of the NIAAA model. **(D)** Curves showing the blood glucose levels (left panel) and the resulting area under curve (right panel) during the IPGTT in Wt and MCJ-KO mice at the 6th day of the NIAAA model. **(E)** Insulin levels during the IPGTT in ethanol-fed Wt versus MCJ-KO mice. **(F)** Number of pancreatic islets in Wt and MCJ-KO mice, control and ethanol fed. **(G)** Measurement of the ATP content in isolated pancreatic islets, isolated from Control and NIAAA fed Wt and MCJ-KO mice, following an overnight resting and 1 hour in 3mM or 22mM Glucose containing media. **(H)** Insulin quantification during the *in vitro* static insulin release assay, using freshly isolated pancreatic islets from ethanol-fed Wt and MCJ-KO mice. **(I)** Pancreas immunohistochemical staining (left panel) and respective quantification (right panel) for Cleaved caspase-3 and iNOS, markers for pancreatic beta cell injury, in Control and NIAAA fed Wt and MCJ-KO mice. **(J)** Pancreatic infiltrating total CD45+ cells and a further characterization of CD4+, CD8+ and B cells populations using FACS in ethanol-fed Wt and MCJ-KO mice.Values are represented as mean ± SEM. Student's t-test was used to compare two groups and one-way ANOVA followed by Tukey post-test was used to compare between multiple groups. *p<0.05, **p<0.01 and ****p< 0.0001 versus Wt.

Interestingly, histological evaluation of the pancreatic islets showed an increase in caspase-3 and iNOS in ethanol-fed MCJ-KO mice (Fig. 5.5I). We also found increased inflammatory infiltration of $CD4^{+}$T, $CD8^{+}$T and B cells in ethanol-fed MCJ-KO mice compared with Wt mice (Fig. 5.5J).

Overall, the pancreas of ethanol-fed MCJ-KO mice suffer from three main damages: ROS due to ethanol metabolism, increased serum LPS and inflammatory infiltration. All these factors impaired pancreatic islet function and resulted in decreased sensitivity of glucose-stimulated insulin secretion, defective insulin secretion and thus hyperglycemia.

5.1.4 MJC-LSS ameliorates liver injury and avoids lipid accumulation following ethanol use

ALD is a systemic affection. After ethanol consumption deficiency of MCJ leads to impairment of intestinal and pancreatic structure and function, by increasing inflammation and permeability and causing apoptosis of pancreatic beta cells. Based on previous studies in which we demonstrated hepatoprotection by silencing *Mcj* in the liver (Barbier-Torres et al. 2017, 2020; Goikoetxea-Usandizaga et al. 2022; Iruzubieta et al. 2021), MCJ-specific siRNA (siMCJ) was used to evaluate whether liver specific *Mcj* silencing could be used as a potential therapy to alleviate liver injury after chronic and acute ethanol abuse. 3-month-old Wt mice were treated with siMCJ or siCtrl by intravenous injection into the tail vein at day 5 of the NIAAA model, and efficient knockdown of MCJ protein expression was confirmed at the end of the model (Fig. 5.6A).

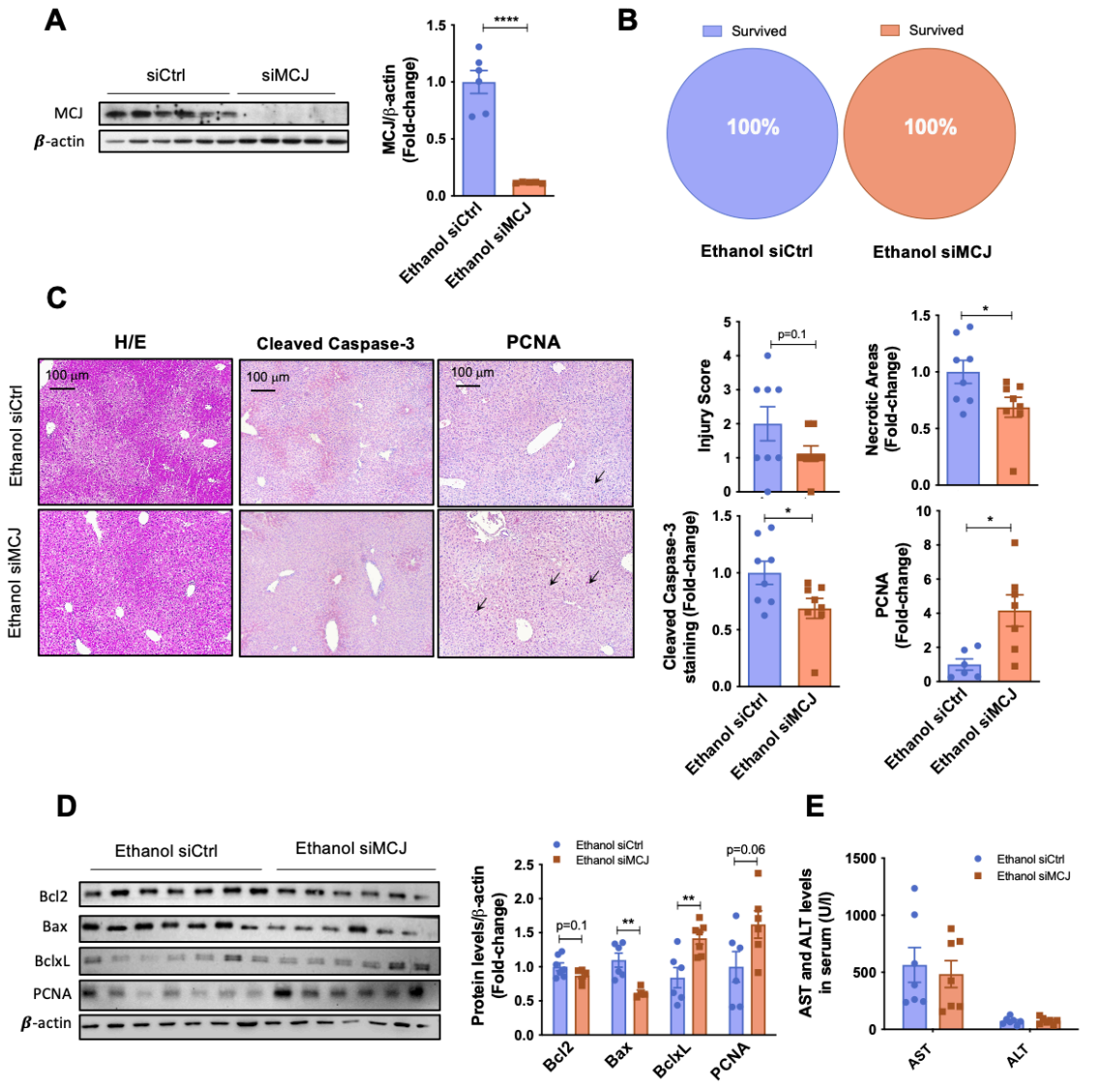

Fig. 5.6 Liver specific silencing of *Mcj* reduces liver damage following the NIAAA model. (A) MCJ levels by western blotting (left panel) and densitometric quantification (right panel) in siCtrl and siMCJ liver extracts after the NIAAA model. ß-actin was used as a loading control. **(B)** Pie charts represent the percentage of Survived and Deceased siCtrl (left panel) and siMCJ (right panel) mice following the NIAAA model. **(C)** Hepatic injury score obtained after the histopathological evaluation and immunohistochemical staining and quantification of Necrotic Areas based on H&E staining, Cleaved Caspase-3, an apoptotic marker, and PCNA in siCtrl versus siMCJ mice following the NIAAA model. **(D)** Apoptotic BCL2, BAX and BclXL and regenerative PCNA protein levels by western blotting (left panel) and densitometric quantification (right panel) in siCtrl and siMCJ liver extracts after the NIAAA model. ß-actin was used as a loading control. **(c)** Serum aspartate aminotransferase (AST) and alanine aminotransferase (ALT) levels in ethanol fed siCtrl and siMCJ mice. Values are represented as mean ± SEM. Student's t-test was used to compare two groups. *p<0.05, **p<0.01 and ****p< 0.0001 versus Wt.

Surprisingly, we achieved a 100% survival percentage in both ethanol-fed siCtrl and siMCJ treated groups (Fig. 5.6B). Importantly, ethanol-fed siMCJ mice exhibited less liver injury and greater hepatic regeneration, as documented by significantly lower number of both necrotic areas and cleaved caspase-3 staining levels, along with an increased PCNA positive immunostainings (Fig. 5.6C). Pathological analysis revealed

that ethanol-fed siCtrl mice had more severe hepatic lesions (steatosis and inflammation), with a final score of 2 versus 1.3 in ethanol-fed siMCJ mice. In addition, pro apoptotic BCL2 and BAX protein levels were reduced and anti-apoptotic BCL-XL and regenerative PCNA were increased in siMCJ mice (Fig. 5.6D). No changes were observed in serum ALT and AST levels (Fig. 5.6E).

In line with previous studies, liver specific MCJ silencing prevented lipid accumulation after ethanol abuse as measured by Sudan red staining and triglyceride accumulation (Fig. 5.7A,B). The activity and mRNA levels of beta oxidation enzymes were significantly higher and those of enzymes controlling lipid synthesis or accumulation were lower in siMCJ mice than in siCtrl mice (Fig. 5.7C,D), confirming that metabolism in siMCJ mice is oriented toward lipid catabolism, thus avoiding one of the main features of ALD.

The inflammatory response was also reduced in siMCJ mice. F4/80 staining showed reduced hepatic monocyte infiltration in siMCJ mice (Fig. 5.7E), and we found reduced mRNA levels of the pro inflammatory cytokines *Tnf*, *Il1b* and *Ccr5* and increased expression of anti-inflammatory *Il-10* and *Ho-1* compared with siCtrl (Fig. 5.7F). We found no evidence of liver fibrosis.

No significant changes were observed in mRNA levels of the main enzymes related to alcohol metabolism (Fig. 5.7G). Measurement of hepatic ethanol and acetaldehyde showed no differences in hepatic ethanol accumulation and a slight trend toward lower hepatic accumulation of acetaldehyde in siMCJ mice (Fig. 5.7H). Importantly, the absence of MCJ prevented excessive production of ROS, as significantly lower DHE staining levels were detected along with decreased 4HNE staining (Fig. 5.7I). Finally, we did not detect any differences in the GSH/GSSG ratio (Fig. 5.7J).

In the context of ethanol-induced systemic changes, ethanol-fed siMCJ mice showed significantly reduced hepatic LPS concentrations(Fig. 5.8A), no changes in *Tlrs* mRNA levels, and significantly decreased *Ap-1* expression, a transcription factor that leads to the production of inflammatory cytokines (Fig. 5.8B). Serum LPS levels were also measured, and no differences were observed between the two groups (Fig. 5.8C). Finally, siCtrl and siMCJ mice exhibited similar glucose levels and glycemic control after a GTT, without severe hyperglycemia (Fig. 5.8D).

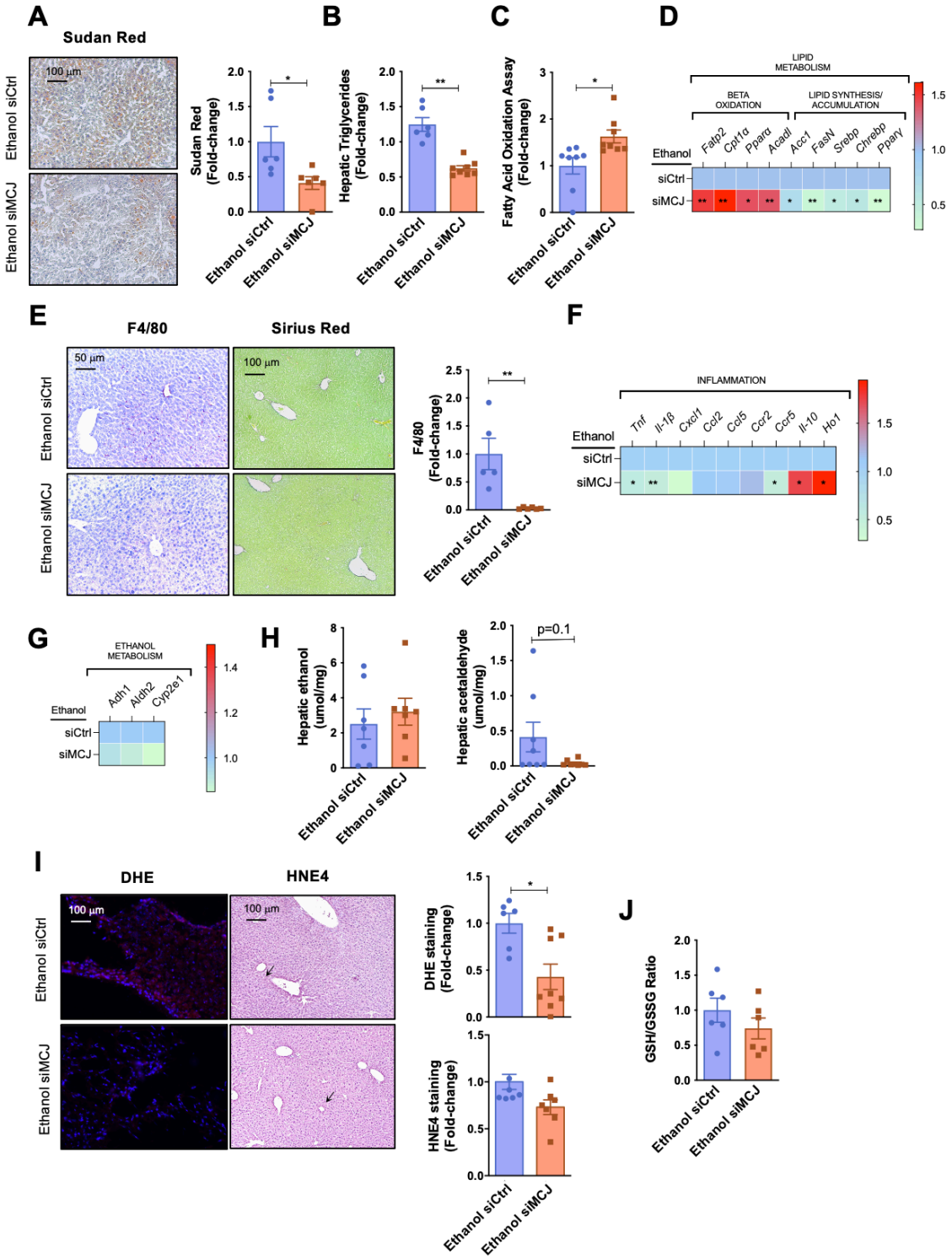

Fig. 5.7 Liver specific silencing of *Mcj* reduces steatosis, inflammation and oxidative stress following the NIAAA model. (A) Liver immunohistochemical staining and quantification for Sudan Red in siCtrl versus siMCJ mice following the NIAAA model. **(B)** Hepatic triglyceride content in siCtrl versus MCJ-LSS mice after the NIAAA model. **(C)** Fatty Acid Oxidation rate was assayed in liver tissue in ethanol-fed siCtrl and siMCJ mice. **(D)** Heatmap showing the differential hepatic expression of mRNA levels from genes involved in Lipid Metabolism in siCtrl and MCJ-LSS mice after NIAAA model (*Fatp2*= Fatty acid transport protein 2; *Cpt1a*= Carnitine Palmitoyltransferase 1A; *Ppara*= Peroxisome proliferator-activated receptor alpha; *Acadl*= Acyl-CoA Dehydrogenase Long Chain; *Acc*= Acetyl-CoA carboxylase; *FasN*= Fatty acid synthase; *Srebp*= Sterol regulatory element-binding protein 1; *Chrebp*= Carbohydrate-responsive element-binding protein; *Pparg*= Peroxisome proliferator-activated receptor gamma). **(E)** Liver immunohistochemical staining and quantification for F4/80 and Sirius Red in siCtrl versus siMCJ mice following the

NIAAA model. **(F)** Heatmap showing the differential hepatic expression of mRNA levels from genes involved in inflammation in siCtrl and MCJ-LSS mice after NIAAA model (*Tnf*= Tumor necrosis factor; *Il-1b*= Interleukin 1 beta; *Cxcl1*= C-X-C Motif Chemokine Ligand 1; *Ccl2*= C-C Motif Chemokine Ligand 2; *Ccl5*= C-C Motif Chemokine Ligand 5; *Ccr2*= C-C Motif Chemokine Receptor 2; *Ccr5*= C-C Motif Chemokine Receptor 5; *Il-10*= Interleukin-10; *Ho-1*= Heme oxygenase-1). **(G)** Heatmap showing the differential hepatic expression of mRNA levels from genes involved in Ethanol metabolism in siCtrl and siMCJ mice after NIAAA model (*Adh1*= Alcohol dehydrogenase 1; *Aldh2*= Aldehyde dehydrogenase 2; *Cyp2e1*= Cytochrome P450 Family 2 Subfamily E Member 1). **(H)** Hepatic ethanol (left panel) and acetaldehyde (right panel) quantification in NIAAA fed siCtrl and siMCJ mice. **(I)** Liver immunohistochemical staining (left panel) and respective quantification (right panel) for DHE and 4-HNE in ethanol-fed siCtrl versus siMCJ mice. **(J)** Hepatic reduced to oxidized glutathione ratio in ethanol fed Wt versus MCJ-KO mice. Values are represented as mean ± SEM. Student's t-test was used to compare two groups. *p<0.05 and **p<0.01 versus Wt.

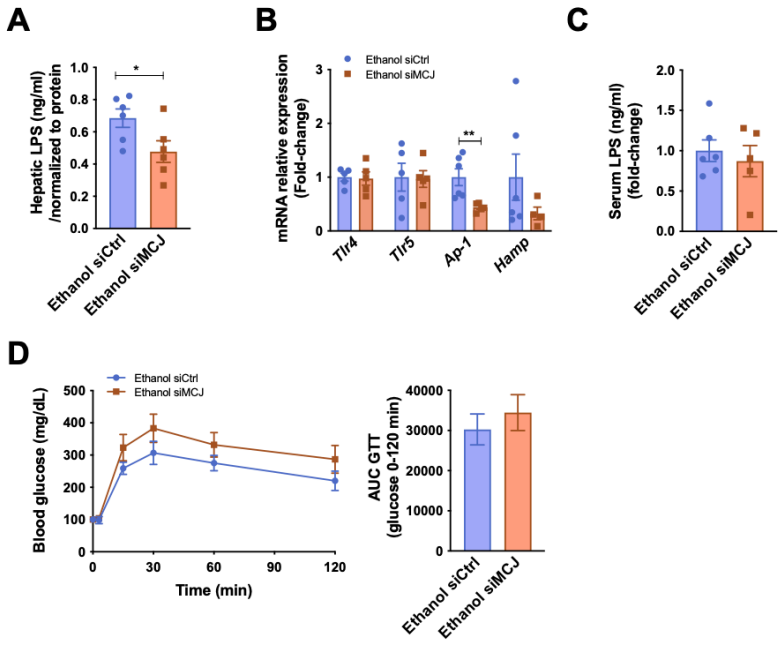

Fig. 5.8 Liver specific silencing of *Mcj* does not induce a systemic alcohol injury. (A) Hepatic amount of LPS in siCtrl versus siMCJ mice following NIAAA model. **(B)** Differential hepatic expression of mRNA levels from genes involved in LPS recognition in siCtrl and siMCJ mice after NIAAA model (*Tlr*= Toll Like receptor; *Ap-1*= Activator protein-1; *Hamp*= Hepcidin antimicrobial peptide). **(C)** Serum amount of LPS in siCtrl versus siMCJ mice following NIAAA model. **(D)** Curves showing the blood glucose levels (left panel) and the resulting area under curve (right panel) during the IPGTT in ethanol-fed siCtrl and siMCJ mice. Values are represented as mean ± SEM. Student's t-test was used to compare two groups. *p<0.05 and **p<0.01 versus Wt.

Thus, siMCJ is hepatoprotective after chronic and acute ethanol consumption and could serve as a new therapeutic approach to treat ALD. siMCJ significantly ameliorates liver injury by targeting the main hallmarks of ALD; it reduces liver steatosis, inflammation and prevents ROS production, thereby avoiding the deleterious effects that MCJ deficiency had in the intestine and the pancreas of ethanol-fed MCJ-KO mice.

5.1.5 siMCJ inhibits mTOR activation and avoids *de novo* lipogenesis

Our goal was to understand the exact mechanism by which siMCJ ameliorates hepatic steatosis and improves ALD. Therefore, we performed high-throughput proteomic analysis based on liquid chromatography-mass spectrometry (LC-MS) in ethanol-fed siCtrl and siMCJ mice. Ingenuity pathway analysis (IPA) was used to identify the major canonical signaling pathways involved in the hepatoprotective effect of siMCJ in ALD, revealing that mTOR signaling and its downstream signaling pathways, which play essential roles in the regulation of lipid metabolism, fatty acid oxidation and *de novo* lipogenesis (Laplante and Sabatini 2009; Ricoult and Manning 2013; Serrano-Maciá et al. 2021), are altered (Fig. 5.9A). All identified hepatic proteins were plotted in a volcano plot (Fig. 5.9B). Among the 69 significantly differentially expressed proteins highlighted within the plot, we focused on the mTOR interactors. Interestingly, we observed proteins whose expression is upregulated by mTOR activation in siCtrl mice (COX1, SERPINA) and siMCJ mice show proteins that are positively regulated when mTOR signaling is inhibited (ATP2B, DMD).

To confirm the results of proteomics analysis, we examined the activation levels of the mTOR pathway and its downstream interactors in both siCtrl and siMCJ mice by Western blot (Fig. 5.9C). siMCJ significantly reduced mTORC1 phosphorylation and thus its activation compared to siCtrl mice. After mTOR inhibition, the phosphorylation of S6 protein (pS6), a downstream target of mTOR, was also reduced in siMCJ mice. mTORC1 regulates *de novo* lipogenesis by increasing the expression of key transcriptional factors for enzymes involved in lipid synthesis (Chen et al. 2018). The expression of transcription factors *Srebp1* and *Chrebp* was previously measured, and we showed that it was significantly reduced in siMCJ mice (Fig. 5.7D). In addition, increased activation of AMPK (Fig. 5.9C), whose downstream signaling inhibits *de novo* lipogenesis (N. L. Price et al. 2013) and increases fatty acid oxidation (Fig. 5.7C) was observed in siMCJ mice.

Aberrant activation of mTORC1 has previously been associated with defects in SIRT1, which appears to be downregulated in ALD patients (Chen et al. 2018; Li et al. 2011; R. Ren et al. 2020). Silencing of MCJ significantly increased both hepatic SIRT1 activity (Fig. 5.9D) and expression (Fig. 5.9E) compared to siCtrl mice. Moreover, SIRT1 activity is dependent on NAD^+, and as previously mentioned, ethanol metabolism significantly

alters the NAD^+/NADH ratio, affecting catabolic pathways such as beta oxidation (Ceni, Mello, and Galli 2014), thus hepatic NAD^+ levels were also measured. A significantly higher NAD^+/NADH ratio was found in siMCJ mice compared to siCtrl mice (Fig. 5.9F).

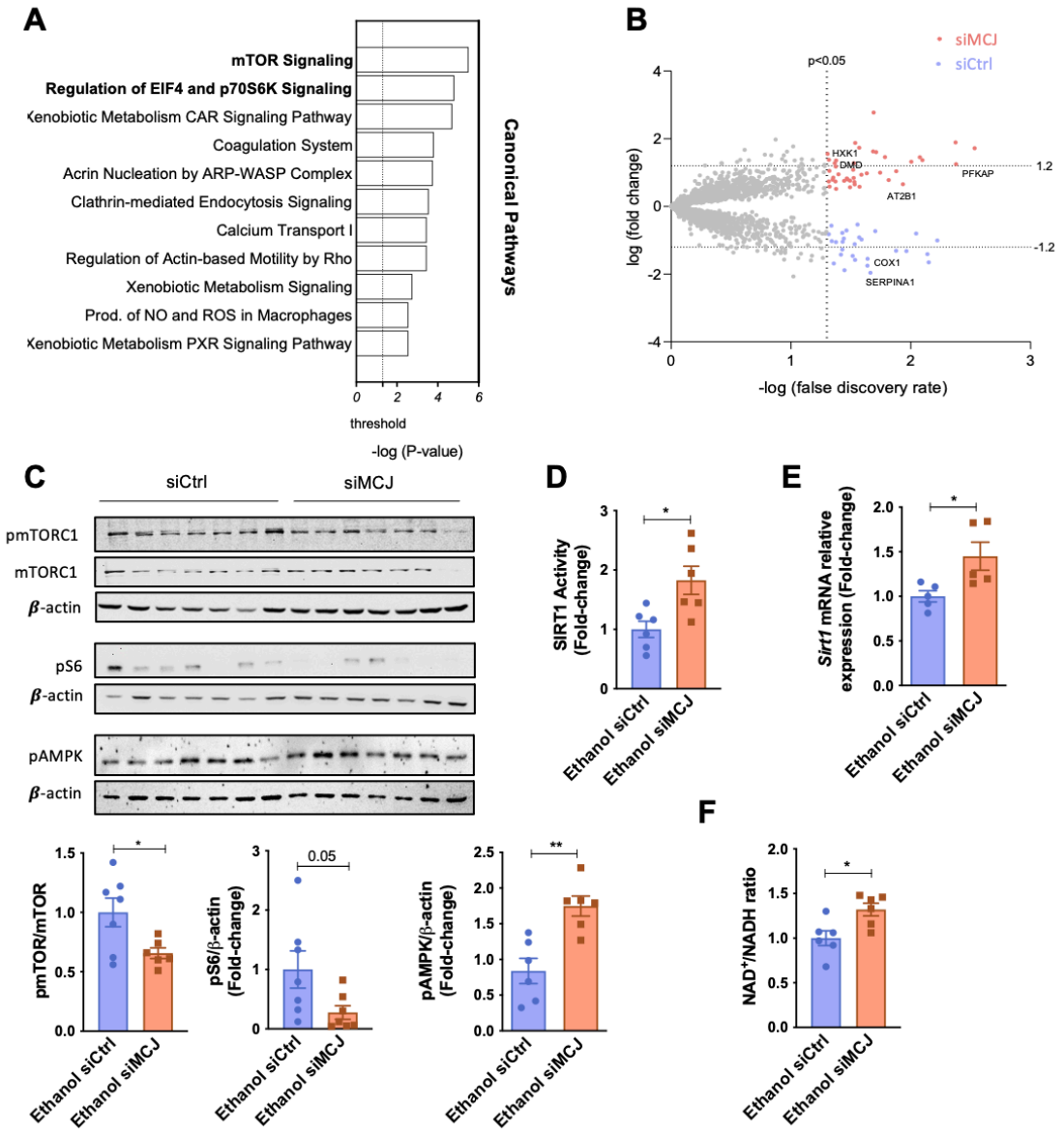

Fig. 5.9 Silencing of MCJ inhibits mTOR activation via increased NAD^+ and improved Sirt1 activity. (A) Ingenuity Pathway Analysis (IPA) of top canonical pathways in siCtrl and siMCJ mice following the NIAAA model. **(B)** Volcano plot showing all the hepatic proteins identified in ethanol-fed siCtrl and siMCJ mice. Statistically significant proteins are shown in the corresponding colors and highlighted proteins were identified as mTOR interactors. **(C)** Activated and total mTOR protein levels, together with activated S6 protein levels by western blotting (upper panel) and densitometric quantification (bottom panel) in siCtrl and siMCJ liver extracts after the NIAAA model. ß-actin was used as a loading control. **(D)** SIRT1 activity assay in liver tissue from ethanol-fed siCtrl and siMCJ mice. **(E)** Differential hepatic expression of mRNA levels from *Sirt1* in siCtrl and siMCJ mice following NIAAA model (*Sirt1*= Sirtuin 1). **(F)** Hepatic NAD^+/NADH ratio in ethanol-fed siCtrl and siMCJ mice. Values are represented as mean ± SEM. Student's t-test was used to compare two groups. *p<0.05 versus Wt.

Overall, our study shows that *Mcj* silencing improves mitochondrial activity and helps restore an appropriate NAD^+/NADH ratio, what promotes lipid beta oxidation and, via SIRT1, also prevents mTORC1 activation and the subsequent *de novo* lipogenesis. Thus, targeting mitochondrial dysfunction prevents alcohol-mediated hepatic steatosis and ALD progression, and thus represents a potential therapeutic approach to treat this disease.

5.2 MITOCHONDRIAL BIOENERGETICS BOOST MACROPHAGES ACTIVATION PROMOTING LIVER REGENERATION IN METABOLICALLY COMPROMISED ANIMALS

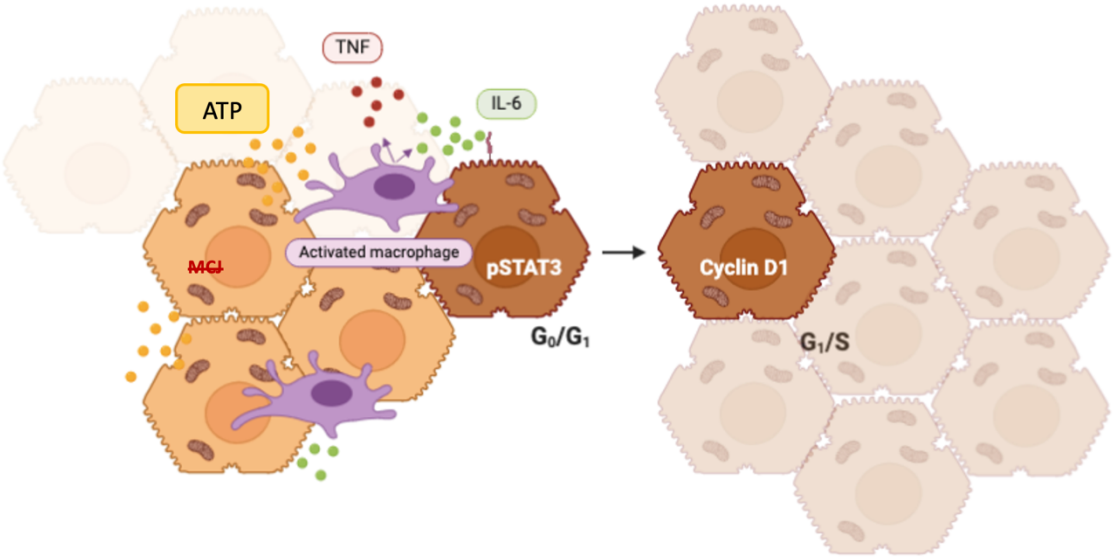

Fig. Increased ATP levels in the absence of *Mcj* mediate accelerated liver regeneration by activating the immune system

The results presented in Chapter 5.1 show the contribution of MCJ to the development of ALD and the outcome of ameliorating mitochondrial dysfunction depending on the targeted organ. In this chapter, we describe the role of mitochondrial activity in the initiation phase of liver regeneration and propose a novel approach based on targeting MCJ to promote regeneration in metabolically compromised individuals.

5.2.1 Expression of MCJ is increased in human liver biopsies after normothermic perfusion and in preclinical models of partial hepatectomy with or without IRI

cDCD is an important source of grafts for liver transplantation. However, changes during the ischemic period negatively affect postoperative outcomes (Hessheimer et al. 2018). To investigate whether MCJ is dysregulated under surgical ischemic conditions and, as a result, associated with susceptibility to IRI in humans, we compared its expression in liver biopsies from DCD donors 60 minutes after the start of the normothermic regional perfusion (NRP) and in healthy control individuals. Our results show that MCJ levels were higher in livers from donor graft patients (n = 17) than in livers from healthy control individuals (n = 7) (Fig. 5.10A).

On the other hand, liver resection is the only curative therapy for most patients with hepatobiliary malignancies. Vascular occlusion is a common strategy to prevent loss of blood during hepatic resection. To assess the possible involvement of MCJ in liver resection that requires vascular occlusion, we examined its expression in livers from two murine models: mice subjected to (1) 70% Phx and (2) 70% hepatectomy with 30 minutes of ischemia (Phx with IRI). We aimed to elucidate whether alterations in MCJ occur in Phx by itself or only during Phx with vascular occlusion.

After 70% Phx, MCJ protein and mRNA levels increased progressively from 5 to 48 h before returning to baseline levels once the hepatic mass was restored after 7 days (Fig. 5.10B,C). Similarly, in mice subjected to Phx with IRI, MCJ was upregulated 24 hours after surgery before returning to baseline after 7 days (Fig 5.10D,E). These results indicate that Phx by itself induces MCJ upregulation. In addition, MCJ upregulation is maintained when vascular occlusion is applied.

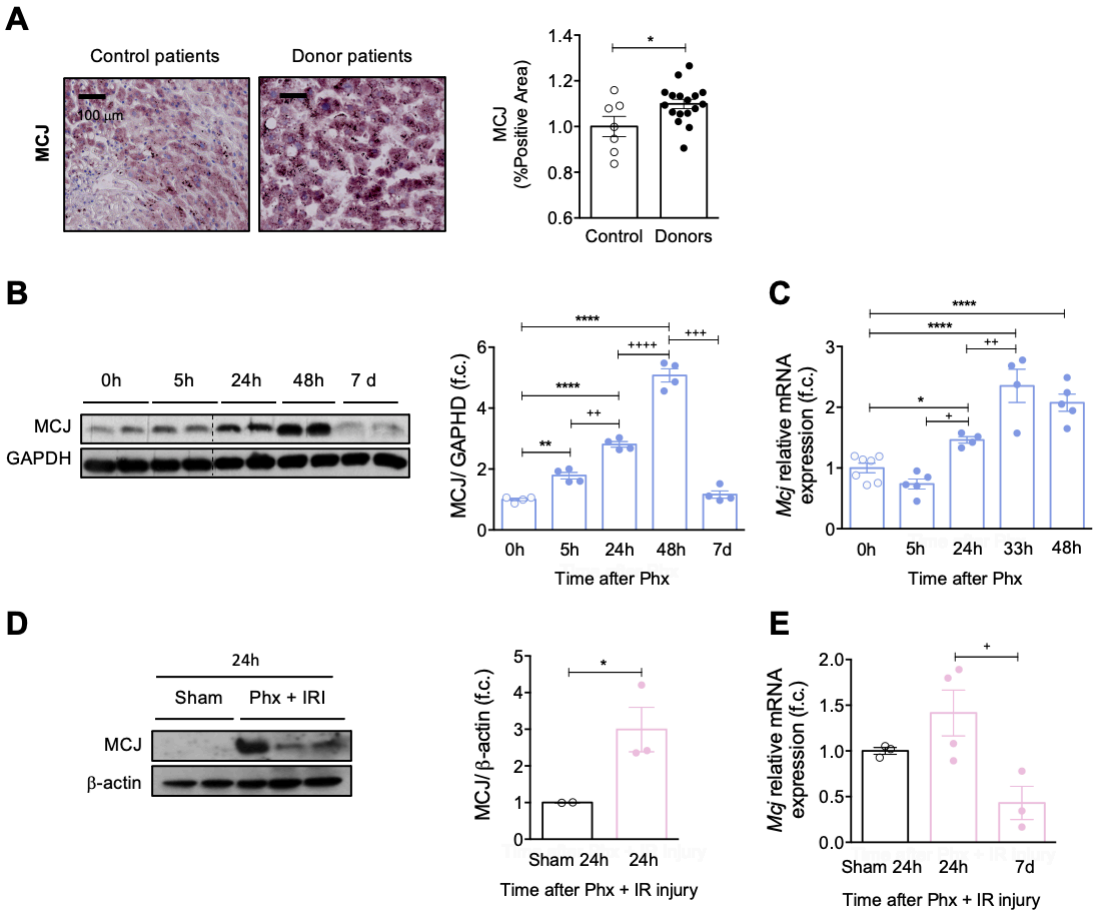

Fig. 5.10 MCJ expression is increased in ischemic injury and graft regeneration. (A) Liver biopsies from transplant donors, 60 minutes after the start of the normothermic regional perfusion (nRP) (n=17), and from healthy control individuals (n=7) where MCJ expression was determined by immunohistochemistry (left panel) and quantified (right panel). Scale bar corresponds to 50µm. Values are represented as Median ± Range. U-test was used to compare two groups. **(B)** MCJ levels by western blotting (left panel) and densitometric quantification (right panel) in WT liver extracts at different time points after 70% Phx. Glyceraldehyde-3-phosphate (GAPDH) was used as a loading control. **(C)** *Mcj* mRNA levels in WT liver extracts at different time points after 70% Phx. At least n=4 was used for each experimental group. **(D)** MCJ levels by western blotting (left panel) and densitometric quantification (right panel) in WT liver extracts at different time points after 70% Phx under IRI. ß-actin was used as a loading control **(E)** *Mcj* mRNA level in WT liver extracts at different time points after 70% Phx under IRI. n=3 was used for sham operated mice and n=10 underwent 70%Phx under IRI. (*Mcj* = Methylation controlled J protein). Values are represented as mean ± SEM. Student's t-test was used to compare two groups and one-way ANOVA followed by Tukey post-test was used to compare between multiple groups. *p<0.05; **p<0.01 and ****p<0.0001 versus control and $^{+}$p<0.05; $^{++}$p<0.01; $^{+++}$p<0.001 and $^{++++}$p<0.0001 versus indicated time points.

5.2.2 In vitro Mcj silencing enhances hepatocyte proliferation following EGF treatment

We first aimed to characterize the effects of *Mcj* silencing and *Mcj* overexpression on hepatocyte proliferation. Twenty-four hours after EGF treatment, silencing of *Mcj* significantly increased the mRNA and protein levels of proliferative markers compared to controls (Fig. 5.11A,B). Conversely, MCJ upregulation blocked the proliferative response (Fig. 5.11C,D). The efficiency of MCJ down- and upregulation was confirmed by Wb (Fig. 5.11E). These data shows that the specific ablation of MCJ in isolated hepatocytes exclusively enhances the proliferative response.

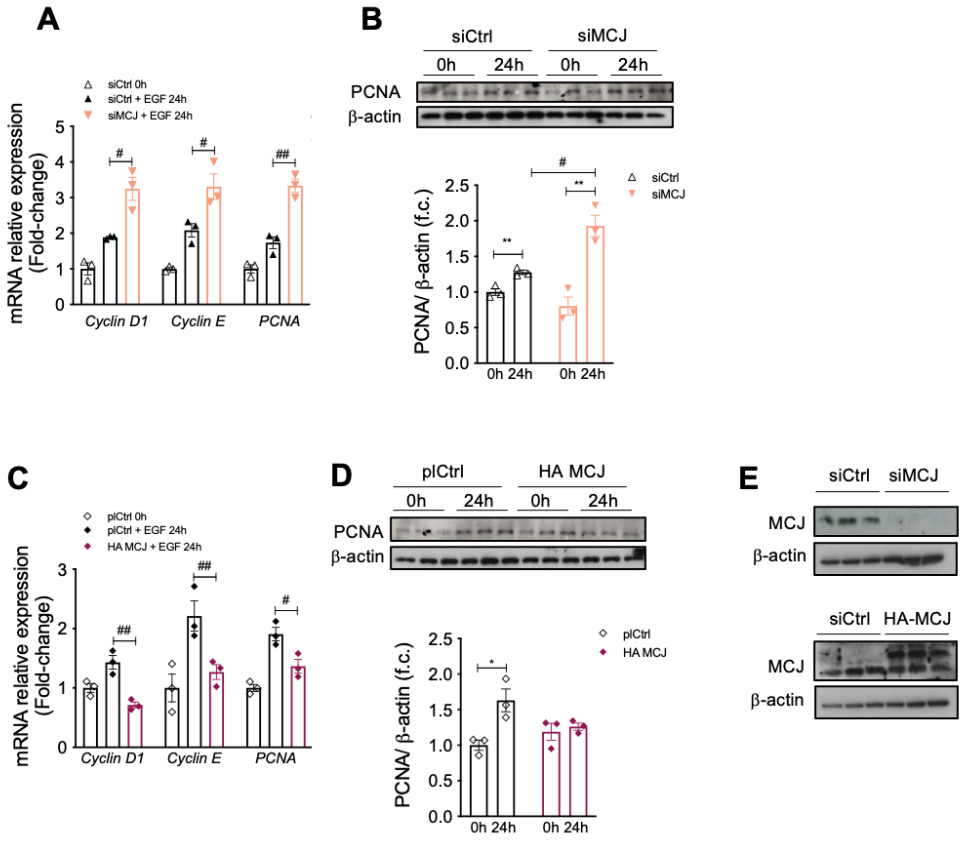

Figure 5.11 Proliferation studies in MCJ silenced hepatocytes 0h and 24h after EGF (20ng/mL) treatment (a-b) **(a)** mRNA levels of Cyclin D1, Cyclin E and PCNA 0h and 24h after EGF treatment (20ng/mL). **(b)** Western blot analysis (upper panel) and densitometric quantification (bottom panel) of total protein levels of PCNA 0h and 24h after EGF treatment. ß-actin was used as a loading control. **Proliferation studies in MCJ overexpressed hepatocytes 0h and 24h after EGF (20ng/mL) treatment (c-d) (c)** mRNA levels of Cyclin D1, Cyclin E and PCNA 0h and 24h after EGF treatment (20ng/mL). **(d)** Western blot analysis (upper panel) and densitometric quantification (bottom panel) of total protein levels of PCNA 0h and 24h after EGF treatment. ß-actin was used as a loading control. **(e)** MCJ levels by western blotting, confirming MCJ silencing and overexpression. Triplicates were used at each experimental condition. Values are represented as mean ± SEM. Student's t-test was used to compare two groups and two-way ANOVA followed by Tukey post-test was used to compare between multiple groups. *p<0.05 and **p<0.01 versus 0h and $^{\#}$p<0.05 and $^{\#\#}$p<0.01 versus siMCJ/HA-MCJ.

5.2.3 MCJ depletion enhances liver regeneration, overcomes liver injury and increases survival after 70% Phx with or without IRI and after prolonged IRI

In mice, the peak of regeneration (S phase) occurs 24-48 h after Phx, and liver mass is usually restored within 5–7 days (Forbes and Newsome 2016). Initially, we observed a faster recovery of liver weight in 3-month-old MCJ KO mice compared to age-matched WT animals 48 h after Phx (Fig. 5.12A). Importantly, no differences in the liver/body weight ratio were observed 5 days after Phx between WT and MCJ KO mice, demonstrating that the original pre-hepatectomy size was reached with high precision in MCJ KO mice, with no overgrowth of liver tissue. In parallel, MCJ KO mice had reduced liver damage in the postoperative period, as demonstrated by lower serum ALT concentrations 5 and 33 h after 70% Phx (Fig. 5.12B). Regenerating hepatocytes in MCJ KO mice entered the cell cycle faster than those in WT, as reflected by an earlier increase in Cyclin D1, PCNA and Ki67-positive immunostaining (Fig 5.12C) and Cyclin D1 protein levels (Fig. 5.12D). Furthermore, cyclin kinase inhibitor *p21*, a known suppressor of hepatocyte proliferation, was expressed at similar levels in both WT and MCJ KO mice 48 h after Phx (Fig. 5.12E). Overall, these data show that the lack of MCJ accelerates liver regeneration until the "hepatostat" (Michalopoulos 2017) is achieved.

To further demonstrate the protective role of MCJ ablation in liver regeneration, we examined the outcome of liver ischemia injury and graft regeneration after 70% Phx with vascular occlusion. We performed 70% Phx with 30 min of IRI in WT and MCJ KO mice and evaluated hepatic injury, hepatic regeneration, and survival 24 h or 7 days after the reperfusion. This procedure is characterized by high mortality rates, with about only 50% of WT mice surviving (Bujaldon et al. 2019); we confirmed this figure in our experimental settings (Fig. 5.13A). Interestingly, the survival rate in MCJ KO mice increased by up to 80% (Fig. 5.13A). This was accompanied by a reduction in serum hepatic transaminases in MCJ KO mice 24 h after the procedure (Fig. 5.13B). Diminished apoptosis and/or necrosis was also observed, as shown by the attenuated activity of calpain proteases (Fig. 5.13C). Moreover, under these conditions, lack of MCJ resulted in significantly increased proliferative markers, including *Cyclin E*, *Pcna* and *Cyclin* B (Fig. 5.13D), compared to WT mice.

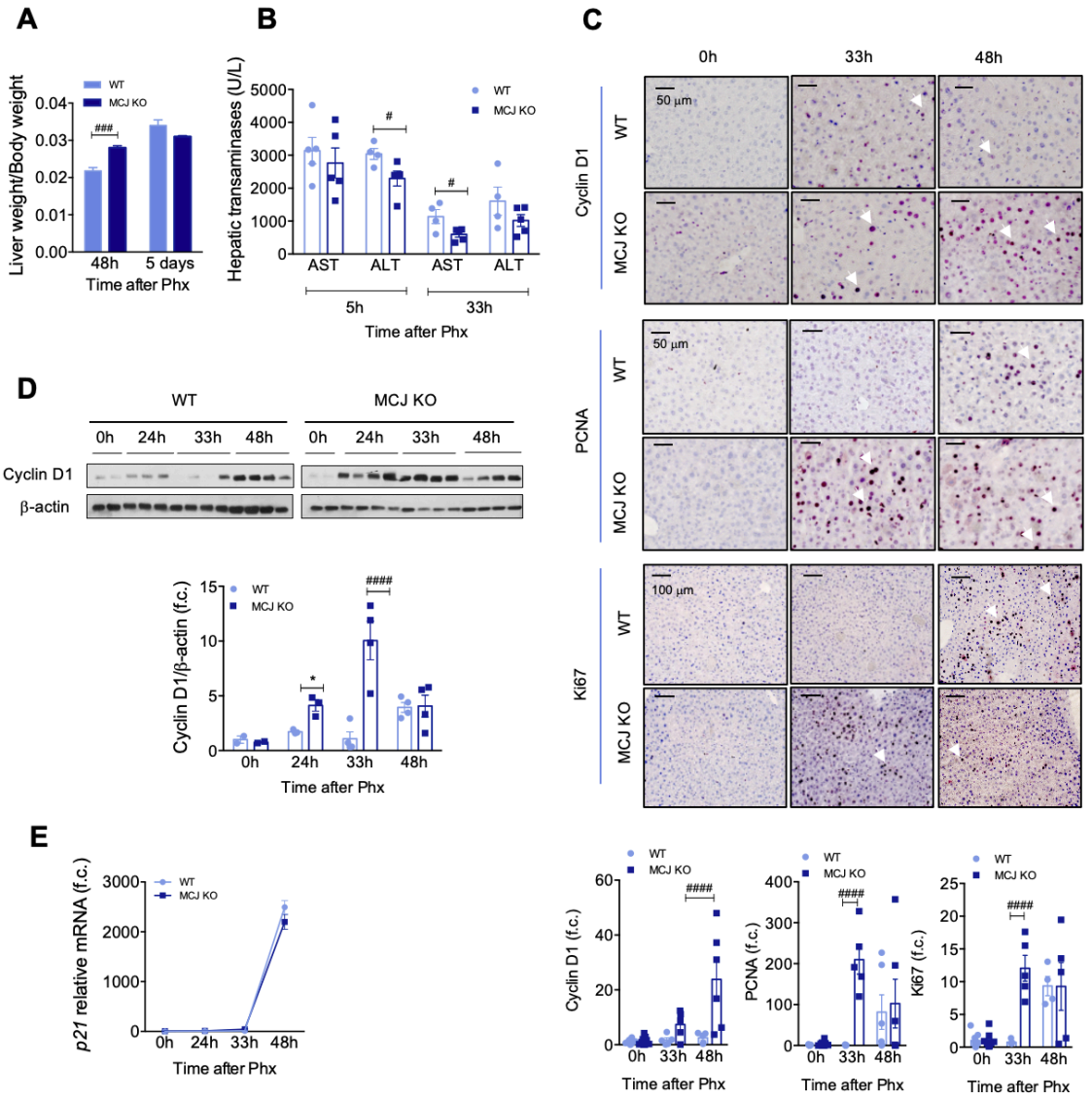

Fig. 5.12 Lack of MCJ enhances graft regeneration and reduces liver damage after 70% Phx. (A) Liver weight/Body weight ratio in WT and MCJ-KO mice, 2 and 5 days after 70% Phx. **(B)** Serum aspartate aminotransferase (AST) and alanine aminotransferase (ALT) levels in WT and MCJ-KO mice 5h and 33h after 70% Phx. **(C)** Liver immunohistochemical staining and respective quantification for Cyclin D1, Ki67 and PCNA, at 0h, 24h, 33h, and 48h after 70% Phx, in WT versus MCJ-KO. Scale bar corresponds to 50µm. **(D)** Western blot analysis (upper panel) and densitometric quantification (bottom panel) of total protein levels of Cyclin D1. ß-actin was used as a loading control. **(E)** mRNA levels of p21 0h, 24h, 33h and 48h after 70% Phx. (*p21*= cyclin-dependent kinase inhibitor 1). Values are represented as mean ± SEM. Two-way ANOVA followed by Tukey post-test was used to compare between multiple groups. $^{\#}p<0.05$ $^{\#\#\#}p<0.001$ and $^{\#\#\#\#}p<0.0001$ versus MCJ-KO.

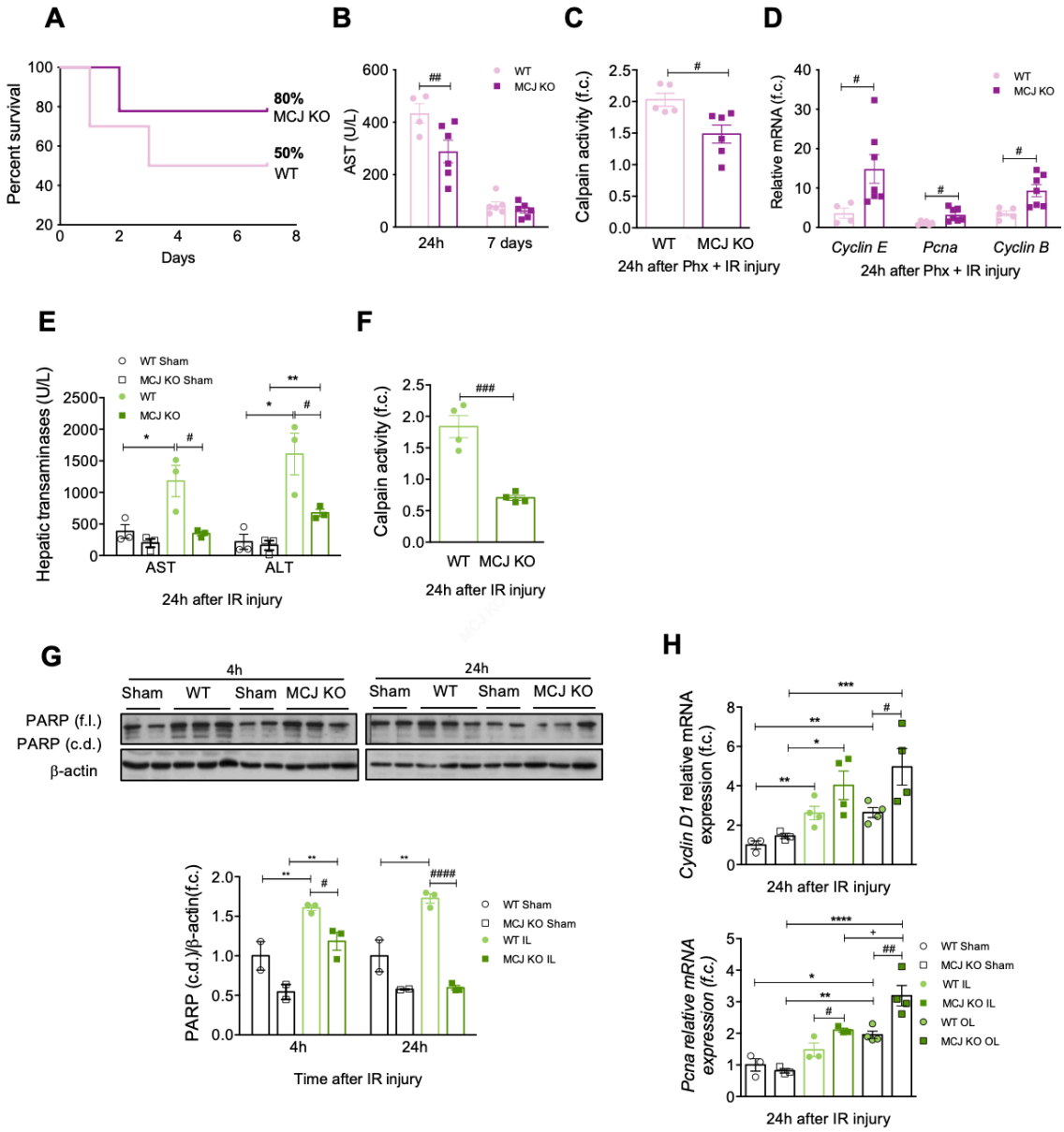

Fig. 5.13 Lack of MCJ enhances graft regeneration, reduces ischemic damage and increases survival after both 70% Phx under IRI and prolonged IRI. (A) Survival percent 7 days after 70% Phx under IRI, WT (n=10) versus MCJ-KO (n=10). **(B)** Serum AST levels in WT and MCJ-KO mice, 24h and 7 days after 70% Phx under IR injury. **(C)** Hepatic calpain activity measured in WT and MCJ-KO mice that underwent the procedure (n=10) 24h after 70% Phx under IRI, relative to sham-operated mice (n=2). **(D)** Differential expression of mRNA levels from genes involved in the cell cycle in WT and MCJ-KO mice, relative to sham operated mice, 24h after 70% Phx under IRI. **(E)** Serum AST and ALT levels in WT and MCJ-KO mice, 24h after IRI. **(F)** Hepatic calpain activity, cell death marker, was measured in the sham operated (n=2) and in the ischemic lobe (IL) of WT and MCJ-KO mice that underwent the procedure (n=5), 24h after IRI. **(G)** Quantification of PARP cleavage cell death marker (bottom panel), by western blotting (upper panel) in WT and MCJ-KO liver extracts, sham operated, 4h and 24h after IRI. Liver extracts correspond to the ischemic lobe. ß-actin was used as a loading control. **(H)** Differential expression of mRNA levels from genes involved in the cell cycle in WT versus MCJ-KO mice, compared to sham operated mice, in both the ischemic and the oxygenated lobes (OL), 24h after IRI. Values are represented as mean ± SEM. Student's t-test was used to compare two groups and two-way ANOVA followed by TUKEY post-test was used to compare between multiple groups. *p<0.05; **p<0.01; ***p<0.001 and ****p<0.0001 versus sham operated and $^{+}$p<0.05 versus different time points and $^{\#}$p<0.05; $^{\#\#}$p<0.01; $^{\#\#\#}$p<0.001 and $^{\#\#\#\#}$p<0.0001 versus MCJ-KO. At least n=5 was used for each experimental condition.

We also aimed to evaluate whether the benefits of MCJ depletion observed after 30 min of ischemia were extended after prolonged ischemic periods without hepatic resection. MCJ KO and WT mice were subjected to 90 minutes of ischemia and sacrificed 4 or 24 h after reperfusion, when we obtained ischemic and oxygenated lobes (Motiño et al. 2019). Serum analysis showed reduced AST and ALT levels in MCJ KO mice 24 h after the ischemic injury (Fig. 5.13E). This was accompanied by decreased calpain activity (Fig. 5.13F) and reduced poly (ADP-ribose) polymerase (PARP) cleavage (Fig. 5.13G). Regarding the regenerative response, there was a sustained increase in *Cyclin D1* and *Pcna* in MCJ KO mice, especially in the oxygenated lobe, compared to WT and sham-operated mice (Fig. 5.13H).

In conclusion, lack of MCJ enhances liver regeneration and overcomes hepatic injury not only after Phx but also following Phx with IRI, and these effects are accompanied by an increase in post-hepatectomy survival. Importantly, these protective effects are also apparent in longer ischemic periods without liver resection, resembling the conditions of liver transplantation.

5.2.4 MCJ absence during liver regeneration increases mitochondrial respiration and ATP synthesis

Liver regeneration is an energetically demanding process. Multiple lines of evidence have indicated that increased ATP levels after injury facilitate liver regeneration (Gonzales et al. 2013). MCJ is a negative regulator of mitochondrial respiration, as it inhibits complex I activity and the formation of supercomplexes, leading to a reduction in ATP synthesis (Hatle et al. 2013).

Both intracellular and extracellular ATP levels were significantly elevated in cultured hepatocytes isolated from WT and MCJ KO mice 24 h after Phx (Fig. 5.14A). ATP can be synthesized through glycolysis in the cytosol or through oxidative phosphorylation (OXPHOS) in mitochondria. Mitochondrial respiration was evaluated in regenerative MCJ KO and WT hepatocytes *in vitro* 3 h after 70% Phx. Our data show a significantly increased oxygen consumption rate (OCR) and higher basal, ATP-linked and maximal respiration in MCJ KO hepatocytes (Fig. 5.14B). Increased ATP production and respiration could be a consequence of an increased number of functional mitochondria in

MCJ KO mice; however, electron microscopy revealed no differences in the number or morphology among basal and regenerative WT and MCJ KO mitochondria (Fig. 5.14C,D). Thus, loss of MCJ during liver regeneration accelerates mitochondrial respiration and increases ATP production, inducing Succinate Dehydrogenase (SDH_2) activity, facilitating the restoration of the hepatic mass (Fig. 5.14E). Overall, our data indicate that MCJ depletion in proliferating hepatocytes enhances mitochondrial function and ATP synthesis and secretion.

In the early postoperative period after partial hepatectomy, ATP is predominantly generated by fatty acid oxidation and, to a lesser extent, by glucose oxidation in hepatic mitochondria (Nakatani et al. 1981; Solhi et al. 2021). We observed a similar trend in the decline of blood glucose levels after Phx in both WT and MCJ KO mice (Fig. 5.14F). Furthermore, using PET-CT scanning, we found that glucose uptake by the liver 24 h after partial hepatectomy was equal between WT and MCJ KO (Fig. 5.14G). Analysis of hepatic fatty acid oxidation revealed significantly enhanced activity in MCJ KO mice, both at baseline and 24 h after Phx (Fig. 5.14H).

The extent of ATP depletion during ischemia and the ability to resynthesize ATP after liver reperfusion play a critical role in graft recovery and facilitate liver regeneration. In line with our previous observations, both intracellular and extracellular ATP levels were significantly increased in MCJ KO hepatocytes 24 h after Phx with IR (Fig. 5.15A). Mitochondrial respiration showed a significant increase in OCR; higher basal, ATP-linked and maximal respiration were observed in MCJ KO regenerative hepatocytes (Fig. 5.15B). Lack of MCJ also induced an increase in SDH_2 activity (Fig. 5.15C).

Similar results were obtained following prolonged IRI injury. ATP production was evaluated in hepatocytes from the oxygenated and the ischemic lobes 4 hours after reperfusion. ATP levels, both intracellular and in the cell culture media, were significantly higher in the ischemic lobe in the absence of MCJ (Fig. 5.15D), along with the induction of mitochondrial SDH2 activity (Fig. 5.15E).

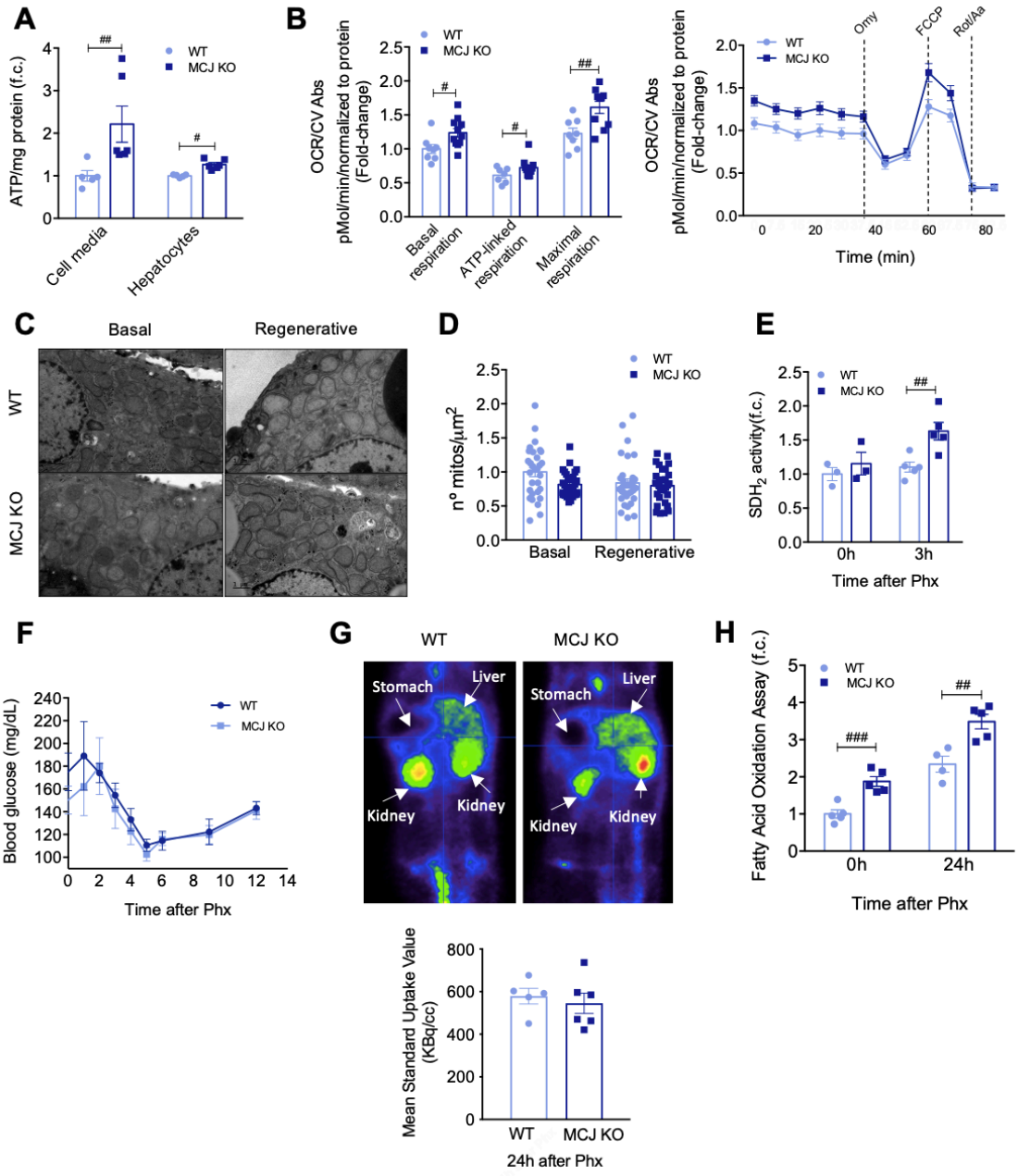

Fig. 5.14 Lack of MCJ increases ATP production following 70% Phx. (A) Cell-media and hepatocyte ATP production in primary WT and MCJ-KO hepatocytes, perfused 24h after 70% Phx. At least quadruplicates were used for each experimental condition. **(B)** Basal, ATP-linked and Maximal respirations using the Mitostress assay in primary WT and MCJ-KO hepatocytes, perfused 3h after 70% Phx. At least quadruplicates were used for each experimental condition. **(C)** Electron microscopy of epon embedded cell sections showing the number of mitochondria and mitochondrial morphology in basal conditions and 24 hours after 70% Phx at 2500X magnification (Scale bar 1µm). **(D)** Number of mitochondria quantified using electron microscopy photos in basal conditions and 24 hours after 70%. **(E)** Hepatic SDH_2 activity was measured in basal conditions and 3h after 70% Phx, in WT vs MCJ-KO mice. (SDH_2 = Succinate Dehydrogenase [ubiquinone] iron-sulfur subunit). **(F)** The tail vein was used to measure blood glucose levels every two hours after 70% Phx in WT and MCJ-KO mice. **(G)** Study of the hepatic uptake of ^{18}F fluorodeoxyglucose (FDG) using a PET-CT scan, 24h after 70% Phx, in WT and MCJ-KO mice. **(H)** Fatty Acid Oxidation rate was assayed in liver tissue at basal conditions and 24h after 70%Phx. Values are represented as mean ± SEM. Two-way ANOVA

followed by Tukey post-test was used to compare between multiple groups. $^{\#}p<0.05$; $^{\#\#}p<0.01$ and $^{\#\#\#}p<0.001$ versus MCJ-KO.

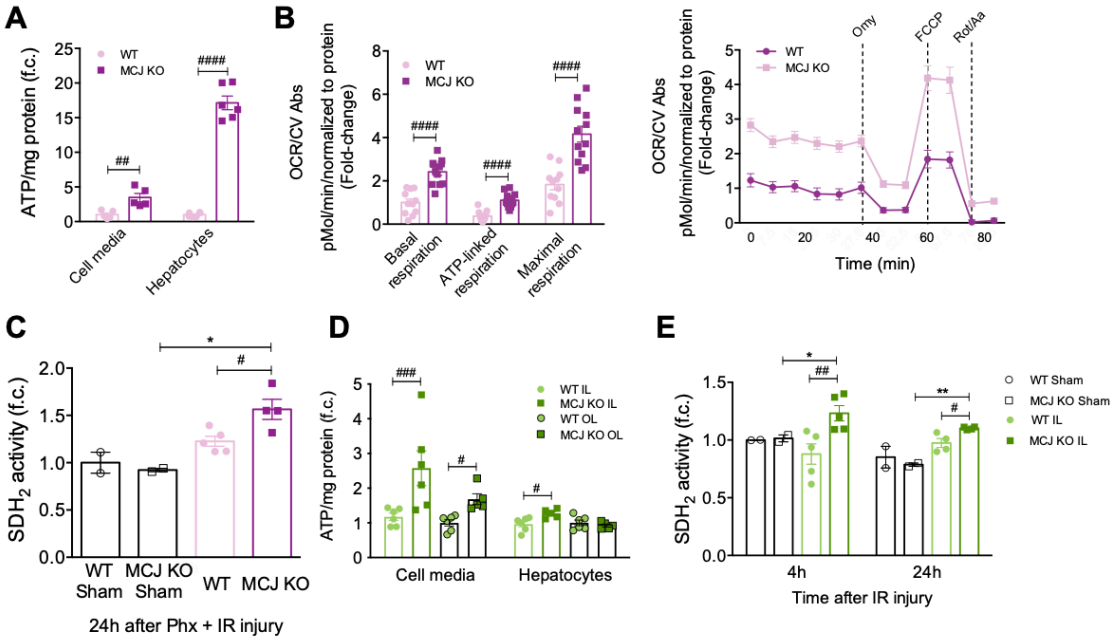

Fig. 5.15 Lack of MCJ increases ATP production following 70% Phx with IRI and after prolonged IRI. (A) Extracellular and intracellular ATP content in WT and MCJ-KO primary hepatocytes, perfused 24h after 70% Phx under IR injury. **(B)** Basal, ATP-linked and maximal respirations using the Mitostress assay in primary WT and MCJ-KO hepatocytes, perfused 24h after 70% Phx under IR injury. At least quadruplicates were used for each experimental condition. **(C)** Hepatic SDH_2 activity was measured in WT and MCJ-KO mice, both in sham operated and in those who underwent the procedure, 24h after 70% Phx under IR injury. **(D)** Cell-media and hepatocyte ATP production in primary WT and MCJ-KO hepatocytes, perfused 24h after IRI. Hepatocytes coming from both the ischemic and the oxygenated lobes were analyzed separately. At least sextuplicates were used for each experimental condition. **(E)** Hepatic SDH_2 activity was measured in WT and MCJ-KO mice, both in sham operated and in those who underwent the procedure, 4h and 24h after IRI. Values are represented as mean ± SEM. Two-way ANOVA followed by Tukey post-test was used to compare between multiple groups. $^{\#}p<0.05$; $^{\#\#}p<0.01$; $^{\#\#\#}p<0.001$ and $^{\#\#\#\#}p<0.0001$ versus MCJ-KO and $^{*}p<0.05$ and $^{**}p<0.01$ versus sham operated.

In summary, MCJ depletion maintains mitochondrial function and ATP levels after Phx as well as after prolonged ischemic damage, likely preventing consequent cell death while enhancing liver regeneration after liver injury.

5.2.5 Lack of MCJ enhances antioxidant defenses during liver regeneration

Enhanced mitochondrial respiration is often related to increased ROS production. However, depletion of MCJ facilitates the formation of respiratory supercomplexes (Barbier-Torres et al. 2017), allowing enhanced complex I activity with a lower risk of

ROS production. Lack of MCJ prevented the hepatic production of ROS after 70% Phx, as shown by reduced levels of dihydroethidium (DHE) staining in liver sections (Fig. 5.16A) and mitoSOX in cultured hepatocytes (Fig. 5.16B) 24 h after Phx. Reduced oxidative damage was further demonstrated by a higher GSH/GSSG ratio in MCJ KO mice (Fig. 5.16C). Decreased levels of mitoSOX staining were also observed in regenerative MCJ KO hepatocytes 24 h after Phx with IRI (Fig. 5.16D).

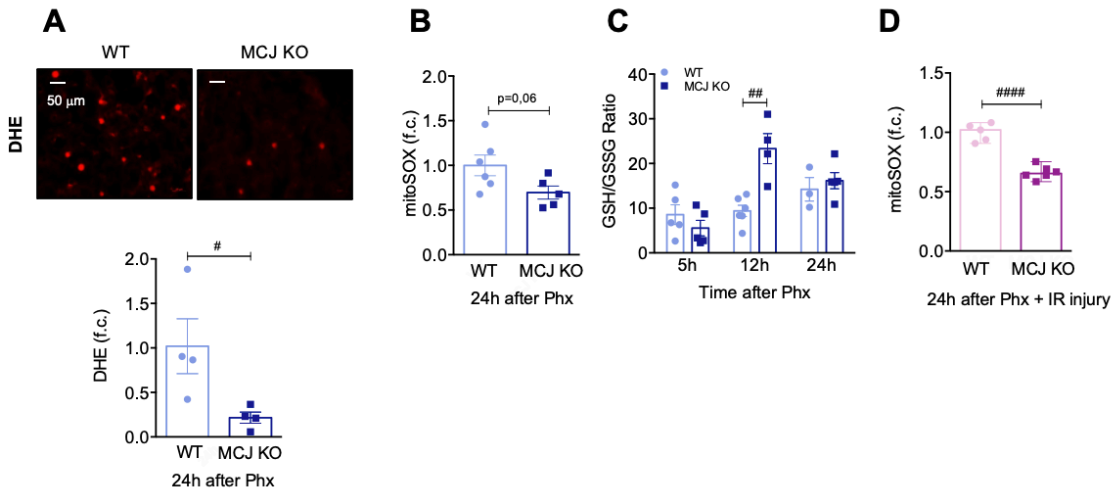

Figure 5.16 (A) ROS in vivo measured by dihydroethidium (DHE) staining in liver sections. Scale bar corresponds to 50 µm. **(B)** Quantification of mitochondrial ROS using mitoSOX in primary WT and MCJ-KO hepatocytes, perfused 24h after 70% Phx. **(C)** GSH/GSSG levels measured by HPLC-MS in WT and MCJ-KO livers. (GSH= Glutathione; GSSG= Glutathione Disulfide). **(D)** Mitochondrial ROS in primary WT and MCJ-KO hepatocytes, perfused 24h after 70% Phx under IR injury, using mitoSOX staining. At least quadruplicates were used for each experimental condition. Values are represented as mean ± SEM. Student's t-test was used to compare two groups and two-way ANOVA followed by TUKEY post-test was used to compare between multiple groups. $^{\#}p<0.05$; $^{\#\#}p<0.01$ and $^{\#\#\#\#}p<0.0001$ versus MCJ-KO.

5.2.5. Secreted ATP activates macrophages, enabling a faster priming phase in the absence of MCJ

Liver regeneration is a complex process involving an inflammatory response (priming phase) that is followed by the proliferation of liver cells to restore the lost mass. ATP plays a crucial role as a signaling molecule in the extracellular space; indeed, purinergic signals regulate the activation of immune cells and the subsequent cytokine production (Ishimaru et al. 2014). Based on these findings, we hypothesized that increased extracellular ATP levels would accelerate the activation of Kupffer cells and, therefore, enable a faster priming phase, accelerating liver regeneration, reducing liver damage and increasing survival in mice lacking MCJ.

We initially confirmed that extracellular ATP was able to stimulate the activation of macrophages. Macrophage-like RAW 264.7 cells, bone marrow-derived macrophages and hepatic Kupffer cells were treated with 3 mM ATP for 4 hours, and the levels of TNF and IL-6 were measured in the supernatants, as reported in previous publications (Ishimaru et al. 2014; Soni et al. 2019). We observed significantly increased levels of both proinflammatory cytokines in ATP-treated supernatants compared to non-stimulated cells (Fig. 5.17A,B,C). Macrophage derived heparin-binding EGF-like growth factor (HB-EGF), a ligand for the EGF receptor (EGFR), has also been identified as a mitogen for hepatocytes (Odegard et al. 2017; Wen et al. 2019). We observed that HB-EGF levels were significantly upregulated in bone marrow derived macrophages and Kupffer cells treated with 3mM ATP for 4 hours compared to non-stimulated cells; besides, MCJ KO showed significantly higher levels (Fig. 5.17D,E).

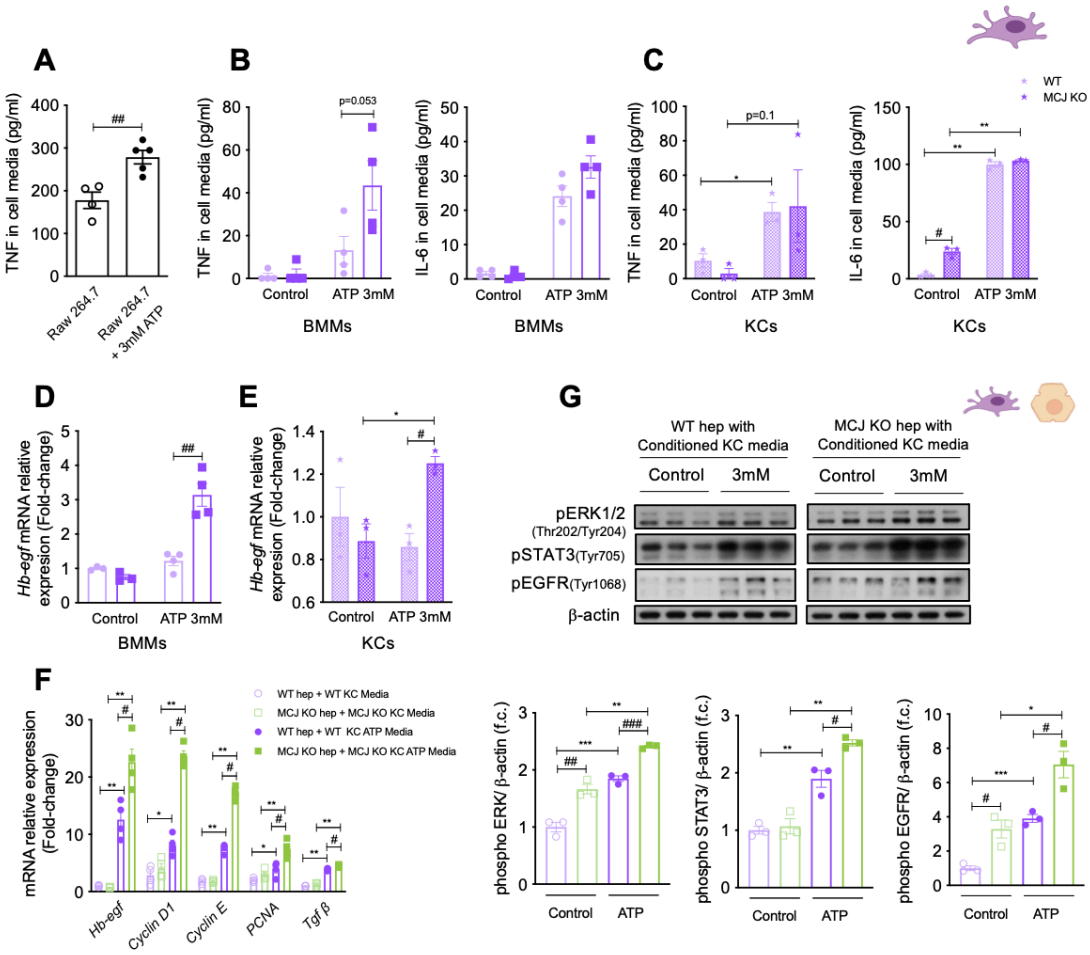

Fig. 5.17 Absence of MCJ activates production of proinflammatory cytokines and initiates the proliferative response due to increased ATP levels. Immune cell activation studies with ATP (A,B,C) Cell-media TNF and IL-6 levels from stimulated and non-stimulated Raw 264.7 **(A),** bone marrow derived cells **(B)** and WT and MCJ-KO hepatic Kupffer cells **(C).** Cells were stimulated with 3mM ATP for 4 hours. **(D,E)** Relative mRNA expression of *Hb-egf* in stimulated and non-stimulated bone marrow derived cells **(D)** and WT and MCJ-KO hepatic Kupffer cells **(E).**

Cells were stimulated with 3mM ATP for 4 hours (*Hb-egf*= heparing binding epidermal groWth factor-like groWth factor). **Proliferation studies with Kupffer cell-derived conditioned media. (F)** mRNA levels of *Hb-Egf, Cyclin D1, Cyclin E*, *PCNA* and *Tgf β* in WT and MCJ-KO hepatocytes following 24 hours of treatment with stimulated and non-stimulated WT and MJC KO Kupffer cell-derived conditioned media. **(G)** Western blot and densitometric quantification of total protein levels of phospho ERK1/2 (Thr 202/Tyr 204), phospho STAT3 (Tyr 705) and phospho EGFR (Tyr 1068) in WT and MCJ-KO hepatocytes following 4 hours of treatment with stimulated and non-stimulated Kupffer cell-derived conditioned media. Kupffer cells were stimulated with 3mM ATP for 4 hours. ß-actin was used as a loading control. Values are represented as mean ± SEM. Student's t-test was used to compare two groups and one-way ANOVA followed by Tukey post-test was used to compare between multiple groups. *p<0.05; **p<0.01 and ***p<0.001 versus control and $^{\#}$p<0.05; $^{\#\#}$p<0.01 and $^{\#\#\#}$p<0.001 versus MCJ-KO.

Kupffer cell-derived TNF and IL-6 play essential roles in the initiation of the priming phase, and HB-EGF promotes the G1/S transition in the hepatocyte cell cycle (Fazel Modares et al. 2019; Mitchell et al. 2005). Thus, to confirm that ATP-mediated Kupffer cell activation and production of inflammatory cytokines enable the initiation of hepatocyte proliferation, we performed proliferation studies with Kupffer cell-derived conditioned media. Proliferation was enhanced in both WT and MCJ KO hepatocytes stimulated with ATP-treated Kupffer cell media; however, mRNA levels of proliferative markers *Cyclin D1, Cyclin E* and *Pcna* were significantly higher in MCJ KO hepatocytes (Fig. 5.17F). *Tgfβ* was also augmented following treatment with conditioned media, with significantly higher levels in MCJ KO hepatocytes; proving that not only regeneration is accelerated in these hepatocytes, but also its termination (Fig. 5.17F). Importantly, the activation of ERK1/2 and STAT3 pathways, which are downstream of HB-EGF and IL-6 signaling respectively, and mediators of the priming phase, along with the activation of EGFR, were increased in hepatocytes in the presence of ATP-Kupffer cell media, with this activation being significantly higher in MCJ KO hepatocytes (Fig. 5.17G). Therefore, increased ATP levels not only enhance the priming phase, but also accelerate the proliferative phase during hepatocyte proliferation.

In vivo, we found increased hepatic *Tnf* and *Il-6* mRNAs and serum levels in MCJ KO mice 3 hours after Phx (Fig. 5.18A,B), along with increased hepatic IL-6/STAT3 signaling (Fig. 5.18C). We also observed the enhanced activation of the EGFR both by Western blotting and IHC in MCJ KO livers 33 h after Phx (Fig. 5.18D,E). Besides, the study of EGFR ligands showed increased expression of *Egf, Betacellulin* and *Hb-egf* in MCJ KO livers, both at early and late phases of liver regeneration (Fig. 5.18F).

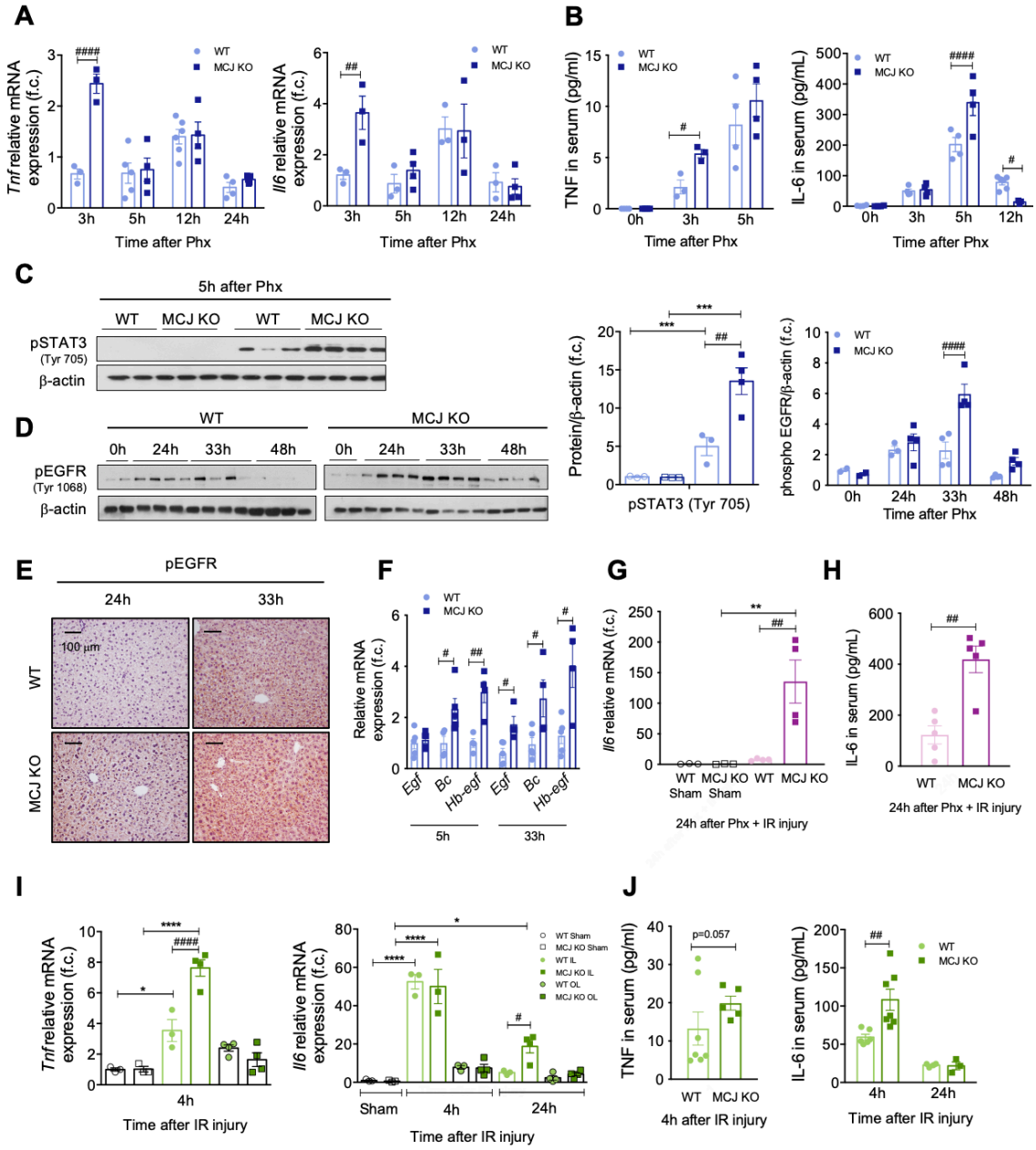

Fig. 5.18 Absence of MCJ accelerates the priming phase *in vivo* due to increased extracellular ATP levels (A) Relative hepatic mRNA expression of *Tnf* and *Il-6* at 3h, 5h, 12h and 24h after 70% Phx, in WT versus MCJ-KO mice. (*Tnf*= Tumor necrosis factor; *Il-6*= Interleukin 6). **(B)** Serum TNF and IL-6 levels, measured by ELISA, at indicated time points after 70% Phx in WT versus MCJ-KO mice. **(C)** Western blot analysis (left panel) and densitometric quantification (right panel) of total protein levels of pSTAT3 5h after Phx. ß-actin was used as a loading control. **(D)** Western blot analysis (left panel) and densitometric quantification (right panel) of total protein levels of pEGFR at 24h, 33h and 48h after 70% Phx. ß-actin was used as a loading control. **(E)** Liver immunohistochemical staining for pEGFR, 24h and 33h after 70% Phx**. (F)** mRNA levels of EGFR ligands *Egf, Bc* and *Hb-egf* 5h and 33h after 70% Phx (Egf= epidermal growth factor, Bc= betacellulin, Hb-egf= heparin binding Egf-like growth factor). mRNA *Il-6* levels in WT and MCJ-KO mice 24h after 70% Phx under IRI. **(H)** Serum IL-6 levels in WT and MCJ-KO mice 24h after 70% Phx under IRI. **(I)** mRNA *Tnf and Il-6* levels in WT and MCJ-KO mice 4 and 24h after IRI. **(J)** Serum TNF and IL-6 levels in WT and MCJ-KO mice 24h after IRI. Values are represented as mean ± SEM. Student's t-test was used to compare two groups and one-way ANOVA followed by Tukey post-test was used to compare between multiple groups. *p<0.05; **p<0.01 and ***p<0.001 versus control and $^{\#}$p<0.05; $^{\#\#}$p<0.01 and $^{\#\#\#\#}$p<0.0001 versus MCJ-KO.

IL-6 plays a major role in ischemia by reducing hepatic injury and promoting regeneration (M. Selzner, Camargo, and Clavien 2003). Notably, mRNA and serum IL-6 levels were significantly increased in MCJ KO mice compared to WT 24 h after 70% Phx with IRI (Fig. 5.18G,H). mRNA and serum levels of both TNF and IL-6 also remained significantly higher in MCJ KO mice 4 and 24 hours after prolonged IRI (Fig. 5.18I,J). Taken together, these findings confirm that increased ATP levels found in mice lacking MCJ are the driving force that enables faster entry into the cell cycle, enhancing liver regeneration.

5.2.5 Silencing MCJ, a new therapeutic approach

MCJ-specific siRNA (siMCJ) was evaluated after 70% Phx to assess whether it could be used as a potential therapy to accelerate liver regeneration following liver resection. Twenty-four hours before 70% Phx, 3-month-old WT mice were treated by intravenous tail injection with siMCJ or siCtrl. Thirty-three hours after this procedure, mice were sacrificed to analyze their hepatic regenerative capacity.

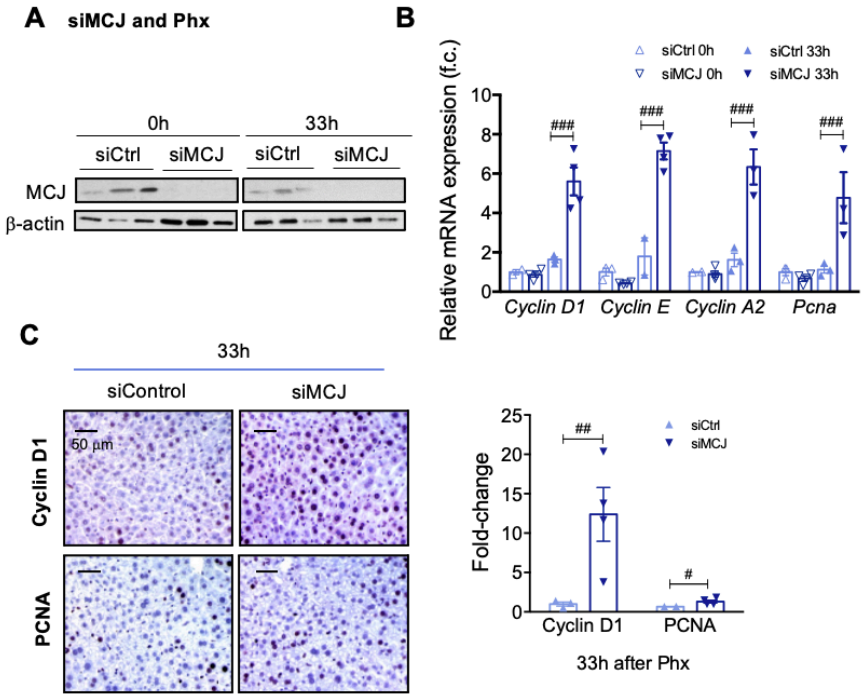

Fig. 5.19 Liver specific *Mcj* silencing accelerates liver regeneration in young mice. (A) MCJ levels by western blotting, confirming MCJ silencing, at basal and 33h after 70% Phx. **(B)** Differential expression of mRNA levels from genes involved in the cell cycle in siControl versus siMCJ WT mice, compared to basal, 33h after 70% Phx. **(C)** Liver immunohistochemical staining and respective quantification for Cyclin D1, and PCNA, proliferative markers, 33h after 70% Phx, in siControl versus siMCJ WT mice. Scale bar corresponds to 50µm. Values are represented as mean ± SEM. Student's t-test was used to compare two groups and two-way ANOVA followed by Tukey post-test was used to compare between multiple groups. $^{\#\#}p<0.01$and $^{\#\#\#}p<0.001$ versus siMCJ.

Efficient knockdown of MCJ (Fig. 5.19A) led to increased mRNA levels of the proliferative genes *Cyclin D1, E, A2* and *Pcna* (Fig. 5.19B). This was confirmed by the increased expression of Cyclin D1 and PCNA proteins in liver sections (Fig. 5.19C). Thus, RNAi-mediated gene targeting of MCJ is as efficient as genetic ablation of MCJ for accelerating liver regeneration after Phx, suggesting that MCJ silencing could constitute a therapeutic alternative.

5.2.6 Targeting MCJ overcomes regenerative limitations associated with steatosis

A large proportion of patients undergoing liver resection have chronic liver diseases, such as steatosis, fibrosis, or aging. These are linked to mitochondrial dysfunction and increase the risk of suffering from PHLF, as they severely limit liver regeneration and exacerbate the susceptibility to IRI (Alexandrino et al. 2018). Therefore, we examined whether MCJ silencing could reduce the susceptibility of steatotic or old livers to IRI and enhance liver regeneration.

Hepatic steatosis is a major risk factor for liver surgery, with postoperative mortality exceeding 14% after major liver resection. We used a murine model of induced steatosis, inflammation, and insulin resistance to test whether MCJ silencing could improve liver regeneration after Phx in steatotic livers. Three-month-old WT mice were fed a high-fat/high-fructose (15%) diet (HFHFD) for 12 weeks; hepatic insulin resistance development and hepatic inflammation were confirmed by an insulin tolerance test (ITT) and F4/80 staining, respectively (Fig. 5.20A,B). Mice were treated with either siMCJ or siCtrl 72 h prior to 70% Phx and euthanized 33 h after the procedure, allowing the analysis of the regenerative phase (Fig. 5.20C). MCJ-silenced mice showed a faster recovery of liver weight, with a significantly increased liver/body weight ratio 33 h after 70% Phx (Fig. 5.20D). These regenerating hepatocytes entered the cell cycle faster, as reflected by earlier increases in *Cyclin D1* and *Pcna* mRNA levels (Fig. 5.20E), Cyclin D1 protein levels (Fig. 5.20F) and Ki67-positive immunostaining (Fig. 5.20G). MCJ silencing not only accelerated liver regeneration in WT mice fed a 12-week HFHFD but also significantly reduced hepatic steatosis, demonstrated by decreased Oil-Red O staining levels (Fig. 5.20G), confirming previous results (Barbier-Torres et al. 2020).

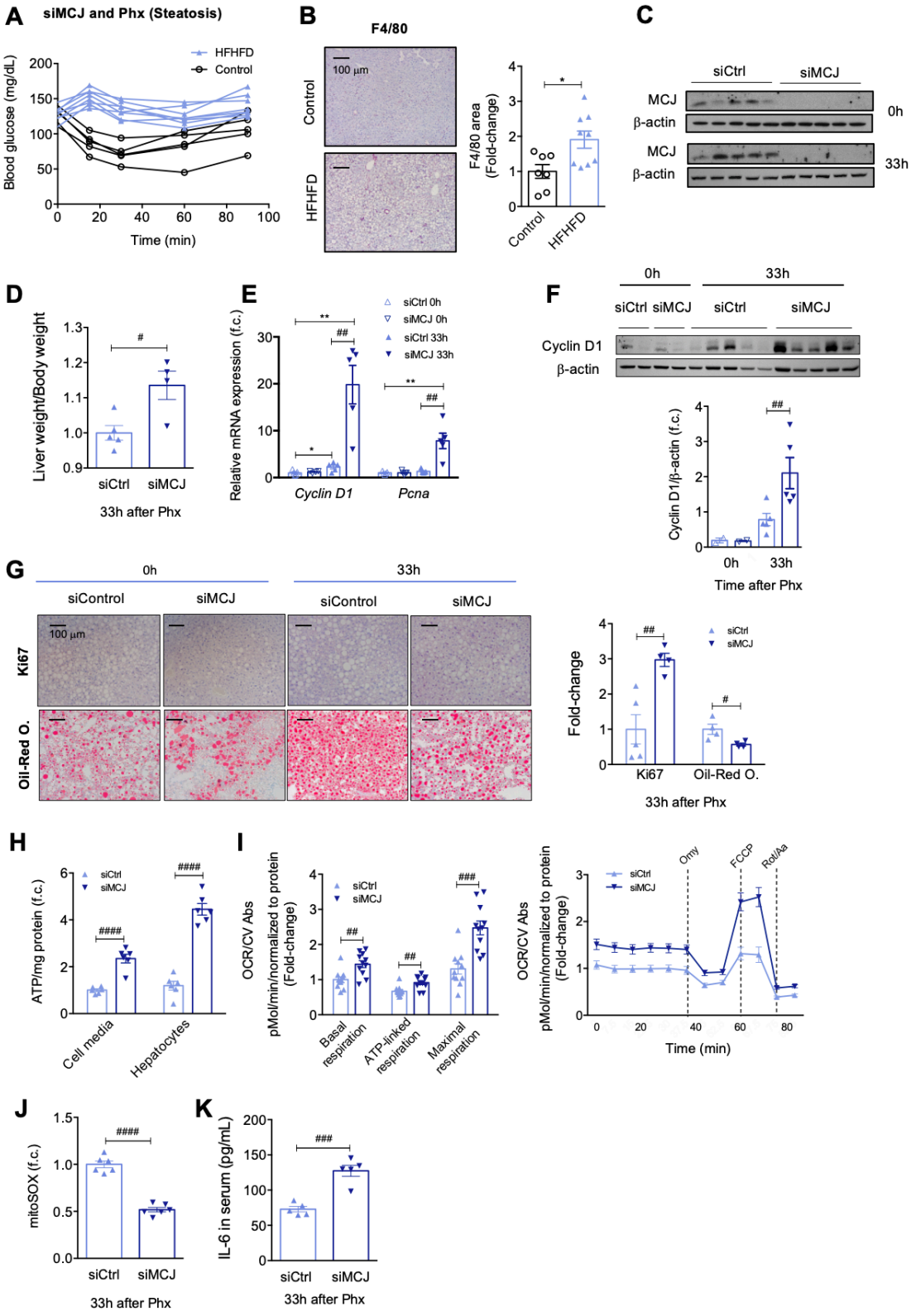

Fig. 5.20 Targeting MCJ overcomes regenerative limitations associated with steatosis. Steatosis was induced following a 12-week High Fat High Fructose Diet (A) Intraperitoneal Insulin Tolerance Test (ITT) before *Mcj* silencing and 70% Phx, to confirm insulin resistance following the HFHFD, compared to control Chow diet. **(B)** Liver immunohistochemical staining (left panel) and respective quantification (right panel) for F4/80, a macrophage marker, in Control diet versus HFHFD mice, before 70% Phx. Scale bar corresponds to 100µm. **(C)** MCJ levels by western blotting, confirming *Mcj* silencing, at basal and 33h after 70% Phx. **(D)** Liver weight/Body weight ratio in steatotic

siControl versus siMCJ WT mice 33h after 70% Phx. **(E)** Differential expression of *Pcna* and *Cyclin D1* mRNA levels in steatotic siControl versus siMCJ WT mice 33h after 70% Phx. **(F)** Western blot analysis of total protein levels of Cyclin D1 33h after 70% Phx in steatotic siControl versus siMCJ WT mice. ß-actin was used as a loading control. **(G)** Liver immunohistochemical staining and respective quantification for Ki67, a proliferative marker, and Oil-Red O., a marker for hepatic steatosis, in steatotic siControl versus siMCJ WT mice at 0 and 33h after 70% Phx. Scale bar corresponds to 100µm. **(H)** Extracellular and intracellular ATP content in primary hepatocytes of steatotic siControl and siMCJ WT mice that were perfused 33h after 70% Phx. At least sextuplicates were used for each experimental condition. **(I)** Oxygen consumption rate (OCR) and Basal, ATP-linked and Maximal respirations using the Mitostress assay in primary hepatocytes of steatotic siControl and siMCJ WT mice perfused 33h after 70% Phx. At least quadruplicates were used for each experimental condition. **(J)** Mitochondrial ROS in primary hepatocytes of steatotic siControl and siMCJ WT mice perfused 33h after 70% Phx, using mitoSOX staining. At least sixtuplicates were used for each experimental condition. **(K)** Serum IL-6 levels, measured by ELISA, 33h after 70% Phx, in steatotic siControl versus siMCJ WT mice. Values are represented as mean ± SEM. Student's t-test was used to compare two groups and two-way ANOVA followed by Tukey post-test was used to compare between multiple groups. *p<0.05 and **p<0.01 versus basal and $^{\#}$p<0.05; $^{\#\#}$p<0.01; $^{\#\#\#}$p<0.001 and $^{\#\#\#\#}$p<0.0001 versus MCJ-KO.

Both extracellular and intracellular ATP levels were measured in cultured hepatocytes isolated from siCtrl- and siMCJ-treated mice 24h after Phx, and in line with previous results, they were significantly elevated in MCJ-silenced hepatocytes (Fig. 5.20H). Furthermore, mitochondrial respiration measured 24h after 70% Phx showed a significant increase in OCR and higher basal, ATP-linked, and maximal respiration in MCJ-silenced hepatocytes (Fig. 5.20I) without ROS overproduction, as lower MitoSOX staining levels were observed (Fig. 5.20J). Additionally, increased serum levels of IL-6 were found in MCJ-silenced mice (Fig. 5.20K). Thus, MCJ silencing proves to be an efficient approach to accelerate mitochondrial activity and overcome the regenerative limitations that characterize insulin-resistant and steatotic livers following a 12-week HFHFD.

5.2.7 Targeting MCJ overcomes regenerative and survival limitations associated with aging

Only 8–15% of patients undergoing hepatic resection are older than 70 years due to the increasing prevalence of comorbidities that confer a high surgical risk (A. I. Fernandes et al. 2015). WT mice aged 15–17 months were treated with either siCtrl or siMCJ, and 24 h later, 70% Phx was performed. The mice were sacrificed 72 h after the procedure. MCJ silencing was equally efficient in aged (Fig. 5.21A) and young mice. We found that hepatic steatosis was significantly corrected by MCJ silencing, as demonstrated by Oil-Red O staining (Fig. 5.21B). This was accompanied by an increase in PCNA staining, showing enhanced liver regeneration (Fig. 5.21B).

Survival after 70% Phx with IR was also studied in 15-month-old MCJ KO and siMCJ-treated mice. Fifteen-month-old MCJ KO and WT mice were subjected to 70% Phx with 30 minutes of ischemia, and the survival rate was assessed 7 days after the procedure (Fig. 5.21C). Only 22% of WT mice survived, while half of MCJ KO mice recovered from the procedure (Fig. 5.21C). Aging is associated with a variety of diminished mitochondrial functions and decreased mitochondrial ATP production in old livers results in lower tolerance to IRI (Seizner et al. 2007). Thus, 24 h after Phx with IRI, extracellular and intracellular ATP levels were measured in cultured hepatocytes isolated from aged WT and MCJ KO mice. ATP levels were significantly elevated in MCJ KO hepatocytes (Fig. 5.21D). Mitochondrial respiration measured 24 h after Phx with IRI showed significantly higher basal, ATP-linked, and maximal respiration in MCJ KO hepatocytes (Fig. 5.21E), which was not accompanied by elevated ROS production, as lower mitoSOX staining levels were detected (Fig. 5.21F).

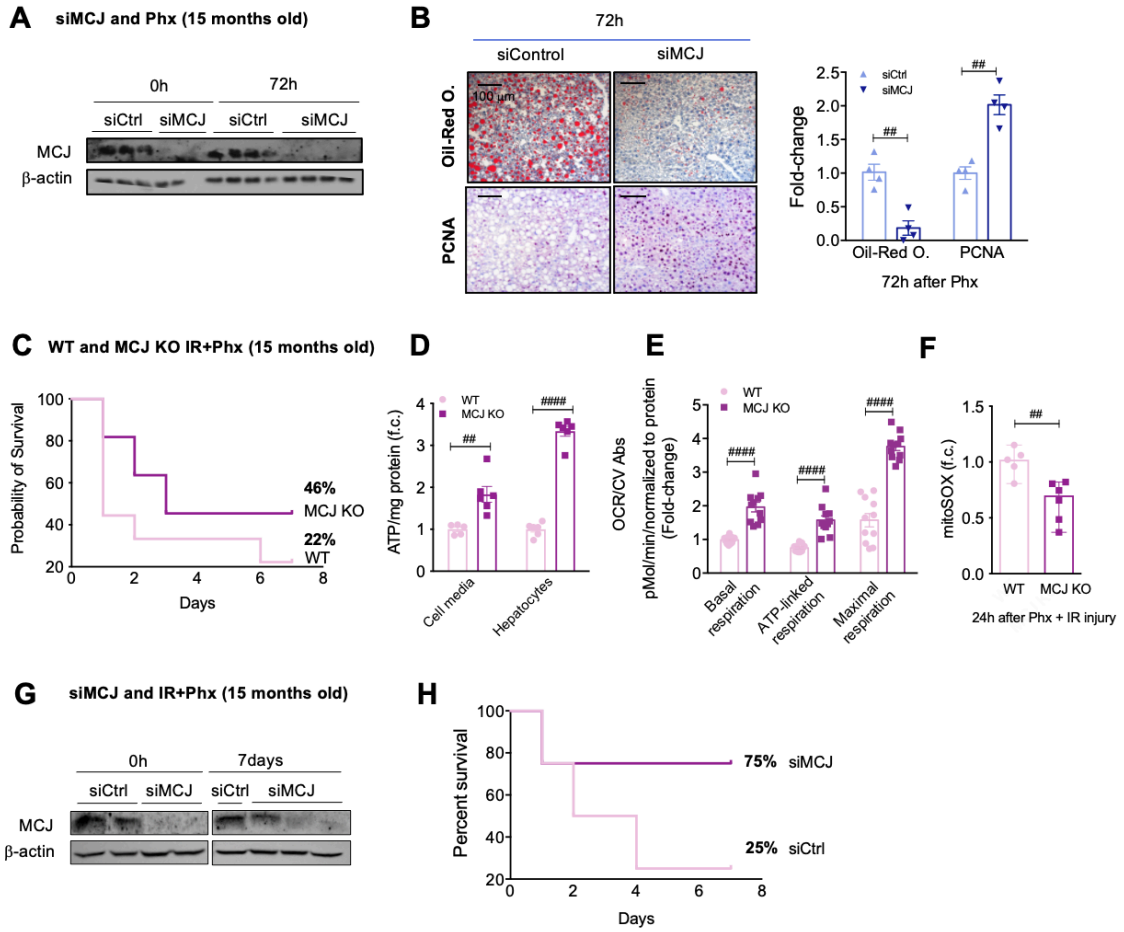

Fig. 5.21 Targeting MCJ overcomes regenerative and survival limitations associated with aging. (A) MCJ levels by western blotting, confirming MCJ silencing, at basal and 72h after 70% Phx. **(B)** Liver immunohistochemical staining and respective quantification for Oil Red O. staining, a marker for hepatic steatosis and for PCNA, proliferative marker 72h after 70% Phx, in siControl versus siMCJ WT. Scale bar corresponds to 100µm. **(C)** Survival percent 7

days after 70% Phx under IRI in 15-months-old WT (n=9) and MCJ-KO (n=11). **(D)** Cell-media and hepatocyte ATP production in primary hepatocytes of 15-months-old WT and MCJ-KO mice, perfused 24h after 70% Phx under IRI. At least sextuplicates were used for each experimental condition. **(E)** Basal, ATP-linked and Maximal respirations using the Mitostress assay in primary hepatocytes of 15-months-old WT and MCJ-KO mice perfused 24h after 70% Phx under IRI. At least quadruplicates were used for each experimental condition. **(F)** Mitochondrial ROS in in primary hepatocytes of 15-months-old WT and MCJ-KO mice, perfused 24h after 70% Phx under IRI, using MitoSOX staining. At least quadruplicates were used for each experimental condition. **(G)** MCJ levels by western blotting, confirming MCJ silencing, at basal and 7 days after 70% Phx. **(H)** Survival percent 7 days after 70% Phx under IRI in 15-months-old siControl (n=4) versus siMCJ (n=4) WT mice. Values are represented as mean ± SEM. Student's t-test was used to compare two groups and two-way ANOVA followed by Tukey post-test was used to compare between multiple groups $^{\#\#}p<0.01$ and $^{\#\#\#\#}p<0.0001$ versus MCJ-KO.

Furthermore, 15-month-old WT mice were treated with either siMCJ or siCtrl 72 h prior to 70% Phx with IR, and they were sacrificed 7 days after the procedure. Efficient MCJ silencing was confirmed (Fig. 5.21G). Mice treated with siCtrl achieved a similar 25% survival rate when compared to 15-month-old WT mice. Notably, 75% of the siMCJ-treated mice survived the procedure, confirming the positive regenerative outcomes already observed in silenced mice subjected to 70% Phx (Fig. 5.21H). Thus, inhibiting MCJ expression reduces both hepatomegaly and steatosis and enhances hepatic regeneration, thereby improving survival in 15-month-old mice.

Overall, the loss of MCJ, increasing ATP production and, therefore, preventing the characteristic ATP depletion, overcomes impaired regeneration and reduces ischemic susceptibility in "marginal" organs (steatotic livers or those originating from old donors), making them suitable for hepatic surgery and liver transplantation.

6. DISCUSSION

6 DISCUSSION

Mitochondrial dysfunction plays a key role in the initiation and development of chronic liver diseases. In this work, we sought to better understand some key players, the direct causes and consequences of mitochondrial dysfunction in order to provide evidence that improving mitochondrial activity, in our case by specifically silencing *Mcj* in the liver, may be the therapeutic approach that could not only ameliorate liver injury but also promote liver regeneration and hopefully alleviate the transplant waiting list.

The morbidity and mortality of CLDs, and thus the global burden, are high and expected to continue to increase (Mokdad et al. 2016).Although viral infections such as hepatitis B and C are declining, alcohol abuse and NAFLD have emerged as important risk factors (Cheemerla and Balakrishnan 2021).Without appropriate therapy, CLDs can progress to cirrhosis and HCC (Mishra and Younossi 2012; Riley and Bhatti 2001; Vernon, Baranova, and Younossi 2011), and liver transplantation (LT) may be the only curative treatment for these end-stage liver diseases. However, current rates cover less than 10% of the global need for organ transplantation (Asrani et al. 2019). These data highlight the window of opportunity to address the increasing prevalence of alcohol abuse and NAFLD and develop new strategies to improve transplantation rates before the global burden of liver disease becomes unsustainable.

The main goal of our laboratory is to understand the underlying pathophysiological mechanisms of CLDs in order to develop new therapeutic strategies. Knowing that most preclinical pharmacological targets fail in clinical trials, likely due to patient heterogeneity, we have tried to find treatments with a broad spectrum of activity. Recently, we have shown that targeting perturbations related to posttranslational modifications (Serrano-Maciá et al. 2021) or Mg^{2+} homeostasis (Simón et al. 2021) ameliorate the progression of NAFLD and NASH. In addition, mitochondrial dysfunction is gaining therapeutic interest.

Because of the high metabolic activity of the liver, hepatocytes have a high density of mitochondria and are therefore susceptible to disorders that affect mitochondrial function (Lee and Sokol 2007). Alterations in mitochondrial function not only affect cellular metabolism, but also have a critical impact on cell-cell signaling pathways, whole-body

metabolism, health, and life expectancy (Sorrentino, Menzies, and Auwerx 2018). Most liver diseases first affect hepatic mitochondria, causing oxidative stress, dysregulation of mitochondrial metabolism, ATP synthesis, mtDNA integrity, Ca2+-compensatory dysfunction, and excessive opening of the mitochondrial membrane permeability transition pore (mPTP), which together trigger hepatocyte death and the release of damage-associated molecular patterns (DAMPs) and enhance the pathogenesis and progression of liver disease (Xiang, Shao, and Chen 2021).

In this context, methylation-controlled J protein (MCJ), also known as DnaJC15, is an endogenous negative regulator of mitochondrial activity that interacts with and inhibits the mitochondrial complex I (Hatle et al. 2013). Significantly elevated MCJ levels have been observed in patients with NAFLD, APAP-induced liver injury, and cholestatic liver disease (Barbier-Torres et al. 2017, 2020; Iruzubieta et al. 2021), and mitochondrial dysfunction is considered a key player in the development of these diseases. Moreover, we have previously shown that liver-specific *Mcj* silencing increases mitochondrial activity and ATP synthesis and (1) leads to reduced formation of ROS and steatosis in nonalcoholic steatohepatitis (NASH) (Barbier-Torres et al. 2020); (2) prevents mitochondrial dysfunction and hepatocyte damage after APAP-induced liver injury (Barbier-Torres et al. 2017); and (3) protects against cholestasis-induced liver injury (Iruzubieta et al. 2021). Therefore, we aimed to investigate the implication of MCJ in alcoholic liver disease and the results of mitochondrial dysfunction improvement.

Excessive alcohol consumption is the leading cause of liver-related mortality in Western countries and represents the second most common indication for LT worldwide (Louvet and Mathurin 2015). The progression of ALD from alcoholic fatty liver to alcoholic steatohepatitis, alcoholic hepatitis, cirrhosis, and eventually hepatocellular carcinoma (HCC) is well characterized but lacks a therapy that could halt and even reverse ALD progression (You and Arteel 2019). Currently, the only options for curing alcohol-related liver damage are abstinence in early stages and liver transplantation in advanced stages (Teschke 2018).

Alcohol abuse significantly impairs mitochondrial function. In fact, mitochondrial dysfunction is one of the earliest indicators of alcohol-related damage (Zhong et al. 2014). Metabolism of high alcohol concentrations leads not only to acetaldehyde, which has

toxic effects, but also to decreased NAD^+/NADH ratio and oxidative stress, altering important metabolic pathways such as beta-oxidation (Ceni, Mello, and Galli 2014). As outlined in Chapter 5.1, our work has attempted for the first time to investigate the implication of the endogenous inhibitor of mitochondrial activity MCJ in the initiation and pathophysiology of ALD. For this purpose, we have worked with the NIAAA mouse model developed by Gao et al. to study the early stages of ALD (Bertola et al. 2013). Herein, we show significantly downregulated hepatic MCJ levels in ethanol-fed mice. Interestingly, we observe that the expression of MCJ in ALD patients depends on the severity and chronicity of the disease; it appears downregulated in early stages, whereas it is overexpressed in late stages. Based on our previous studies, the downregulation of MCJ is an unexpected finding. However, it may indicate a possible key role of MCJ in the initiation and development of the disease. As discussed previously, mitochondria increase oxygen consumption after alcohol consumption, in part as an adaptive response to oxidize the toxic metabolite acetaldehyde and increase NAD^+ supply for alcohol metabolism more rapidly. This phenomenon is termed "Swift Increase in Alcohol Metabolism" (SIAM) (Zhong et al. 2014). Consistently, increased mitochondrial activity, depolarization, and hepatic hypermetabolism have been measured during early ALD (Bradford and Rusyn 2005; Lemasters and Holmuhamedov 2006). Downregulation of MCJ in the early stages of liver injury may be a strategy to enhance mitochondrial respiration, NAD^+ production, and to support metabolism of the high levels of alcohol that hepatocytes must cope with, as mitochondria are still fit enough to do so.

The mechanism for SIAM remains unclear and most likely involves multiple factors (Bradford and Rusyn 2005; Thurman, McKenna, and McCaffrey 1976). Lemasters et al. showed that increased oxygen consumption during SIAM is mediated by reversible uncoupling of hepatocellular mitochondria, as increased mitochondrial respiration does not lead to increased ATP production; alcohol consumption actually leads to a decrease in hepatic ATP levels. The closure of VDAC, which is responsible for the permeability of the outer mitochondrial membrane to hydrophilic metabolites (e.g., ADP, Pi) and mitochondrial substrates (e.g., fatty acyl-CoA), plays a key role in this phenomenon (Lemasters and Holmuhamedov 2006). However, prolonged alcohol abuse and acetaldehyde accumulation lead to mitochondrial damage, ROS overproduction, and decreased overall metabolic efficiency due to VDAC closure, resulting in lipid accumulation, fibrogenesis, and inflammation (Ceni, Mello, and Galli 2014; Levine,

Harris, and Morgan 2000). Overexpression of MCJ at late stages may be an attempt to slow mitochondrial oxidative metabolism, reduce oxidative stress, and arrest mitochondrial damage. However, it would also reduce the formation of NAD^+, which is essential for alcohol metabolism. As a result, ethanol in this condition would be metabolized primarily via CYP2E1, which consumes NADPH, generates ROS, and leads to toxic acetaldehyde accumulation that promotes disease progression (Abdelmegeed et al. 2013; Lu and Cederbaum 2008). Overall, preventing mitochondrial dysfunction and ROS overproduction by silencing *Mcj* may be the firewall that delays or even prevents the downfall of ALD patients.

Expression of MCJ is regulated by the methylation of three specific CpG sites in its promotor (Barbier-Torres et al. 2020). Indeed, this epigenetic process is inversely correlated with expression, where lower DNA methylation is associated with higher levels of transcripts. Prolonged alcohol abuse is known to decrease MAT1A activity, and, thereby, SAMe levels (Barbier-Torres et al. 2022). Therefore, the ratio SAMe/SAH, an index for methylation reactions, is significantly reduced in late ALD stages, causing MCJ overexpression. Further studies are needed to elucidate the exact mechanism by which MCJ is downregulated at early stages.

The contribution of MCJ to the development of ALD has been further confirmed by preclinical in vivo studies. Following the NIAAA model, whole body MCJ-KO mice showed nearly fourfold increased mortality compared to Wt mice. This result is shocking, to say the least, because we had previously demonstrated hepatoprotection in NAFLD, APAP-induced liver injury, and cholestasis in MCJ-KO mice (Barbier-Torres et al. 2017, 2020; Iruzubieta et al. 2021). Ethanol-fed MCJ-KO mice exhibit mildly increased liver injury associated with altered lipid metabolism, increased FA deposition, and increased expression of *Ccl2* and *Ccr2*, with no differences in immune cell infiltration. In the context of alcohol metabolism, expression of *Cyp2e1* is significantly increased in ethanol-fed MCJ-KO mice, leading to increased oxidative stress and lipid peroxidation. We find no significant differences in hepatic accumulation of toxic acetaldehyde. Overall, liver injury is higher in ethanol-fed MCJ-KO mice than in ethanol-fed Wt mice, but it is still moderate and not sufficient to cause such differences in survival.

Alcohol abuse causes a systemic disease (González-Reimers et al. 2014). Since alcohol dehydrogenase, CYP2E1, and aldehyde dehydrogenase are mainly expressed in hepatocytes, most of the direct cellular toxicity of ethanol involves these cells (Louvet and Mathurin 2015). However, the effects of acetaldehyde and ROS extend far beyond the liver and affect other organs as well (Rao 2009). Indeed, intestinal damage has been identified as an aggravating factor in ethanol-fed MCJ-KO mice. Pascual-Itoiz et al. have previously described that under inflammatory conditions, deficiency of MCJ plays a detrimental role in the gut. Following the dextran sulfate sodium (DSS) model, which causes clinically relevant loss of gut barrier function, deficiency of MCJ activates intestinal macrophages and enhances inflammatory TNF signaling, leading to more severe ulcerative colitis (Pascual-Itoiz et al. 2020). Consistent with their study, increased immune infiltration, dysbiosis, augmented permeability, and altered gut-liver axis are observed in ethanol-fed MCJ-KO mice. In addition, ethanol-fed MCJ-KO mice exhibit significantly increased plasma LPS levels compared to ethanol-fed Wt mice. LPS translocation is associated with low-grade systemic inflammation and disease exacerbation (Boutagy et al. 2016; Mohammad and Thiemermann 2021). The altered gut-liver axis prompted us to measure LPS concentration in the liver in case it might be influencing the observed liver injury. Ethanol-fed MCJ-KO mice have significantly increased hepatic LPS concentrations. Interestingly, Abdulla et al. previously found that LPS increases hepatic *Cyp2e1* mRNA expression (Abdulla, Goralski, and Renton 2006), Roe et al. proposed that this increase could be mediated by hepatocyte nuclear factor-1 (HNF-1), AP-1 or NF*k*B (Roe et al. 2001) and Lu et al. showed that increased CYP2E1 potentiates LPS hepatotoxicity (Lu and Cederbaum 2010), creating a vicious cycle that may be responsible for the significantly increased *Cyp2e1* expression and subsequent oxidative stress and lipid peroxidation in ethanol-fed MCJ-KO mice. In addition, Ambade et al. and Hua et al. have highlighted the importance of CCR2/CCL2 signaling in mediating LPS-induced hepatocellular damage (Ambade et al. 2019; Hua et al. 2020).

Nevertheless, enhanced translocation of bacterial endotoxins may have a broader systemic effect; they are by no means restricted to the liver (Rao 2009). We observe markedly elevated blood glucose levels in ethanol-fed MCJ-KO mice, indicating possible pancreatic injury . Chronic pancreatitis is indeed common in alcoholic individuals (Ren et al. 2016). The study of the endocrine pancreatic function shows deteriorated glycemic regulation in ethanol-fed MCJ-KO mice, as they are unable to control their blood glucose

levels during the IPGTT, and even reach hyperglycemic levels (< 600mg/dL), leading to their sudden death. Consistently, insulin secretion is also defective in ethanol-fed MCJ-KO mice. Mechanistically, insulin secretion depends on ATP production and Ca^{+2} signaling (Klec et al. 2019); although the MCJ-KO pancreatic islets have significantly higher ATP levels both in the basal state and after ethanol consumption, the static insulin secretion assay shows a decreased ability to sense glucose. Since metabolic endotoxemia is known to play a key role in the development and pathophysiology of diabetes mellitus (DM) (Gomes, Costa, and Alfenas 2017; Lassenius et al. 2011; Orokorov et al. 2011), we hypothesize that circulating LPS may have blunted the ability of MCJ-KO pancreatic beta cells to sense glucose, leading to elevated blood glucose levels that, in the worst case, result in fatal hyperglycemia (Fig. 6.1).

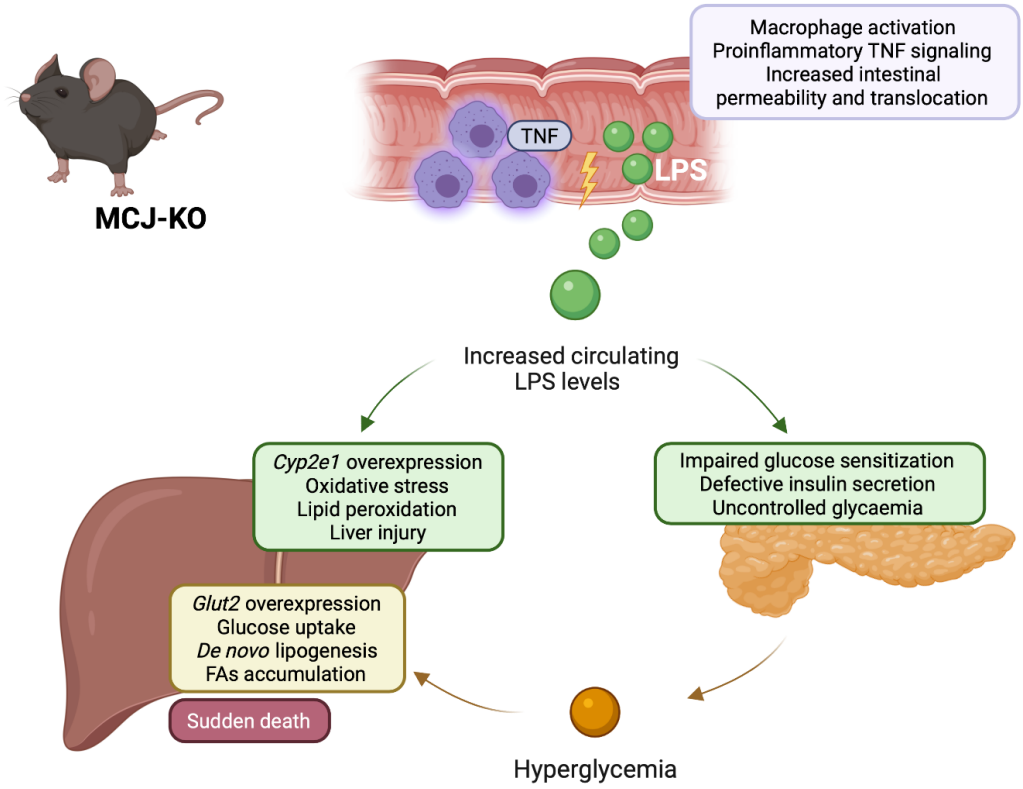

Figure 6.1 After ethanol abuse, whole body lack of MCJ results in increased mortality due to exacerbated systemic affection driven by circulating LPS. (Cyp2e1=Cytochrome P450 2E1; FAs=Fatty acids; Glut2=Glucose transporter 2; LPS=Lipopolysaccharide; TNF=Tumor necrosis factor)

Significantly increased expression of the hepatic glucose transporter *Glut2* and several genes involved in *de novo* lipogenesis, particularly *Chrebp*, whose expression is upregulated by substrate, suggest that circulating glucose uptake is increased in ethanol-fed MCJ-KO mice, which in turn leads to the formation of FAs and increased deposition. Although intrinsic MCJ-KO capacity appears to be directed toward catabolism and hepatoprotection, after ethanol consumption intestinal injury and LPS translocation exacerbate hepatic oxidative stress, liver injury and overall mortality.

On the contrary, liver-specific Mcj silencing shows hepatoprotective effects. First, a survival rate of 100% is observed in both groups of mice. We consider that the difference in survival between Wt and siCtrl mice is negligible (the mortality rate of 15% observed in the first group refers to the death of one mouse). Importantly, after ethanol consumption, liver-specific deficiency of MCJ significantly reduces liver injury and promotes liver regeneration. In addition, ethanol-fed siMCJ mice clearly exhibit metabolism directed toward lipid catabolism, as well as reduced immune response and oxidative stress. In terms of systemic effects, no changes are observed in the gut-liver axis, consistent with similar circulating and hepatic LPS levels and *Cyp2e1* expression. In addition, glycemic control is comparable in both groups. Overall, these results confirm the detrimental role of MCJ in nonhepatic tissues, particularly in the gut, after chronic and acute alcohol abuse.

siMCJ exerts hepatoprotective functions by promoting lipid beta-oxidation, as previously published by our group (Barbier-Torres et al. 2020), but also modulates de novo lipogenesis. Alcohol-induced hepatic steatosis occurs at early ALD stages, and is reversible, raising the possibility of therapeutic intervention for ALD prevention. In silico analysis of results from LC-MS shows lower enrichment of mTOR and its downstream signaling pathways in siMCJ mice. The mTORC1 signaling plays an important role in the regulation of lipid metabolism, such as de novo lipogenesis, by enhancing the transcription of SREBP1 (Caron, Richard, and Laplante 2015). Chen et al. have previously shown that mTORC1 activity is increased in experimental animals and ALD patients (H. Chen et al. 2018). Interestingly, aberrant activation of mTORC1 has been associated with defects in NAD^+-dependent SIRT-1 activity (H. Chen et al. 2018; Li et al. 2011). Ethanol exposure downregulates the expression of SIRT-1 (H. Chen et al. 2018), and its deacetylase activity is sensitive to the NADH redox state, so changes in the

NAD^+/NADH ratio caused by alcohol metabolism also impair its function (You and Arteel 2019). Thus, increasing NAD^+ by silencing hepatic *Mcj* restores both the expression and activity of SIRT-1 and prevents mTOR activation and subsequent de novo lipogenesis. In addition, SIRT-1 also activates AMPK (Price et al. 2012), whose downstream signals inhibit ATP-consuming processes such as *de novo* lipogenesis by phosphorylating and inhibiting ACC, ChREBP, and SREBP-1, key lipogenic enzymes and transcription factors (Fig. 6.2).

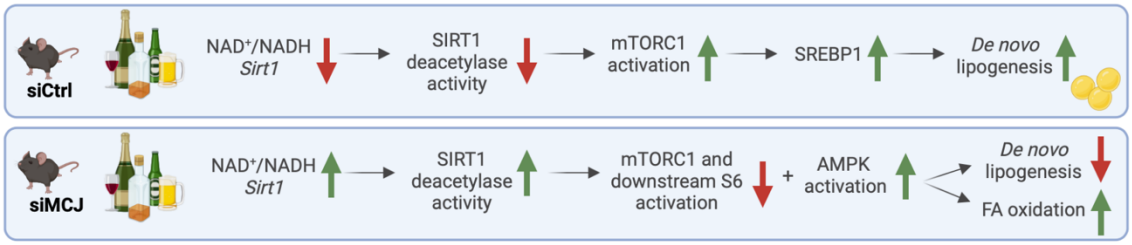

Figure 6.2 Schematic representation of the hepatoprotection exerted by liver specific *Mcj* silencing after alcohol abuse. (AMPK=AMP-activated protein kinase; FA=Fatty acids; mTORC1=Mammalian target of rapamycin complex 1; NAD=nicotinamide adenine dinucleotide; SIRT1=Sirtuin; SREBP1= Sterol regulatory element-binding protein 1)

We have already explained that the mechanisms for SIAM are still unclear and most likely involve multiple factors. Indeed, downregulation of MCJ in early ALD stages may be a new key player. As a result of chronic alcohol abuse, toxic acetaldehyde accumulation, mitochondrial damage, and VDAC closure, SIAM becomes maladaptive. We hypothesize that liver-specific knockdown of *Mcj* may prevent this. Although we were unable to measure this, we hypothesize that liver-specific *Mcj* silencing enables SIAM without VDAC closure. VDAC closure is mediated by various metabolites such as tubulin, actin, and NADH, and opening is mediated by BCL-XL (Rostovtseva and Bezrukov 2008). We suggest that the increase in oxygen consumption and enhanced OXPHOS favored by liver-specific *Mcj* silencing are sufficient to initiate SIAM; VDAC remains open, substrates and metabolites can circulate freely, and mitochondria can produce ATP, catabolize FAs, oxidize excess NADH and acetaldehyde, and generate NAD^+. Further studies are needed to elucidate the exact mechanism, but an increased NAD^+/NADH ratio and BCL-XL protein levels found in ethanol-fed siMCJ mice, together with increased FA oxidation activity, may be indicative.

Overall, on the one hand, organ specificity needs to be considered when boosting mitochondrial activity to halt ALD, and on the other hand, liver-specific *Mcj* silencing

might be a novel therapeutic approach to stop, ameliorate and even prevent the progression of ALD by alleviating mitochondrial dysfunction and restoring NAD^+/NADH ratio.

There is no effective FDA-approved therapy for ALD. We have shown that targeting mitochondrial dysfunction in early stages could be a good strategy to halt disease progression and, together with abstinence, could help alleviate liver damage and restore homeostasis. ALD, however, has a silent progression, and may not be diagnosed until the late stages, when LT is the only therapeutic option. The remarkable regenerative capacity of the liver allows the implementation of several therapeutic strategies. Nevertheless, LT is also associated with complications such as ischemia-reperfusion injury, which is the main cause of graft dysfunction after transplantation (Gracia-Sancho, Casillas-Ramírez, and Peralta 2015), as well as a shortage of donor organs due to the widening gap between supply and demand (Campana et al. 2021). Strategies to improve the donor pool, proper attention to patients on the waiting list and ease the economic burden are crucial. The results in Chapter 5.2 highlight the relevance of mitochondrial dysfunction in impaired liver regeneration and ischemia-reperfusion injury and point to a new approach to increase the donor organ pool by alleviating mitochondrial dysfunction in metabolically compromised, and frequently disposed organs.

Liver regeneration is determined by the energy status of the hepatocyte (Alexandrino et al. 2016). In this regard, liver biopsies from controlled donation after circulatory death (cDCD) show significantly increased MCJ levels 60 minutes after the onset of normothermic regional perfusion (NRP) compared with control, suggesting a possible link between MCJ and IRI susceptibility. In the preclinical study, 70% partial hepatectomy (Phx), prolonged IRI, and Phx under IRI allow analysis of the regenerative response and ischemic injury. Interestingly, after Phx with or without occlusion, mice show increased MCJ levels compared with baseline or sham-operated mice, and once the damage is alleviated, MCJ is downregulated. Overexpression of MCJ may be a strategy to reduce the overproduction of ROS and could be driven by changes in the methylation status. Although hepatocyte proliferation is required after liver injury, excessive mitochondrial activity may lead to oxidative stress that damages rather than heals liver tissue. We have previously shown that the expression of MCJ is regulated by methylation of three specific CpG sites in its promoter (Barbier-Torres et al. 2020). SAMe levels are

known to decrease markedly during liver regeneration, which is due to a switch between MAT1A and MAT2A gene expression (L. Chen et al. 2004) along with increased formation of S-adenosylhomocysteine (SAH). Therefore, the SAMe/SAH ratio is significantly reduced, leading to the previously observed overexpression of MCJ during Phx and ischemic injury. Overall, MCJ expression, and thus mitochondrial activity, plays a key role during the regenerative phase and ischemic injury.

Both *in vitro* and *in vivo*, lack of MCJ significantly accelerates cell cycle entry, which is associated with faster recovery of liver weight after Phx and increased survival after Phx under IRI. In terms of liver weight/body weight ratio, the absence of MCJ promotes accelerated liver regeneration until the "hepatostat" is reached, implying that although regeneration is enhanced, it is not uncontrolled. In addition, hepatic IRI is widely used in liver surgery, especially in liver transplantation, liver resection, and trauma. It is also the leading cause of organ failure immediately after transplantation; oxygen deprivation during ischemia directly affects mitochondrial coupling as ATP is depleted, and liver injury is further exacerbated during reperfusion (Soares et al. 2019). Deficiency of MCJ after prolonged IRI attenuates liver injury and improves the regeneration response.

Mitochondrial function also correlates with post-hepatectomy liver function (Alexandrino et al. 2018). Alexandrino et al. demonstrated in a cohort of 30 patients that decreased oxidative phosphorylation correlates with worse postoperative liver function and increased risk of PHLF (Alexandrino et al. 2016). The increased expression of MCJ observed in our patient cohort may be one reason for this. Restoration of ATP levels is not a novel therapeutic approach; ischemic preconditioning, a brief period of portal triad occlusion and reperfusion before sustained IR, induces adenosine-mediated tissue protection (Wang, Jia, and Zhang 2020). Studies demonstrating the hepatoprotective effects of purinergic signaling agonists after IRI and LT highlight the possibility to target mitochondrial dysfunction and restore ATP production during liver regeneration and ischemic injury (Tang et al. 2010). However, alleviating mitochondrial dysfunction and improving respiration has been challenging because it may involve collateral ROS overproduction. Our results show that the absence of MCJ significantly improves mitochondrial function and increases ATP production in all three preclinical models, without collateral oxidative stress, even after ischemic injury.

But what is fueling the increased mitochondrial respiration in MCJ-KO mice? During regeneration, hepatocytes undergo a series of metabolic adaptations to meet the increased ATP demand. Phx-induced hypoglycemia is known to promote liver regeneration by triggering specific pro-regenerative signals and suppressing certain anti-regenerative signaling pathways (Huang et al. 2016). We confirm similar levels of hypoglycemia in MCJ WT and MCJ-KO mice after Phx, and by PET-CT scanning we can exclude the possibility of a more glycolytic phenotype in MCJ-KO mice. Importantly, we have identified that hepatic fatty acid oxidation provides the energy required for liver regeneration after major resection or ischemic injury. Therefore, silencing of MCJ represents a potential mechanism for enhancing mitochondrial activity to rapidly meet the energy demands of liver regeneration while avoiding the deleterious side effects of oxidative stress.

Liver regeneration is a complex process involving an inflammatory response (priming phase) followed by proliferation of liver cells to restore lost mass. ATP plays a crucial role as a signaling molecule in the extracellular space; in fact, purinergic signals regulate immune cell activation and subsequent cytokine production (Ishimaru et al. 2014). Kupffer cell-derived IL-6 trans signaling is not only critically involved in normal liver regeneration (Fazel Modares et al. 2019), but also plays an important protective role in chronic (Streetz et al. 2003) and acute liver diseases (Gao et al. 2020). A recent study associated higher preoperative serum levels of IL-6 and TNF with early liver graft regeneration after liver transplantation (Chae et al. 2018). We therefore hypothesized that increased ATP levels would accelerate Kupffer cell activation, allowing for a faster priming phase that promotes liver regeneration, reduces liver injury, and increases survival in MCJ-KO mice. Ishimaru et al. showed that ATP-stimulated Kupffer cells produced significantly higher IL-6 levels compared to non-stimulated cells (Ishimaru et al. 2014). We show similar results in macrophage-like RAW 264.7, BMMs and hepatic Kupffer cells in the presence of ATP, not only with IL-6 but also with TNF. In addition, ATP-stimulated MCJ-KO BMM and Kupffer cells have significantly higher levels of HB-EGF, an activator of the ERK1/2 pathway and a ligand for EGFR, which is considered a key factor in the progression of hepatocytes through the G1/S transition during regeneration (Mitchell et al. 2005). Interestingly, proliferation studies in Wt and MCJ-KO hepatocytes using Kupffer cell-derived conditioned media confirm increased activation of ERK1/2, STAT3, and EGFR signaling pathways (Fig. 6.3). *In vivo*,

significantly elevated levels of IL-6 and TNF as well as activation of STAT3 and EGFR are also observed in MCJ-KO mice after Phx, IRI and Phx under IRI, providing further evidence that increased ATP levels are the driving force enabling the accelerated regeneration and explaining the 12-hour gap between the regeneration peaks of Wt and MCJ-KO (S phase).

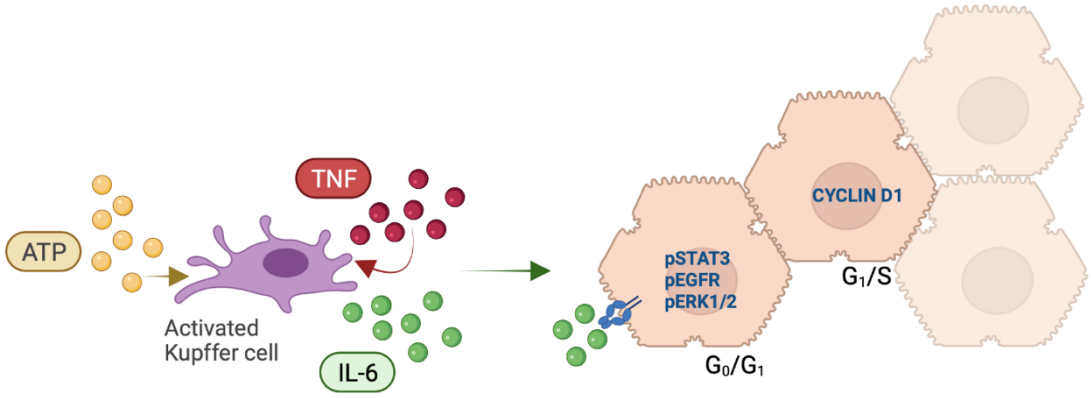

Figure 6.3 Extracellular ATP activates liver resident Kupffer cells and initiates the priming phase, promoting hepatocyte proliferation. (ATP=Adenosine triphosphate; pEGFR=phosphorylated epidermal growth factor receptor; pERK1/2=phosphorylated extracellular signal-regulated kinase ½; IL-6=Interleukin-6; STAT3=Signal transducer and activator of transcription-3; TNF=Tumor necrosis factor)

Moreover, LT faces a major organ shortage. Among the strategies to improve the donor pool, the use of extended-criteria livers has been proposed. Unfortunately, the use of these marginal organs increases the incidence of allograft dysfunction and post-reperfusion syndrome (Trapero-Marugán, Little, and Berenguer 2018; Younossi et al. 2021). Therefore, we decided to mimic steatotic and aging mouse models and study the effects of MCJ silencing on hepatic damage, liver regeneration and survival after Phx with IRI.

Recipients of organs from aged donors may have increased morbidity and mortality after transplantation due to increased susceptibility to IRI. Mitochondria in aged livers produce less ATP and more free radicals (Navarro and Boveris 2007), and since intracellular energy metabolism is considered a key mechanism in the ischemic phase, aging allografts respond poorly. Our data show a survival rate of 75% in 17-month-old *Mcj*-silenced mice subjected to Phx under IRI after silencing via a single tail vein 72 h before the procedure, compared with a survival rate of 25% in Wt mice. After 70% Phx in 15–17-month-old Wt mice, we observe improved liver regeneration and reduced liver steatosis with *Mcj* silencing, along with increased mitochondrial activity and ATP production. Thus,

silencing *Mcj* reduces susceptibility to ischemic damage in old livers by improving mitochondrial activity and ATP production.

Hepatic steatosis is a major risk factor for liver surgery, with postoperative mortality exceeding 14% after major liver resection compared with 2% in patients with non-fatty livers (Behrns et al. 1998). Steatosis is associated with impaired mitochondrial function and inadequate ATP production, causing an unfavorable necrotic form of cell death during periods of ischemia (Selzner et al. 2003). Our results show increased mitochondrial activity and increased ATP production exerting a protective effect in fatty livers and causing accelerated liver regeneration in Mcj-silenced mice fed HFHFD (15%) for 12 weeks compared with Wt mice. A simple tail vein injection 72 hours before surgery was able to overcome the impaired liver regeneration associated with hepatic steatosis.

Several siRNA-based therapeutics have been successfully tested in experimental transplantation models to reduce IRI. However, there are limitations to the *in vivo* use of RNAi in terms of delivery method, uptake, selectivity, and stability. Thijssen et al. hypothesized that machine perfusion preservation could be used as a platform for gene interference therapeutics and have shown positive results: administering siRNA in the perfusion solution allows for more efficient delivery, lower doses, is cost-saving, and has fewer side effects on other organs (Thjissen et al. 2019). As explained previously, ANRP-ECMO is becoming the standard procedure for solid organ transplantation in Spain. We propose a possible strategy for the use of siMCJ (Fig. 6.4): it could be administered at the beginning of ANRP-ECMO; once ECMO is interrupted for organ retrieval, siMCJ would also be included in the cold preservation fluid; and finally, the recipient would also receive siMCJ during recovery. In this way, especially for organs with extended criteria, the liver can recover before it reaches the recipient.

Overall, the silencing of *Mcj* may be a means to achieve the long-sought balance between the number of organs needed and the number of organs available for liver transplantation by restoring and maintaining mitochondrial activity and ATP levels, allowing the successful use of donor livers with expanded criteria.

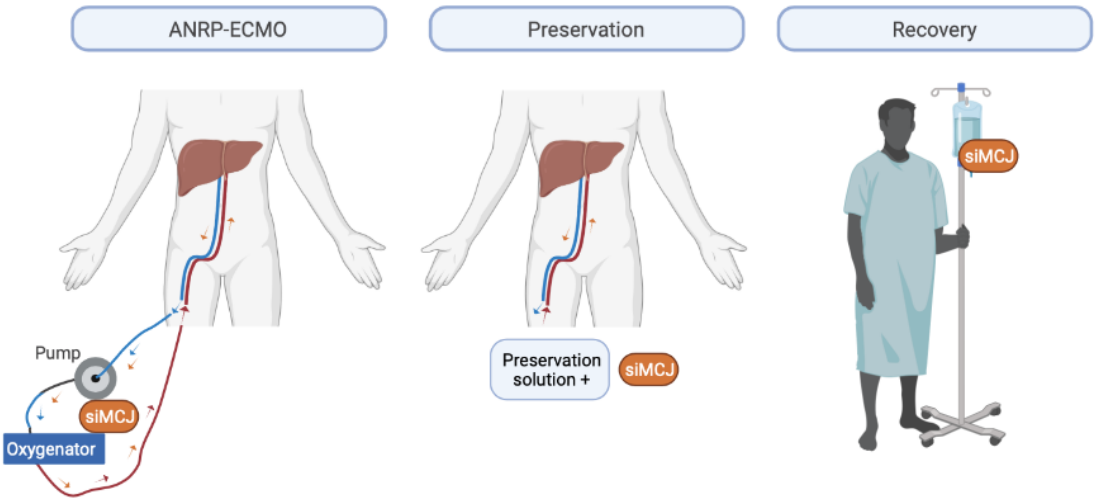

Figure 6.4 Proposal for siMCJ implementation during liver transplantation (ANRP-ECMO: Abdominal normothermic perfusion with extracorporeal membrane oxygenation; siMCJ=small interfering MCJ)

The present work highlights the implication of mitochondrial dysfunction in the development and progression of ALD as well as in impaired liver regeneration and increased susceptibility to ischemic injury, particularly in individuals with compromised metabolism. This is consistent with previous studies that underscore the importance of altered mitochondrial function in the pathophysiology of chronic liver disease and provides robust results that support targeting mitochondrial dysfunction through liver-specific *Mcj* silencing as a therapeutic approach to ameliorate liver injury and promote regeneration. Overexpression of MCJ in patients with advanced liver disease is evidence for this.

The search for targets with broad action has become the trademark of our group. Interestingly, MCJ shows therapeutic effect in more than one hallmark. First, liver-specific Mcj silencing alleviates mitochondrial dysfunction and significantly reduces oxidative stress in NAFLD, ALD, APAP-induced liver injury, cholestatic liver injury, and IRI (Barbier-Torres et al. 2017, 2020; Iruzubieta et al. 2021). Thereby, it enhances oxidation of FAs, which alleviates steatosis, increases ATP production, which reduces ischemic damage, activates priming phase and provides additional energy for liver regeneration, and overall reduces inflammation and hepatocellular injury. Thus, liver-specific silencing of Mcj ameliorates one of the earliest indicators and potential triggers of CLDs, preventing their progression.

The findings in Chapter 5.1 reinforce the need for targeted, specific therapeutic approaches. As treatments advance toward precision medicine, RNA-based therapies are gaining particular recognition. Recently, the first siRNA drug was approved by the FDA for clinical use, opening a new avenue for novel approaches with diverse clinical applications. However, as mentioned above, their application in vivo is still challenging. Although the addition of siMCJ in machine perfusion preservation fills the gap for transplantation, it is not as practical for other CLDs. In this sense, Barbier-Torres et al. have used nanoparticulate and GalNAc-formulated siRNA to efficiently target hepatic MCJ (Barbier-Torres et al. 2020). Briefly, the approach is based on the fact that only hepatocytes express the asialoglycoprotein receptor (ASGPR) that binds and clears circulating Gal-NAc molecules, laying the foundation for a direct, rapid, and already accessible therapeutic approach (Debacker et al. 2020). The knowledge that MCJ KO mice are healthy supports the minimal toxicity of Mcj silencing as a therapy. In addition, the use of GalNAc-formulated siRNA molecules has already been approved by the FDA, which could enable the transition from preclinical approaches to clinical trials.

Even if our results demonstrate the feasibility of targeting MCJ to alleviate liver damage and improve regeneration, further work in both preclinical and clinical trials is needed to demonstrate efficacy and, hopefully, reach patients.

7. CONCLUSIONS

7 CONCLUSIONS

Based on Hypothesis and Aims in Chapter 3, Results in Chapter 4 and the Discussion of those in Chapter 5, the following can be concluded:

1) MCJ is downregulated in clinical and preclinical models of early ALD and overexpressed in patients with advanced ALD
2) Whole body deficiency of MCJ exacerbates ALD *in vivo*
    a. Downregulation of the protein exacerbates systemic effects of alcohol
        i. Overactivation of intestinal macrophages triggers a proinflammatory cascade that alters gut microbiota, increases gut permeability and facilitates LPS translocation
        ii. Circulating LPS aggravates liver injury through increased *Cyp2e1* expression and oxidative stress
        iii. Circulating LPS impairs pancreatic function and MCJ-KO mice show poor glycemic control
        iv. Elevated blood glucose levels facilitate hepatic glucose entry, *de novo* lipogenesis of FAs and cause steatosis
    b. After alcohol abuse, MCJ-KO mice die due to hyperglycemia
3) Liver-specific *Mcj* silencing improves ALD *in vivo*
    a. Downregulation of the protein prevents steatosis
        i. Increased OXPHOS promotes fatty acid oxidation and restores NAD^+/NADH ratio
        ii. Restored NAD^+ increases SIRT1 deacetylase activity
        iii. SIRT1 inhibits mTORC1 activation and subsequent SREBP1 expression and *de novo* lipogenesis
    b. Downregulation of the protein reduces oxidative stress
    c. Alleviating steatosis and reducing oxidative stress prevents inflammation and hepatocellular damage
4) MCJ is overexpressed during liver regeneration and ischemia reperfusion injury in clinical and preclinical models
5) Targeted silencing of *Mcj* improves liver regeneration and reduces ischemic damage *in vivo*

   a. Downregulation of the protein improves mitochondrial respiration and increases ATP production
   b. Increased ATP production provides additional energy for liver regeneration and initiates the regenerative cascade
      i. Extracellular ATP activates liver resident Kupffer cells and subsequently the production of cytokines (TNF, IL-6) and growth factors (HB-EGF)
      ii. STAT3 and EGFR are then activated and facilitate the migration of CyclinD1 to the nucleus
      iii. Hepatocytes start rapidly proliferating
   c. Increased ATP production prevents ATP depletion characteristic of ischemic injury
   d. Overall liver injury is ameliorated
6) Targeted silencing of *Mcj* overcomes regenerative limitations and reduces susceptibility to ischemic injury in metabolically compromised preclinical models
   a. Downregulation of the protein improves mitochondrial bioenergetics, increases ATP production, attenuates steatosis, and promotes regeneration in steatotic mice
   b. Downregulation of the protein improves mitochondrial bioenergetics, increases ATP production, decreases oxidative stress, promotes regeneration and increases survival in aged mice

8. BIBLIOGRAPHY

8 BIBLIOGRAPHY

Abdelmegeed, Mohamed A, Atrayee Banerjee, Sehwan Jang, and Seong-Ho Yoo. 2013. "CYP2E1 Potentiates Binge Alcohol-Induced Gut Leakiness, Steatohepatitis and Apoptosis." *Free Radical Biology and Medicine* 65.

Abdulla, Dalya, Kerry B. Goralski, and Kenneth W. Renton. 2006. "The Regulation of Cytochrome P450 2E1 during LPS-Induced Inflammation in the Rat." *Toxicology and Applied Pharmacology* 216(1): 1–10.

Acín-Pérez, Rebeca et al. 2008. "Respiratory Active Mitochondrial Supercomplexes." *Mol Cell* 32(4): 529–39.

Alexandrino, Henrique et al. 2016. "Mitochondrial Bioenergetics and Posthepatectomy Liver Dysfunction." *European Journal of Clinical Investigation* 46(7): 627–35.

———. 2018. "Mitochondria in Liver Regeneration: Energy Metabolism and Posthepatectomy Liver Dysfunction." *Mitochondrial Biology and Experimental Therapeutics*: 127–52.

Ambade, Aditya et al. 2019. "Pharmacological Inhibition of CCR2/5 Signaling Prevents and Reverses Alcohol-Induced Liver Damage, Steatosis and Inflammation in Mice." *Hepatology* 69(3): 1105–21.

Andringa, Kelly K. et al. 2010. "Analysis of the Liver Mitochondrial Proteome in Response to Ethanol and S-Adenosylmethionine Treatments: Novel Molecular Targets of Disease and Hepatoprotection." *American Journal of Physiology - Gastrointestinal and Liver Physiology* 298(5): 732–45.

Arduini, Alessandro et al. 2012. "Mitochondrial Dysfunction in Cholestatic Liver Diseases." *Fron Biosci (Elite Ed)* 4(6): 2233–52.

Argemi, Josepmaria et al. 2019. "Defective HNF4alpha-Dependent Gene Expression as a Driver of Hepatocellular Failure in Alcoholic Hepatitis." *Nature Communications* 10(1).

Argemi, Josepmaria, Meritxell Ventura-Cots, Vikrant Rachakonda, and Ramon Bataller. 2021. "Alcoholic-Related Liver Disease: Pathogenesis, Management and Future Therapeutic Developments." *Revista Espanola de Enfermedades Digestivas* 112(11): 869–78.

Arsene, Diana, Omar Farooq, and Ramon Bataller. 2016. "New Therapeutic Targets in Alcoholic Hepatitis." *Hepatology Int* 10(4): 538–52.

Asrani, Sumeet K, Harshad Devarbhavi, John Eaton, and Patrick S Kamath. 2019. "Burden of Liver Diseases in the World." *Journal of Hepatology* 70(1): P151-171.

Avila, Matias A et al. 2021a. "Recent Advances in Alcohol-Related Liver Disease (ALD): Summary of a Gut Round Table Meeting." *Gut* 69(4): 764–80.

———. 2021b. "Summary of a Gut Round Table Meeting." 69(4): 764–80.

Bagy, Kornélia, Renato V Iozzo, and Ilona Kovalszky. 2012. "Decorin-TGFβ Axis in Hepatic Fibrosis and Cirrhosis." *J Histochem Cytochem* 60(4): 262–68.

Bajaj, Jasmohan S et al. 2017. "Fecal Microbiota Transplant Fromo a Rational Stool Donor Improves Hepatic Encephalopathy: A Randomized Clinical Trial." *Hepatology* 66(6): 1727–38.

Bala, Shashi et al. 2016. "The Pro-Inflammatory Effects of MiR-155 Promote Liver Fibrosis and Alcohol-Induced Steatohepatitis." *J Hepatol* 64(6): 1378–87. file:///C:/Users/Carla Carolina/Desktop/Artigos para acrescentar na qualificação/The impact of birth weight on cardiovascular disease risk in the.pdf.

Barbier-Torres, Lucía et al. 2017. "The Mitochondrial Negative Regulator MCJ Is a Therapeutic Target for Acetaminophen-Induced Liver Injury." *Nature Communications* 8(1).

———. 2020. "Silencing Hepatic MCJ Attenuates Non-Alcoholic Fatty Liver Disease (NAFLD) by Increasing Mitochondrial Fatty Acid Oxidation." *Nature Communications* 11(1): 1–15. http://dx.doi.org/10.1038/s41467-020-16991-2.

———. 2022. "Depletion of Mitochondrial Methionine Adenosyltransferase A1 Triggers Mitochondrial Dysfunction in Alcohol-Associated Liver Disease." *Nature Communications* 13(1): 1–17.

Bardallo, Raquel G. et al. 2021. "Role of Peg35, Mitochondrial Aldh2, and Glutathione in Cold Fatty Liver Graft Preservation: An Igl-2 Approach." *International Journal of Molecular Sciences* 22(10): 1–13.

———. 2022. "PEG35 and Glutathione Improve Mitochondrial Function and Reduce Oxidative Stress in Cold Fatty Liver Graft Preservation." *Antioxidants* 11(1).

Bass, Nathan M. et al. 2010. "Rifaximin Treatment in Hepatic Encephalopathy." *New England Journal of Medicine* 362(12): 1071–81.

Behrns, KE et al. 1998. "Hepatic Steatosis as a Potential Risk Factor for Major Hepatic Resection." *J Gastrointest Surg* 2(3): 292–98.

Benedé-Ubieto, Raquel et al. 2021. "An Experimental DUAL Model of Advanced Liver Damage." *Hepatology Communications* 5(6): 1051–68.

Bernal, William, and Julia Wendon. 2013. "Acute Liver Failure." *N Engl J Med* 369(26): 2525–34.

Bertola, Adeline et al. 2013. "Mouse Model of Chronic and Binge Ethanol Feeding (the NIAAA Model)." *Nature*

Protocols 8(3): 627–37. http://dx.doi.org/10.1038/nprot.2013.032.

Bhatti, Jasvinder Singh, Gurjit Kaur Bhatti, and P Hemachandra Reddy. 2017. "Mitochondrial Dysfunction and Oxidative Stress in Metabolic Disorders - A Step towards Mitochondria Based Therapeutic Strategies." *Biochimica et Biophysica Acta - Molecular Basis of Disease* 1863(5): 1066–77.

Bhushan, Bharat et al. 2014. "Pro-Regenerative Signaling after Acetaminophen-Induced Acute Liver Injury in Mice Identified Using a Novel Incremental Dose Model." *Am J Pathol* 184(11): 3013–25.

———. 2017. "Dual Role of Epidermal Growth Factor Receptor in Liver Injury and Regeneration after Acetaminophen Overdose in Mice." *Toxicol Sci* 155(2): 363–78.

Bhushan, Bharat, and Udayan Apte. 2019. "Liver Regeneration after Acetaminophen Hepatotoxicity: Mechanisms and Therapeutic Opportunities." *American Journal of Pathology* 189(4): 719–29. https://doi.org/10.1016/j.ajpath.2018.12.006.

Biberthaler, Peter et al. 2001. "Ischemia at 4°C: A Novel Mouse Model to Investigate the Effect of Hypothermia on Postiscnemic Hepatic Microcirculatory Injury." *Research in Experimental Medicine* 200(2): 93–105.

Biewald, J., R. Nilius, and J. Langner. 1998. "Occurrence of Acetaldehyde Protein Adducts Formed in Various Organs of Chronically Ethanol Fed Rats: An Immunohistochemical Study." *International journal of molecular medicine* 2(4): 389–96.

Bishehrashi, Faraz et al. 2017. "Alcohol and Gut-Derived Inflammation." *Alcohol Res* 38(2): 163–71.

Boteon, Yuri L. et al. 2017. "Mechanisms of Autophagy Activation in Endothelial Cell and Their Targeting during Normothermic Machine Liver Perfusion." *World Journal of Gastroenterology* 23(48): 8443–51.

Boutagy, Nabil E, Ryan P McMillan, Madlyn I Frisard, and Hulver W Matthew. 2016. "Metabolic Endotoxemia with Obesity: Is It Real and Is It Relevant?" *Biochimie* 124: 11–20.

Bradbury, Michael W. 2006. "Lipid Metabolism and Liver Inflammation. I. Hepatic Fatty Acid Uptake: Possible Role in Steatosis." *American Journal of Physiology - Gastrointestinal and Liver Physiology* 290(2): 194–98.

Bradford, Blair U., and Ivan Rusyn. 2005. "Swift Increase in Alcohol Metabolism (SIAM): Understanding the Phenomenon of Hypermetabolism in Liver." *Alcohol* 35(1): 13–17.

Brandon-Warner, Elizabeth, Laura W Schrum, C Maz Schmidt, and Iain H McKillop. 2012. "Rodent Models of Alcoholic Liver Disease: Of Mice and Men." *Alcohol* 46(8): 715–25.

Brinkmann, Anneliese, Norbert Katz, Dieter Sasse, and Kurt Jungermann. 1978. "Increase of the Gluconeogenic and Decrease of the Glycolytic Capacity of Rat Liver with a Change of the Metabolic Zonation after Partial Hepatectomy." *De Gruyter* 359(2): 1561–72.

Bujaldon, Esther et al. 2019. "Relevance of VEGFA in Rat Livers Subjected to Partial Hepatectomy under Ischemia-Reperfusion." *J Mol Med (Berl)* 97(9): 1299–1314.

Buraschi, Simone et al. 2010. "Decorin Antagonizes Met Receptor Activity and Down-Regulates {beta}-Catenin and Myc Levels." *J Biol Chem* 285(53): 42075–85.

Caldez, Matias J. et al. 2018. "Metabolic Remodeling during Liver Regeneration." *Developmental Cell* 47(4): 425-438.e5.

Callahan, Benjamin J et al. 2016. "DADA2: High-Resolution Sample Inference from Illumina Amplicon Data." *Nat Methods* 13(7): 581–83.

Campana, Lara, Hannah Esser, Meritxell Huch, and Stuart Forbes. 2021. "Liver Regeneration and Inflammation: From Fundamental Science to Clinical Applications." *Nature Reviews Molecular Cell Biology* 22(9): 608–24. http://dx.doi.org/10.1038/s41580-021-00373-7.

Campbell, Christopher T., Jill E. Kolesar, and Brett A. Kaufman. 2012. "Mitochondrial Transcription Factor A Regulates Mitochondrial Transcription Initiation, DNA Packaging, and Genome Copy Number." *Biochimica et Biophysica Acta - Gene Regulatory Mechanisms* 1819(9–10): 921–29. http://dx.doi.org/10.1016/j.bbagrm.2012.03.002.

Cani, Patrice D. 2018. "Human Gut Microbiome: Hopes, Threats and Promises." *Gut* 67(9): 1716–25.

Caporaso, J Gregory et al. 2011. "QIIME Allows Analysis of High-Throughput Community Sequencing Data." *Nat Methods* 7(5): 335–36.

Caron, Alexandre, Denis Richard, and Mathieu Laplante. 2015. "The Roles of MTOR Complexes in Lipid Metabolism." *Annual Review of Nutrition* 35(1): 321–48.

Carr, Rotonya M., and Andrea E. Reid. 2015. "FXR Agonists as Therapeutic Agents for Non-Alcoholic Fatty Liver Disease." *Current Atherosclerosis Reports* 17(4).

Cauley, Ryan P, Khashayar Vakili, and Nora Fullington. 2016. "Deceased Donor Split Liver Transplantation in Japan -Report on the Meeting-." *Japanese Journal of Transplantation* 51(6): 464–69.

Cederbaum, Arthur I. 2012. "Alcohol Metabolism." *Clinics in Liver Disease* 16(4): 667–85.

Celli, Romulo, and Xuchen Zhang. 2014. "Review Article Pathology of Alcoholic Liver Disease." *Journal of Clinical and Translational Hepatology* 2: 103–9.

Ceni, Elisabetta, Tommaso Mello, and Andrea Galli. 2014. "Pathogenesis of Alcoholic Liver Disease: Role of

Oxidative Metabolism." *World Journal of Gastroenterology* 20(47): 17756–72.

Chae, Min Suk et al. 2018. "Serum Interleukin-6 and Tumor Necrosis Factor-α Are Associated with Early Graft Regeneration after Living Donor Liver Transplantation." *PLoS ONE* 13(4): 1–13.

Champagne, Devin P. et al. 2016. "Fine-Tuning of CD8 T Cell Mitochondrial Respiration by MCJ/ DnaJC15 Dictates Protection to Influenza Virus." *Immunity* 44(6): 1299–1311.

Chandramouleeswaran, Prasanna M. et al. 2020. "Autophagy Mitigates Ethanol-Induced Mitochondrial Dysfunction and Oxidative Stress in Esophageal Keratinocytes." *PLoS ONE* 15(9 September 2020): 1–29. http://dx.doi.org/10.1371/journal.pone.0239625.

Chang, Binxia et al. 2015. "Short- or Long-Term High Fat Diet Feeding plus Acute Ethanol Binge Synergistically Induce Acute Liver Injury in Mice: An Important Role for CXCL1." *Hepatology* 62(4): 1070–85.

Chedid, A. et al. 1986. "Significance of Megamitochondria in Alcoholic Liver Disease." *Gastroenterology* 90(6): 1858–64.

Cheemerla, Shantan, and Maya Balakrishnan. 2021. "Global Epidemiology of Chronic Liver Disease." *Clinical Liver Disease* 17(5): 365–70.

Chen, Hanqing et al. 2018a. "DEPTOR Suppresses Lipogenesis and Ameliorates Hepatic Steatosis and Acute-on-Chronic Liver Injury in Alcoholic Liver Disease." *Hepatology* 68(2): 496–514.

———. 2018b. "DEPTOR Suppresses Lipogenesis and Ameliorates Hepatic Steatosis and Acute-on-Chronic Liver Injury in Alcoholic Liver Disease." *Hepatology* 68(2): 496–514.

Chen, Lixin et al. 2004. "Impaired Liver Regeneration in Mice Lacking Methionine Adenosyltransferase 1A." *FASEB J* 18(7): 914–16.

Choi, Eun Kyung et al. 2020. "Role of Remote Ischemic Preconditioning in Hepatic Ischemic Reperfusion Injury." *Dose-Response* 18(3): 1–6.

Choi, Ja Sung, Hyun Aae Ryu, Sae Hee Cheon, and Sung Whan Kim. 2019. "Human Adipose Derived Stem Cells Exhibit Enhanced Liver Regeneration in Acute Liver Injury by Controlled Releasing Hepatocyte Growth Factor." *Cellular Physiology and Biochemistry* 52(4): 935–50.

Chu, Michael J J, Anna J Dare, Anthony R J Phillips, and Adam S J R Bartlett. 2015. "Donor Hepatic Steatosis and Outcome After Liver Transplantation: A Systematic Review." *J Gastrointest Surg* 19(9): 1713–24.

Clemens, Dahn L., and Katrina J. Mahan. 2010. "Alcoholic Pancreatitis: Lessons from the Liver." *World Journal of Gastroenterology* 16(11): 1314–20.

Cornell, R P. 1985. "Gut-Derived Endotoxin Elicits Hepatotrophic Factor Secretion for Liver Regeneration." *Am J Physiol* 249(5): R551-562.

Crabb, D W. 1995. "Ethanol Oxidizing Enzymes: Roles in Alcohol Metabolism and Alcoholic Liver Disease." *Prog Liver Dis* 13: 151–72.

Cruise, J L et al. 1987. "Alpha 1-Adrenergic Effects and Liver Regeneration." *Hepatology* 7(6): 1189–94.

Czigany, Zoltan et al. 2020. "Ischemia-Reperfusion Injury in Marginal Liver Grafts and the Role of Hypothermic Machine Perfusion: Molecular Mechanisms and Clinical Implications." *Journal of Clinical Medicine* 9(3).

———. 2022. "What Is Hot and New in Basic and Translational Science in Liver Transplantation in 2020–2021?—Report of the Basic and Translational Research Committee of the International Liver Transplantation Society." *Transplantation* 106(2): 227–33.

D'Souza El-Guindy, Nympha B. et al. 2010. "Laboratory Models Available to Study Alcohol-Induced Organ Damage and Immune Variations: Choosing the Appropriate Model." *Alcoholism: Clinical and Experimental Research* 34(9): 1489–1511.

Day, Christopher P., and Oliver F.W. James. 1998. "Hepatic Steatosis: Innocent Bystander or Guilty Party?" *Hepatology* 27(6): 1463–66.

Debacker, Alexandre J. et al. 2020. "Delivery of Oligonucleotides to the Liver with GalNAc: From Research to Registered Therapeutic Drug." *Molecular Therapy* 28(8): 1759–71. https://doi.org/10.1016/j.ymthe.2020.06.015.

Delire, Bénédicte, Peter Stärkel, and Isabelle Leclercq. 2015. "Animal Models for Fibrotic Liver Diseases: What We Have, What We Need, and What Is under Development." *Journal of Clinical and Translational Hepatology* 3(1): 53–66.

Demetriou, Achilles A. et al. 1988. "Transplantation of Microcarrier-attached Hepatocytes into 90% Partially Hepatectomized Rats." *Hepatology* 8(5): 1006–9.

Demetris, Anthony J. et al. 2006. "Pathophysiologic Observations and Histopathologic Recognition of the Portal Hyperperfusion or Small-for-Size Syndrome." *American Journal of Surgical Pathology* 30(8): 986–93.

Demirakca, Traute et al. 2011. "Effects of Alcoholism and Continued Abstinence on Brain Volumes in Both Genders." *Alcoholism: Clinical and Experimental Research* 35(9): 1678–85.

Detlefsen, Sönke, Bence Sipos, Bernd Feyerabend, and Günter Klöppel. 2006. "Fibrogenesis in Alcoholic Chronic Pancreatitis: The Role of Tissue Necrosis, Macrophages, Myofibroblasts and Cytokines." *Modern Pathology*

19(8): 1019–26.
Detre, Katherine M. et al. 1995. “Influence of Donor Age on Graft Survival after Liver Transplantation—United Network for Organ Sharing Registry.” *Liver Transplantation and Surgery* 1(5): 311–19.
Dicker, Daniel et al. 2018. “Global, Regional, and National Age-Sex-Specific Mortality and Life Expectancy, 1950-2017: A Systematic Analysis for the Global Burden of Disease Study 2017.” *The Lancet* 392(10159): 1684–1735.
Ding, Wen-Xing, and Xiao-Ming Yin. 2012. “Mitophagy: Mechanisms, Pathophysiological Roles, and Analysis.” *Biol Chem* 393(7): 547–64.
Duan, Yi et al. 2020. “HHS Public Access.” 575(7783): 505–11.
Dutkowski, Philipp et al. 2015. “First Comparison of Hypothermic Oxygenated Perfusion versus Static Cold Storage of Human Donation after Cardiac Death Liver Transplants.” *Annals of Surgery* 262(5): 764–71.
European Association for the Study of the Liver. 2017. “EASL Clinical Practice Guidelines: The Diagnosis and Management of Patients with Primary Biliary Cholangitis.” *J Hepatol* 67(1): 145–72.
Fairfield, Bradley, and Bernd Schnabl. 2021. “Gut Dysbiosis as a Driver in Alcohol-Induced Liver Injury.” *JHEP Reports* 3(2): 1–9.
Fan, Shicheng et al. 2022. “YAP-TEAD Mediates PPAR α–Induced Hepatomegaly and Liver Regeneration in Mice.” *Hepatology* 75(1): 74–88.
Farooq, M. Omar, and Ramon Bataller. 2016. “Pathogenesis and Management of Alcoholic Liver Disease.” *Digestive Diseases* 34(4): 347–55.
Fausto, N. 2000. “Liver Regeneration.” *J Hepatol* 32(1 Suppl): 19–31.
Fausto, Nelson, Jean S. Campbell, and Kimberly J. Riehle. 2006. “Liver Regeneration.” *Hepatology* 43(2 SUPPL. 1): 45–53.
Fazel Modares, Nastaran et al. 2019. “IL-6 Trans-Signaling Controls Liver Regeneration After Partial Hepatectomy.” *Hepatology* 70(6): 2075–91.
Fernandes, Alexandra I et al. 2015. “Functional Hepatocellular Regeneration in Elderly Patients Undergoing Hepatectomy.” *Liver International* 35(4): 1116–23.
Fernandes, Andrew D et al. 2014. “Unifying the Analysis of High-Throughput Sequencing Datasets: Characterizing RNA-Seq, 16S RRNA Gene Sequencing and Selective Growth Experiments by Compositional Data Analysis.” *Microbiome* 2.
Fernández-Cabezudo, Maria J et al. 2016. “Deficiency of Mitochondrial Modulator MCJ Promotes Chemoresistance in Breast Cancer.” *JCI insight* 1(7).
Fiel, M. Isabel, Kemal Deniz, Ferhan Elmali, and Thomas D. Schiano. 2011. “Increasing Hepatic Arteriole Wall Thickness and Decreased Luminal Diameter Occur with Increasing Age in Normal Livers.” *Journal of Hepatology* 55(3): 582–86. http://dx.doi.org/10.1016/j.jhep.2010.12.018.
Foley, David P. et al. 2011. “Biliary Complications After Liver Transplantation From Donation After Cardiac Death Donors.” *Annals of Surgery* 253(4): 817–25.
Forbes, Stuart J., and Philip N. Newsome. 2016. “Liver Regeneration-Mechanisms and Models to Clinical Application.” *Nature Reviews Gastroenterology and Hepatology* 13(8): 473–85.
Freeman, Thomas L. et al. 2005. “Recent Advances in Alcohol-Induced Adduct Formation.” *Alcoholism: Clinical and Experimental Research* 29(7): 1310–16.
Friedl, Peter, and Darren Gilmour. 2009. “Collective Clel Migration in Morphogenesis, Regeneration and Cancer.” *Nature Reviews Molecular Cell Biology* 10: 445–57.
Friedman, Jonathan R., and Jodi Nunnari. 2014. “Mitochondrial Form and Function.” *Nature* 505(7483): 335–43.
Friedman, Scott L. 2008a. “Hepatic Stellate Cells: Protean, Multifunctional, and Enigmatic Cells of the Liver.” *Physiological Reviews* 88(1): 125–72.
———. 2008b. “Mechanisms of Hepatic Fibrogenesis.” *Gastroenterology* 134(6): 1655–69.
Friedman, Scott L, Brent A Neuschwander-Tetri, Mary Rinella, and Arun J Sanyal. 2018. “Mechanisms of NAFLD Development and Therapeutic Strategies.” *Nat Med* 24(7): 908–22.
Furrer, Katarzyna et al. 2011. “Serotonin Reverts Age-Related Capillarization and Failure of Regeneration in the Liver through a VEGF-Dependent Pathway.” *Proceedings of the National Academy of Sciences of the United States of America* 108(7): 2945–50.
Gäbele, Erwin et al. 2011. “A New Model of Interactive Effects of Alcohol and High-Fat Diet on Hepatic Fibrosis.” *Alcoholism: Clinical and Experimental Research* 35(7): 1361–67.
Gao, Bin, and Ramon Bataller. 2011. “Alcoholic Liver Disease: Pathogenesis and New Therapeutic Targets.” *Gastroenterology* 141(5): 1572–85.
Gao, Rachel Y et al. 2020. “Hypoxia-Inducible Factor-2α Reprograms Liver Macrophages to Protect Against Acute Liver Injury Through the Production of Interleukin-6.” *Hepatology* 71(6): 2105–17.
Gazit, Vered et al. 2010. “Liver Regeneration Is Impaired in Lipodystrophic Fatty Liver Dystrophy Mice.” *Hepatology*

52(6): 2109–17.
Giddings, Emily L. et al. 2021. “Mitochondrial ATP Fuels ABC Transporter-Mediated Drug Efflux in Cancer Chemoresistance.” *Nature Communications* 12(1): 1–19.
Gitto, Stefano et al. 2016. “Multidisciplinary View of Alcohol Use Disorder: From a Psychiatric Illness to a Major Liver Disease.” *Biomolecules* 6(1): 1–12.
Gkretsi, Vasiliki et al. 2008. “Liver-Specific Ablation of Integrin-Linked Kinase in Mice Results in Abnormal Histology, Enhanced Cell Proliferation, and Hepatomegaly.” *Hepatology* 48(6): 1932–41.
Gloor, Gregory B, Jean M Macklaim, Vera Pawlosky-Glahn, and Juan J Egozcue. 2017. “Microbiome Datasets Are Compositional: And This Is Not Optional.” *Frontiers in Microbiology*.
Goikoetxea-Usandizaga, Naroa et al. 2022. “Mitochondrial Bioenergetics Boost Macrophage Activation, Promoting Liver Regeneration in Metabolically Compromised Animals.” *Hepatology* 75(3): 550–66.
Goldberg, D S et al. 2014. “Superior Survival Using Living Donors and Donor-Recipient Matching Using a Novel Living Donor Risk Index.” *Hepatology* 60(5): 1717–26.
Gomes, Júnia Maria Geraldo, Jorge de Assis Costa, and Rita de Cássia Gonçalves Alfenas. 2017. “Metabolic Endotoxemia and Diabetes Mellitus: A Systematic Review.” *Metabolism: Clinical and Experimental* 68: 133–44. http://dx.doi.org/10.1016/j.metabol.2016.12.009.
Gonzales, Emmanuel et al. 2013. “ATP Release after Partial Hepatectomy Regulates Liver Regeneration in the Rat.” *J Hepatol* 52(1): 54–62.
González-Reimers, Emilio et al. 2014. “Alcoholism: A Systemic Proinflammatory Condition.” *World Journal of Gastroenterology* 20(40): 14660–71.
Gottlieb, Roberta A, and Asa B Gustafsson. 2011. “Mitochondrial Turnover in the Heart.” *Biochimica et Biophysica Acta (BBA)-Molecular Cell Researh* 1813(7): 1295–1301.
Gracia-Sancho, Jordi, Araní Casillas-Ramírez, and Carmen Peralta. 2015. “Molecular Pathways in Protecting the Liver from Ischaemia/Reperfusion Injury: A 2015 Update.” *Clinical Science* 129(4): 345–62.
Gulbins, Erich, Stephan Dreschers, and Jurgen Bock. 2003. “Role of Mitochondria in Apoptosis.” *Exp Physiol* 88(1): 85–90.
Hai, Hao-Han, Phoebe Aw, Thomas Zheng Jie Teng, and Vishal G Shelat. 2021. “Perioperative Steroid Administration Reduces Overall Complications in Patients Undergoing Liver Resection: A Meta-Analysis.” *World Journal of Gastrointestinal Surgery* 13(9): 1079–94.
Hardardottir, I, W Doerrler, KR Feingold, and C Grunfeld. 1992. “Cytokines Stimulate Lipolysis and Decrease Lipoprotein Lipase Activity in Cultured Fat Cells by a Prostagaldin Independent Mechanism.” *Biochem Biophys Res Commun* 186(1): 237–43.
Hasumura, Yasushi, Rolf Teschke, and Charles S. Lieber. 1975. “AcetaldehydeOxidationbyHepaticMitochondria: DecreaseAfterChronicEthanolConsumption.” *Science* 189(August): 727–29.
Hatle, Ketki M. et al. 2007. “Methylation-Controlled J Protein Promotes c-Jun Degradation To Prevent ABCB1 Transporter Expression.” *Mol Cell Biol* 27(8): 2952–66.
———. 2013. “MCJ/DnaJC15, an Endogenous Mitochondrial Repressor of the Respiratory Chain That Controls Metabolic Alterations.” *Molecular and Cellular Biology* 33(11): 2302–14.
He, Jinhan, Jung Hoon Lee, Maria Febbraio, and Wen Xie. 2011. “The Emerging Roles of Fatty Acid Translocase/CD36 and the Aryl Hydrocarbon Receptor in Fatty Liver Disease.” *Experimental Biology and Medicine* 236(10): 1116–21.
von Heesen, Maximilian et al. 2015. “Preconditioning by Cilostazol Protects against Cold Hepatic Ischemia-Reperfusion Injury.” *Annals of Transplantation* 20: 160–68.
Hessheimer, Amelia J. et al. 2022. “Abdominal Normothermic Regional Perfusion in Controlled Donation after Circulatory Determination of Death Liver Transplantation: Outcomes and Risk Factors for Graft Loss.” *American Journal of Transplantation* 22(4): 1169–81.
Hessheimer, Amelia J et al. 2018. “Normothermic Regional Perfusion vs. Super-Rapid Recovery in Controlled Donation after Circulatory Death Liver Transplantation.” *J Hepatol* 70(4): 658–65.
Heymann, Helen M., Adriana M. Gardner, and Eric R. Gross. 2018. “Aldehyde-Induced DNA and Protein Adducts as Biomarker Tools for Alcohol Use Disorder.” *Trends in Molecular Medicine* 24(2): 144–55. http://dx.doi.org/10.1016/j.molmed.2017.12.003.
Hide, Diana et al. 2016. “Effects of Warm Ischemia and Reperfusion on the Liver Microcirculatory Phenotype of Rats: Underlying Mechanisms and Pharmacological Therapy.” *Scientific Reports* 6(February): 1–12. http://dx.doi.org/10.1038/srep22107.
Higgins, G M, and R M Anderson. 1931. “Experimental Pathology of the Liver I. Restoration of the Liver of the White Rat Following Partial Surgicla Removal.” *Arch Pathol Lab Med* 12: 186–202.
Hirao, Hirofumi, Kojiro Nakamura, and Jerzy W. Kupiec-Weglinski. 2022. “Liver Ischaemia–Reperfusion Injury: A New Understanding of the Role of Innate Immunity.” *Nature Reviews Gastroenterology and Hepatology* 19(4):

239–56.
Hu, Chenxia, Zhongwen Wu, and Lanjuan Li. 2020. “Mesenchymal Stromal Cells Promote Liver Regeneration through Regulation of Immune Cells.” *International Journal of Biological Sciences* 16(5): 893–903.
Hu, Chenxia, Lingfei Zhao, Fen Zhang, and Lanjuan Li. 2021. “Melatonin and Its Protective Role in Attenuating Warm or Cold Hepatic Ischaemia/Reperfusion Injury.” *Cell Proliferation* 54(4): 1–11.
Hu, Huili et al. 2018. “Long-Term Expansion of Functional Mouse and Human Hepatocytes as 3D Organoids.” *Cell* 175(6): 1591-1606.e19.
Hua, Renyi et al. 2020. “CCR2 Mediates the Adverse Effects of LPS in the Pregnant Mouse.” *Biology of Reproduction* 102(2): 445–55.
Huang, Jiansheng et al. 2016. “Postponing the Hypoglycemic Response to Partial Hepatectomy Delays Mouse Liver Regeneration.” *American Journal of Pathology* 186(3): 587–99. http://dx.doi.org/10.1016/j.ajpath.2015.10.027.
Huang, Jiansheng, and David A. Rudnick. 2014. “Elucidating the Metabolic Regulation of Liver Regeneration.” *American Journal of Pathology* 184(2): 309–21. http://dx.doi.org/10.1016/j.ajpath.2013.04.034.
Huang, Wendong et al. 2006. “Nuclear Receptor-Dependent Bile Acid Signaling Is Required for Normal Liver Regeneration.” *Science* 312(5771): 233–36.
Huprikar, S. et al. 2015. “Solid Organ Transplantation from Hepatitis B Virus-Positive Donors: Consensus Guidelines for Recipient Management.” *American Journal of Transplantation* 15(5): 1162–72.
Iruzubieta, Paula et al. 2021. “Boosting Mitochondria Activity by Silencing MCJ Overcomes Cholestasis-Induced Liver Injury.” *JHEP Reports* 3(3).
Isayama, Fuyumi et al. 2006. “LPS Signaling Enhances Hepatic Fibrogenesis Caused by Experimental Cholestasis in Mice.” *Am J Physiol Gastrointest Liver Physiol* 290(6): G1318-1328.
Ishak, Kamal G., Hyman J. Zimmerman, and Mukunda B. Ray. 1991. “Alcoholic Liver Disease: Pathologic, Pathogenetic and Clinical Aspects.” *Alcoholism: Clinical and Experimental Research* 15(1): 45–66.
Ishimaru, Makiko et al. 2014. “Purinergic Signaling via P2Y Receptors Up-Mediates IL-6 Production by Liver Macrophages/Kupffer Cells.” *Journal of Toxicological Sciences* 39(3): 413–23.
Ivanics, Tommy, Phillipe Abreu, Eleonora De Martin, and Gonzalo Sapisochin. 2021. “Changing Trends in Liver Transplantation: Challenges and Solutions.” *Transplantation* 105(4): 743–56.
Jackson, Dakota N, and Arianne L Theiss. 2020. “Gut Bacteria Signaling to Mitochondria in Intestinal Inflammation and Cancer.” *Gut Microbes* 11(3): 285–304.
Jaeschke, H. 1998. “Mechanisms of Reperfusion Injury after Warm Ischemia of the Liver.” *J Hepatobiliary Pancreat Surg* 5(4): 402–8.
Jassem, W et al. 2019. “Normothermic Machine Perfusion (NMP) Inhibits Proinflammatory Responses in the Liver and Promotes Regeneration.” *Hepatology* 70: 682–95.
Ji, Haofeng et al. 2014. “T-Cell Immunoglobulin and Mucin Domain 4 (TIM-4) Signaling in Innate Immune-Mediated Liver Ischemia-Reperfusion Injury.” *Hepatology* 60(6): 2052–64.
Ji, Ru et al. 2012. “The Differentiation of MSCs into Functional Hepatocyte-like Cells in a Liver Biomatrix Scaffold and Their Transplantation into Liver-Fibrotic Mice.” *Biomaterials* 33(35): 8995–9008.
Jian, Yanchao et al. 2020. “Alcohol Metabolizing Enzymes, Microsomal Ethanol Oxidizing System, Cytochrome P450 2E1, Catalase, and Aldehyde Dehydrogenase in Alcohol-Associated Liver Disease.” *Biomedicines* 8(50): 1–16.
Jung, Kyeo Woon et al. 2020. “Effect of Remote Ischemic Preconditioning Conducted in Living Liver Donors on Postoperative Liver Function in Donors and Recipients Following Liver Transplantation: A Randomized Clinical Trial.” *Annals of Surgery* 271(4): 646–53.
Kageyama, Shoichi et al. 2014. “Graft Reconditioning with Nitric Oxide Gas in Rat Liver Transplantation from Cardiac Death Donors.” *Transplantation* 97(6): 618–25.
Kaplowitz, Neil, and Cheng Ji. 2006. “Unfolding New Mechanisms of Alcoholic Liver Disease in the Endoplasmic Reticulum.” *Journal of Gastroenterology and Hepatology (Australia)* 21(SUPPL. 3): 10–12.
Katoh, Kazutaka, and Daron M Standley. 2013. “MAFFT Multiple Sequence Alignment Software Version 7: Improvements in Performance and Usability.” *Molecular Biology and Evolution* 30(4): 772–80.
Kharbanda, Kusum K. et al. 2009. “Betaine Administration Corrects Ethanol-Induced Defective VLDL Secretion.” *Molecular and Cellular Biochemistry* 327(1–2): 75–78.
Klec, Christiane et al. 2019. “Calcium Signaling in SS-Cell Physiology and Pathology: A Revisit.” *Int J Mol Sci* 20(24): 6110.
Klingensmith, J S, and H M Mehendale. 1982. “Chlordecone-Induced Fat Depletion in the Male Rat.” *J Toxicol Environ Health* 10(1): 121–29.
Koh, Won Uk et al. 2019. “Remote Ischemic Preconditioning and Diazoxide Protect from Hepatic Ischemic Reperfusion Injury by Inhibiting HMGB1-Induced TLR4/MyD88/NF-KB Signaling.” *International Journal of Molecular Sciences* 20(23).
Kong, Ling Zu et al. 2019. “Pathogenesis, Early Diagnosis, and Therapeutic Management of Alcoholic Liver Disease.”

International Journal of Molecular Sciences 20(11).

Kotsch, Katja et al. 2008. "Methylprednisolone Therapy in Deceased Donors Reduces Inflammation in the Donor Liver and Improves Outcome after Liver Transplantation a Prospective Randomized Controlled Trial." *Annals of Surgery* 248(6): 1042–49.

Kwong, A. J. et al. 2021. "OPTN/SRTR 2019 Annual Data Report: Liver." *American Journal of Transplantation* 21(S2): 208–315.

Lamas-Paz, Arantza et al. 2018. "Alcoholic Liver Disease: Utility of Animal Models." *World Journal of Gastroenterology* 24(45): 5063–75.

Laplante, Mathieu, and David M Sabatini. 2009. "An Emerging Role of MTOR in Lipid Biosynthesis." *Curr Biol* 19(22): R1046-1052.

Lassenius, Mariann I. et al. 2011. "Bacterial Endotoxin Activity in Human Serum Is Associated with Dyslipidemia, Insulin Resistance, Obesity, and Chronic Inflammation." *Diabetes Care* 34(8): 1809–15.

Lawler, Joseph F. et al. 1998. "Tumor Necrosis Factor-α Stimulates the Maturation of Sterol Regulatory Element Binding Protein-1 in Human Hepatocytes through the Action of Neutral Sphingomyelinase." *Journal of Biological Chemistry* 273(9): 5053–59.

Lazaro, Raul et al. 2015. "Osteopontin Deficiency Does Not Prevent but Promotes Alcoholic Neutrophilic Hepatitis in Mice." *Hepatology* 61(1): 129–40. https://www.ncbi.nlm.nih.gov/pmc/articles/PMC3624763/pdf/nihms412728.pdf.

Lee, Jun-hee et al. 2020. "Mitochondrial Double-Stranded RNA in Exosome Promotes Interleukin-17 Production through Toll-like Receptor 3 in Alcoholic Liver Injury." *Hepatology* 72(2): 609–25.

Lee, Seong Min et al. 2021. "Effect of Mesenchymal Stem Cell in Liver Regeneration and Clinical Applications." *Hepatoma Research* 7.

Lee, Way S, and Ronald J Sokol. 2007. "Liver Disease in Mitochondrial Disorders." *Seminars in Liver Disease* 27(3): 259–73.

Lemasters, John J., and Ekhson Holmuhamedov. 2006. "Voltage-Dependent Anion Channel (VDAC) as Mitochondrial Governator - Thinking Outside the Box." *Biochimica et Biophysica Acta - Molecular Basis of Disease* 1762(2): 181–90.

Levine, Harris, and Morgan. 2000. "Energy Expenditure in Chronic Alcohol Abuse." *European Journal of Clinical Investigation* 30(9): 779–86.

Li, Yu et al. 2011. "Hepatic Overexpression of SIRT1 in Mice Attenuates Endoplasmic Reticulum Stress and Insulin Resistance in the Liver." *FASEB J* 25(5): 1664–79.

Lieber, C. S. 1988. "Metabolic Effects of Acetaldehyde." *Biochemical Society Transactions* 16(3): 241–47.

Lieber, Charles S. 1994. "Alcohol and the Liver: 1994 Update." *Gastroenterology* 106(4): 1085–1105.

———. 1997. "Cytochrome P-4502E1: Its Physiological and Pathological Role." *Physiological Reviews* 77(2): 517–44.

———. 2001. "Alcohol: Its Metabolism and Interaction with Nutrients." *Handbook of Nutrition and Food*: 915–40.

———. 2004. "Alcoholic Fatty Liver: Its Pathogenesis and Mechanism of Progression to Inflammation and Fibrosis." *Alcohol* 34(1): 9–19.

Lieber, Charles S., Maria A. Leo, Xiaolei Wang, and Leonore M. DeCarli. 2008. "Effect of Chronic Alcohol Consumption on Hepatic SIRT1 and PGC-1α in Rats." *Biochemical and Biophysical Research Communications* 370(1): 44–48.

Lin, Fan et al. 2021. 45 Artificial Organs *Hypothermic Oxygenated Perfusion with Defatting Cocktail Further Improves Steatotic Liver Grafts in a Transplantation Rat Model*.

Lin, Jie et al. 2020. "Protective Effects of Ischemic Preconditioning Protocols on Ischemia-Reperfusion Injury in Rat Liver." *Journal of Investigative Surgery* 33(9): 876–83. https://doi.org/10.1080/08941939.2018.1556753.

Liu, Raymond, and David C. Chan. 2015. "The Mitochondrial Fssion Receptor Mff Selectively Recruits Oligomerized Drp1." *Molecular Biology of the Cell* 26(24): 4466–77.

Llopis, M. et al. 2016. "Intestinal Microbiota Contributes to Individual Susceptibility to Alcoholic Liver Disease." *Gut* 65(5): 830–39.

Locasale, Jason W, and Lewis C Cantley. 2011. "Metabolic Flux and the Regulation of Mammalian Cell Growth." *Cell Metab* 14(4): 443–51.

Locher, Kaspar P. 2016. "Mechanistic Diversity in ATP-Binding Cassette (ABC) Transporters." *Nat Struct Mol Biol* 23(6): 487–93.

Louvet, Alexandre, and Philippe Mathurin. 2015. "Alcoholic Liver Disease: Mechanisms of Injury and Targeted Treatment." *Nature Reviews Gastroenterology and Hepatology* 12(4): 231–42.

Lu, Yongke, and Arthur I. Cederbaum. 2008. "CYP2E1 and Oxidative Liver Injury by Alcohol." *Free Radical Biology and Medicine* 44(5): 723–38.

———. 2010. "CYP2E1 Potentiation of LPS and TNFα-Induced Hepatotoxicity by Mechanisms Involving Enhanced

Oxidative and Nitrosative Stress, Activation of MAP Kinases, and Mitochondrial Dysfunction." *Genes and Nutrition* 5(2): 149–67.

Luedde, Tom, Neil Kaplowitz, and Robert F Schwabe. 2014. "Cell Death and Cell Death Responses in Liver Disease: Mechanisms and Clinical Relevance." *Gastroenterology* 147(4): 765–83.

Ma, Zhiqiang et al. 2017. "Melatonin and Mitochondrial Function during Ischemia/Reperfusion Injury." *Cellular and Molecular Life Sciences* 74(21): 3989–98.

MacDonald, Richad A. 1961. "Autoradiographic Study Using Tritiated Thymidine in Normal, Cirrhotic, and Partially Hepatectomized Rats." *Arch Intern Med* 107(3): 335–43.

Magdaleno, Fernando, Chuck C. Blajszczak, and Natalia Nieto. 2017. "Key Events Participating in the Pathogenesis of Alcoholic Liver Disease." *Biomolecules* 7(1).

Magoč, Tanja, and Steven L Salzberg. 2011. "FLASH: Fast Length Adjustment of Short Reads to Improve Genome Assemblies." *Bioinformatics* 27(11): 2957–63.

Malnick, Stephen, and Yaakov Maor. 2020. "The Interplay between Alcoholic Liver Disease, Obesity, and the Metabolic Syndrome." *Visceral Medicine* 36(3): 198–205.

Mansouri, Abdellah, Charles-Henry Gattolliat, and Tarik Asselah. 2018. "Mitochondrial Dysfunction and Signaling in Chronic Liver Diseases." *Gastroenterology* 155(3): 629–47.

Mao, Shennen A, Jaime M Glorioso, and Scott L Nyberg. 2014. "Liver Regeneration." *Transl Res* 163(4): 352–62.

Mao, Xin Li et al. 2022. "Novel Targets and Therapeutic Strategies to Protect Against Hepatic Ischemia Reperfusion Injury." *Frontiers in Medicine* 8(January): 1–15.

Marchesini, Giulio et al. 2016. "EASL-EASD-EASO Clinical Practice Guidelines for the Management of Non-Alcoholic Fatty Liver Disease." *Journal of Hepatology* 64(6): 1388–1402. http://dx.doi.org/10.1016/j.jhep.2015.11.004.

Martín, F et al. 1999. "Mechanisms of Glucose Hypersensitivity in Beta-Cells from Normoglycemic, Partially Pancreatectomized Mice." *American Diabetes Association* 48(10): 1954–61.

Marubashi, Shigeru et al. 2004. "Effect of Portal Hemodynamics on Liver Regeneration Studied in a Novel Portohepatic Shunt Rat Model." *Surgery* 136(5): 1028–37.

Mathurin, P et al. 2011. "Early Liver Transplantation for Severe Alcoholic Hepatitis." *The New England Journal of Medicina* 365(19): 1790–1800.

Mathurin, Philippe, and Ramon Bataller. 2015. "Trends in the Management and Burden of Alcoholic Liver Disease." *Journal of Hepatology* 62(1): S38–46.

Mathurin, Philippe, and Michael R. Lucey. 2020. "Liver Transplantation in Patients with Alcohol-Related Liver Disease: Current Status and Future Directions." *The Lancet Gastroenterology and Hepatology* 5(5): 507–14. http://dx.doi.org/10.1016/S2468-1253(19)30451-0.

McDonald, Braedon et al. 2017. "Platelets and Neutrophil Extracellular Traps Collaborate to Promote Intravascular Coagulation during Sepsis in Mice." *Blood* 129(10): 1357–67.

Mehta, Ashish J., and David M. Guidot. 2012. "Alcohol Abuse, the Alveolar Macrophage and Pneumonia." *American Journal of the Medical Sciences* 343(3): 244–47.

de Meijer, Vincent Erwin, Masato Fujiyoshi, and Robert Jack Porte. 2019. "Ex Situ Machine Perfusion Strategies in Liver Transplantation." *Journal of Hepatology* 70(1): 203–5.

Mencin, A., J. Kluwe, and R. F. Schwabe. 2009. "Toll-like Receptors as Targets in Chronic Liver Diseases." *Gut* 58(5): 704–20.

Mendes-Braz, M. et al. 2012. "The Current State of Knowledge of Hepatic Ischemia-Reperfusion Injury Based on Its Study in Experimental Models." *Journal of Biomedicine and Biotechnology* 2012.

Messina, Antonietta, Eléanor Luce, Marwa Hussein, and Anne Dubart-Kupperschmitt. 2020. "Pluripotent-Stem-Cell-Derived Hepatic Cells: Hepatocytes and Organoids for Liver Therapy and Regeneration." *Cells* 9(2).

Michalopoulos, George K. 2013. "Principles of Liver Regeneration and Growth Homeostasis." *Comprehensive Physiology* 3(1): 485–513.

———. 2017. "Hepatostat: Liver Regeneration and Normal Liver Tissue Maintenance." *Hepatology* 65(4): 1384–92.

Michalopoulos, George K., and Bharat Bhushan. 2021. "Liver Regeneration: Biological and Pathological Mechanisms and Implications." *Nature Reviews Gastroenterology and Hepatology* 18(1): 40–55. http://dx.doi.org/10.1038/s41575-020-0342-4.

Middleton, Paul, and Nikhil Vergis. 2021. "Mitochondrial Dysfunction and Liver Disease: Role, Relevance, and Potential for Therapeutic Modulation." *Therapeutic Advances in Gastroenterology* 14: 1–19.

Miñambres, Eduardo, Juan J. Rubio, Elisabeth Coll, and Beatriz Domínguez-Gil. 2018. "Donation after Circulatory Death and Its Expansion in Spain." *Current Opinion in Organ Transplantation* 23(1): 120–29.

Mishra, Alita, and Zobair M. Younossi. 2012. "Epidemiology and Natural History of Non-Alcoholic Fatty Liver Disease." *Journal of Clinical and Experimental Hepatology* 2(2): 135–44.

Mitchell, Claudia et al. 2005. "Heparin-Binding Epidermal Growth Factor-like Growth Factor Links Hepatocyte

Priming with Cell Cycle Progression during Liver Regeneration." *J Biol Chem* 280(4): 2562–68.

Mitra, Souveek, Arka De, and Abhijit Chowdhury. 2020. "Epidemiology of Non-Alcoholic and Alcoholic Fatty Liver Diseases." *Translational Gastroenterology and Hepatology* 5: 1–17.

Mohammad, Shireen, and Christoph Thiemermann. 2021. "Role of Metabolic Endotoxemia in Systemic Inflammation and Potential Interventions." *Frontiers in Immunology* 11(January): 1–16.

Mokdad, Ali H. et al. 2016. "Global Burden of Diseases, Injuries, and Risk Factors for Young People's Health during 1990–2013: A Systematic Analysis for the Global Burden of Disease Study 2013." *The Lancet* 387(10036): 2383–2401.

Morgan, T R, S Mandayam, and M M Jamal. 2004. "Alcohol and Hepatocellular Carcinoma." *Gastroenterology* 127(5): S87–96.

Motiño, Omar et al. 2019. "Protective Role of Hepatocyte Cyclooxygenase-2 Expression Against Liver Ischemia-Reperfusion Injury in Mice." *Hepatology* 70(2): 650–65.

Mullany, Lisa K et al. 2008. "Distinct Proliferative and Transcriptional Effects of the D-Type Cyclins in Vivo." *Cel Cycle* 7(14): 2215–24.

Nachiappan, V, D Curtiss, B E Corkey, and L Kilpatrick. 1994. "Cytokines Inhibit Fatty Acid Oxidation in Isolated Rat Hepatocytes: Synergy among TNF, IL-6 and IL-1." *Shock* 1(2): 123–29.

Nadi, Akram, Lida Moradi, Jafar Ai, and Shiva Asadpour. 2020. "Stem Cells and Hydrogels for Liver Tissue Engineering: Synergistic Cure for Liver Regeneration." *Stem Cell Reviews and Reports* 16(6): 1092–1104.

Nakatani, T et al. 1981. "Differences in Predominant Energy Substrate in Relation to the Resected Hepatic Mass in the Phase Immediately after Hepatectomy." *J Lab Clin Med* 97(6): 887–98.

Nasralla, David et al. 2018. "A Randomized Trial of Normothermic Preservation in Liver Transplantation." *Nature* 557(7703): 50–56.

Navarro, Ana, and Alberto Boveris. 2007. "The Mitochondrial Energy Transduction System and the Aging Process." *American Journal of Physiology - Cell Physiology* 292(2): C670-686.

Navasa, Nicolás et al. 2015. "Regulation of Oxidative Stress by Methylation-Controlled j Protein Controls Macrophage Responses to Inflammatory Insults." *Journal of Infectious Diseases* 211(1): 135–45.

Nebrig, Maxim, Peter Neuhaus, and Andreas Pascher. 2014. "Advances in the Management of the Explanted Donor Liver." *Nature Reviews Gastroenterology and Hepatology* 11(8): 489–96.

Nevzorova, Yulia A. et al. 2016. "Enhanced Expression of C-Myc in Hepatocytes Promotes Initiation and Progression of Alcoholic Liver Disease." *Journal of Hepatology* 64(3): 628–40. http://dx.doi.org/10.1016/j.jhep.2015.11.005.

Nevzorova, Yulia A., Zoe Boyer-Diaz, Francisco Javier Cubero, and Jordi Gracia-Sancho. 2020. "Animal Models for Liver Disease – A Practical Approach for Translational Research." *Journal of Hepatology* 73(2): 423–40. https://doi.org/10.1016/j.jhep.2020.04.011.

Nishida, Takeshi et al. 2013. "Spontaneous Onset of Nonalcoholic Steatohepatitis and Hepatocellular Carcinoma in a Mouse Model of Metabolic Syndrome." *Hepatic and Pancreatic Systems* 93: 230–41.

Northup, Patrick Grant et al. 2015. "Excess Mortality on the Liver Transplant Waiting List: Unintended Policy Consequences and Model for End-Stage Liver Disease (MELD) Inflation." *Hepatology* 61(1): 285–91.

Ntamo, Yonela et al. 2022. "Clinical Use of N-Acetyl Cysteine during Liver Transplantation: Implications of Oxidative Stress and Inflammation as Therapeutic Targets." *Biomedicine and Pharmacotherapy* 147(October 2021): 112638. https://doi.org/10.1016/j.biopha.2022.112638.

Nunnari, Jodi, and Anu Suomalainen. 2012. "Mitochondria: In Sickness and in Health." *Cell* 148(6): 1145–59.

Odegard, J et al. 2017. "Differential Effects of Epidermal Growth Factor (EGF) Receptor Ligands on Receptor Binding, Downstream Signalling Pathways and DNA Synthesis in Hepatocytes." *Growth Factors* 35(6): 239–48.

Orokorov, PL, IA Anikhovskaia, IE Volkov, and M Iu Ikovlev. 2011. "Intestinal Endotoxin in Induction of Type 1 Diabetes." *Fiziol Cheloveka* 37(2): 138–41.

Osellame, Laura D., Thomas S. Blacker, and Michael R. Duchen. 2012. "Cellular and Molecular Mechanisms of Mitochondrial Function." *Best Practice and Research: Clinical Endocrinology and Metabolism* 26(6): 711–23. http://dx.doi.org/10.1016/j.beem.2012.05.003.

Panel, Mathieu, Bijan Ghaleh, and Didier Morin. 2018. "Mitochondria and Aging: A Role for the Mitochondrial Transition Pore?" *Aging Cell* 17(4): 1–15.

Papageorgiou, Dimitris N, Jeroen Demmers, and John Strouboulis. 2013. "NP-40 Reduces Contamination by Endogenous Biotinylated Carboxylases during Purification of Biotin Tagged Nuclear Proteins." *Protein Expr Purif* 89(1): 80–83.

Paranjpe, Shirish et al. 2016. "Combined Systemic Elimination of MET and Epidermal Growth Factor Receptor Signaling Completely Abolishes Liver Regeneration and Leads to Liver Decompensation." *Hepatology* 64(5): 1711–24.

Pascual-Itoiz, Miguel Angel et al. 2020. "The Mitochondrial Negative Regulator MCJ Modulates the Interplay between

Microbiota and the Host during Ulcerative Colitis." *Scientific Reports* 10(1): 1–13.
Peralta, Carmen et al. 1999. "Protective Effect of Liver Ischemic Preconditioning on Liver and Lung Injury Induced by Hepatic Ischemia-Reperfusion in the Rat." *Hepatology* 30(6): 1481–89.
Peralta, Carmen, Mónica B Jiménez, and Jordi Gracia-Sancho. 2013. "Hepatic Ischemia and Reperfusion Injury: Effects on the Liver Sinusoidal Milieu." *J Hepatol* 59(5): 1094–1106.
Pernas, Lena, and Luca Scorrano. 2016. "Mito-Morphosis: Mitochondrial Fusion, Fission, and Cristae Remodeling as Key Mediators of Cellular Function." *Annual Review of Physiology* 78(November 2015): 505–31.
Petrasek, Jan et al. 2012. "IL-1 Receptor Antagonist Ameliorates Inflammasome-Dependent Alcoholic Steatohepatitis in Mice." *Journal of Clinical Investigation* 122(10): 3476–89.
Philips, Cyriac Abby et al. 2017. "Healthy Donor Fecal Microbiota Transplantation in Steroid-Ineligible Severe Alcoholic Hepatitis: A Pilot Study." *Clinical Gastroenterology and Hepatology* 15(4): 600–602. http://dx.doi.org/10.1016/j.cgh.2016.10.029.
Pimpin, Laura et al. 2018. "Burden of Liver Disease in Europe: Epidemiology and Analysis of Risk Factors to Identify Prevention Policies." *J Hepatol* 69(3): 718–35.
Poole, Lauren G., Christine E. Dolin, and Gavin E. Arteel. 2017. "Organ-Organ Crosstalk and Alcoholic Liver Disease." *Biomolecules* 7(3): 1–16.
Price, Morgan N, Paramvir S Dehal, and Adam P Arkin. 2010. "FastTree 2 – Approximately Maximum-Likelihood Trees for Large Alignments." *PLoS ONE*.
Price, Nathan L et al. 2012. "SIRT1 Is Required for AMPK Activation and the Beneficial Effects of Resveratrol on Mitochondrial Function." *Cell Metab* 15(5): 675–90.
———. 2013. "SIRT1 Is Required for AMPK Activation and the Beneficial Effects of Resveratrol on Mitochondrial Function." *Cell Metab* 15(5): 675–90.
Purohit, Vishnudutt, and David A. Brenner. 2006. "Mechanisms of Alcohol-Induced Hepatic Fibrosis: A Summary of the Ron Thurman Symposium." *Hepatology* 43(4): 872–78.
Qi, Bo et al. 2021. "Effect of Remote Ischemic Preconditioning among Donors and Recipients Following Pediatric Liver Transplantation: A Randomized Clinical Trial." *World Journal of Gastroenterology* 27(4): 345–57.
Qi, Meirigeng et al. 2017. "Encompassing ATP, DNA, Insulin, and Protein Content for Quantification and Assessment of Human Pancreatic Islets." *Cell and Tissue Banking* 19: 77–85.
Qin, Liya et al. 2007. "Systemic LPS Causes Chronic Neuroinflamamtion and Progressive Neurodegeneration." *Glia* 55(5): 453–62.
Ramachandran, Anup, and Hartmut Jaeschke. 2019. "Acetaminophen Hepatotoxicity." *Seminars in Liver Disease* 39(2): 221–34.
Ramaiah, Shashi K., Chantal Rivera, and Gavin E. Arteel. 2004. "Early-Phase Alcoholic Liver Disease: An Update on Animal Models, Pathology, and Pathogenesis." *International Journal of Toxicology* 23(4): 217–31.
Ramanan, Poornima, and Raymund R. Razonable. 2013. "Cytomegalovirus Infections in Solid Organ Transplantation: A Review." *Infection and Chemotherapy* 45(3): 260–71.
Rao, RK. 2009. "Endotoxemia and Gut Barrier Dysfunction in Alcoholic Liver Disease." *Hepatology* 50(2): 638–44.
Rasineni, Karuna et al. 2020. "Recent Advances in Understanding the Complexity of Alcohol-Induced Pancreatic Dysfunction and Pancreatitis Development." *Biomolecules* 10(5).
Ren, Ruixue, Ziming Wang, Miaomiao Wu, and Hua Wang. 2020. "Emerging Roles of SIRT1 in Alcoholic Liver Disease." *International Journal of Biological Sciences* 16(16): 3174–83.
Ren, Zhenhua et al. 2016. "Chronic plus Binge Ethanol Exposure Causes More Severe Pancreatic Injury and Inflammation." *Toxicol Appl Pharmacol* 308: 11–19.
Ricoult, Stéphane JH, and Brendan D Manning. 2013. "The Multifaceted Role of MTORC1 in the Control of Lipid Metabolism." *EMBO Rep* 14(3): 242–51.
Riley, T. R., and A. M. Bhatti. 2001. "Preventive Strategies in Chronic Liver Disease: Part II. Cirrhosis." *American Family Physician* 64(10): 1735–40.
Roe, Amy L et al. 2001. "The Effect of Endotoxin on Hepatocyte Nuclear Factor 1 Nuclear Protein Binding: Potential Implications on CYP2E1 Expression in the Rat." *Journal of Pharmacy and Pharmacology* 53(10): 1365–71.
Rosello, Arnau Panisello et al. 2020. "Polyethylene Glycol 35 as a Perfusate Additive for Mitochondrial and Glycocalyx Protection in Hope Liver Preservation." *International Journal of Molecular Sciences* 21(16): 1–16.
Rostovtseva, Tatiana K., and Sergey M. Bezrukov. 2008. "VDAC Regulation: Role of Cytosolic Proteins and Mitochondrial Lipids." *Journal of Bioenergetics and Biomembranes* 40(3): 163–70.
de Rougemont, Olivier, Kuno Lehmann, and Pierre-Alain Clavien. 2009. "Preconditioning, Organ Preservation, and Postconditioning to Prevent Ischemia-Reperfusion Injury to the Liver." *Liver Transpl* 15(10): 1172–82.
Rousselle, T et al. 2020. "Intravenous Administration of Mitochondria Minimizes Liver Ischemia Reperfusion Injury in Lean and Diet Induced Obese Mice." *Am J Transplant* 20(Suppl 3).
Roychowdhury, Sanjoy et al. 2012. "Inhibition of Apoptosis Protects Mice from Ethanol-Mediated Acceleration of

Early Markers of CCl4-Induced Fibrosis but Not Steatosis or Inflammation." *Alcoholism: Clinical and Experimental Research* 36(7): 1139–47.

Rubio Muñoz, J. J. et al. 2022. "Role of Normothermic Perfusion with ECMO in Donation after Controlled Cardiac Death in Spain." *Medicina Intensiva* 46(1): 31–41.

Rudnick, David A., and Nicholas O. Davidson. 2012. "Functional Relationships between Lipid Metabolism and Liver Regeneration." *International Journal of Hepatology* 2012: 1–8.

Runge, D M et al. 1999. "STAT 1α/1β, STAT 3 and STAT 5: Expression and Association with c-MET and EGF-Receptor in Long-Term Cultures of Human Hepatocytes." *Biochem Biophys Res Commun* 265(2): 376–81.

Russel, W E, R J Coffey, A J Ouellette, and H L Moses. 1988. "Type Beta Transforming Growth Factor Reversibly Inhibits the Early Proliferative Response to Partial Hepatectomy in the Rat." *Proceedings of the National Academy of Sciences of the United States of America* 85(14): 5126–30.

Russo, Lucia et al. 2012. "Addition of Simvastatin to Cold Storage Solution Prevents Endothelial Dysfunction in Explanted Rat Livers." *Hepatology* 55(3): 921–30.

Saravia, Jordy et al. 2020. "Signaling Networks in Immunometabolism." *Cell Res* 30(4): 328–42.

Satishchandran, Abhishek et al. 2018. "MicroRNA 122, Regulated by GRLH2, Protects Livers of Mice and Patients from Ethanol-Induced Liver Disease." *Gastroenterology* 154(1): 1–22. file:///C:/Users/Carla Carolina/Desktop/Artigos para acrescentar na qualificação/The impact of birth weight on cardiovascular disease risk in the.pdf.

Schlegel, Andrea et al. 2020. "Hypothermic Oxygenated Perfusion Protects from Mitochondrial Injury before Liver Transplantation." *EBioMedicine* 60: 103014. https://doi.org/10.1016/j.ebiom.2020.103014.

Schmieder, Robert, and Robert Edwards. 2011. "Quality Control and Preprocessing of Metagenomic Datasets." *Bioinformatics* 27(6): 863–64.

Schusdziarra, Christina, Marta Blamowska, Abdussalam Azem, and Kai Hell. 2013. "Methylation-Controlled J-Protein MCJ Acts in the Import of Proteins into Human Mitochondria." *Hum Mol Genet* 22(7): 1348–57.

Secinaro, Michael A. et al. 2019. "Glycolysis Induces MCJ Expression That Links T Cell Proliferation with Caspase-3 Activity and Death." *Frontiers in Cell and Developmental Biology* 7(MAR): 1–10.

Seizner, Markus et al. 2007. "Increased Ischemic Injury in Old Mouse Liver: An ATP-Dependent Mechanism." *Liver Transplantation* 13(3): 382–90.

Selzner, Markus, Carlos A. Camargo, and Pierre Alain Clavien. 1999. "Ischemia Impairs Liver Regeneration after Major Tissue Loss in Rodents: Protective Effects of Interleukin-6." *Hepatology* 30(2): 469–75.

Selzner, Markus, Carlos A Camargo, and Pierre-Alain Clavien. 2003. "Ischemia Impairs Liver Regeneration after Major Tissue Loss in Rodents: Protective Effects of Interleukin-6." *Hepatology* 30(2): 469–75.

Selzner, Nazia, Markus Selzner, Wolfram Jochum, and Pierre-Alain Clavien. 2003a. "Ischemic Preconditioning Protects the Steatotic Mouse Liver against Reperfusion Injury: An ATP Dependent Mechanism." *Journal of Hepatology* 39(1): P55-61.

Selzner, Nazia, Markus Selzner, Wolfram Jochum, and Pierre Alain Clavien. 2003b. "Ischemic Preconditioning Protects the Steatotic Mouse Liver against Reperfusion Injury: An ATP Dependent Mechanism." *Journal of Hepatology* 39(1): 55–61.

Serrano-Maciá, Marina et al. 2021. "Neddylation Inhibition Ameliorates Steatosis in NAFLD by Boosting Hepatic Fatty Acid Oxidation via the DEPTOR-MTOR Axis." *Mol Metab* 53.

Shah, Neil D et al. 2019. "Alcohol-Related Liver Disease Is Rarely Detected at Early Stages Compared With Liver Diseases of Other Etiologies Worldwide: Lack of Early Detection of Alcoholic-Related Liver Disease." *Clin Gastroenterol Hepatol* 17(11): 2320–29.

Shi, Ming et al. 2017. "A Pilot Study of Mesenchymal Stem Cell Therapy for Acute Liver Allograft Rejection." *Stem Cells Translational Medicine* 6(12): 2053–61.

Shimano, Hitoshi et al. 1997. "Isoform 1c of Sterol Regulatory Element Binding Protein Is Less Active than Isoform 1a in Livers of Transgenic Mice and in Cultured Cells." *Journal of Clinical Investigation* 99(5): 846–54.

Shkoporov, Andrey N. et al. 2019. "The Human Gut Virome Is Highly Diverse, Stable, and Individual Specific." *Cell Host and Microbe* 26(4): 527-541.e5. https://doi.org/10.1016/j.chom.2019.09.009.

Shridhar, V et al. 2001. "Loss of Expression of a New Member of the DNAJ Protein Family Confers Resistance to Chemotherapeutic Agents Used in the Treatment of Ovarian Cancer." *Cancer Res* 61(10): 4258–65.

Simón, Jorge et al. 2021. "Magnesium Accumulation upon Cyclin M4 Silencing Activates Microsomal Triglyceride Transfer Protein Improving NASH." 75(1): 34–45.

Singal, Ashwani K. et al. 2018. "ACG Clinical Guideline: Alcoholic Liver Disease." *American Journal of Gastroenterology* 113(2): 175–94.

Singal, Ashwani K., and Vijay H. Shah. 2019. "Current Trials and Novel Therapeutic Targets for Alcoholic Hepatitis." *Journal of Hepatology* 70(2): 305–13. https://doi.org/10.1016/j.jhep.2018.10.026.

Sinha, D., and P. D'Silva. 2014. "Chaperoning Mitochondrial Permeability Transition: Regulation of Transition Pore

Complex by a J-Protein, DnaJC15." *Cell Death and Disease* 5(3): 1–11.
Smilkstein, M J, G L Knapp, K W Kulig, and B H Rumack. 1988. "Efficacy of Oral N-Acetylcysteine in the Treatment of Acetaminophen Overdose. Analysis of the National Multicenter Study (1976 to 1985)." *N Engl J Med* 319(24): 1557–62.
Soares, Ricardo OS et al. 2019. "Ischemia/Reperfusion Injury Revisited: An Overview of the Latest Pharmacological Strategies." *Int J Mol Sci* 20(20): 5034.
Solhi, Roya et al. 2021. "Metabolic Hallmarks of Liver Regeneration." *Trends in Endocrinology and Metabolism* 32(9): 731–45.
Soni, Sanooj et al. 2019. "ATP Redirects Cytokine Trafficking and Promotes Novel Membrane TNF Signaling via Microvesicles." *FASEB J* 33(5): 6442–55.
Sorrentino, Vincenzo, Keir J. Menzies, and Johan Auwerx. 2018. "Repairing Mitochondrial Dysfunction in Disease." *Annual Review of Pharmacology and Toxicology* 58: 353–89.
Stickel, Felix, Christian Datz, Jochen Hampe, and Ramon Bataller. 2017. "Pathophysiology and Management of Alcoholic Liver Disease: Update 2016." *Gut and Liver* 11(2): 173–88.
Strathdee, G et al. 2004. "Cell Type-Specific Methylation of an Intronic CpG Island Controls Expression of the MCJ Gene." *Carcinogenesis* 25(5): 693–701.
Strathdee, Gordon et al. 2005. "Demethylation of the MCJ Gene in Stage III/IV Epithelial Ovarian Cancer and Response to Chemotherapy." *Gynecol Oncol* 97(3): 898–903.
Streetz, Konrad L. et al. 2003. "Interleukin 6/Gp130-Dependent Pathways Are Protective during Chronic Liver Diseases." *Hepatology* 38(1): 218–29.
Suk, Ki Tae, Moon Young Kim, and Soon Koo Baik. 2014. "Alcoholic Liver Disease: Treatment." *World Journal of Gastroenterology* 20(36): 12934–44.
Suriawinata, Arief A., and Swan N. Thung. 2002. "Malignant Liver Tumors." *Clinics in Liver Disease* 6(2): 527–54.
Suter, Paolo, Eric Jequier, and Yves Schutz. 1994. "Effect of Ethanol on Energy Expenditure." *America Phsiological Society*: R1204–12.
Suter, Paolo M, Eric Jéquier, and Yves Schutz. 1994. "Effect of Ethanol on Energy Expenditure." *American Physiological Society* 35: 1204–12.
Tammineni, Prasad et al. 2013. "The Import of the Transcription Factor STAT3 into Mitochondria Depends on GRIM-19, a Component of the Electron Transport Chain." *J Biol Chem* 288(7): 4723–32.
Tang, LM et al. 2010. "Activation of Adenosine A2A Receptor Attenuates Inflammatory Response in a Rat Model of Small-for-Size Liver Transplantation." *Transplant Proc* 42(5): 1915–20.
Tao, Yachao, Menglan Wang, Enqiang Chen, and Hong Tang. 2017. "Liver Regeneration: Analysis of the Main Relevant Signaling Molecules." *Mediators of Inflammation* 2017.
Tarlá, Marissa Rabelo et al. 2006. "A Molecular View of Liver Regeneration." *Acta Cirurgica Brasileira* 21(SUPPL.1): 58–62.
Tashiro, Hirotaka, Shintaro Kuroda, Yoshihiro Mikuriya, and Hideki Ohdan. 2014. "Ischemia-Reperfusion Injury in Patients with Fatty Liver and the Clinical Impact of Steatotic Liver on Hepatic Surgery." *Surgery Today* 44(9): 1611–25.
Taub, Rebecca. 1996. "Liver Regeneration 4: Transcriptional Control of Liver Regeneration." *FASEB J* 10(4): 413–27.
———. 2004. "Liver Regeneration: From Myth to Mechanism." *Nature Reviews Molecular Cell Biology* 5: 836–47.
Teodoro, João S. et al. 2022. "Shaping of Hepatic Ischemia/Reperfusion Events: The Crucial Role of Mitochondria." *Cells* 11(4): 1–24.
Teschke, Rolf. 2018a. "Alcoholic Liver Disease: Alcohol Metabolism, Cascade of Molecular Mechanisms, Cellular Targets, and Clinical Aspects." *Biomedicines* 6(4).
———. 2018b. "Alcoholic Steatohepatitis (ASH) and Alcoholic Hepatitis (AH): Cascade of Events, Clinical Aspects, and Pharmacotherapy Options." *Expert Opinion on Pharmacotherapy* 19(8): 779–93. https://doi.org/10.1080/14656566.2018.1465929.
Thiele, Todd E., and Montserrat Navarro. 2014. "'Drinking in the Dark' (DID) Procedures: A Model of Binge-like Ethanol Drinking in Non-Dependent Mice." *Alcohol* 48(3): 235–41.
Thijssen, Max F. et al. 2019. "Gene Silencing With Small Interfering RNA: A New Therapeutic Option During Ex Vivo Machine Liver Perfusion Preservation." *Liver Transplantation* 25(1): 140–51.
Thjissen, Max F et al. 2019. "Gene Silencing With SiRNA (RNA Interference): A New Therapeutic Option During Ex Vivo Machine Liver Perfusion Preservation." *Liver Transplantation* 140–151(25): 1.
Thurman, R. G. et al. 1982. "Swift Increase in Alcohol Metabolism (SIAM) in the Mouse: Comparison of the Effect of Short-Term Ethanol Treatment on Ethanol Elimination in Four Inbred Strains." *Journal of Pharmacology and Experimental Therapeutics* 223(1): 45–49.
Thurman, R G, W R McKenna, and T B McCaffrey. 1976. "Pathways Responsible for the Adaptive Increase in Ethanol

Utilization Following Chronic Treatment with Ethanol: Inhibitor Studies with the Hemoglobin-Free Perfused Rat Liver." *Mol Pharmacol* 12(1): 156–66.

Trapero-Marugán, María, Ester Coelho Little, and Marina Berenguer. 2018. "Stretching the Boundaries for Liver Transplant in the 21st Century." *The Lancet Gastroenterology and Hepatology* 3(11): 803–11. http://dx.doi.org/10.1016/S2468-1253(18)30213-9.

Tripathi, Anupriya et al. 2018. "The Gut-Liver Axis and the Intersection with the Microbiome." *Nat Rev Gastroenterol Hepatol* 15(7): 397–411.

Truant, Stéphanie et al. 2013. "Volumetric Gain of the Liver after Major Hepatectomy in Obese Patients: A Case-Matched Study in 84 Patients." *Ann Surg* 258(5): 696–704.

Tsukamoto, H., R. D. Reidelberger, S. W. French, and C. Largman. 1984. "Long-Term Cannulation Model for Blood Sampling and Intragastric Infusion in the Rat." *American Journal of Physiology - Regulatory Integrative and Comparative Physiology* 16(3).

Tsukamoto, Hidekazu, Keigo Machida, Alla Dynnyk, and Hasmik Mkrtchyan. 2009. "'Second Hit' Models of Alcoholic Liver Disease." *Seminars in Liver Disease* 29(2): 178–87.

Tuma, Dean J. 2002. "Role of Malondialdehyde-Acetaldehyde Adducts in Liver Injury." *Free Radical Biology and Medicine* 32(4): 303–8.

Tyanova, Stefka et al. 2016. "The Perseus Computational Platform for Comprehensive Analysis of (Prote)Omics Data." *Nat Methods* 13: 731–40.

Venkatesan, S., R. J. Ward, and T. J. Peters. 1988. "Effect of Chronic Ethanol Feeding on the Hepatic Secretion of Very-Low-Density Lipoproteins." *Biochimica et Biophysica Acta (BBA)/Lipids and Lipid Metabolism* 960(1): 61–66.

Verma, Sudhir et al. 2021. "Liver Regeneration: Metabolic and Epigenetic Regulation." *Hepatoma Research* 7.

Vernon, G., A. Baranova, and Z. M. Younossi. 2011. "Systematic Review: The Epidemiology and Natural History of Non-Alcoholic Fatty Liver Disease and Non-Alcoholic Steatohepatitis in Adults." *Alimentary Pharmacology and Therapeutics* 34(3): 274–85.

Veteläinen, Reeta, Arlène K van Vliet, and Thomas M van Gulik. 2007. "Severe Steatosis Increases Hepatocellular Injury and Impairs Liver Regeneration in a Rat Model of Partial Hepatectomy." *Ann Surg* 245(1): 44–50.

Villarreal, Daniel et al. 2019. "A Simple High Efficiency Protocol for Pancreatic Islet Isolation from Mice." *J Vis Exp* 150.

Wan, Ping, Qigen Li, Jianjun Zhang, and Qiang Xia. 2015. "Right Lobe Split Liver Transplantation versus Whole Liver Transplantation in Adult Recipients: A Systematic Review and Meta-Analysis." *Liver Transplantation* 21: 928–43.

Wang, H. Joe, Samir Zakhari, and M. Katherine Jung. 2010. "Alcohol, Inflammation, and Gut-Liver-Brain Interactions in Tissue Damage and Disease Development." *World Journal of Gastroenterology* 16(11): 1304–13.

Wang, Hua, Wajahat Mehal, Laura E. Nagy, and Yaron Rotman. 2021. "Immunological Mechanisms and Therapeutic Targets of Fatty Liver Diseases." *Cellular and Molecular Immunology* 18(1): 73–91. http://dx.doi.org/10.1038/s41423-020-00579-3.

Wang, Jinglin et al. 2022. "Developing Tissue Engineering Strategies for Liver Regeneration." *Engineered Regeneration* 3(1): 80–91. https://doi.org/10.1016/j.engreg.2022.02.003.

Wang, Ping, Jidong Jia, and Dong Zhang. 2020. "Purinergic Signalling in Liver Diseases: Pathological Functions and Therapeutic Opportunities." *JHEP Reports* 2(6): 100165. https://doi.org/10.1016/j.jhepr.2020.100165.

Wang, Yuhua et al. 2013. "Lactobacillus Rhamnosus GG Reduces Hepatic TNFα Production and Inflammation in Chronic Alcohol-Induced Liver Injury." *Journal of Nutritional Biochemistry* 24(9): 1609–15.

Wei, Xiaoli et al. 2013. "Chronic Alcohol Exposure Disturbs Lipid Homeostasis at the Adipose Tissue-Liver Axis in Mice: Analysis of Triacylglycerols Using High-Resolution Mass Spectrometry in Combination with In Vivo Metabolite Deuterium Labeling." *PLoS ONE* 8(2).

Wen, Hui-Ju et al. 2019. "Myeloid Cell-Derived HB-EGF Drives Tissue Recovery After Pancreatitis." *Cell Mol Gastroenterol Hepatol* 8(2): 173–92.

West, A Phillip et al. 2011. "TLR Signalling Augments Macrophage Bactericidal Activity through Mitochondrial ROS." *Nature* 472: 476–80.

Weymann, Alexander et al. 2009. "P21 Is Required for Dextrose-Mediated Inhibition of Mouse Liver Regeneration." *Hepatology* 50(1): 2017–2215.

Wisnieski, Jacek R, Alexandre Zougman, Nagarjuna Nagaraj, and Matthias Mann. 2009. "Universal Sample Preparation Method for Proteome Analysis." *Nat Methods* 6(5): 359–62.

Wrzosek, Laura et al. 2021. "Microbiota Tryptophan Metabolism Induces Aryl Hydrocarbon Receptor Activation and Improves Alcohol-Induced Liver Injury." *Gut* 70(7): 1299–1308.

Xia, Si Wei et al. 2020. "Endoplasmic Reticulum Stress and Protein Degradation in Chronic Liver Disease." *Pharmacological Research* 161: 105218. https://doi.org/10.1016/j.phrs.2020.105218.

Xiang, Li, Yaru Shao, and Yuping Chen. 2021. "Mitochondrial Dysfunction and Mitochondrion-Targeted Therapeutics in Liver Diseases." *Journal of Drug Targeting* 29(10): 1080–93. https://doi.org/10.1080/1061186X.2021.1909051.

Yamada, Y et al. 1998. "Analysis of Liver Regeneration in Mice Lacking Type 1 or Type 2 Tumor Necrosis Factor Receptor: Requirement for Type 1 but Not Type 2 Receptor." *Hepatology* 28(4): 959–70.

Yamashita, Hiromi et al. 2001. "A Glucose-Responsive Transcription Factor That Regulates Carbohydrate Metabolism in the Liver." *Proceedings of the National Academy of Sciences of the United States of America* 98(16): 9116–21.

Yamauchi, Hidemi, and B. 1982. "Postischemic Liver Damage in Rats: Effect of Some Therapeutic Interventions on Survival Rate." *Baca, Ibo Mittmann, Ulrich Geisen, Hans Peter Salzer, Manfred* 138(1): 63–70.

Yan, Ming et al. 2007. "Ethanol Induced Mitochondria Injury and Permeability Transition Pore Opening: Role of Mitochondria in Alcoholic Liver Disease." *World Journal of Gastroenterology* 13(16): 2352–56.

Yang, An Ming et al. 2017. "Intestinal Fungi Contribute to Development of Alcoholic Liver Disease." *Journal of Clinical Investigation* 127(7): 2829–41.

You, Min, and Gavin E. Arteel. 2019. "Effect of Ethanol on Lipid Metabolism." *Journal of Hepatology* 70(2): 237–48. https://doi.org/10.1016/j.jhep.2018.10.037.

You, Min, and Christopher Q. Rogers. 2009. "Adiponectin: A Key Adipokine in Alcoholic Fatty Liver." *Experimental Biology and Medicine* 234(8): 850–59.

Younossi, Zobair M. et al. 2021. "Nonalcoholic Steatohepatitis Is the Most Rapidly Increasing Indication for Liver Transplantation in the United States." *Clin Gastroenterol Hepatol* 19(3): 580–89.

Zhang, Pengcheng et al. 2015. "Demethyleneberberine, a Natural Mitochondria-Targeted Antioxidant, Inhibits Mitochondrial Dysfunction, Oxidative Stress, and Steatosis in Alcoholic Liver Disease Mouse Model." *Journal of Pharmacology and Experimental Therapeutics* 352(1): 139–47.

Zhang, Sen et al. 2022. "Role of Mitochondrial Pathways in Cell Apoptosis during He-Patic Ischemia/Reperfusion Injury." *International Journal of Molecular Sciences* 23(4).

Zhang, Yu et al. 2018. "Hepatic Ischemic Preconditioning Alleviates Ischemia-Reperfusion Injury by Decreasing TIM4 Expression." *International Journal of Biological Sciences* 14(10): 1186–95.

Zheng, Danping et al. 2017. "Accuracy of Computed Tomography for Detecting Hepatic Steatosis in Donors for Liver Transplantation: A Meta-Analysis." *Clin Transplant* 31(8).

Zheng, Yi et al. 2019. "Deficiency of the Mitochondrial Glycerol 3-Phosphate Dehydrogenase Contributes to Hepatic Steatosis." *Hepatology* 70(1): 84–97.

Zhong, Wei et al. 2012. "Chronic Alcohol Exposure Stimulates Adipose Tissue Lipolysis in Mice: Role of Reverse Triglyceride Transport in the Pathogenesis of Alcoholic Steatosis." *American Journal of Pathology* 180(3): 998–1007. http://dx.doi.org/10.1016/j.ajpath.2011.11.017.

Zhong, Zhi et al. 2014. "Acute Ethanol Causes Hepatic Mitochondrial Depolarization in Mice: Role of Ethanol Metabolism." *PLoS ONE* 9(3).

Zhou, Hao et al. 2019. "DNA-PKcs Promotes Alcohol-Related Liver Disease by Activating Drp1-Related Mitochondrial Fission and Repressing FUNDC1-Required Mitophagy." *Signal Transduction and Targeted Therapy* 4(1). http://dx.doi.org/10.1038/s41392-019-0094-1.

Zhou, Sheng Li et al. 1998. "Ethanol Up-Regulates Fatty Acid Uptake and Plasma Membrane Expression and Export of Mitochondrial Aspartate Aminotransferase in HepG2 Cells." *Hepatology* 27(4): 1064–74.

9. SUPPORT

9 SUPPORT

This work was supported and funded by Asociación Española Contra el Cáncer (AECC), National Health Institute (NIH), Gobierno Vasco-Departamentos de Industria y de Salud, ELKARTEK, Ministerio de Ciencia, Innovación y Universidades (MICINN), BioEF, EiTB Maratoia and La Caixa Foundation Program to Dr. Ma Luz Martínez-Chantar. It has been also funded by a pre-doctoral grant from Gobierno Vasco-Departamento de Educación to Naroa Goikoetxea-Usandizaga.